Properties of boson-exchange superconductors

J. P. Carbotte

Department of Physics, McMaster University, Hamilton, Ontario, Canada L8S 4M1

The author reviews some of the important successes achieved by Eliashberg theory in describing the observed superconducting properties of many conventional superconductors. Functional derivative techniques are found to help greatly in understanding the observed deviations from BCS laws. Approximate analytic formulas with simple correction factors for strong-coupling corrections embodied in the single parameter $T_c/\omega_{\ln}$ are also found to be very helpful. Here T_c is the critical temperature and $\omega_{\ln}$ is an average boson energy mediating the pairing potential in Eliashberg theory. In view of the discovery of high-T_c superconductivity in the copper oxides, results in the very strong coupling limit of $T_c/\omega_{\ln}\sim 1$ are also considered, as is the asymptotic limit when $T_c/\omega_{\ln}\rightarrow\infty$. This case is of theoretical interest only, but it is nevertheless important because simple analytic results apply that give insight into the more realistic strong-coupling regime. A discussion more specific to the oxides is included in which it is concluded that some high-energy boson-exchange mechanism must be operative, with, possibly, some important phonon contribution in some cases. A more definitive application of boson-exchange models to the oxides awaits better experimental results.

CONTENTS

I. INTRODUCTION AND OVERVIEW

A. Purpose and limit on scope

Much that was known at the time about Eliashberg theory and its application to real superconductors was reviewed by Scalapino (1969) and by McMillan and Rowell (1969) in Parks's two-volume series on superconductivity. Since then, the book by Ginzburg and Kirzhnits [(1982); Dolgov and Maksimov (1982a, 1982b)] has appeared. It contains some discussion of the more recent developments of strong-coupling theory, as does the excellent and comprehensive review of Allen and Mitrović (1982), which is, however, limited to a discussion of the critical temperature. In this review I want to survey and emphasize some of the more important results obtained as well as ideas developed since 1969, and to look at Eliashberg theory in the light of the discovery of superconductivity at high temperature in the oxides.

In order to keep this review within a manageable length, it was necessary to restrict considerably the developments covered. None of the well-known derivations of the Eliashberg equations themselves and of the associated formulas for the free energy, the optical properties, etc., are repeated. Moreover, the effects of magnetic impurities within the theories of Abrikosov and Gor'kov [(1960, 1961), weak scattering—Born's approximation; Ambegaokar and Griffin (1965); Skalski *et al.* (1964); Maki (1969); Schachinger *et al.* (1980)] and of Shiba (1968) and Rusinov [(1969a, 1969b), strong scattering—a t-matrix approach)] are not covered. Another effect necessarily neglected is that of anisotropy [Allen (1980); Daams and Carbotte (1980a, 1980b, 1981); Allen and Mitrović (1982); Zarate and Carbotte (1983a, 1983b); and Whitmore (1984)] in the electron-boson interaction and even in the Fermi surface, although, in some sense, these effects are included in an average way when experimental data are used for the electron-boson spectral density. New developments concerned with the energy dependence in the electronic density of states [Pickett (1980, 1982), Mitrović and Carbotte (1981a, 1983a, 1983b), Carbotte (1982), and Kieselmann and Rietschel (1982)] and with energy dependence in the pairing interaction have also been omitted. This leaves the isotropic Eliashberg equations without magnetic impurities, spin fluctuations [Mitrović and Carbotte (1982); Zarate and Carbotte (1987)] (paramagnons), and other forms of magnetism [Schossmann and Carbotte (1986), Schachinger, Stephan, and Carbotte (1988)] (spin glass effects). Proximity systems will also not be reviewed, although considerable interesting new developments (Zarate and Carbotte, 1985) have taken place.

Even within the limited scope just described, I shall not be able to cover all developments and shall, undoubtedly, leave out many contributions that could have been included. Some choices had to be made.

B. Overview of each section

1. The critical temperature

Section II deals exclusively with the critical temperature T_c. It starts with the Eliashberg equations in their nonlinear form, applicable at any temperature below T_c and written on the imaginary Matsubara frequency axis. No derivation is given. The kernels are the electron-phonon or, more generally, the electron-boson spectral density $\alpha^2F(\omega)$ describing an effective electron-electron interaction due to any form of boson exchange, and the Coulomb pseudopotential μ^*, usually treated as an adjustable parameter. For the reader who is not as familiar with the complexity of the Eliashberg equations, we first reduce the equations in a BCS-type approximation to obtain a renormalized BCS form in which the role of the pairing potential $N(0)V$ [with $N(0)$ the single-spin electron density of states at the Fermi energy] is played by $N(0)V=(\lambda-\mu^*)/(1+\lambda)$, where λ is the electron-boson mass-renormalization parameter. The BCS equation is then linearized and the usual equation for the critical temperature obtained. It is used to calculate a first estimate of the maximum value of T_c possible within BCS theory for a given characteristic boson energy ω_c. This estimate will later be seen to be in need of revision and is, in fact, quite wrong, although often quoted.

Next, the familiar BCS result for the ratio of T_c to the gap edge (Δ_0) at zero temperature is obtained and is used to illustrate the first important difference between Eliashberg theory and BCS theory—that dimensionless ratios such as $2\Delta_0/k_BT_c$ are not universal in Eliashberg formal-

ism, while they are universal in the BCS limit of the theory.

A much used, approximate formula for T_c, superior to BCS and first derived by McMillan (1968) and later modified and improved by Dynes (1972) and by Allen and Dynes (1975), is introduced, discussed, and used to make a second estimate of the maximum critical temperature possible within Eliashberg theory. The estimate assumes that arbitrary values are possible for the kernels, and concerns about lattice stability are ignored.

In addition to λ and μ^*, the improved McMillan equation involves a definite characteristic phonon energy $\omega_{\ln}$, which is related to a logarithmic moment of the spectral density $\alpha^2F(\omega)$. While this analytic formula for T_c has been very useful, it remains approximate and its limitations are discussed through comparison with exact numerical solutions of the full Eliashberg equations. In particular, it is noted that the McMillan equation leads to a saturation of T_c as $\lambda\rightarrow\infty$, while the exact results do not. Thus the concept of a maximum possible T_c value, based on such an equation, is an artifact of the approximations that were made to be able to obtain a simple analytic equation and is not intrinsic to Eliashberg theory.

An asymptotic equation, valid for large λ, is derived that gives $T_c=0.183\sqrt{\lambda}\,\omega_E$, where ω_E is a characteristic boson energy in a model in which the spectral density is taken to be a delta function at a particular Einstein-oscillator frequency ω_E. Thus, in more exact approaches to T_c, the limit of infinite electron-boson mass renormalization ($\lambda\rightarrow\infty$ with ω_E constant) gives a continuous increase of T_c, following the law $\sqrt{\lambda}$. It is clear, then, that maximum T_c discussions need to be posed within the framework of lattice or other instabilities and are not contained in Eliashberg theory. As λ increases indefinitely, the lattice will surely reach a point when it is no longer stable because of the very large electron-phonon interaction. At present, there is no universally accepted, simple, and quantitative stability criterion.

The concept of the functional derivative of T_c with respect to $\alpha^2F(\omega)$ has helped greatly in understanding the exact relationship between phonons of a particular frequency ω_0 and the size of the critical temperature. In fact, this functional derivative denoted by $\delta T_c/\delta\alpha^2F(\omega_0)$ gives the limit of the ratio of the change in T_c (δT_c) to the infinitesimal perturbation when the electron-phonon spectral density is augmented by $\epsilon\delta(\omega-\omega_0)$ at a particular frequency ω_0. That is, $\delta T_c/\delta\alpha^2F(\omega_0)\equiv\lim_{\epsilon\rightarrow 0}\delta T_c/\epsilon$ and describes the effectiveness in T_c of the spectral weight at frequency ω_0.

Approximate universal analytic equations for $\delta T_c/\delta\alpha^2F(\omega)$, applicable to any superconductor in the weak-coupling limit, are derived. From these it is found that high- and low-frequency phonons contribute little to T_c, while there exists an intermediate optimum phonon region for which the phonons are most effective. A nearly universal finding is that the optimum phonon energy $\omega_{\rm op}$ equals approximately $7k_BT_c$, with k_B the Boltzmann constant. A simple, physical argument is offered to explain qualitatively the calculated shape of $\delta T_c/\delta\alpha^2F(\omega)$. General formulas for the functional derivative are also given and numerical results, based on these, are presented. They confirm the idea that an optimum phonon frequency exists and that very low frequency phonons are not very effective in raising T_c. Phonon softening with constant spectral area A (see below) can only be beneficial if it occurs at frequencies above the optimum value. In this regard the phonon softening with decreasing temperature, observed in Nb_3Sn by Shirane and Axe (1973) for a specific acoustic branch, is interesting. But, using functional derivatives, it can be shown that the softened modes mainly fall in a region where $\delta T_c/\delta\alpha^2F(\omega)$ is small; so they contribute very little to T_c.

The idea of an optimum phonon energy in $\alpha^2F(\omega)$ is used to prove a theorem that states that, for a given strength of the spectral density, defined as the area under it, namely, $A=\int_0^\infty\alpha^2F(\omega)d\omega$, the best shape that will maximize T_c is a delta function placed at the maximum of its own functional derivative. Choosing any other shape for $\alpha^2F(\omega)$, with fixed A, will only lead to a lowering of T_c. This fact is described by the inequality $T_c\leq Ac(\mu^*)$, where $c(\mu^*)$ is a universal number determined by Eliashberg theory. It is only slightly decreasing with increasing μ^*. The equality holds for a δ function and the inequality for any other realistic shape. Some values in real materials can, in fact, fall reasonably close to the optimum value. The inequality mentioned above represents a more sophisticated formulation of a previous empirical observation of Leavens and Carbotte (1974), which led them to suggest that, for many materials with λ bounded by $1.2<\lambda<2.4$, a reasonable formula for T_c is $T_c=0.148A$. This formula, as well as the equality $T_c=c(\mu^*)A$ for a δ-function spectral density, leads to the conclusion that T_c can be increased indefinitely if A is increased without limit, and that the mathematical structure of the Eliashberg equations does not lead to saturation of T_c. With the discovery of superconductivity at very elevated temperatures in the copper oxides, it is interesting to note that the formula $T_c=c(\mu^*)A$ can give a value of $T_c=160$ K for a modest value of mass enhancement of $\lambda=1.54$ and fixed μ^*. For this to occur, we need to take ω_E to be of order 100 meV, which falls around the maximum phonon energy observed in the oxides. The corresponding value of $A=77$ meV, which is much larger than the value of $A=13.5$ meV for Nb_3Ge, is probably unrealistically large for a phonon mechanism, while it may not be for another kind of boson-exchange process.

Section II ends with a discussion of the isotope effect. For a pure electron-phonon system with $\mu^*=0$, it can be shown that $\beta\equiv -d\ln T_c/d\ln M$ is, quite generally, equal to 0.5. No simplification of the Eliashberg equations are required in order to prove this theorem, which is, of course, consistent with simple BCS theory. When μ^* is

not zero, however, $\beta \neq \frac{1}{2}$. This can be seen easily from the McMillan equation. It predicts that, for reasonably small values of λ, β can become small and, indeed, can even be negative, as has been observed in some systems. But a small λ value and a finite μ^* of order 0.1 usually implies a small value of T_c. For large T_c, we expect large λ's and β near 0.5. Of the many complications that can, in principle, change β, an unusually large value of Coulomb pseudopotential μ^* or a high-energy additional attractive mechanism unconnected to ion mass, which we simulate through a finite negative μ^*, are real possibilities. It is very important to understand that, in compounds people often talk about partial isotope effects (β_i) for each mass species rather than the total $\beta_{\text{tot}} = \sum \beta_i$. A beautiful, formal, but quite general and powerful formulation of partial contributions to the total isotope effect, has been given by Rainer and Culetto (1979), and we review this work. In view of the controversy that remains around the value of β for the oxides, it is important to realize that if β_i, for a particular i, is zero, this only means that those particular vibrations are not involved in the superconductivity. Alternatively, if it is large, they certainly are involved. In either case, it does not say anything about the effect of other phonon modes and, in that sense, does not address the question of mechanism directly. For this, the total isotope effect is more relevant, but still not unambiguous.

2. Tunneling and its relation to electron-phonon interaction

In Section III we start with the real-axis formulation of the Eliashberg equations, which we write without derivation since it is our aim to use these in applications to real superconductors and to understand, as much as possible, their implications for superconducting properties. The equations themselves, which apply at any temperature T below T_c, are a set of two complicated nonlinear integral equations for a complex frequency-dependent gap $\Delta(\omega)$ and renormalization function $Z(\omega)$, the latter of which exists in both normal and superconducting states. Both quantities are temperature dependent. In order to give the reader some feeling for these equations, which, we admit, are rather formidable, we start by reducing them to a BCS form through a number of appropriate approximations. This involves, among other simplifications, keeping only the real part of both gap and renormalization and assuming they are frequency independent and, in the case of the renormalization Z, temperature independent as well (i.e., it is evaluated at $T=0$ in the normal state).

A more sophisticated two-step model for the gap near $T=T_c$ can be used to derive a McMillan-like equation for T_c. We can introduce arbitrary numerical parameters into the basic derived functional form, so as to account for errors made during the simplifications. Definite choices for the parameters introduced result when we compare with exact numerical solutions of the full equations in specific cases. The end result of such a procedure is the Allen-Dynes equation, which is valid for values of λ that are not too large. Another equation that follows directly from an approximate solution of the real-axis Eliashberg equations is that of Leavens and Carbotte (1974). It has the advantage of having no numerical adjustable parameter, but it has the disadvantage that a further moment of $\alpha^2F(\omega)$ besides $\lambda = 2\int_0^\infty \alpha^2F(\omega)/\omega \, d\omega$ is needed. It was constructed from a consideration of the behavior of exact numerical solutions to the Eliashberg equations and reduces to an Allen-Dynes–type formula in the appropriate limit.

A second issue considered in this section is the relation between real-axis and imaginary-axis formulation of the Eliashberg equations. In a real-axis formulation, the gap is complex and defined for all frequencies ω while, in the Matsubara formulation, Δ is real and defined only at an infinite discrete set of imaginary frequencies $i\omega_n \equiv i\pi T(2n-1)$ with $n = 0, \pm 1, \pm 2, \ldots$. The two formulations can be related to each other through formal analytic continuation of the gap and gap equations. The two sets of equations are then equivalent, except for a small complication that should be noted, but that is of little consequence in practice. In both formulations, a sharp step-function cutoff is introduced into the Coulomb pseudopotential term at some definite frequency ω_c. But a sharp cutoff on the real axis does not analytically continue to a sharp cutoff on the imaginary axis and vice versa. Therefore there is a difference between the two cases, and, for a given $\alpha^2F(\omega)$, slightly different μ^* parameters are needed to get a common T_c value.

To go from exact *numerical* solutions for the Matsubara gaps and renormalization factors at discrete, imaginary frequencies to the real-axis solutions, we can employ the Padé approximant technique first introduced by Vidberg and Serene (1977). The technique is standard and straightforward and involves a continued fraction that can be used for real frequencies, after the numerical coefficients have been fitted to imaginary-frequency data. The method has been used mainly at $T=0$ and gives reliable values for the gap edge Δ_0 in most cases. It does not always, however, give a faithful representation of the phonon structure at higher frequencies. This is a serious limitation if we want to discuss tunneling experiments, but it may not be so important if we simply want to use the resulting gaps inside integrals that weigh all frequencies fairly equally.

A new, more accurate, and compact method for going from the imaginary-axis gaps to the real axis has been developed recently by Marsiglio, Schossmann, and Carbotte (1988). It involves new equations that still require iteration for the real-frequency renormalization function $\tilde{\omega}(\omega) = \omega Z(\omega)$ and pairing energy $\tilde{\phi}(\omega)$, but they do not contain any principal-value integrals. Instead, the imaginary-axis solutions enter. The equations converge very rapidly compared with the real-axis ones and give results that are identical and, in particular, can be used to discuss tunneling experiments.

For a given model of $\alpha^2F(\omega)$ and μ^*, the gap equations

at zero temperature can be solved for the frequency-dependent gap $\Delta(\omega)$ and, from it, the quasiparticle density of states in the superconductor calculated. This function is measured in tunneling experiments using superconductor–oxide–normal-metal junctions. Structure in the current-voltage I-V characteristics reflects the details of the frequency dependence of the spectral density $\alpha^2F(\omega)$, and a measurement of I-V characteristics offers an opportunity to measure $\alpha^2F(\omega)$ in electron-phonon superconductors. The procedure is called inversion of tunneling data and gives a unique $\alpha^2F(\omega)$ as well as μ^* value [McMillan and Rowell (1969)]. In a given case, the Eliashberg equations are repeatedly solved for model $\alpha^2F(\omega)$'s, which are constantly adjusted until convergence is reached between predicted I-V structure and experimental data. This spectroscopy has now been applied to many s, p, and d elements and alloys as well as compounds including the A15's.

In the case of Pb, there exists a beautiful proof of the validity of the Eliashberg equations that needs to be stressed, since recent claims have been made that the electron-phonon interaction may not be operative even in conventional metals (Hirsch, 1989a, 1989b, 1989c; Hirsch and Marsiglio, 1989). To invert tunneling data and get the kernels $\alpha^2F(\omega)$ and μ^* for a given material, it is only necessary to use $I(V)$ data extending to voltages equal to the end of the phonon spectrum (ω_0) plus the gap edge (Δ_0). We can then use the Eliashberg equations with the measured kernels to predict the $I(V)$ structure in the multiphonon region beyond $\Delta_0+\omega_0$. In Pb, the predicted phonon structure in this high-energy region agrees very well with experiment. This is taken as a strong proof of the consistency of the Eliashberg equations when applied to Pb.

There is much additional evidence that we are really measuring the electron-phonon spectral density in tunneling inversion. As a first observation, the shape that is obtained for the spectral density $\alpha^2F(\omega)$ as a function of ω looks very much like the phonon frequency distribution of the material of interest, with some small differences. In addition, there is now an entire industry in which band-structure calculations, giving the electronic wave functions as well as eigenenergies, are extended to calculate electron-phonon matrix elements and from them, the spectral density. Besides the gradient of the self-consistent crystal potential, such computations require a knowledge of the lattice dynamics, i.e., phonon frequencies and polarization vectors. But these are known from coherent inelastic neutron-scattering data on the phonon-dispersion curves. A Born–von Kármán fit to limited data gives the force constants between atoms, which can be used to calculate the phonons everywhere.

The formula for the spectral density $\alpha^2F(\omega)$, which is evaluated and which is exact, involves two Fermi-surface integrals. One is over the initial electron states ($\mathbf{k}$), the other over final states ($\mathbf{k}'$). The transitions involved describe electron scattering from the Fermi surface to the Fermi surface with crystal momentum $\mathbf{k}-\mathbf{k}'$ transfer to the phonon system. A Dirac delta function in the integrand puts phonons $\omega_j(\mathbf{k}-\mathbf{k}')$, with j being a branch index, in bins according to energy ω. In addition, each phonon mode is weighted by the strength of its coupling to the electron system due to the electron-phonon interaction. This prescription for $\alpha^2F(\omega)$ is similar to, but slightly different from, that for the phonon frequency distribution $F(\omega)$. For this latter function, the momentum label in the phonon frequency is restricted to the first Brillouin zone, and each phonon is weighted by 1. Thus, except for a different weighting factor for the phonons and a somewhat different phase-space sum, which is determined by phonon variables for $F(\omega)$ and electronic variables for $\alpha^2F(\omega)$, the two functions are related.

A long discussion is given of the similarities and differences between $\alpha^2F(\omega)$ and $F(\omega)$. A general conclusion is that when the phonons are well characterized by a Born–von Kármán model, $F(\omega)$ and $\alpha^2F(\omega)$ look very much the same, although it is important, in such comparisons, to account for phonon lifetime effects, particularly in alloys. When the ratio $\alpha^2F(\omega)/F(\omega)$ is taken, the resulting $\alpha^2(\omega)$ does have some variation with ω, but this is usually not sufficient to significantly distort the shape of $\alpha^2F(\omega)$ compared with $F(\omega)$. More specifically, the high-energy longitudinal phonon peaks are often found to be somewhat attenuated and broaden in tunneling measurements. Moreover, an overall shift towards some softening of the $\alpha^2F(\omega)$ spectrum is sometimes observed when compared with $F(\omega)$.

The review of calculations of the electron-phonon interaction in conventional superconductors is limited to those works in which a full spectral density is computed and displayed. This includes calculations for s-p metals, such as Pb, Al, and Zn, with multiple plane-wave pseudopotential and Fermi surface. Those calculations based on a single plane wave and a spherical Fermi surface are not included. In the transition element series, we mention calculations in Nb, Pt, and Pd. The compounds reviewed include the refractory compounds such as TiN, SnN, VN, and NbN, and some of the A15 compounds. It is important to be aware that many calculations do not compute $\alpha^2F(\omega)$ directly. Rather, only the McMillan-Hopfield parameter η is computed [Grimvall (1981)]. This parameter is related to the first frequency moment of $\alpha^2F(\omega)$ and does not depend on phonon variables. The mass-enhancement parameter λ is then calculated from the formula $\lambda=\eta/M\langle\omega^2\rangle$, where M is the ion mass and $\langle\omega^2\rangle$ is some average squared phonon frequency. A value for this last quantity is then required, and usually only an approximate estimate of λ results. In principle, we are usually interested in the entire function $\alpha^2F(\omega)$ and not just in λ, even if it were known exactly.

Computations of $\alpha^2F(\omega)$ that use results of band-structure calculations have proceeded along two distinct lines. In the first kind of calculations, the microscopic equation for $\alpha^2F(\omega)$ is evaluated directly. In the second, the phonon lifetimes $\gamma_j(\mathbf{k})$ due to the electron-phonon interaction are computed first, and a formula due to Al-

len (1980) is used to relate $\gamma_j(\mathbf{k})$ to $\alpha^2F(\omega)$. This formula is exact and can have some special advantages in specific cases. For example, the intermediate quantity $\gamma_j(\mathbf{k})$ can be tested directly against phonon linewidth data, and the parameters in the calculations adjusted to get better agreement. Extensive comparisons of this kind exist for Nb. In addition, in some cases, Nb_3Sn, for example, neutron groups have been measured for some phonons at different temperatures. As we lower the temperature through the superconducting transition temperature, the electrons become condensed in the superconducting state and a definite energy $2\Delta_0$ is required to excite a hole-particle pair out of the condensate. This implies that, in the superconducting state, phonons with energy $\omega<2\Delta_0$ will have no lifetime coming from the electron-phonon interaction, and the neutron groups will, as a result, sharpen up, as is observed.

Tunneling spectroscopy has been instrumental in delineating the role played by the electron-phonon interaction in conventional superconductors, as have calculations of the spectral density $\alpha^2F(\omega)$. With the discovery of superconductivity in the oxides with large values of T_c, an interest has developed in understanding better the kind of information that might be available from tunneling in those systems, should we be able to fabricate good-quality junctions. This brings us to a discussion of tunneling inversion when a joint phonon-plus-high-energy electronic mechanism is present, which is a possible model for the oxides. The high-energy mechanism need not be specified in detail. Its origin is certainly not known at this time, and therefore it is modeled by introducing a sharp extra peak in the spectral density at some high energy. This is assumed to be additional to a phonon contribution, which is present but not sufficiently important to give a very high value of T_c. In this case it is found that the resulting phonon structure in the quasiparticle density of states can still be quite pronounced. This could lead one to believe that we are more strongly coupled to the phonons than we actually are if the existence of the high-energy electronic peak is not recognized. Inversion of such characteristics would lead to a small value for an effective electron-phonon spectral density relative to the size of the gap. In fact, we would find $\alpha^2_{\rm eff}F(\omega)\cong\alpha^2F(\omega)/(1+\lambda_{\rm ex})$, where $\lambda_{\rm ex}$ is the contribution to the electronic mass renormalization coming from the electronic mechanism. Moreover, the effective μ^* would be negative and it would never be possible to get perfect agreement between the calculated I-V curve and the experimental data. Thus the existence of a second, unrecognized high-energy mechanism leads to a breakdown of the usual inversion procedure with a recognizable pattern of failure, namely, small $\alpha^2_{\rm eff}F(\omega)$, negative μ^*, and a less than perfect fit.

3. The energy gap at zero temperature

Section IV is concerned exclusively with the zero-temperature energy gap that exists in the quasiparticle excitation spectrum of real superconductors. It starts with Eliashberg calculations of the dimensionless ratio $2\Delta_0/k_BT_c$ for a large number of materials for which the microscopic parameters $\alpha^2F(\omega)$ and μ^* are known from tunneling inversion or, in a few cases, from some other source. The calculations, which can be taken as another test of the validity of the Eliashberg equations for the systems considered, show that most materials do not obey the BCS universal law $2\Delta_0/k_BT_c=3.53$. Furthermore, when calculated values are compared with experiment, excellent overall agreement is obtained at the level of a few percent in most cases. This agreement leaves no doubt that Eliashberg theory, with an electron-phonon kernel and Coulomb pseudopotential (much less important), applies while BCS does not.

A simple, approximate formula that includes a correction of the general form $a(T_c/\omega_{\ln})^2\ln(\omega_{\ln}/bT_c)$ is derived from Eliashberg theory through a series of simplifying assumptions. The constants a and b are parameters to be described later, and $\omega_{\ln}$ is the characteristic phonon energy introduced by Allen and Dynes (1975). Formulas of the form just mentioned that include strong-coupling corrections in terms of the parameter $T_c/\omega_{\ln}$ have appeared early in the literature, but $\omega_{\ln}$ was not well defined. In addition, it is only recently that such a form could be tested against exact numerical solutions on a large number of specific cases, and that the data in conventional materials could be used to give definite values for the arbitrary constants a and b through a best visual fit to the exact results. In this way it is found that the formula $2\Delta_0/k_BT_c=3.53[1+12.5(T_c/\omega_{\ln})^2\ln(\omega_{\ln}/2T_c)]$ fits remarkably well a great deal of theoretical as well as experimental data on $2\Delta_0/k_BT_c$. There is some fluctuation off the main-trend curve in specific cases, but this can be understood as being due to some dependence on details of the shape of $\alpha^2F(\omega)$ that are not captured in the single parameter $T_c/\omega_{\ln}$. An analysis of the variation in $2\Delta_0/k_BT_c$ for fixed T_c and $\omega_{\ln}$, but for different measured shapes of $\alpha^2F(\omega)$, helps to explain the observed deviations.

The functional derivative of the gap edge Δ_0 with $\alpha^2F(\omega)$ is interesting because it gives information about the effect on Δ_0 of various frequencies in $\alpha^2F(\omega)$. As for $\delta T_c/\delta\alpha^2F(\omega)$, detailed brute-force calculations of $\delta\Delta_0/\delta\alpha^2F(\omega)$ based on the full Eliashberg equations give a curve that goes to zero in the limit $\omega\rightarrow0$ and $\omega\rightarrow\infty$ and exhibits a single peak in between. The peak is now sharper and falls at an energy lower than that for T_c. A rule of thumb, established on the basis of a few typical cases, give $2\Omega^*(\Delta_0)\sim\Omega^*(T_c)\sim7k_BT_c$, where Ω^* is the optimum frequency, i.e., at the maximum in the functional derivative. For the ratio $2\Delta_0/k_BT_c$, the functional derivative is found to be yet sharper and to peak at yet lower energies with $\Omega^*(2\Delta_0/k_BT_c)\sim\frac{4}{3}k_BT_c$, but the general shape is the same. Such curves lead to the idea of the existence of an optimum spectrum for Δ_0 and $2\Delta_0/k_BT_c$. Before going into such ideas, a long technical

discussion is given of a method for obtaining these functional derivatives, developed by Coombes and Carbotte (1986), which is more elegant than the brute-force method often employed before. It gives the same results, of course. Some readers may want to skip the details. The essence of the method is that the infinitesimal change in the gap on changing the electron-phonon spectral density is isolated and separately continued analytically to the real-frequency axis using Padé approximates.

Turning to the case of a δ-function spectral density $\alpha^2F(\omega)=A\,\delta(\omega-\omega_E)$, we can show that the gap edge Δ_0 normalized to A is a universal function of ω_E/A and μ^*. Further, as a function of the universal dimensionless frequency $\bar{\omega}_E\equiv\omega_E/A$, numerical solutions for Δ_0/A give a curve similar in shape to the functional derivative. It exhibits a single distinct maximum at a definite optimum frequency $\bar{\omega}_E^*$ (just a number), and $\bar{\Delta}_0\equiv\Delta_0/A$ takes on the definite value $[b(\mu^*)]$. Thus for a δ-function spectral density of weight A, $\Delta_0=b(\mu^*)A$; and so Δ_0, as does T_c, can grow indefinitely with A. Any other shape should lead to a smaller value of Δ_0 for the same A value, as is verified for a large number of real systems. As for T_c, the maximum value for $\Delta_0/A=b(\mu^*)$ is a weakly varying function of μ^* decreasing slightly with increasing μ^*. From the shape found for $\delta[2\Delta_0/k_BT_c]/\delta\alpha^2F(\omega)$, we expect a similar story to hold for $2\Delta_0/k_BT_c$. For a delta-function spectral density, we can, in fact, demonstrate that this ratio is independent of A and is only a function of ω_E/A for a given μ^*. In this case we find that $2\Delta_0/k_BT_c$ keeps increasing as ω_E/A is decreased, and that a maximum is only reached in the limit of $\omega_E/A\to 0$. Using functional derivatives, we can show that this upper limit of 13 for $2\Delta_0/k_BT_c$ also holds for any other shape, since removing weight from the delta function at zero frequency and placing it anywhere else is found to reduce this ratio. The relevant functional derivative is negative definite and exactly zero at $\omega=0$. Curves of $2\Delta_0/k_BT_c$ as a function of $T_c/\omega_{\ln}$ confirm this effect as $T_c/\omega_{\ln}$ gets large; i.e., they show saturation.

The formal discussion of the maximum value of $2\Delta_0/k_BT_c$ in Eliashberg theory, which holds for any kernel whatever its origin, shape, or size, is followed by a simplified but analytic discussion of the same problem, which yields the approximate answer 11.6 instead of 13 for the maximum value of $2\Delta_0/k_BT_c$. This reasonable agreement can be taken as confirmation of the numerical work and of the approximate derivations.

The section ends with a discussion of the jump observed at energy Δ_0 in the *I-V* characteristics of a superconductor–insulator–normal-metal tunneling junction. This jump is found to correlate well with the strong-coupling parameter $T_c/\omega_{\ln}$ and to grow large as $T_c/\omega_{\ln}$ gets large, a result found to be consistent with its functional derivative.

4. Thermodynamics for specific materials

Section V is mainly concerned with the comparison between theory and experiment of thermodynamic properties for a large number of conventional superconductors, for which the microscopic kernels $\alpha^2F(\omega)$ and μ^* are known from tunneling. In general, the theory predicts results that are quite different from BCS and are in good agreement with experiments confirming, once more, the remarkable accuracy of Eliashberg theory when applied to conventional superconductivity.

From the general formula for the free-energy difference between normal and superconducting state, which depends only on the Matsubara gaps and renormalization functions, we can obtain all of the thermodynamics. In particular, the temperature dependence of the electronic specific-heat difference between superconducting and normal state $\Delta C(T)$ and of the critical magnetic-field deviation function $D(t)$ are of special interest.

As an illustration of the agreement between theory and experiment that can be achieved with the Eliashberg equations and tunneling-derived kernels, we compare $C_{es}(T_c)/(\gamma T_c)$, the electronic specific heat in the superconducting state at T_c normalized by its normal-state value, with γ, the coefficient of the electronic specific heat at T equal to zero (Sommerfeld constant); $\gamma T_c^2/H_c^2(0)$ with $H_c(0)$, the zero-temperature thermodynamic critical magnetic field; and the extremum values of $D(t)$ for the case of Pb and Nb. The agreement is very good and the disagreement with BCS predictions clear. Comparison in other materials is similar with the main remaining uncertainty having to do with some variability in the available data. The absolute value of $H_c(0)$, of the jump in the specific heat at T_c, $\Delta C(T_c)$, and of $[\partial H_c(T)/\partial T]_{T_c}$ are all dependent on the electronic density of states at the Fermi energy for single spin $[N(0)]$, in addition to depending on the kernels $\alpha^2F(\omega)$ and μ^*. To determine this quantity we use the measured Sommerfeld constant γ, and the resulting agreement between theory and experiment for the three quantities mentioned above is excellent. In addition, the derived value of $N(0)$ agrees well with band-structure calculations.

Next we compare the theoretical results for the full temperature variation of the critical magnetic-field deviation function $D(t)$ with experiment for Al (BCS), Ta, Sn, Tl, In, Nb, Hg, and Pb and find remarkable qualitative and good quantitative agreement. The temperature variation of the specific heat for the same materials, as just mentioned, is also presented and a detailed comparison with experiment given for the case of Pb. The agreement is almost exact throughout most of the temperature range. As a further illustration of an *s-p* material, we consider the alloy $Pb_{0.9}Bi_{0.1}$ with equally good results. For the alloy $Nb_{0.75}Zr_{0.25}$, a comparison with pure Nb is presented as well as a direct comparison with experimental data. The comparison with data is important because, in this case, a recent accurate determination of the thermodynamics is available, and the agreement is essentially exact. The comparison with Nb is also significant because the $\alpha^2F(\omega)$ for $Nb_{0.75}Zr_{0.25}$ shows considerable softening over Nb leading to an important enhancement of strong-coupling effects in thermodynamic quantities as

well as in the gap to critical temperature ratio $2\Delta_0/k_BT_c$. This is discussed in detail using functional derivative ideas.

The thermodynamics measured for the A15 compounds can also be understood quite satisfactorily within Eliashberg theory. To illustrate this, the case of V_3Si is considered in detail and a comparison with experiment presented for various dimensionless ratios as well as for $D(t)$ and the temperature variation of the specific heat. One problem that should be mentioned is that the electronic density of states $N(0)$ derived from the measured value of $H_c(0)$ and Eliashberg calculations for the same quantity is not in good agreement with band-structure calculations. In most other cases, it is. An explanation of this discrepancy, in terms of energy dependence in the electronic density of states and a slight deviation from perfect stoichiometry, is offered.

Instead of continuing with further comparison of Eliashberg results with experiment in more specific cases, we next derive approximate but analytic formulas for some of the dimensionless ratios of interest and fit the arbitrary constants introduced (to make up for errors in the simplifications) to the results of a large number of exact numerical calculations on real materials. In almost all the cases considered, a correction of the same form $a(T_c/\omega_{\ln})^2\ln(\omega_{\ln}/bT_c)$, as described before for $2\Delta_0/k_BT_c$, is found to fit the numerical results remarkably well. The quantities considered are $\Delta C(T_c)/(\gamma T_c)$, the slope of the specific heat at T_c, $\gamma T_c^2/H_c^2(0)$, and the reduced critical field $h_c(t)$ at zero reduced temperature with $h_c(t)\equiv H_c(T)/|dH_c(t)/dt|_{t=1}$. The formulas derived here clearly imply that definite relationships exist between these various quantities for an Eliashberg superconductor, at least at the level of accuracy represented by the analytic formulas themselves. These relations put important constraints on results of the theory. In reality, some materials do fall slightly off the main-trend curves represented by our approximate formulas. An analysis of the deviations is given, and it is concluded that such deviations depend on detailed features of $\alpha^2F(\omega)$ not captured in the single strong-coupling parameter $T_c/\omega_{\ln}$.

Presently known conventional superconductors fall in the range $T_c/\omega_{\ln}\lesssim 0.25$. With the discovery of the high-T_c oxides, it is of interest to know what Eliashberg theory predicts when $T_c/\omega_{\ln}$ is increased beyond this restricted range. Results are presented for the normalized specific-heat jump $\Delta C(T_c)/\gamma T_c$, for its slope at T_c, $[T_c d\Delta C(T)/dT]_{T_c}/\gamma T_c$, for the normalized slope $[T_c d\Delta C/dT]_{T_c}/\Delta C(T_c)$, for $\gamma T_c^2/H_c^2(0)$, and for the extrema in $D(t)$ for values up to $T_c/\omega_{\ln}\simeq 1.4$. In the very strong coupling regime, the results are found to behave in a completely unexpected fashion. For example, the normalized specific-heat jump $\Delta C(T_c)/(\gamma T_c)$ is predicted to be smaller than the BCS value of 1.43 and is opposite to the results for the usual strong-coupling regime. Thus the very strong coupling regime can be distinguished easily from the usual one, at least in principle. Of course, to achieve this regime, very large values of λ would be needed. This may not be compatible with lattice stability for an electron-phonon mechanism. On the other hand, some other mechanism may be operative. This would require the existence of low-frequency bosons of the order of T_c.

5. Thermodynamics: Some formal results and applications

Section VI, as did Sec. V, deals with thermodynamic properties, but considers mainly formal aspects. It starts with the equation for the free-energy difference ΔF, between normal and superconducting state, given by Wada (1964). It is less compact then the Bardeen-Stephen (1964) equation, but it has the great advantage, when considering functional derivatives, that its variation with gap and renormalization function is zero. These variations give, respectively, the two Eliashberg equations for the gap and normal-state channels. From the Wada formula, we derive formal, but completely general, formulas for the total functional derivative of ΔF with $\alpha^2F(\omega)$ from which follows the functional derivative of the critical-field deviation function $D(t)$ at a fixed value of reduced temperature and of the critical magnetic field. This formal section is followed by a simple application of the functional derivative [which gives the response of a given property to an infinitesimal change in $\alpha^2F(\omega)$ at a given frequency] to a discussion of the effect of hydrostatic pressure on the critical temperature, the zero-temperature thermodynamic critical field, and the deviation function $D(t)$ in superconducting Pb. It is found that most of the observed shift in T_c is due to the changes in μ^*. The phonon contribution largely cancels, because some frequency regions in the shift in $\alpha^2F(\omega)$ add on to T_c while others subtract, as can be seen very clearly from functional derivative considerations. In contrast, for $H_c(0)$, we can understand that the cancellation among phonon shifts is less important, and phonon shifts are as important as μ^* changes in determining the full observed change in $H_c(0)$. Finally, for $D(t)$, the shift is found to originate mainly from the change in $\alpha^2F(\omega)$, with the change in μ^* being of lesser importance.

A second application of the functional derivative is to optimum spectra for the thermodynamics. The first quantity considered is the normalized specific-heat jump. That an optimum spectra exists is indicated by the shape of the functional derivative of the normalized jump $\Delta C(T_c)/(\gamma T_c)$. This derivative increases slowly from zero as ω is reduced from ∞, shows a maximum around $5k_BT_c$ (with some variation in position of maximum with the different base materials considered), and then drops through zero before diverging like $-1/\omega$ for $\omega\rightarrow 0$. This indicates that, for a given area A under the spectral density, the best shape is a delta function centered at the Einstein frequency ω_E placed right at the position of the maximum in its own functional derivative. For a delta-

function spectrum, it is shown that, for a given value of μ^*, the normalized jump is a unique function of ω_E/T_c and independent of A. As the dimensionless parameter $\omega_E/T_c \equiv \bar{\omega}_E$ is varied, a single maximum is traced out for $\Delta C(T_c)/(\gamma T_c)$ in accordance with our expectation. This maximum occurs at $\bar{\omega}_E^* \equiv d(\mu^*)$, with $d(\mu^*)$ a well-defined number for a given μ^*. The height at maximum has value $c(\mu^*)$, which is the maximum value attainable for any shape whatsoever. This statement is supported by the fact that the functional derivative for such an optimum delta-function base is negative definite and exactly zero at $\omega_E^*/T_c = d(\mu^*)$. Thus adding or removing weight to the delta function at $\bar{\omega}_E^*$ leaves the specific-heat jump unchanged, while adding weight anywhere else decreases it. We have thus found a local maximum that should be valid for any boson-exchange mechanism that can be described by the Eliashberg equations and that is quite independent of shape, size, or origin of the kernels in these equations. A test of this assertion for many known superconductors is positive, and new superconductors could be tested. Should the test fail, we would need to conclude that the isotropic Eliashberg equations are inapplicable to that material and that a new or modified theory is required.

The same kind of argument leads us to conclude that an optimum spectrum also exists for the normalized slope of the specific heat at T_c, the critical field at $T=0$ $H_c(0)/[\sqrt{2N(0)}\,A]$, for the dimensionless ratio $\gamma T_c^2/H_c^2(0)$, as well as for the critical-field deviation function $D(t)$. For the first, second, and last of these quantities Q, there exists a maximum universal number for Q^*, while for the third, a minimum exists and none of these extrema can be violated by any Eliashberg superconductor.

Next, the asymptotic limit of the free energy with electron-phonon mass enhancement $\lambda \to \infty$ is considered. We can prove that in this limit the free-energy difference $\Delta F/N(0) = \frac{1}{4}\lambda\omega_E^2 g(t)$ with ω_E the boson frequency involved and $g(t)$ a universal function determined through the numerical solution of a dimensionless form of the Eliashberg equations. The only restriction is that $\sqrt{\lambda}\,t \gg 1$; so only finite temperatures are treated. This universal limit is, in a sense, the opposite of the BCS limit, which corresponds to very weak coupling. Numerical values are obtained for $g(t)$ and are presented in the form of the reduced thermodynamic critical magnetic field $h_c(t)$. The effective reduced field is found to behave completely differently from its BCS counterpart. It has upward curvature throughout the reduced temperature range considered and diverges as $t \to 0$. From a knowledge of $h_c(t)$, we can also determine the free energy in the limit $\lambda \to \infty$ and, consequently, the specific-heat difference between the normal and superconducting state. As an example, the specific-heat jump at T_c is found to behave like $19.9/\lambda$, while the normalized derivative of the jump $(d/dt)[\Delta C(T)/\gamma T]|_{t=1}$ goes like $39.2/\lambda$. These are exact numerical results obtained from complete numerical solutions of the Eliashberg equations in the appropriate limit. The section ends with a simple one Matsubara gap solution of this same problem. It is useful because it turns out to be qualitatively correct and aids in understanding the exact results.

6. The upper critical magnetic field

Section VII deals with the upper critical magnetic field $H_{c2}(T)$ and starts from the strong-coupling equations of Schossmann and Schachinger (1986), which are valid for any impurity content and depend only on the electron-phonon spectral density, Coulomb pseudopotential, and Fermi velocity. These equations, which involve Matsubara gaps $\tilde{\Delta}(i\omega_n)$, are linearized because they describe a second-order phase boundary between normal and superconducting state in an external magnetic field H. In a two-square-well model, they reduce to the well-known equations of Werthamer *et al.* (1966), but with important renormalizations that cannot be ignored and that affect the Fermi velocity, the impurity content, and the Pauli limiting term $i\mu_B H$, where μ_B is the Bohr magneton. When a fit to data is used, the renormalizations of the Fermi velocity and of the impurity scattering time are, in a sense, already included, and the renormalized WHH (Werthamer, Helfand, and Hohenberg) theory (BCS) gives results, in some cases, that are not very different from those based on the full Eliashberg equations. A detailed comparison with experiment is given for the case of Nb, which includes full calculations as well as WHH results. In this case, Pauli limiting is not an important factor. On the other hand, when Pauli limiting does play a role, WHH without renormalization fails because it greatly overestimates the effect of Pauli limiting with attendant need for large unphysical values of spin-orbit scattering in order to restore agreement with experiment. The difficulty is that BCS leaves out a $(1+\lambda)$ renormalization that greatly reduces the band-splitting term. This was recognized by Orlando *et al.* (1979). They used free-energy arguments to derive the Clogston-Pauli limiting field, which gives a factor of $(\sqrt{1+\lambda})^{-1}$ for the renormalization while a complete microscopic derivation by Schossmann and Carbotte (1989) gives $(1+\lambda)^{-1}$ [Tedrow and Meservey (1982)]. Within a two-square-well model, it is shown that a universal curve applies for the renormalized field $H_{c2}(0)/(1+\lambda)T_c$ as a function of renormalized slope at T_c, namely, $[dH_{c2}(T)/dT]_{T_c}/(1+\lambda)T_c$. Dirty and clean limits are considered and compared with the results that apply when Pauli limiting is unimportant, which corresponds to the limit of $\dot{H}_{c2}/(1+\lambda)T_c \lesssim 1$. Strong-coupling corrections beyond $1+\lambda$ renormalizations are also discussed.

The discussion then shifts to the derivation of simple formulas for strong-coupling corrections. We start by showing that, in the dirty limit, the complete strong-coupling equations of Schossmann and Schachinger (1986) properly reduce to the well-known equations of Bergmann and Rainer (1973). These are much simpler

than the equations for a general impurity content and apply only when impurity scattering parameter $t^+ \to \infty$ ($t^+ = 1/2\pi\tau$ with τ the scattering time). The comparison of the derived approximate analytic form with results of exact numerical calculations for a large number of real materials leads to a form for the reduced field $h_{c2}(0)$ at zero temperature that contains a $(T_c/\omega_{\ln})^2 \ln(\omega_{\ln}/bT_c)$ correction. An additional linear term is also required for a good fit. The same holds for the clean limit. Strong-coupling corrections for the Ginzburg-Landau parameter κ_1 ($\kappa_1 = H_{c2}/\sqrt{2}\,H_c$) are also derived and compared with exact results. It is noted that a very simple relationship holds between $k(T,t^+) \equiv \kappa_1(T,t^+)/\kappa_1(T_c,t^+)$, where T is the temperature and t^+ is the impurity parameter, and the dimensionless ratio $2\Delta_0/k_B T_c$. Other more complex relationships also hold.

Next, the strong-coupling parameter associated with the upper critical field $\eta_{H_{c2}}$ is calculated on the basis of a La-Sr-Cu-O and Pb-type spectrum as a function of $T_c/\omega_{\ln}$ for small and large values. This includes the very strong coupling limit. Results are given for $T = T_c$ and $T = 0$ in the clean ($t^+ = 0$) and dirty ($t^+ = 100$ meV) limits. The choice of underlying spectral density is not crucial. As the coupling is increased, $\eta_{H_{c2}}$ starts first to increase above the BCS value of 1, displays a maximum, and then drops below 1 for very strong coupling. This characteristic behavior is opposite to the conventional strong-coupling case.

The temperature variation of the reduced critical field $h_{c2}(t) \equiv H_{c2}(T)/\{|[dH_{c2}(T)/dT]_{T=T_c}|T_c\}$ is examined for a number of delta-function-based spectra with increasing value of T_c/ω_E where ω_E is the Einstein frequency of the base δ function. Such curves do not depend on the strength of the spectral density A, a parameter that simply sets the size of T_c, but drops out of the dimensionless ratio T_c/ω_E. As T_c/ω_E increases from the BCS limit $T_c/\omega_E \to 0$, the reduced $h_{c2}(t)$ curves change in shape and eventually acquire an upward curvature with value at $t = 0$ considerably larger than the corresponding BCS value. Eventually $h_{c2}(0)$ reaches a maximum value which depends on impurity content and then drops toward an asymptotic value of 0.57.

The Ginzburg-Landau parameter $\kappa_1(T,t^+)$ is also displayed for different values of $T_c/\omega_{\ln}$, and its behavior in the very strong coupling regime is again found to be opposite to our expectation based on the results for the conventional regime.

Asymptotic limits that result when the electron-phonon mass-renormalization parameter λ tends towards infinity are considered. In the dirty limit, indicated by the superscript "di," we find that $H_{c2}^{\rm di}(T)$ is equal to $(0.1833\pi/eD)\omega_E\sqrt{\lambda}\,k(t)$, where $k(t)$ is a universal function of reduced temperature determined from Eliashberg theory. Its exact numerical value is obtained for any $t > 0$ such that $t\sqrt{\lambda} \gg 1$. It shows upward curvature for all t considered and increases indefinitely as $t \to 0$. In the above relationship, ω_E is the phonon frequency and D the diffusion constant characteristic of electron scattering in the dirty limit. An approximate one-Matsubara-gap theory gives results for $h_{c2}^{\rm di}(t)$ in the asymptotic limit that are not very different from the exact value and are very simple, namely, $h_{c2}^{\rm di}(t) \cong \frac{1}{2}(1/t - t)$. Near $T = T_c$, the exact numerical work gives $H_{c2}^{\rm di}(T) = (2.24\pi T_c/eD)(1-t)$ to be compared with $(2\pi T_c/eD)(1-t)$ when a one-gap approximation is used.

Results are obtained in the clean limit and are also shown to hold for any finite impurity content. This is not surprising since, as the electron-phonon interaction becomes very large, the electron scattering coming from this effect alone overwhelms any finite impurity contribution. We find that the same function $k(t)$ as previously introduced also determines the clean limit (now represented by the superscript "cl") $H_{c2}^{\rm cl}(t)$, which is equal to $(6\pi^2 T_c^2/ev_F^2)\lambda k(t)t$: a function that is well behaved at $t \to 0$. Near $t = 1$, we get $H_{c2}^{\rm cl}(t) = (13.4\pi^2 T_c^2\lambda/ev_F^2)(1-t)$, and near $t \to 0$, $H_{c2}^{\rm cl}(t) = 7.64\pi^2 T_c^2\lambda/ev_F^2$, in serious disagreement with another estimate in the literature. In the one-gap model, the analytic results are $H_{c2}^{\rm cl}(t) \cong (12\pi^2\lambda T_c^2/ev_F^2)(1-t)$ for $t \sim 1$ and $\cong 6\pi^2\lambda T_c^2/ev_F^2$ for $t \to 0$, in good qualitative agreement with the exact numerical values.

In a later section the idea of the functional derivative of H_{c2} with spectral density $\alpha^2F(\omega)$ is introduced and general exact formulas from which it can be calculated are given. Numerical results based on these general equations are given, from which the idea of the existence of an optimum spectrum follows. These are investigated after a scaling theorem, valid for any delta-function spectrum, is established. Results for the maximum value of strong-coupling corrections to $H_{c2}(T)$ at $t = 0$ and $t = 1$ for $t^+ = 0$, 50, and 500 meV are presented in tabular form and tested against results for real materials in a few cases using a graphical representation. Finally, functional derivatives are used to verify that a local maximum was reached in each case of interest.

7. Optical properties

Section VIII deals with specific optical properties, namely, the local and London limits of the penetration depth and electromagnetic coherence length. General formulas, valid for any coupling strength, are given for these quantities. At any temperature they depend only on the solutions of the Eliashberg equations. Evaluation of the equations for the local limit requires only a knowledge of $\Delta(i\omega_n)$, while the London limit depends additionally on $Z(i\omega_n)$ which, in turn, has an impurity dependence. For large impurity content, the London limit reduces exactly to the local limit, which applies only to dirty systems. An exact relationship holds be-

tween the London $[\lambda_L(T)]$, local $[\lambda_l(T)]$ penetration depths and the coherence length $[\xi(T)]$, which involves the mean free path l, namely, $[\lambda_l(T)/\lambda_L(T)]^2=\xi(T)/l$. This relation is useful in testing results of numerical calculations.

To start, we present results for the temperature dependence of the penetration depth in V_3Si in the pure London ($l=\infty$) limit as well as for the case of finite mean free path chosen to represent a particular experimental sample. The results are presented in the form $[\lambda(0)/\lambda(t)]^2-(1-t^4)$, where the two-fluid result has been subtracted out, and are compared with a BCS temperature variation, which is also the result that we obtain when the aluminum spectrum is used for $\alpha^2F(\omega)$. For the spectral density of V_3Si, two different tunneling-derived spectra are used. The first is from the work of Kihlstrom (1985), and the other from Bangert, Geerk, and Schweiss (1985). This last spectrum is not considered realistic and is used only to show that any arbitrary shape spectrum will not do in calculating the temperature variation of the penetration depth. Comparison of our theoretical results with the experimental data of Christen *et al.* (1984) reveals good agreement with the results of our full Eliashberg calculations based on the spectrum of Kihlstrom (1985) and poor agreement with BCS and with the results obtained from the Bangert *et al.* (1985) $\alpha^2F(\omega)$. We can conclude that when reliable data are available on normal-state properties, good agreement can be obtained for electromagnetic properties. Furthermore, BCS theory does not apply and strong-coupling theory is needed to achieve quantitative agreement.

The discussion turns next to the theoretical derivations of approximate equations for the strong-coupling corrections associated with optical properties. Through a fit of the resultant formulas (with arbitrary coefficients) to exact numerical data on a large number of conventional materials, we find specific formulas for the strong-coupling parameters η_{λ_L}, η_{λ_l}, and η_ξ at $T=0$ and $T=T_c$, as well as for related properties. The resulting forms fit the numerical data very well. Finally, asymptotic limits are considered. In the limit $\lambda\to\infty$, we are able to establish that $\lambda_l(t)$ is given by $\lambda_l^{-2}(t)=(\sqrt{\lambda}\,\omega_E\sigma_N\mu_0/\sqrt{2}\hbar)g^{-2}(t)$, where ω_E is the characteristic phonon energy and σ_N the normal-state resistivity with $g(t)$ a universal dimensionless function that can be calculated numerically for $t>0$ with $\sqrt{\lambda}\,t\gg1$. The same function also determines $\lambda_L(t)$. In fact, $\sqrt{n}\;\lambda_L(t)/\sqrt{\lambda}=1.274\overline{\Lambda}g(t)\sqrt{t}$, where n is the carrier density per cubic centimeters and $\overline{\Lambda}$ is the classical penetration depth. The temperature dependence of each of these quantities is distinct, in the asymptotic limit, from a BCS variation. In addition, we can show that the coherence length takes the form $\xi(t)=0.87v_F\hbar/\omega_E\lambda^{3/2}t$. Approximate, one-Matsubara-gap results are derived and compared with the exact results and found to be qualitatively valid with some important quantitative differences.

8. Mainly about the oxides

Section IX deals specifically with superconductivity in the oxides. It starts with a discussion of phonon models applied to the high-T_c case. A T_c value of 125 K is easily and naturally obtained within Eliashberg theory and an electron-phonon mechanism. In some cases, but not in all, the necessary value of the mass enhancement λ is usually large and may not be compatible with lattice stability, although we are not aware of any reliable quantitative criterion for stability that could be used to definitely settle this question. Objections to a phonon mechanism therefore fall outside Eliashberg theory and would need to be found through considerations other than simply the large observed value for T_c.

After a review of existing information on the partial oxygen isotope effect in La-Sr-Cu-O, we review the theory of such a quantity and conclude that many purely phononic models can be constructed that would be consistent with the data. Another possibility is a joint phononic-plus-high-energy excitonic mechanism. In the discussion of the partial isotope effect, the formulation of Rainer and Culetto (1979) proves useful, since it allows us to determine the role played separately in the total β by each phonon mode. A long discussion is also included on total isotope effects and on possible exotic mechanisms that might contribute to it.

The thermodynamic properties predicted on the basis of a spectral density for La-Sr-Cu-O given by Weber (1987a, 1987b) are presented with a view at a comparison with experiment. The calculated spectral density is based on a pure phonon model and follows a procedure for calculation that has proved very successful in the A15 compounds. It does give a value for T_c of order 35 K, but only if the material is near a structural phase transition. Another limitation of the model is that the predicted oxygen isotope effect is a little too large in comparison with experiment.

When we attempt to compare calculated superconducting properties, such as the gap-to-critical-temperature dimensionless ratio $2\Delta_0/k_BT_c$ or the normalized specific-heat jump at T_c, $\Delta C(T_c)/\gamma T_c$ with γ the Sommerfeld constant, it is found that there exists too much variability in the present data for any firm conclusion to be drawn. As an example, the value obtained for $2\Delta_0/k_BT_c$ varies significantly with material used and method of measurement. While far-infrared determinations on the whole favor a value around 3.54, much larger values are indicated in tunneling experiments that, in general, give an uncomfortably large range of possible values.

The electronic specific-heat jump at T_c is also uncertain and, in any case, the value of the Sommerfeld constant, needed in comparison with experiment, is not known. It cannot be measured directly from the specific heat above T_c because, in this temperature range, the phonons make the dominant contribution. Moreover, a

magnetic field of sufficient strength to quench the superconductivity cannot be used at low temperature because its value is too large. Other methods are indirect and require simplifying assumptions to extract γ. For example, to extract it from the magnetic susceptibility requires an unknown Stoner enhancement factor, and to use the slope of the upper critical field requires knowledge of the normal-state resistivity as well as strong-coupling corrections, not to mention the large variability in value of slope found in different experiments.

While a knowledge of thermodynamic properties can, in principle, give invaluable information on mechanism, the variability in the present existing data is too large for any definitive conclusion to be drawn. This leaves open the possibility that La-Sr-Cu-O has a joint phononic-plus-high-energy excitonic contribution to the pairing. The superconducting properties for such a joint mechanism are calculated and are found to be more consistent with available data than is a pure phonon model, although significant uncertainty remains. In particular, a joint model is definitely more consistent with present band-structure calculations for the value of the electronic density of states at the Fermi energy. On the other hand, it is as yet unclear whether band-structure calculations can be applied directly to such highly correlated systems, although fairly convincing evidence is starting to accumulate in favor of band theory.

After a short review of electron-phonon calculations of the electron mass renormalization λ in Y-Ba-Cu-O, the isotope effect is reviewed. It is stressed that the total isotope effect is likely to be small even though very recent partial isotope effect measurement on the oxygen indicates that it may not be negligible. Nevertheless, this is strong, although not completely compelling, evidence for a joint mechanism. The properties of such a joint mechanism for a 96-K superconductor are calculated in a model consistent with present isotope effect measurements (Akis and Carbotte, 1989c). Interesting deviations from pure BCS laws are predicted, but comparison with experiment is unsuccessful at this time because of limitation in the accuracy of the data.

Finally, we discuss recent experiments on the ratio of the slope in the specific heat at T_c to its jump. The value of this ratio is large compared with BCS and, in fact, large with respect to the maximum value possible in an Eliashberg superconductor, whatever the size, shape, or origin of the kernels in these equations. The observation is also inconsistent with a pure excitonic mechanism and remains a puzzle at this point.

The temperature variation of the London penetration depth in Y-Ba-Cu-O has been measured by several groups. The different early sets of results are consistent with the strong-coupling calculations of Blezius *et al.* (1988) and of Rammer (1988a) and indicate a phonon model. Unfortunately, this conclusion is not firm, since other data favor a BCS temperature variation that would be consistent with a pure exciton model or a joint mechanism. If consensus on the data could be achieved, we would be able to say something fairly definitive about the mechanism, but, at present, this is not yet possible.

II. THE CRITICAL TEMPERATURE

A. The Eliashberg equations and their reduction to BCS

The equations that underlie all of the work to be described in this review are the Eliashberg [Eliashberg (1960a, 1960b); Schrieffer (1964); Scalapino (1969); Bergmann and Rainer (1973); Rainer and Bergmann (1974); and Daams and Carbotte (1981)] gap equations, which involve two nonlinear coupled equations for the Matsubara gaps $\Delta(i\omega_n)$ and the renormalization factors $Z(i\omega_n)$. On the imaginary-frequency axis, they take the form [Rainer and Bergmann (1974); Allen and Dynes (1975); Allen and Mitrović (1982)]

$$\Delta(i\omega_n)Z(i\omega_n)=\pi T\sum_m [\lambda(i\omega_m-i\omega_n) -\mu^*(\omega_c)\theta(\omega_c-|\omega_m|)] \times\frac{\Delta(i\omega_m)}{\sqrt{\omega_m^2+\Delta^2(i\omega_m)}} \tag{2.1}$$

and

$$Z(i\omega_n)=1+\frac{\pi T}{\omega_n}\sum_m\lambda(i\omega_m-i\omega_n)\frac{\omega_m}{\sqrt{\omega_m^2+\Delta^2(i\omega_m)}}\ , \tag{2.2}$$

where $\mu^*(\omega_c)$ is the Coulomb pseudopotential opposing superconductivity. It comes with a cutoff at ω_c; otherwise, the sum over m will not converge in Eq. (2.1). In both (2.1) and (2.2), $\lambda(i\omega_m-i\omega_n)$ is related to the electron-boson attraction between two electrons interacting around the Fermi energy and is related to the electron-boson spectral density $\alpha^2F(\omega)$ (McMillan and Rowell, 1969), with ω the frequency of the exchanged boson, through the relation

$$\lambda(i\omega_m-i\omega_n)=2\int_0^\infty\frac{\Omega\alpha^2F(\Omega)d\Omega}{\Omega^2+(\omega_n-\omega_m)^2}\equiv\lambda(m-n)\ , \tag{2.3}$$

where $i\omega_n=i\pi T(2n-1)$ is the nth Matsubara frequency and $n=0,\pm1,\pm2,\ldots$ with T being the temperature. These equations are derived with the help of thermodynamic Green's functions [Nambu (1960); Abrikosov *et al.* (1963); Rickayzen (1965, 1980)].

Equations (2.1) and (2.2) can be reduced to the much simpler BCS [Bardeen *et al.* (1957)] form if a two-square-well model [Allen and Dynes (1975)] is used for $\lambda(n-m)$. In this model we take

$$\lambda(i\omega_m-i\omega_n)=\begin{cases}\lambda & \text{for both } |\omega_n|,|\omega_m|<\omega_c\ ,\\ 0 & \text{otherwise}\ ,\end{cases} \tag{2.4}$$

with λ the usual effective mass-renormalization parameter given by

$$\lambda(m=n)=\lambda(0)\equiv\lambda=\int_0^\infty \frac{2\alpha^2F(\Omega)d\Omega}{\Omega} . \tag{2.5}$$

If in Eq. (2.2) we further neglect the gap in the denominator on the right-hand side, we get [Allen and Dynes (1975)]

$$Z(i\omega_n)=1+\frac{\pi T}{\omega_n}\sum_m \lambda(i\omega_m-i\omega_n)\mathrm{sgn}(\omega_m)=1+\lambda . \tag{2.6}$$

Inserting this result into Eq. (2.1), we obtain for the two-square-well model

$$\Delta(i\omega_n)=\begin{cases}\Delta(T), & |\omega_n|<\omega_c ,\\ 0, & |\omega_n|>\omega_c ,\end{cases} \tag{2.7}$$

with

$$\Delta(T)=\frac{\lambda-\mu^*}{1+\lambda}\pi T\sum_{\substack{m\\ |\omega_m|<\omega_c}}\frac{\Delta(T)}{\sqrt{\omega_m^2+\Delta^2(T)}} . \tag{2.8}$$

This last equation is just the finite temperature version of the BCS gap equation [Bardeen *et al.* (1957)] written in terms of Matsubara frequencies and with the usual pairing parameter $N(0)V$ given by

$$N(0)V\equiv\frac{\lambda-\mu^*}{1+\lambda} , \tag{2.9}$$

with $N(0)$ being the single-spin electronic density of states at the Fermi energy, and V being the pairing potential.

For a temperature T near T_c, we can linearize Eq. (2.8) to get

$$1=\frac{\lambda-\mu^*}{1+\lambda}\pi T\sum_{\substack{m\\ |\omega_m|<\omega_c}}\frac{1}{|\omega_m|}\cong\frac{\lambda-\mu^*}{1+\lambda}\sum_{n=1}^{\omega_c/2\pi T_c+\frac{1}{2}}\frac{1}{n-\frac{1}{2}}$$
$$=\frac{\lambda-\mu^*}{1+\lambda}\left[\psi\left(\frac{\omega_c}{2\pi T_c}+\frac{1}{2}\right)-\psi\left(\tfrac{1}{2}\right)\right] \tag{2.10}$$

with $\psi(Z)$ the digamma function. For large Z, $\psi(Z)$ goes like $\ln(Z)$, so that

$$1=\frac{\lambda-\mu^*}{1+\lambda}\ln\left[\frac{2e^\gamma\omega_c}{\pi T_c}\right] , \tag{2.11}$$

where γ is the Euler constant. Thus

$$k_BT_c=1.13\hbar\omega_c\exp\left[-\frac{1+\lambda}{\lambda-\mu^*}\right] , \tag{2.12}$$

where we have reintroduced the Boltzmann constant k_B and Planck's constant $\hbar$.

B. A first estimate of maximum T_c

If this last equation is used to get an estimate for the maximum possible value for the critical temperature by letting $\lambda\to\infty$, we get

$$(k_BT_c)^{\max}=1.13\frac{\hbar\omega_c}{e} , \tag{2.13}$$

which is a very optimistic estimate. Phonons in the high-T_c oxides, as an example, extend up to 100 meV. Should we be coupled entirely to such modes, which is not likely to be the case, Eq. (2.13) gives 42 meV ($\sim$487 K) for the maximum T_c. We shall soon see that Eq. (2.12) is inadequate as $\lambda\to\infty$ and that the above estimate is not valid. Nevertheless, it does indicate that changing the scale of ω_c from a phonon to an electronic energy scale might increase T_c substantially. This argument is often brought forward as favoring an electronic mechanism in the high-T_c oxides with T_c up to 125 K [Sleight *et al.* (1975); Bednorz and Müller (1986); Cava *et al.* (1987); Chen *et al.* (1987); Chu *et al.* (1987); M. K. Wu *et al.* (1987); Maeda *et al.* (1988); Sheng and Hermann (1988); Subramanian *et al.* (1988)].

For the temperature $T=0$, Eq. (2.8) reads

$$1=\frac{\lambda-\mu^*}{1+\lambda}\frac{1}{2}\int_{-\omega_c}^{\omega_c}\frac{d\omega}{\sqrt{\omega^2+\Delta(0)^2}}\cong\frac{\lambda-\mu^*}{1+\lambda}\ln\left[\frac{2\hbar\omega_c}{\Delta(0)}\right] , \tag{2.14}$$

and we get

$$\frac{2\Delta(0)}{k_BT_c}=3.54 \tag{2.15}$$

for the dimensionless ratio of twice the gap to critical temperature. For actual superconductors (Meservey and Schwartz, 1969) Eq. (2.15) is rarely obeyed, and complete numerical solutions of Eqs. (2.1) and (2.2) are required to get quantitative agreement with experiment, as will be seen later.

C. McMillan equation and related issues

In order to solve Eqs. (2.1) and (2.2) so as to get an accurate T_c value, we need to know the input parameters $\alpha^2F(\Omega)$ and μ^*. These microscopic parameters are known for many conventional superconductors from McMillan and Rowell (1969) inversion of tunneling data. This technique will be described in detail in the next section. References to the $\alpha^2F(\omega)$ used in this work are given in Table I. in Fig. 1, we show results of tunneling inversion for the electron-phonon spectral density of Pb (Grimvall, 1981; solid curve) and compare with similarly obtained spectra for Sn* (dotted curve) and In* (dashed curve). Here the asterisk indicates that these two last spectra have been renormalized to have the same value of T_c and of $\omega_{\ln}$ as Pb. The characteristic phonon energy $\omega_{\ln}$ is, as is also λ, a much used moment of $\alpha^2F(\omega)$. The

mass-renormalization λ is twice the first inverse moment and has already been introduced [formula (2.5)], while $\omega_{\ln}$, which was first used by Allen and Dynes (1975), is defined as

$$\omega_{\ln}=\exp\left[+\frac{2}{\lambda}\int_0^\infty \ln(\omega)\frac{\alpha^2F(\omega)}{\omega}d\omega\right]. \tag{2.16}$$

It can be taken to represent an important measure of the average boson frequency associated with the spectral density $\alpha^2F(\omega)$. For a delta function centered around the Einstein frequency ω_E, i.e., for

$$\alpha^2F(\omega)=A\,\delta(\omega-\omega_E)\,, \tag{2.17}$$

with A the area under $\alpha^2F(\omega)$, Eq. (2.16) clearly gives $\omega_{\ln}=\omega_E$. In other cases, when there is a spread in frequencies, the low-energy part is weighted more heavily in $\omega_{\ln}$ than the high, and the value of $\omega_{\ln}$ will depend on the shape of the spectral density. For the case of Pb, $\lambda=1.55$ and $\omega_{\ln}=4.83$ meV. With this spectrum a numerical solution of the linearized version of Eqs. (2.1) and (2.2) gives $T_c=0.6198$ meV ($\sim$7.2 K) for $\mu^*=0.144$ with $\omega_c=66$ meV. This result will now be compared with the prediction of the McMillan (1968) formula, which is an approximate but analytic equation for T_c. This formula, which has been extremely popular, is much more quantitative than the BCS result (2.12). It was first developed by McMillan and then later refined by Allen and Dynes (1975) to read

$$k_BT_c=\frac{\hbar\omega_{\ln}}{1.2}\exp\left[-\frac{1.04(1+\lambda)}{\lambda-\mu^*(1+0.62\lambda)}\right]. \tag{2.18}$$

A complete derivation of this equation will be given in the next section. As a first check on its accuracy, we consider Pb. In this case, it gives a $T_c\cong0.496$ meV ($\sim$5.76 K), which is about 20 percent smaller than the exact result. Already we see some problem with the McMillan equation (2.18). Furthermore, it is not at all clear which value of μ^* should be used in (2.18). It certainly should not be the value used in the complete numerical solution, as we have done, but unfortunately no

TABLE I. Spectral-function sources. We tabulate here the sources for the $\alpha^2F(\nu)$ spectra used in our calculations. Most of the spectra come from a tabulation of Rowell *et al.* (1970).

1. Al comes from a theoretical calculation of Leung *et al.* (1976a, 1975b).
2. Several sources are available for Nb. Nb(R) comes from Robinson and Rowell (1972); Nb(A) comes from Arnold *et al.* (1980). These have been measured through tunneling. A theoretical calculation [Nb(B)] comes from Butler *et al.* (1977).
3. V has been obtained through tunneling by Zasadzinski *et al.* (1982).
4. Amorphous Bi and Ga have been obtained through tunneling by Chen *et al.* (1969).
5. La is from Lou and Tomasch (1972), through tunneling.
6. Mo is from Kimhi and Geballe (1980), through tunneling
7. Nb_3Sn has been obtained from Shen (1972) through tunneling.
8. V_3Si(Kihl.) has been obtained through tunneling by Kihlstrom (1985). We have scaled it to give $\lambda=1$ and used $T_c=16.4$ K (rather than 15.4 K as measured by Kihlstrom), which is in better agreement with the single-crystal T_c value.
9. V_3Si was obtained from scaling $G(\Omega)$ obtained through inelastic neutron scattering, such that $\lambda=1$, by Schweiss *et al.* (1976).
10. Nb_3Al has three possibilities. Two of them [(1) and (2)] were obtained from tunneling measurements by Kwo and Geballe (1981); the third [(3)] is a phonon spectrum obtained by Schweiss *et al.* (1972) and scaled to give $\lambda=1.7$.
11. Nb_3Ge (1) was obtained through tunneling by Geerk *et al.* (1982), whereas Nb_3Ge (2) was scaled from neutron-scattering data obtained by Müller *et al.* (1982) to give $\lambda=1.6$. μ^* has been fitted to give $T_c=20$ K.
12. V_3Ga has been obtained through tunneling by Zasadzinski *et al.* (1980).
13. Finally, the spectra by Weber (1987a, 1987b) have been obtained by theoretical calculations.

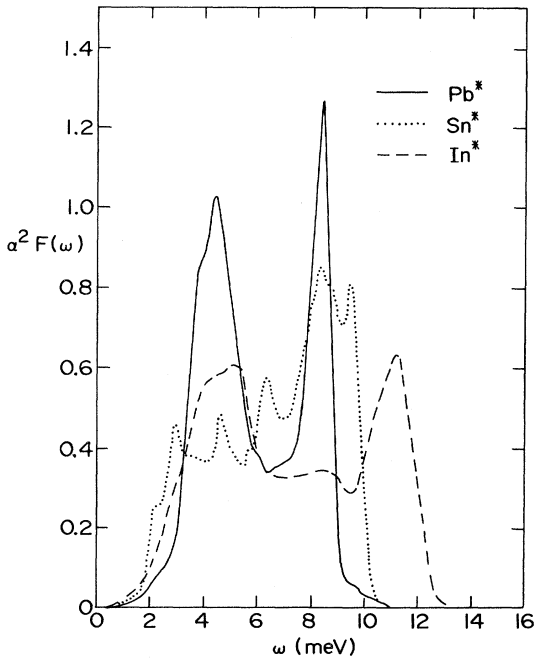

FIG. 1. Scale electron-phonon spectral densities based on the spectral density of Sn (dotted curve) and In (dashed curve) compared with that for Pb (solid curve). Each curve has the same $\omega_{\ln}$ and T_c value as pure Pb, and $\alpha^2F(\omega)=B\alpha_0^2F(\omega b)$ with B and b being appropriately chosen constants.

precise correction formula is known. Despite these problems, it is of interest to proceed with caution to estimate from Eq. (2.18) a maximum value of T_c as $\lambda \to \infty$. We get for $\mu^*=0$

$$(k_B T_c)^{\max} \cong \frac{\hbar\omega_{\ln}}{1.2} e^{-1.04} . \tag{2.19}$$

In general, the value of $\omega_{\ln}$ will depend on the shape of $\alpha^2F(\omega)$. If, for the purpose of argument, we take it as roughly $\frac{1}{2}$ the largest phonon energy in the system, we get a value for $(k_B T_c)^{\max}$ that is about $\frac{1}{3}$ of the value estimated on the basis of Eq. (2.12) or 14 meV ($\sim$162.5 K). We shall soon see that both estimates are wrong and that Eliashberg theory itself does not give a maximum value for T_c. Rather, the critical temperature must be limited for the electron-phonon case, by lattice stability arguments and not by the mathematical structure of the theory of superconductivity itself [Cohen and Anderson (1972); Varma (1982)].

D. A scaling theorem

We start by establishing a scaling theorem (Coombes and Carbotte, 1986a, 1988) for T_c that applies exactly when $\mu^*=0$ and is approximately true when μ^* is not an important player in T_c as compared with the role played by the electron-phonon spectral density. Consider a base spectrum $\alpha_0^2F(\omega)$ and another denoted by $\alpha_M^2F(\omega)$, which is constructed from the base spectrum through scaling of the frequency axis by a constant factor of b; i.e.,

$$\alpha_M^2F(\omega)=\alpha_0^2F(b\omega) . \tag{2.20}$$

We note that $b>1$ means that we have compressed the base spectrum and $b<1$ extends it to higher frequencies. Reference to Eq. (2.16) gives that $\omega_{\ln}^M=\omega_{\ln}^0/b$ and reference to Eq. (2.5) yields $\lambda_M=\lambda_0$; i.e., the mass-renormalization function λ is unchanged.

When we substitute (2.20) into the Eliashberg equations (2.1) and (2.2), we can rewrite them to read (Coombes and Carbotte, 1986a)

$$\bar{\Delta}(i\bar{\omega}_n)Z(i\bar{\omega}_n)=\pi\bar{T}\sum_m \left[\lambda^0(i\bar{\omega}_n-i\bar{\omega}_m)-\mu^*\left[\frac{\bar{\omega}_c}{b}\right]\right] \times \frac{\bar{\Delta}(i\bar{\omega}_m)}{\sqrt{\bar{\omega}_m^2+\bar{\Delta}^2(i\bar{\omega}_m)}} , \tag{2.21}$$

$$Z(i\bar{\omega}_n)=1+\frac{\pi\bar{T}}{\bar{\omega}_n}\sum_m \lambda^0(i\bar{\omega}_n-i\bar{\omega}_m)\frac{\bar{\omega}_m}{\sqrt{\bar{\omega}_m^2+\bar{\Delta}^2(i\bar{\omega}_m)}} , \tag{2.22}$$

with $\bar{\Delta}(i\bar{\omega}_n)=b\Delta(i\omega_n)$, $\bar{\omega}_n=\omega_n b$, and $\bar{\omega}_c=b\omega_c$. If we ignore the extra factor of $1/b$ in $\mu^*(\bar{\omega}_c/b)$ as being unimportant, we see that (2.21) and (2.22) are identical to the equations for the base spectrum $\alpha_0^2F(\omega)$ with $\bar{T}\equiv Tb$ playing the role of temperature, so that we immediately conclude that

$$T_c^M=T_c^0/b . \tag{2.23}$$

This relationship implies that the characteristic strong-coupling ratio $T_c/\omega_{\ln}$ is completely unaffected by a uniform stretch or compression of the frequency scale for the electron-boson spectral density. At the same time, on varying b, we can get any value of T_c we wish. To increase it, b needs to be made less than 1. This corresponds to increasing $\omega_{\ln}$. This result is in agreement with both approximate equations for T_c, namely, Eq. (2.12), the two-square-well result (Allen and Mitrović, 1982), and Eq. (2.18), the McMillan (1968) equation as modified by Allen and Dynes (1975).

A given spectrum $\alpha_0^2F(\omega)$ can be scaled by b on the frequency axis to give any desired value of $\omega_{\ln}$. After this is done, we can multiply by another constant factor B to get a model spectral density

$$\alpha_M^2F(\omega)=B\alpha_0^2F(b\omega) , \tag{2.24}$$

which has any desired value of T_c. All we need to do is adjust B in an appropriate manner. This is how the two spectra Sn* and In* of Fig. 1 were obtained. This leads us to consider a plot of $T_c/\omega_{\ln}$ as a function of λ for a spectrum $B\alpha_0^2F(\omega)$ where $\lambda=B\lambda_0$ as a function of λ.

Figure 2 displays results based on Pb, Nb_3Sn, Hg, and V_3Si. All plots are for $\mu^*=0.1$ in the range up to $\lambda=10$. Similar plots have been given by Allen and Dynes (1975) and by Marsiglio and Carbotte (1987c), but in a much more restricted range of λ. On the same plot we also

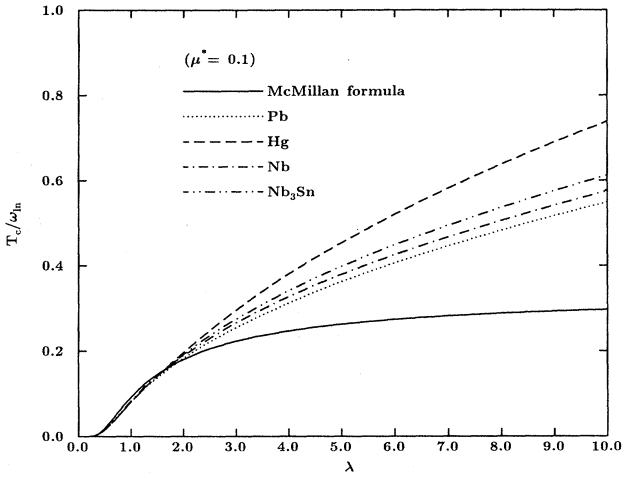

FIG. 2. $T_c/\omega_{\ln}$ as a function of λ given by the McMillan equation (solid curve) for $\mu^*=0.1$. Exact results are also given for scaled Pb (dotted curve), Hg (dashed curve), Nb (dot-dashed curve), and Nb_3Sn (dashed-double-dotted curve) spectra from the full numerical solutions of the Eliashberg equations.

show the McMillan equation results (solid line). It is striking that for large values of λ, $T_c/\omega_{\ln}$ keeps rising when the exact equations (2.21) and (2.22) are used, while the McMillan equation predicts saturation. This prediction, which leads to a finite maximum critical temperature for infinite λ as we have seen, is clearly an artifact of the approximate solution (2.18), which does not apply for large λ and is, therefore, not real. There is, in fact, no limit to T_c in Eliashberg theory. This leads us to a consideration of the exact asymptotic limit for the critical temperature T_c.

E. Asymptotic limit of $\lambda \to \infty$

We return to Eqs. (2.1) and (2.2) and substitute the equation for $Z(i\omega_n)$ into that for $\Delta(i\omega_n)$ to get

$$\Delta(i\omega_n)=\pi T\sum_m \lambda(i\omega_m-i\omega_n)\frac{\left[\Delta(i\omega_m)-\dfrac{\omega_m}{\omega_n}\Delta(i\omega_n)\right]}{\sqrt{\omega_m^2+\Delta^2(i\omega_m)}}\ , \tag{2.25}$$

where we have taken $\mu^*(\omega_c)=0$. This is sufficient for our purposes but is by no means essential to the arguments that follow. We first note that the term $m=n$ on the right-hand side of Eq. (2.25) drops out of the sum because, in that case, the quantity in the large parentheses is exactly zero [Marsiglio *et al.* (1989)]. It is therefore permissible to restrict the sum over m to $m\neq n$, so that $\lambda(i\omega_m-i\omega_n)$ is needed only for $m\neq n$. If we use for the spectral density the delta function of (2.7), we find

$$\lambda(i\omega_m-i\omega_n)=\frac{2\omega_E A}{\omega_E^2+(2\pi T)^2(m-n)^2} \quad \text{with } m\neq n\ . \tag{2.26}$$

If we assume $\omega_E \ll 2\pi T$ for any temperature of interest, we can drop ω_E in the denominator of (2.26) and obtain

$$\lambda(i\omega_m-i\omega_n)=\frac{2}{(2\pi\bar{T})^2(m-n)^2}\ , \tag{2.27}$$

where we have introduced the dimensionless temperature $\bar{T}\equiv T/\sqrt{A\omega_E}$. If we further introduce into (2.25) dimensionless Matsubara gaps $\bar{\Delta}(i\bar{\omega}_n)\equiv\Delta(i\omega_n)/\sqrt{A\omega_E}$, we can rewrite it in the universal form:

$$\bar{\Delta}(i\bar{\omega}_n)=\pi\bar{T}\sum_{m\neq n}\frac{2}{(2\pi\bar{T})^2(m-n)^2} \times\frac{\left[\bar{\Delta}(i\bar{\omega}_m)-\dfrac{\bar{\omega}_m}{\bar{\omega}_n}\bar{\Delta}(i\bar{\omega}_n)\right]}{\sqrt{\bar{\omega}_m^2+\bar{\Delta}^2(i\bar{\omega}_m)}}, \tag{2.28}$$

which is a dimensionless equation that does not refer to any particular material parameters. Numerical solution of this equation gives universal Matsubara gaps $\bar{\Delta}(i\bar{\omega}_n)\equiv f_n(t)$, which are well-defined functions of the reduced temperature $t\equiv T/T_c$. The single universal number $\bar{T}_c$ is obtained from a numerical solution of the linearized version of (2.28) and gives

$$\bar{T}_c=0.2584 \quad \text{or} \quad T_c=0.258\sqrt{\omega_E A}=0.183\sqrt{\lambda}\,\omega_E\ , \tag{2.29}$$

a result first obtained by Allen and Dynes [(1975); Owen and Scalapino (1971)] which holds for $\mu^*=0$. We shall see later that a single-Matsubara-gap approximation would have given $1/(\pi\sqrt{2})$ for the coefficient in (2.29) rather than 0.258. In both cases for a fixed value of the boson Einstein frequency ω_E, T_c goes to infinity as $\lambda\to\infty$. This contradicts the results obtained for $(k_B T_c)^{\max}$ in Eqs. (2.13) and (2.19), which were based on the approximate equations (2.12) and (2.18), respectively. These equations break down when λ is large, as is also illustrated in Fig. 2.

Leavens (1975, 1977) and Leavens and Carbotte (1974, 1977) arrived at the conclusion that T_c is not bounded in Eliashberg theory by using very different arguments from those presented so far. We shall discuss these briefly, but before doing so, we want to stress once more that limits on T_c that may exist for a given boson-exchange mechanism must be found outside Eliashberg theory. For example, in the case of the electron-phonon interaction the criterion of lattice instability is probably involved. Since such criteria are at best qualitative, a firm limit cannot be placed on T_c, although rough estimates are certainly useful.

F. Functional derivatives

Before the work of Leavens (1975, 1977) can be understood properly, it is necessary to introduce the idea of functional derivatives, first discussed within Eliashberg theory by Bergmann and Rainer [(1973); Karakosov *et al.* (1975, 1976)]. These authors considered the problem of the response of T_c to an infinitesimal (ϵ) addition to the base $\alpha^2F(\omega)$ at a specific frequency Ω. By definition, the functional derivative of T_c with respect to $\alpha^2F(\Omega)$ is given by

$$\frac{\delta T_c}{\delta\alpha^2F(\Omega)}=\lim_{\epsilon\to 0}\frac{\Delta T_c}{\epsilon}\ , \tag{2.30}$$

where ΔT_c is the change in T_c that results when one adds on to the spectral density a new piece of the form $\epsilon\delta(\omega-\Omega)$.

In Appendix A we give a simple analytic but approximate equation for the functional derivative of T_c. The calculations follow the work of Mitrović and Carbotte (1981b) in which the infinitesimal addition term is treated exactly. For the remaining part, a two-square-well model is employed. This leads to a universal function $G(\bar{\Omega})$ with

$$\frac{\delta T_c}{\delta\alpha^2F(\Omega)}=\frac{1}{1+\lambda}G(\bar{\Omega}) \tag{2.31a}$$

and [Eq. (A15)]

$$G(\bar{\Omega})=\sum_{n=1}^{\infty}\frac{4\bar{\Omega}}{\bar{\Omega}^2+4\pi^2n^2}B_n\ , \tag{2.31b}$$

where $\bar{\Omega}\equiv\Omega/k_BT_c$, and the B_n are numbers given by [Eq. (A16)]

$$B_n=\sum_{m=1}^{n}\left[\frac{1}{n}\frac{2}{2m-1}+\frac{2}{(2m-1)^2}\right]-\frac{\pi^2}{4}\ . \tag{2.32}$$

The universal function $G(\bar{\Omega})$ is shown in Fig. 3. The shape of this curve is characteristic of all functional derivatives of T_c, even when they are computed exactly. It goes to zero like $\bar{\Omega}$ as $\bar{\Omega}$ goes to zero and like $1/\bar{\Omega}$ as $\bar{\Omega}$ goes to infinity. In between, the curve exhibits a single broad maximum at $\bar{\Omega}^*\cong10.0$ with maximum value $G(\bar{\Omega}^*)=0.8$. This means that all phonon frequencies have the effect of increasing T_c, but for given area low and high frequencies are less effective than those around $\Omega=10.0k_BT_c$. This leads to the idea of the existence of an optimum frequency for T_c.

The shape of $\delta T_c/\delta\alpha^2F(\Omega)$, exhibited in Fig. 3, and the existence of an optimum frequency can be understood with the help of a simple classical model for lattice dynamics. Consider a single positively charged ion that can perform harmonic motion with frequency ω about its equilibrium position on the perfect lattice. Let U be its excursion off equilibrium and A be the amplitude of the harmonic motion [Carbotte (1987)]

$$U=A\sin(\omega t)\ , \tag{2.33}$$

where t is the time. If we introduce an electron into the system, it will pull the ion towards itself, because of the attractive ion-electron interaction, and so build up an ion polarization cloud about itself. The maximum polarization that can be obtained occurs when the oscillator is fully stretched at maximum amplitude. This occurs for $\omega_{op}t=\pi/2$, where the subscript "op" stands for optimum. For this lattice polarization to be effective in creating an overall electron-electron attraction, it is necessary that the first electron, which travels with the Fermi velocity (v_F), still be within the coherence length ξ_0 (which is the typical length associated with superconductivity) when full polarization occurs. The condition is $t=\xi_0/v_F$, and therefore

$$\omega_{op}=\frac{\pi v_F}{2\xi_0}\sim7k_BT_c\ , \tag{2.34}$$

where use has been made of the simple formula $\xi_0=\hbar v_F/\pi\Delta(0)$ [Grimvall (1981)]. Thus we expect the functional derivative to peak around $7k_BT_c$ and to show a broad maximum because there is nothing sharp in the argument just given. It should then drop to zero at both high and low frequencies. If the lattice oscillates too slowly compared with the typical time ξ_0/v_F, there will be no polarization. If it oscillates too rapidly, the polarization will simply average out to zero over the time of interest. Thus $\delta T_c/\delta\alpha^2F(\Omega)$ should indeed go to zero at both $\Omega\to0$ and $\Omega\to\infty$.

So far, we have based our arguments on the approximate form (2.31) for the functional derivative. An exact formulation has been given by Bergmann and Rainer (1973; for a formulation including anisotropy, see Daams and Carbotte, 1980a). For the discussion it is convenient to rewrite Eqs. (2.1) and (2.2) in terms of the alternate quantities $\tilde{\omega}(i\omega_n)\equiv\omega_nZ(i\omega_n)$ and $\tilde{\Delta}(i\omega_n)\equiv\Delta(i\omega_n)\tilde{\omega}(i\omega_n)/\omega_n$. The equations are now

$$\tilde{\Delta}(i\omega_n)=\pi T\sum_m[\lambda(i\omega_n-i\omega_m)-\mu^*]\times\frac{\tilde{\Delta}(i\omega_m)}{\sqrt{\tilde{\omega}^2(i\omega_m)+\tilde{\Delta}^2(i\omega_m)}} \tag{2.35}$$

and

$$\tilde{\omega}(i\omega_n)=\omega_n+\pi T\sum_m\lambda(i\omega_n-i\omega_m)\times\frac{\tilde{\omega}(i\omega_m)}{\sqrt{\tilde{\omega}^2(i\omega_m)+\tilde{\Delta}^2(i\omega_m)}}\ . \tag{2.36}$$

For the functional derivative of T_c with respect to $\alpha^2F(\omega)$ we need only the linearized form of Eqs. (2.35) and (2.36), which apply near T_c. Introducing $\bar{\Delta}_n=\tilde{\Delta}(i\omega_n)/[|\tilde{\omega}(i\omega_n)|+\rho]$, where ρ is a pair-breaking parameter that will be zero at T_c, and substituting (2.36) into (2.35) yields the equation

$$\rho\bar{\Delta}_n=\pi T_c\sum_m\left[\lambda(i\omega_n-i\omega_m)-\mu^*-\delta_{n,m}\frac{|\tilde{\omega}(i\omega_n)|}{\pi T_c}\right]\bar{\Delta}_m\ , \tag{2.37}$$

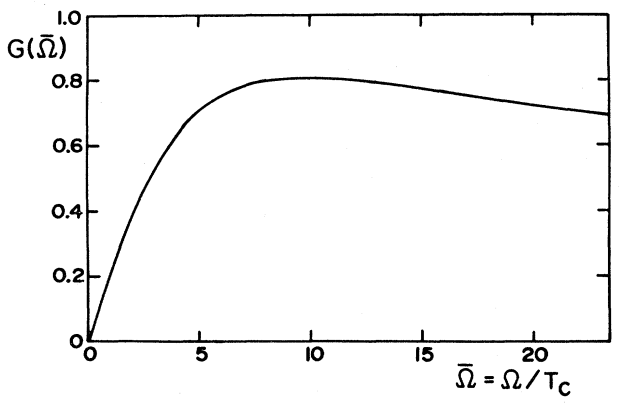

FIG. 3. Universal function $G(\bar{\Omega})$ as a function of normalized phonon energy $\bar{\Omega}=\Omega/T_c$, which enters the curve for the functional derivative of T_c with respect to $\alpha^2F(\omega)$ in the $\lambda^{\Theta\Theta}$ model of Mitrović and Carbotte.

which is an eigenvalue equation with kernel

$$K_{n,m}=\pi T_c\left[\lambda(i\omega_n-i\omega_m)-\mu^*-\delta_{n,m}\frac{|\bar{\omega}(i\omega_n)|}{\pi T_c}\right]. \tag{2.38}$$

A variation $\delta K_{n,m}$ in the kernel leads to a change in ρ of $\delta\rho$, which can be written in the form

$$\delta\rho=\frac{\sum_{n,m}\bar{\Delta}_n\delta K_{n,m}\bar{\Delta}_m}{\sum_n\bar{\Delta}_n^2} \tag{2.39}$$

with $\bar{\Delta}_n$ in this last equation being the eigenvector for $\rho=0$ and $T=T_c$.

The functional derivative of the critical temperature is given by

$$\frac{\delta T_c}{\delta\alpha^2F(\omega)}=-\frac{\dfrac{\delta\rho}{\delta\alpha^2F(\omega)}}{\left[\dfrac{\partial\rho}{\partial T}\right]_{T_c}}, \tag{2.40}$$

where $\delta\rho/\delta\alpha^2F(\omega)$ means the variation in ρ due to the explicit dependence of $K_{n,m}$ on $\alpha^2F(\omega)$ only, i.e.,

$$\frac{\delta\rho}{\delta\alpha^2F(\omega)}=\frac{\sum_{n,m}\bar{\Delta}_n\left[\pi T_c\left[\dfrac{\delta\lambda(i\omega_n-i\omega_m)}{\delta\alpha^2F(\omega)}-\delta_{n,m}\sum_{m'}\dfrac{\delta\lambda(i\omega_n-i\omega_{m'})}{\delta\alpha^2F(\omega)}\mathrm{sgn}(\omega_n\omega_{m'})\right]\right]\bar{\Delta}_m}{\sum_n\bar{\Delta}_n^2}, \tag{2.41}$$

also $\partial\rho/\partial T$ takes account only of the explicit T dependence and is

$$\frac{\partial\rho}{\partial T}=\frac{\sum_{n,m}\bar{\Delta}_n\left[\pi T_c\left[\dfrac{\partial\lambda(i\omega_n-i\omega_m)}{\partial T}-\delta_{n,m}\sum_{m'}\dfrac{\partial\lambda(i\omega_n-i\omega_{m'})}{\partial T}\mathrm{sgn}(\omega_{m'}\omega_n)\right]\right]\bar{\Delta}_m}{\sum_n\bar{\Delta}_n^2}. \tag{2.42}$$

Finally,

$$\frac{\delta\lambda(i\omega_n-i\omega_m)}{\delta\alpha^2F(\omega)}=\frac{2\omega}{\omega^2+(\omega_n-\omega_m)^2} \tag{2.43}$$

and

$$\frac{\partial\lambda(i\omega_n-i\omega_m)}{\partial T}=\int_0^\infty\left[-\frac{2\omega\alpha^2F(\omega)}{[\omega^2+(\omega_n-\omega_m)^2]^2}\frac{2(\omega_n-\omega_m)^2}{T}\right]d\omega. \tag{2.44}$$

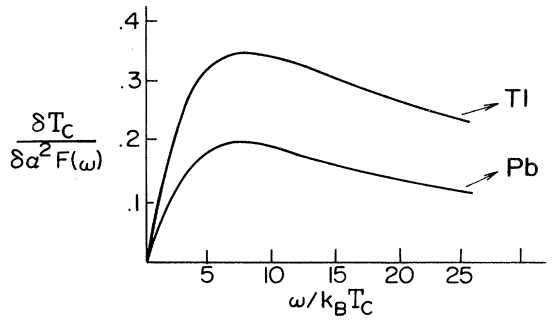

FIG. 4. Functional derivative of T_c with respect to $\alpha^2F(\omega)$ $[\delta T_c/\delta\alpha^2F(\omega)]$ as a function of the normalized phonon frequency ω/k_BT_c for Pb and Tl. The two curves show the same general behavior but have distinct amplitudes. They were obtained from exact numerical work based on Eq. (2.40).

To evaluate Eq. (2.40) numerically, we only need the numerical solutions of (2.37) for a given $\alpha^2F(\omega)$ spectrum and μ^* at the critical temperature of the unperturbed system with $\rho(T_c)=0$ in (2.37). Numerical evaluation of the relevant formulas for Pb and Tl are shown in Fig. 4. We see that the exact theory is not qualitatively different from our approximate analytic two-square-well-model solution. There are, of course, quantitative differences; in particular, the maximum in the exact curves occurs around $7.0k_BT_c$ rather than $10.0k_BT_c$.

As previously mentioned, the shape of the functional derivative curve suggests a method of optimizing the shape of $\alpha^2F(\omega)$ for a given spectral weight A, which is the area under $\alpha^2F(\omega)$ $[A=\int_0^\infty\alpha^2F(\omega)d\omega]$. We expect that taking infinitesimal weight out of the base $\alpha^2F(\omega)$ at a frequency away from the maximum in its functional derivative and placing the same amount of weight at the position of the maximum (where the phonons are more effective in T_c) should increase the critical temperature. If, for any base function, the functional derivative retains its shape, i.e., displays a maximum, then we should be able to repeat the procedure step after step and conclude that, for a given spectral weight A, the best shape of $\alpha^2F(\omega)$ in order to maximize T_c is a delta function at an optimum Einstein frequency ω_E^*, which should also be the frequency defining the maximum in its own functional derivative.

G. A delta-function spectral density

We can quantify this concept through use of a delta-function spectrum for $\alpha^2F(\omega)$ [Eq. (2.17)]. Substitution

of (2.17) into the Eliashberg equations (2.1) and (2.2) leads to dimensionless equations of the form [Blezius and Carbotte (1987, 1988)]

$$\overline{\Delta}(i\overline{\omega}_n)Z(i\overline{\omega}_n)=\pi\overline{T}\sum_m\left[\frac{2\overline{\omega}_E}{\overline{\omega}_E^2+(\overline{\omega}_n-\overline{\omega}_m)^2}-\mu^*\theta(\omega_c-|\overline{\omega}_m|A)\right]\times\frac{\overline{\Delta}(i\overline{\omega}_m)}{\sqrt{\overline{\omega}_m^2+\Delta^2(i\overline{\omega}_m)}} \tag{2.45}$$

and

$$Z(i\overline{\omega}_n)=1+\frac{\pi\overline{T}}{\overline{\omega}_n}\sum_m\frac{2\overline{\omega}_E}{\overline{\omega}_E^2+(\overline{\omega}_n-\overline{\omega}_m)^2}\frac{\overline{\omega}_m}{\sqrt{\overline{\omega}_m^2+\overline{\Delta}^2(i\overline{\omega}_m)}}, \tag{2.46}$$

where $\overline{\Delta}(i\overline{\omega}_n)=\Delta(i\omega_n)/A$, $\overline{T}=T/A$, $\overline{\omega}_E=\omega_E/A$, and $\overline{\omega}_n=\omega_n/A$. Equations (2.45) and (2.46) depend only on the single material parameter $\overline{\omega}_E$ and on μ^*, provided as did Leavens (1975), we neglect the A dependence that appears in the cutoff on the Coulomb repulsion term. For many superconductors, μ^* is not an important parameter and the above approximation is justified. It follows directly from the scaled equations (2.45) and (2.46) that

$$T_c=Af(\overline{\omega}_E,\mu^*), \tag{2.47}$$

where the function $f(\overline{\omega}_E,\mu^*)$ is to be determined through numerical calculation and is a universal curve for a fixed Coulomb repulsion μ^*. In Fig. 5, we plot this universal function for three different values of μ^*, namely, $\mu^*=0.0$, 0.1, and 0.2. We see that all three curves have the same shape as a function of $\overline{\omega}_E=\omega_E/A$. Each exhibits a maximum at some intermediate value of $\overline{\omega}_E$, which decreases with increasing μ^*, and each curve goes to zero at $\overline{\omega}_E=0$ and $\overline{\omega}_E=\infty$. It is clear that, for a delta-function spectral density, there is a unique optimum frequency that makes T_c largest for a fixed value of A. If we denote by $\overline{\omega}_E^*(\mu^*)$ the normalized frequency $\overline{\omega}_E$ at which the maximum occurs, we find that at this frequency

$$\frac{T_c}{A}=c(\mu^*)\quad\text{and}\quad\omega_E^*(\mu^*)=d(\mu^*), \tag{2.48}$$

where c and d are universal functions of μ^*.

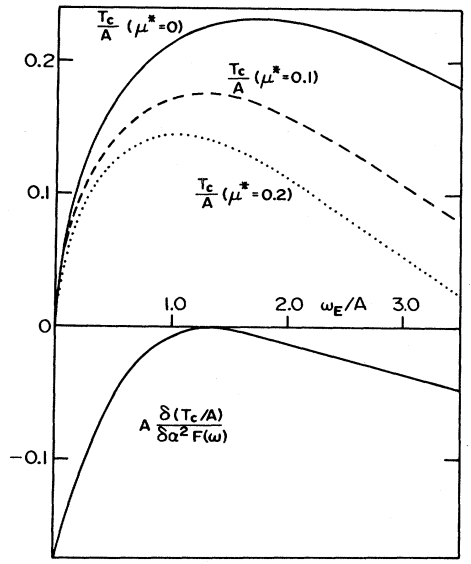

FIG. 5. Critical temperature T_c divided by A, the area under the spectral density, for an underlying delta-function-model spectra density $\alpha^2F(\omega)=A\delta(\omega-\omega_E)$, as a function of normalized Einstein frequency ω_E/A. For a given value of Coulomb pseudopotential μ^* ($\mu^*=0$, solid curve; $\mu^*=0.1$, dashed curve; and $\mu^*=0.2$, dotted curve), the curve T_c/A vs ω_E/A is universal and independent of A. In the lower frame is the functional derivative $A\delta(T_c/A)/\delta\alpha^2F(\omega)$ for the base δ function with $\mu^*=0.1$. It is seen to be exactly zero at the optimum frequency indicated by the maximum of the T_c/A vs ω_E/A curve and is negative definite for all other frequencies.

H. The optimum spectrum for T_c

We can prove that (2.48) represents a local maximum for any shape of $\alpha^2F(\omega)$ with a fixed A. In the lower part of Fig. 5, we show the functional derivative of T_c/A with respect to $\alpha^2F(\omega)$ for the optimum base delta-function spectrum

$$\alpha^2F(\omega)=A\delta(\omega-\omega_E^*(\mu^*)) \tag{2.49}$$

with $\omega_E^*(\mu^*)=1.3A$ for $\mu^*=0.1$. In this case $A\delta(T_c/A)/\delta\alpha^2F(\omega)$ is negative definite and zero exactly at $\overline{\omega}_E=1.3\equiv\overline{\omega}_E^*(\mu^*)$. That is, the functional derivative is exactly zero at the frequency of the base delta function (2.49) and negative everywhere else. This means that adding weight to the spectral density at this frequency leaves T_c/A unchanged, and adding weight anywhere else reduces it. Thus we have maximized T_c/A with the optimum spectrum (2.49) for arbitary A. It follows that the inequality

$$T_c\le Ac(\mu^*) \tag{2.50}$$

holds. The equality applies to a delta function and the inequality to any other spectral shape. This result was first established by Leavens (1975) using somewhat different arguments.

The inequality (2.50) is tested against conventional superconductors in Fig. 6, where we show $c(\mu^*)$ as a function of μ^* [solid line with open circles, Leavens (1975), Mitrović and Carbotte (1981b)]. On the same figure we have plotted the ratio T_c/A (solid dots) for a large number of the conventional superconductors to be identified in the next section. It is clear that several fall close to our theoretical maximum, indicating that, in nature,

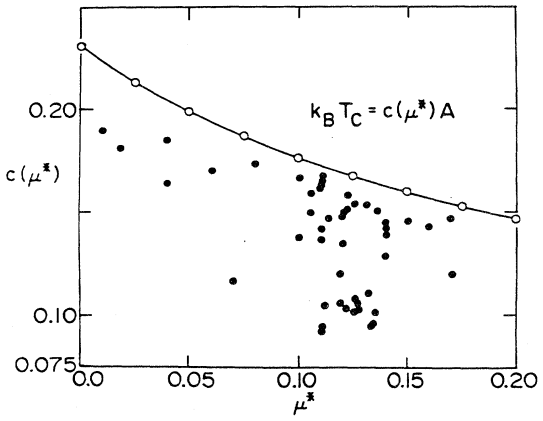

FIG. 6. Constant $c(\mu^*)$ in the relation $k_B T_c = c(\mu^*) A$ for the maximum T_c associated with a given A as a function of μ^*. Placed on the same figure (solid dots) are the results for T_c/A obtained in the case of many strong-coupling superconductors for which $\alpha^2F(\omega)$ is known from tunneling spectroscopy. The solid points all fall below the maximum curve, as they must.

some systems have boson modes that fall near the broad maximum around the optimum frequency. In these cases T_c is nearly as large as it can be made for a given A.

Equation (2.48), like the asymptotic form (2.29), implies that there is no limit placed on T_c by the theory of superconductivity itself. An infinite T_c can be reached in Eliashberg theory for a fixed ω_E by increasing λ indefinitely because $T_c = 0.183\sqrt{\lambda}\,\omega_E$ [Allen and Dynes (1975)] for $\lambda \to \infty$. On the other hand, an infinite T_c value can also be obtained for a fixed λ by increasing A indefinitely. This follows from Eq. (2.48). To be specific, for $\mu^* = 0.1$, $c(\mu^*) \cong 0.175$ and $\omega_E^*(\mu^*) \cong 1.3A$. In this case the optimum value of mass renormalization is quite finite, namely, $\lambda^* = 1.54$, which is very close to the value for Pb. Yet because $T_c = 0.175A$, it can be made infinitely large by taking $A \to \infty$. At the same time, of course, ω_E^* also goes toward infinity. Both cases just described achieve an infinite T_c, but in very different ways. We conclude, as previously described, that the criteria for maximum T_c need to be found outside Eliashberg theory.

To end this discussion, we make two final points. Supposing we could find a system for which the bosons (phonons) fall close to the optimum value, how large could we make T_c if $\omega_E^*(\mu^*)$ is to remain within the range of phonon energies? For the high-T_c oxides, phonons are measured to exist up to energies of the order of 100 meV. This implies a value of $A \cong 77$ meV for $\mu^* = 0.1$, and hence a T_c value of 13.5 meV or about 160 K for a mass renormalization of $\lambda^* = 1.54$. For this to occur, however, we would need to be preferentially strongly coupled only to the 100-meV phonons and have an A value that is unusually large. The highest value of A known to us from tunneling inversion is ~ 13.5 meV for Nb_3Ge. We stress, however, that the value of λ that is required is perfectly modest.

The other point we wish to make is to introduce briefly the equation of Leavens and Carbotte (1971, 1972, 1974) for T_c, which was established on the basis of a version of the McMillan equation of the form (2.18) but with $\omega_{\ln}$ replaced by $\langle\omega\rangle$. This was introduced by Dynes (1972) with

$$\langle\omega\rangle = \frac{2\int \alpha^2F(\omega)d\omega}{2\int \frac{\alpha^2F(\omega)}{\omega}d\omega} \equiv \frac{2A}{\lambda} . \tag{2.51}$$

Thus

$$\frac{T_c}{A} = \frac{2}{1.2\lambda}\exp\left[-\frac{1.04(1+\lambda)}{\lambda-\mu^*(1+0.62\lambda)}\right] . \tag{2.52}$$

For λ in the range $1.2 < \lambda < 2.4$, Leavens and Carbotte (1974) noticed that the function on the right-hand side of (2.52) was approximately constant, which suggested the simple relation

$$T_c = 0.148\,A \tag{2.53}$$

with the constant fit to numerical data on T_c obtained from solutions of the full Eliashberg equations (2.35) and (2.36) using several known spectral density functions. That this is a reasonable formula for T_c can also be seen from a close examination of Fig. 5. In the range $0.6 \lesssim \omega_E/A \lesssim 1.5$, the curves for T_c/A are reasonably flat, and so $T_c = \text{const} \times A$ is a good first approximation. For $\mu^* = 0.1$, we should take the constant somewhat below the maximum value of 0.175, and 0.148 is reasonable. The range defined above, over which Eq. (2.53) should be valid, is roughly $1.3 \lesssim \lambda \lesssim 3.3$. The more rigorous approach on which (2.53) is based gave the slightly smaller range quoted above.

I. Other equations for T_c

Over the years many other analytic equations have been suggested for T_c [Allen and Mitrović (1982)]. They all have certain advantages and disadvantages and usually a limited range of validity, although this may not be explicitly stated. Allen and Dynes (1975) extended the range of validity of the McMillan equation (2.18) by adding modifications to the prefactor on the right-hand side. These changes were designed to introduce into the T_c equation some dependence on the shape of spectral density and to increase the range of validity to higher values of λ. For an assessment of its accuracy, see Cai *et al.* (1979).

An equation by Rowell (1976) is equally simple and similar to our equation (2.53). There is also very extensive work on T_c equations by Wu and collaborators [H. Wu *et al.* (1977, 1987); Kung *et al.* (1978) Wu and Ji

(1979); Wang *et al.* (1980); Wu *et al.* (1980); Zhou *et al.* (1980)], by Kirzhnits *et al.* (1973), and by Khan and Allen (1980). Other works, too numerous to quote [Dolgov and Maksimov (1982a, 1982b); Combescot (1989)], also exist. The interested reader is referred to the review of Allen and Mitrović (1982) for further details on these alternate equations. At the present time, we recommend a complete numerical solution of the linearized version of Eqs. (2.1) and (2.2) when $\alpha^2F(\omega)$ is known from tunneling. When only an estimate of λ is available, the McMillan equation may be most useful.

The functional derivative technique introduced in this section for T_c has proven to be quite helpful in our discussion of the existence of an optimum spectrum for T_c. It has many other uses. We shall illustrate only two others here. In Fig. 7 we show phonon-dispersion curves along [110] for Nb_3Sn as determined by inelastic neutron scattering by Shirane and Axe (1971). The measurements were carried out at the four temperatures indicated in the figure, namely, 295, 120, 80, and 46 K. Considerable softening of this acoustic branch is observed as T is reduced. The question arises: is this softening directly related to superconductivity? Cowan and Carbotte (1978) have argued that it is not. In Fig. 8, we show the electron-phonon spectral density for Nb_3Sn as obtained by Shen (1972). On the same figure we also plot the functional derivative of T_c with respect to $\alpha^2F(\omega)$ and note that the phonons below 4 meV, which are the modes most affected by the softening depicted in Fig. 7, fall in a region that is mostly ineffective for T_c. In fact, performing a full Eliashberg calculation of the critical temperatures with the omission of the entire range ($\omega \leq 3.8$) in $\alpha^2F(\omega)$ decreases T_c by only 0.16 K. Phonon softening is not the answer to the relatively high T_c value found in Nb_3Sn

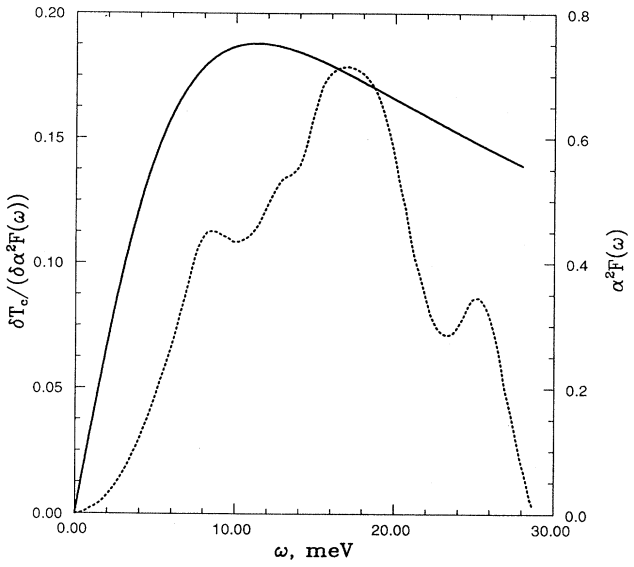

FIG. 8. Electron-phonon spectral density $\alpha^2F(\omega)$ (dotted curve) for Nb_3Sn measured from tunneling inversion as a function of ω compared with the functional derivative $\delta T_c/\delta\alpha^2F(\omega)$ (solid curve) for the same system.

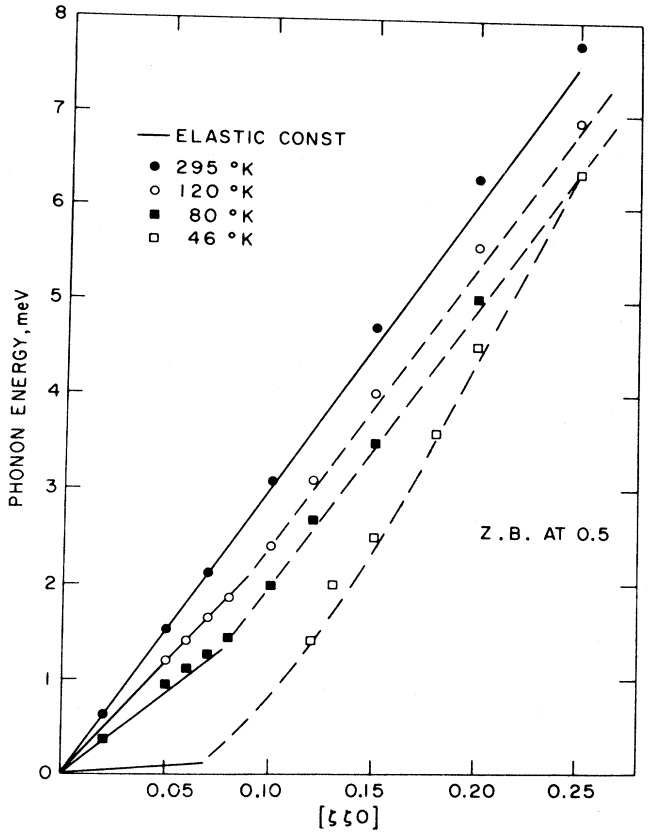

FIG. 7. Phonon-dispersion curves for Nb_3Sn along the [$\zeta\zeta$0] direction measured by inelastic neutron scattering at several different temperatures [from Shirane and Axe (1971)].

J. The isotope effect

The functional derivative of T_c with respect to $\alpha^2F(\omega)$ also enters into a very elegant formulation of the isotope effect given by Rainer and Culetto (1979). Before describing their work it is instructive to start with a brief discussion of the dependence of T_c on isotope mass M based on the simple BCS-type equation (2.12) with μ^* set equal to zero. First, we note that λ is independent of isotopic mass. In the next section, when the electron-phonon spectral density $\alpha^2F(\omega)$ is written explicitly in terms of microscopic quantities, we shall show that for a single component system the ion mass enters only as a multiplicative factor on the frequency ω, namely,

$$\alpha^2F(\omega) \equiv \mathcal{F}(\sqrt{M}\,\omega)\ , \tag{2.54}$$

where the entire mass dependence has been exhibited and therefore $\lambda = 2\int \mathcal{F}(\sqrt{M}\,\omega)/\omega d\omega$ is independent of M, as can be verified by introducing the variable $\sqrt{M}\,\omega \equiv x$ in this integral.

If ω_c in Eq. (2.12) with $\mu^*=0$ is interpreted as a phonon energy, it will vary as the inverse of M to the power $\frac{1}{2}$ and the only mass dependence of T_c will be through this factor, so that the isotope coefficient β defined by

$$\beta \equiv -\frac{d\ln T_c}{d\ln M}=\frac{1}{2}\ , \tag{2.55}$$

which is the classical BCS result. In general, (2.55) does not hold exactly for real materials except in special cases. This can be seen readily if we use the McMillan equation (2.18) and keep the Coulomb pseudopotential μ^*, which does depend on ω_c and hence on mass M for a phonon mechanism. The well-known equation for μ^* is [Morel and Anderson (1962)]

$$\mu^*=\frac{\mu}{1+\mu\ln\left[\frac{E_F}{\omega_c}\right]}\ , \tag{2.56}$$

where μ is a purely electronic quantity referring to the average Coulomb potential on the Fermi surface and E_F is the Fermi energy. Differentiation of (2.56) with respect to M gives

$$\frac{d\mu^*}{d\ln M}=-\frac{1}{2}\mu^{*2}\ . \tag{2.57}$$

Noting (2.57) and differentiating Eq. (2.18) gives

$$\beta \equiv \frac{1}{2}\left[1-\frac{1.04(1+\lambda)(1+0.62\lambda)}{[\lambda-\mu^*(1+0.62\lambda)]^2}\mu^{*2}\right]\ , \tag{2.58}$$

which reduces to $\frac{1}{2}$ when $\mu^*=0$ and is, in general, less then this when μ^* is finite. A plot is given in Fig. 9 as a function of λ for three values of μ^*, namely, $\mu^*=0.1$, 0.13, and 0.2. It is clear that β is different from $\frac{1}{2}$ only when λ is small, in which case it can even be negative when λ and μ^* are nearly balanced, as is observed in αU.

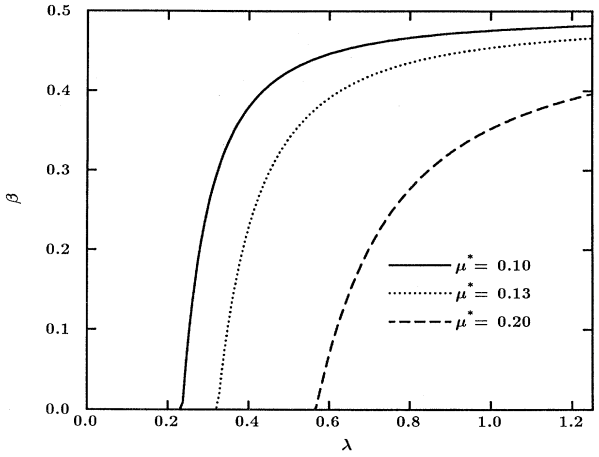

FIG. 9. Isotope effect coefficient β as a function of λ obtained from the McMillan equation [see Eq. (2.58)] for three values of μ^* ($\mu^*=0.1$, solid curve; $\mu^*=0.13$, dotted curve; and $\mu^*=0.2$, dashed curve). For small values of λ, it is possible for β to be small and even to be negative, although this region is not shown on the figure.

When λ gets much larger than μ^*, which is expected for an electron-phonon system with large T_c, the isotope effect will be close to its ideal value.

The above results were obtained using approximate T_c equations, but we can show quite generally that for $\mu^*=0$ the exact numerical solution of the linearized version of Eqs. (2.1) and (2.2) do indeed give $\beta=\frac{1}{2}$, whatever the shape of the spectral density. The proof of this fact depends on the observation that any spectral density $\alpha^2F(\omega)$ depends on M only through $\alpha^2F(\omega)=\mathcal{F}(\sqrt{M}\,\omega)$. Inserting this into the eigenvalue equation (2.37) for T_c with $\rho=0$ gives the equation

$$0=\pi\hat{T}_c\sum_m\left[\int_0^\infty\frac{\mathcal{F}(x)x\,dx}{x^2+(2\pi\hat{T}_c)^2(n-m)^2}-\delta_{n,m}\left[|2n-1|+\sum_{m'}\int_0^\infty\frac{\mathcal{F}(x)x\,dx}{x^2+(2\pi\hat{T}_c)^2(m'-n)^2}\mathrm{sgn}(\omega_{m'}\omega_n)\right]\right]\bar{\Delta}_m\ , \tag{2.59}$$

where $\hat{T}_c\equiv\sqrt{M}\,T_c$ and is a number independent of M, since it is given by Eq. (2.59) which makes no reference to the ion mass. It follows therefore that $T_c\sim 1/\sqrt{M}$ and that $\beta=\frac{1}{2}$ for $\mu^*=0$ and any $\alpha^2F(\omega)$.

K. The Rainer and Culetto approach to the partial isotope effect

When exact numerical calculations of β are contemplated, in specific cases, the method of Rainer and Culetto (1979) is very revealing. It was first derived for a multimass system M_i with corresponding isotopic coefficients $\beta_i\equiv -d\ln T_c/d\ln M_i$. If we refer each mass in a compound to some reference mass M according to the equation $M_i=\alpha_i M$ with α_i some appropriate constant that depends on i, we can show that Eq. (2.54) still holds. It follows directly from this that if all nuclear masses are changed by the same ratio $\delta M_i/M_i\equiv\delta M/M'$, the total isotope effect $\beta_{\rm tot}$, defined as $-d\ln T_c/d\ln M$, is just the sum of all the partial β_i's. That is,

$$\beta_{\rm tot}=\sum_i\beta_i\ ; \tag{2.60a}$$

and, for $\mu^*=0$, $\beta_{\rm tot}=\frac{1}{2}$ even in a compound involving several different mass species. Further,

$$\delta\alpha^2F(\omega)=\frac{1}{2}\omega\left[\frac{d}{d\omega}[\alpha^2F(\omega)]\right]\frac{\delta M}{M}\ . \tag{2.60b}$$

This formula follows directly from the fact that $\alpha^2F(\omega)\equiv\mathcal{F}(\sqrt{M}\,\omega)$, which we have used already to show that λ is unaffected by isotopic mass.

The corresponding change in T_c is given by

$$\delta T_c=\int\delta\alpha^2F(\omega)\frac{\delta T_c}{\delta\alpha^2F(\omega)}d\omega\ , \tag{2.61}$$

which can be rewritten, after an integration by parts, in the form

$$\delta\ln T_c=-\int_0^\infty d\omega\,\alpha^2F(\omega)\delta\ln M\frac{d}{d\omega}\left[\frac{\omega}{2T_c}\frac{\delta T_c}{\delta\alpha^2F(\omega)}\right]\ . \tag{2.62}$$

This form suggested to Rainer and Culetto (1979) that a partial isotope effect coefficient for the phonons of frequency ω be introduced according to

$$\beta(\omega)\equiv R(\omega)\alpha^2F(\omega) \tag{2.63}$$

with

$$R(\omega)=\frac{d}{d\omega}\left[\frac{\omega}{2T_c}\frac{\delta T_c}{\delta\alpha^2F(\omega)}\right]\ . \tag{2.64}$$

The total isotope effect is then

$$\beta_{\rm tot}=\int_0^\infty d\omega\,\beta(\omega)\ . \tag{2.65}$$

The weighting function $R(\omega)$ looks much like the functional derivative of T_c, itself, and is presented in Fig. 10 for a five-wide-bins model of $\alpha^2F(\omega)$, which is also shown on the same figure. The three $R(\omega)$ curves are for $\mu^*=-0.15$ (solid), $\mu^*=0.0$ (short dash), and $\mu^*=0.15$ (long dash). While these curves all have the same general shape, they vary considerably in absolute value. The three systems considered include one in which some high-energy nonphonon mechanism is involved in addition to a phonon contribution. The high-energy contribution is simulated by a negative μ^*. In all three cases, which are summarized in Table II, the T_c is equal to 36 K, which is the value observed for the oxide La-Sr-Cu-O. Other cases could have been considered, but the data of Table II are sufficient to illustrate our main points and to give some understanding of how the partial isotope effect works. When thinking about the curves presented in Fig. 10, it is important to remember that the $\alpha^2F(\omega)$ shown (five wide bins of equal width and height) is to be normalized differently in each of the three cases considered. It has the smallest overall value for $\mu^*=-0.15$ and the largest for $\mu^*=0.15$ since, in this case, the electron-phonon attraction must overcome some Coulomb repulsion. This is clearly illustrated in the second column of Table II where the corresponding values of λ are entered. We note that for $\mu^*=0.15$, λ is more than 5 times larger than for $\mu^*=-0.15$, with the case of $\mu^*=0.0$ intermediate.

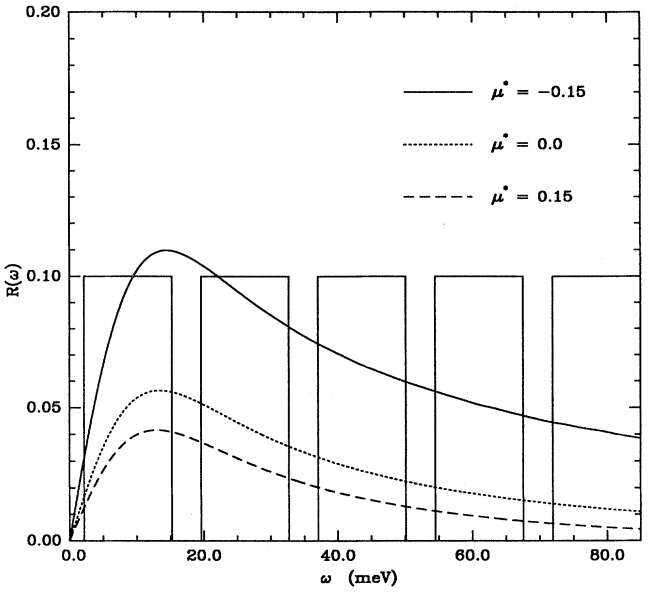

FIG. 10. Function $R(\omega)$ vs ω (in meV) entering the partial isotope effect given by formula (2.64) for three values of μ^* ($\mu^*=-0.15$, solid curve; $\mu^*=0.0$, short dashed curve; and $\mu^*=0.15$, longer dashed curve). This function is based on a model α^2F composed of five bins of equal width, which is shown for comparison.

Returning to Fig. 10 and $R(\omega)$, we note that this function goes to zero at $\omega=0$ and $\omega\to\infty$ and has a single fairly broad peak falling somewhere at the end of the first bin in $\alpha^2F(\omega)$ and hence at relatively low energy compared with the maximum phonon energy in the system. This shape for $R(\omega)$ means that very low and very high energy phonons contribute less to the isotope effect than do phonons around the maximum in $R(\omega)$. The data entered in Table II help to illustrate this. The third column gives the total isotope effect. This is followed by the partial contributions β_i from bins $i=1,5$, respectively. Starting with the case $\mu^*=-0.15$, we see that even

TABLE II. Total and partial isotope effect for the five bins of equal-width model for $\alpha^2F(\omega)$ shown in Fig. 10.

μ^*	λ	$\beta_{\rm tot}$	β_1	β_2	β_3	β_4	β_5
−0.15	0.491	0.31	0.079	0.087	0.054	0.048	0.039
0.0	1.797	0.50	0.152	0.149	0.092	0.061	0.043
0.15	2.643	0.49	0.166	0.152	0.100	0.047	0.027

though each bin is of equal size, the first two bins contribute the most to β because they fall around the maximum of $R(\omega)$ while the last three contribute less because they fall in the slowly decaying tail of $R(\omega)$. We note, also, that in all cases each of the last three bins contributes somewhat less as the index i increases from 3 to 5, because $R(\omega)$ drops with increasing ω in this region. For $\mu^*=-0.15$, the total isotope effect $\beta_{\rm tot}$ is 0.315, with more than half of this value coming from the first two peaks. This case could be thought of as simulating the situation observed in La-Sr-Cu-O for a model in which a joint mechanism of high-energy-boson-plus-phonon exchange is considered [Allender *et al.* (1973); Marsiglio, Akis, and Carbotte (1987a, 1988); Marsiglio and Carbotte (1987b, 1987c); Marsiglio and Carbotte (1988a)]. For the phonon contribution, the oxygen modes would be thought of as roughly described by the last three higher-energy bins contributing together 0.141 to the oxygen isotope effect, which is close to the measured value 0.16–0.20 [Batlogg, Kourouklis, *et al.* (1987); Faltens *et al.* (1987)]. The reason the total β is considerably below $\frac{1}{2}$ in this case is due to the excitonic contribution. For a pure phonon model $\beta=0.5$, as we see in the second row of Table II, and for $\mu^*=0.15$, it is only slightly less, namely, 0.475, which is representative of many strong-coupling conventional superconductors. It is clear from our discussion so far that the total isotope effect can be reduced from 0.5 in two ways: either the Coulomb pseudopotential μ^* is accounted for or some high-energy nonphonon mechanism is present. In addition, not all phonons contribute the same amount to β. The very low and very high energy phonons are less effective than those around 1/5 the maximum phonon energy in the system, at least in the models considered here and by Rainer and Culetto.

III. TUNNELING AND ITS RELATION TO THE ELECTRON-PHONON INTERACTION

A. Real-axis Eliashberg equations and reduction to BCS

Discussions of the current-voltage characteristics of a tunneling junction have traditionally made use of the real-frequency-axis formulation of the Eliashberg [Schrieffer *et al.* (1963); Schrieffer (1964); Scalapino *et al.* (1965); Scalapino *et al.* (1966)] equations, which are derived in many places including the review of Allen and Mitrović (1982). They consist of two coupled nonlinear integral equations with singular kernels involving a frequency (ω) and temperature (T) dependent complex gap $\Delta(\omega,T)$ and renormalization $Z_s(\omega,T)$. They take the form [Scalapino (1969)]

$$\Delta(\omega,T)Z_s(\omega,T)=\int_0^{\omega_c}d\omega'\,\mathrm{Re}\left[\frac{\Delta(\omega',T)}{\sqrt{\omega'^2-\Delta^2(\omega',T)}}\right]\int_0^{\infty}d\nu\,\alpha^2F(\nu)\times\left[[n(\nu)+f(-\omega')]\left[\frac{1}{\omega+\omega'+\nu+i0^+}-\frac{1}{\omega-\omega'-\nu+i0^+}\right]-[n(\nu)+f(\omega')]\left[\frac{1}{\omega+\nu-\omega'+i0^+}-\frac{1}{\omega-\nu+\omega'+i0^+}\right]\right]-\mu\int_0^{\omega_c}d\omega'\,\mathrm{Re}\left[\frac{\Delta(\omega',T)}{\sqrt{\omega'^2-\Delta^2(\omega',T)}}\right][1-2f(\omega')] \tag{3.1}$$

and

$$[1-Z_s(\omega,T)]\omega=\int_0^{\infty}d\omega'\,\mathrm{Re}\left[\frac{\omega'}{\sqrt{\omega'^2-\Delta^2(\omega',T)}}\right]\int_0^{\infty}d\nu\,\alpha^2F(\nu)\times\left[[n(\nu)+f(-\omega')]\left[\frac{1}{\omega+\omega'+\nu+i0^+}+\frac{1}{\omega-\omega'-\nu+i0^+}\right]+[n(\nu)+f(\omega')]\left[\frac{1}{\omega-\omega'+\nu+i0^+}+\frac{1}{\omega-\nu+\omega'+i0^+}\right]\right], \tag{3.2}$$

where ω_c is a boson energy cutoff introduced into the Coulomb repulsion term proportional to μ in order to achieve convergence in Eq. (3.1). It is often taken to be 10 times the maximum boson energy in the spectral density $\alpha^2F(\omega)$. If this is done, the first integral over ω' in (3.1), which deals with the boson kernel, can be extended to infinite if one wishes, because convergence has already been achieved by $\omega'=\omega_c$. In Eqs. (3.1) and (3.2), $f(\omega)$ is the Fermi function $1/(e^{\beta\omega}+1)$ and $n(\nu)$ is the Bose factor $1/(e^{\beta\nu}-1)$ with $\beta\equiv(k_BT_c)^{-1}$. The real part of the product $\Delta(\omega,T)Z_s(\omega,T)$ and of $Z_s(\omega,T)$ itself is determined by the principal-value integrals in (3.1) and (3.2), while the imaginary part comes from the delta-function parts with $1/(x\pm i0^+)=P/x\mp i\pi\delta(x)$, where P denotes a principal part. Because of the oc-

currence of denominators that vanish, the integrals in (3.1) and (3.2) need to be done carefully when numerical work is attempted.

To get some feeling for these complex equations, it is instructive to reduce them to BCS. To achieve this end, several approximations are required. First, all the boson factors in (3.1) and (3.2) are ignored, i.e., real boson scattering processes are left out. Further, the imaginary parts of Δ and Z_s are neglected; $\Delta(\omega,T)$ is replaced by its $\omega=0$ value, up to $\omega=\omega_c$ and taken to be zero after that; and Z_s is replaced by its value in the normal state at $\omega=0$ and $T=0$. With these approximations, we get

$$\Delta_0 Z_N(0,0)=\int_{\Delta_0}^{\omega_c} d\omega' \mathrm{Re}\left[\frac{\Delta_0}{\sqrt{\omega'^2-\Delta_0^2}}\right]\int_0^\infty d\nu\,\alpha^2F(\nu)\left[f(-\omega')\left[\frac{2}{\omega'+\nu}\right]-f(\omega')\left[\frac{2}{\nu-\omega'}\right]\right]$$

$$-\mu\int_{\Delta_0}^{\omega_c} d\omega' \mathrm{Re}\left[\frac{\Delta_0}{\sqrt{\omega'^2-\Delta_0^2}}\right][1-2f(\omega')] \tag{3.3a}$$

and

$$[1-Z_N(0,T)]\omega=\int_0^\infty d\omega'\int_0^\infty d\nu\,\alpha^2F(\nu)\left[\frac{2\omega}{\omega^2-(\omega'+\nu)^2}f(-\omega')+f(\omega')\frac{2\omega}{\omega^2-(\omega'-\nu)^2}\right], \tag{3.3b}$$

where Δ_0 in the first equation (3.3a) is $\Delta(0,T)$. In the last equation, we must cancel a factor of ω that appears on both right- and left-hand sides and then take the limit of $\omega\to 0$. This gives the mass-renormalization factor $\lambda(T)$ at finite temperature (Grimvall, 1968, 1969):

$$Z_N(0,T)-1\equiv\lambda(T) \tag{3.4a}$$

with

$$\lambda(T)=2\int_0^\infty d\omega'\int_0^\infty d\nu\,\alpha^2F(\nu)\left[\frac{f(-\omega')}{(\omega'+\nu)^2}+\frac{f(\omega')}{(\omega'-\nu)^2}\right]. \tag{3.4b}$$

Taking now the $T=0$ limit of Eq. (3.4) gives

$$Z_N(0,0)-1=\int_0^\infty d\nu\,\alpha^2F(\nu)\int_0^\infty\frac{2\,d\omega'}{(\omega'+\nu)^2}$$

$$=\int_0^\infty 2\frac{\alpha^2F(\nu)}{\nu}d\nu\equiv\lambda\,. \tag{3.5}$$

In addition, if we neglect ω' in each of the denominators in the first integral of (3.3a), we arrive at

$$\Delta_0(T)=\int_{\Delta_0}^{\omega_c} d\omega'\frac{\Delta_0}{\sqrt{\omega'^2-\Delta_0^2}}\frac{\lambda-\mu}{1+\lambda}[1-2f(\omega')]\,, \tag{3.6}$$

where we have made explicit the temperature dependence of Δ_0 and where the cutoff ω_c is now important for both λ and μ contributions. Finally, setting $\epsilon\equiv\sqrt{\omega'^2-\Delta_0^2}$, we obtain

$$\Delta_0(T)=\frac{\lambda-\mu}{1+\lambda}\int_0^{\omega_c} d\epsilon\frac{\Delta_0(T)}{\sqrt{\epsilon^2+\Delta_0^2(T)}}\times\{1-2f[\sqrt{\epsilon^2+\Delta_0^2(T)}]\}\,, \tag{3.7}$$

which is the usual BCS equation at finite temperature [Bardeen *et al.* (1957)] with the temperature T made explicit in Δ_0 on both sides of the equation.

B. Better solutions

Less approximate but still analytical solutions of (3.1) and (3.2) are possible and have been discussed in the literature. Of these, the McMillan (1968) equation for the critical temperature is the best known and is also the most widely used. We take a two-step model for the gap [Leavens and Carbotte (1974)]

$$\Delta(\omega,T)=\begin{cases}\Delta_0(T), & 0<\omega<\omega_0\,,\\ \Delta_\infty, & \omega>\omega_0\,,\end{cases} \tag{3.8a}$$

and

$$Z_S(\omega,T)=\begin{cases}1+\lambda, & 0<\omega<\omega_0,\\ 1, & \omega>\omega_0\,,\end{cases} \tag{3.8b}$$

with ω_0 some cutoff frequency that is assumed to be much less than ω_c. All boson factors are again neglected and the limit $T=T_c$ is taken, which means that Eq. (3.1) can be linearized in the gap value. Equation (3.1) now reads

$$\Delta_0=\frac{1}{1+\lambda}\int_0^{\omega_0} d\omega'\frac{\Delta_0}{\omega'}\int_0^\infty d\nu\,\alpha^2F(\nu)\left[\frac{2f(-\omega')}{\omega'+\nu}+\frac{2f(\omega')}{\omega'-\nu}\right]+\frac{1}{1+\lambda}\int_{\omega_0}^{\omega_c}\frac{d\omega'}{\omega'}\Delta_\infty\int_0^\infty d\nu\,\alpha^2F(\nu)\frac{2}{\omega'+\nu}$$

$$-\frac{\mu}{1+\lambda}\left[\Delta_0\int_0^{\omega_0}\frac{d\omega'}{\omega'}[1-2f(\omega')]+\Delta_\infty\int_{\omega_0}^{\omega_c}\frac{d\omega'}{\omega'}[1-2f(\omega')]\right] \tag{3.9}$$

and

$$\Delta_\infty = -\mu^* \Delta_0 \ln\left[\frac{1.13\omega_0}{k_B T_c}\right], \tag{3.10}$$

where the last two terms in (3.9) are just $\Delta_\infty/(1+\lambda)$, which has been solved for explicitly in (3.10). The second term in (3.9) can be worked out to be

$$\frac{\Delta_\infty}{1+\lambda}\int_0^\infty d\nu\,\alpha^2F(\nu)\frac{2}{\nu}\ln\left[1+\frac{\nu}{\omega_0}\right]. \tag{3.11}$$

Here we have used the fact that $\omega_c \gg \omega_0$ and $\omega_c \gg \nu$ for all important frequencies ν in $\alpha^2F(\nu)$. Moreover (Morel and Anderson, 1962),

$$\mu^* = \mu \Big/ \left[1+\mu\ln\left[\frac{\omega_c}{\omega_0}\right]\right]. \tag{3.12}$$

If we take $\nu/\omega_0 \ll 1$, Eq. (3.9) reduces to an eigenvalue equation for T_c of the form

$$1+\lambda = \int_0^{\omega_0}\frac{d\omega'}{\omega'}\int_0^\infty d\nu\,\alpha^2F(\nu)2\left[\frac{f(-\omega')}{\omega'+\nu}+\frac{f(\omega')}{\omega'-\nu}\right] - \mu^*\ln\left[\frac{1.13\omega_0}{k_BT_c}\right]\frac{2A}{\omega_0} - \mu^*\ln\left[\frac{1.13\omega_0}{k_BT_c}\right], \tag{3.13}$$

where $A=\int_0^\infty \alpha^2F(\nu)d\nu$ is just the area under the spectral density [Leavens (1977)]. If we define an average phonon energy by [Dynes (1972)]

$$\langle\omega\rangle = 2A/\lambda$$

and replace the denominators $\omega'+\nu$ and $\nu-\omega'$ in the first integral of (3.13) simply by ν, we get

$$1+\lambda = \int_0^{\omega_0}\frac{d\omega'}{\omega}[1-2f(\omega')]\lambda - \mu^*\left[\lambda\frac{\langle\omega\rangle}{\omega_0}+1\right]\ln\left[\frac{1.13\omega_0}{k_BT_c}\right] \tag{3.14}$$

or

$$k_BT_c = 1.13\omega_0\exp\left[-\frac{1+\lambda}{\lambda-\mu^*(1+\lambda\langle\omega\rangle/\omega_0)}\right]. \tag{3.15}$$

This suggests taking $\omega_0 = c^{-1}\langle\omega\rangle$ where c is some constant and trying, as a semiphenomenological form, an equation

$$k_BT_c = \langle\omega\rangle a\exp\left[-\frac{b(1+\lambda)}{\lambda-\mu^*(1+c\lambda)}\right], \tag{3.16}$$

with the constants a, b, and c to be fit to data on real materials. Following McMillan (1968), Dynes (1972) suggested, on the basis of many solutions of the Eliashberg equations for real materials for which $\alpha^2F(\omega)$ were known from tunneling inversion, the explicit form

$$k_BT_c = \frac{\langle\omega\rangle}{1.2}\exp\left[-\frac{1.04(1+\lambda)}{\lambda-\mu^*(1+0.62\lambda)}\right], \tag{3.17}$$

which is one version of the famous McMillan equation. Later, Allen and Dynes (1975) suggested substituting for $\langle\omega\rangle$ the value $\omega_{\ln}$ given by Eq. (2.16). One limitation of (3.17) is that it is not always made clear what value of μ^* should go with this choice of $\langle\omega\rangle$. Formula (3.12) suggests that the appropriate choice is certainly not the value used in a full Eliashberg numerical solution with cutoff ω_c. It should correspond to a somewhat lower cutoff equal to ω_0 that might be associated with the maximum boson energy in the system. Even if this problem about the choice of μ^* is overlooked, we have seen in the previous section that McMillan's approximate equation stops being satisfactory when λ get large. In that case, we need to solve numerically the full Eliashberg equations.

C. Solution of Leavens and Carbotte

Leavens and Carbotte (1974) have suggested a completely analytic formula for T_c without the need of introducing numerically fitted parameters as was done by McMillan. Their equation, however, introduces a new moment of $\alpha^2F(\omega)$, namely,

$$\bar{\lambda} \equiv 2\int_0^\infty d\nu\frac{\alpha^2F(\nu)}{\nu}\ln\left[1+\frac{\omega_0}{\nu}\right]. \tag{3.18}$$

Their arguments are based on the following observation. In Figs. 11 and 12, we show complete numerical solu-

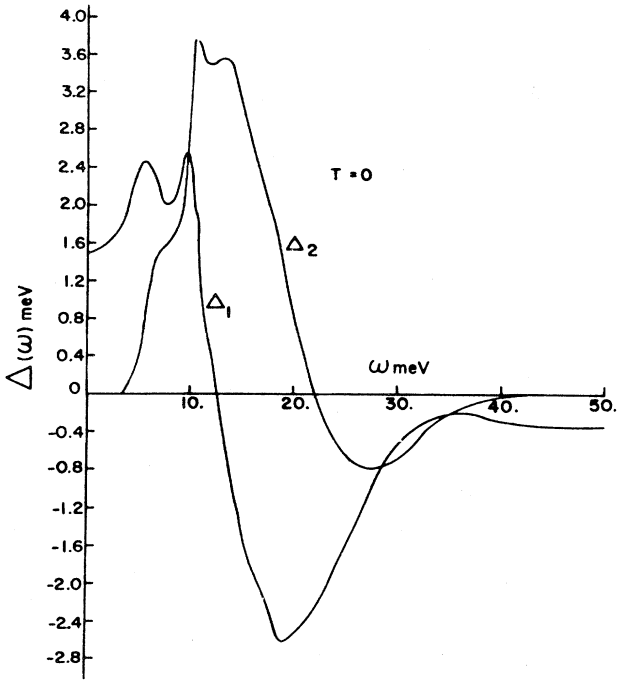

FIG. 11. Real, $\Delta_1(\omega)$, and imaginary, $\Delta_2(\omega)$, part of the complex real-frequency-axis gap $\Delta(\omega)\equiv\Delta_1(\omega)+i\Delta_2(\omega)$ for $Pb_{0.9}Bi_{0.1}$ at $T=0$ as a function of ω in meV.

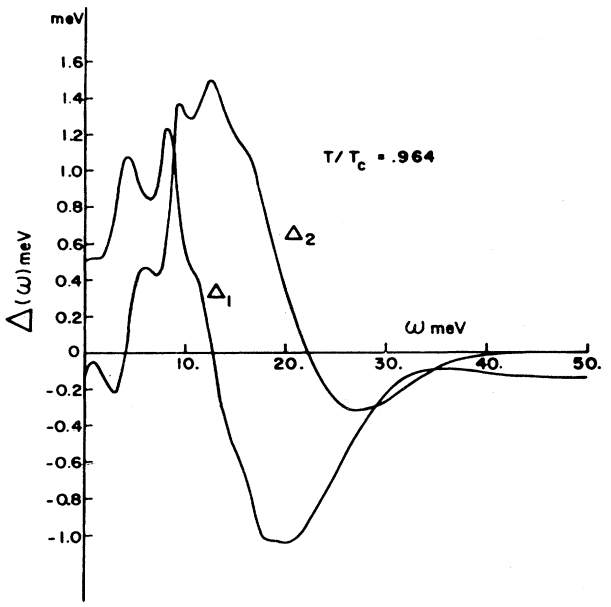

FIG. 12. Real, $\Delta_1(\omega)$, and imaginary, $\Delta_2(\omega)$, part of the complex real-frequency-axis gap $\Delta(\omega)=\Delta_1(\omega)+i\Delta_2(\omega)$ for $Pb_{0.9}Bi_{0.1}$ at $T=0.964T_c$ as a function of ω in meV.

tions of the Eliashberg equations (3.1) and (3.2) for the real and imaginary part of the gap. The material is $Pb_{0.9}Bi_{0.1}$ and the solutions, by Vashishta and Carbotte (1973), are based on a tunneling-derived spectral density. The figures apply, respectively, to a temperature $T=0$ and $T/T_c=0.964$ (very near T_c). Both real (Δ_1) and imaginary (Δ_2) parts show a great deal of structure and cannot be fit easily to a simple function. The real part of the gap shows a small increase as ω increases from the value zero; then it exhibits two peaks corresponding to the transverse and longitudinal peaks in the phonon spectrum of $Pb_{0.9}Bi_{0.1}$. At approximately the maximum phonon frequency in $\alpha^2F(\omega)$, it is seen to drop precipitously through zero and to become negative, showing a deep minimum and then a gradual increase toward a constant small negative value. Leavens and Carbotte (1974) noticed that approximating $\Delta(\omega')$ by a constant Δ_0 in the right-hand side of (3.1) for the entire range $\omega'=(0,\omega_0)$, with ω_0 the maximum phonon energy in $\alpha^2F(\omega)$, underestimates the contribution of this integral in this region. This arises because the full $\Delta(\omega')$ actually increases as we increase ω' from $\omega'=0$, as we have noted. This led Leavens and Carbotte to suggest that ω_0 be fixed at the maximum frequency in the spectral density, which now gives μ^* a definite value, and that additionally the Δ_∞ contribution for $\omega'>\omega_0$ be dropped to compensate for the underestimation of the real part of the gap in the first integral. It seems reasonable then to approximate the gap equation at T_c by (3.13), but with the second term left out on the right-hand side. This suggests the approximate form

$$1+\lambda=\int_0^{\omega_0}\frac{d\omega'}{\omega'}\int_0^{\infty}d\nu\,\alpha^2F(\nu)2\left[\frac{f(-\omega')}{\omega'+\nu}+\frac{f(\omega')}{\omega'-\nu}\right]-\mu^*\ln\left[\frac{1.13\omega_0}{k_BT_c}\right]. \tag{3.19}$$

Further, Leavens and Carbotte note that $(1/\omega')f(\omega')/(\nu-\omega')$ is peaked about $\omega'\cong 0$. If the important frequencies in $\alpha^2F(\nu)$ are large compared with k_BT_c [which measures the exponential decay of $f(\omega')$], we can replace this factor by $(1/\omega')f(\omega')/(\nu+\omega')$ and get

$$1+\lambda=2\int_0^{\infty}d\nu\,\alpha^2F(\nu)\int_0^{\omega_0}\frac{d\omega'}{\omega'}\frac{\tanh\left[\frac{\omega'}{2k_BT_c}\right]}{\omega'+\nu}-\mu^*\ln\left[\frac{1.13\omega_0}{k_BT_c}\right]. \tag{3.20}$$

The first integral in (3.20) can be worked out to read

$$-\bar{\lambda}+\lambda\ln\left[\frac{1.13\omega_0}{k_BT_c}\right], \tag{3.21}$$

which gives a final equation for T_c of the form

$$k_BT_c=1.13\omega_0\exp\left[-\frac{1+\lambda+\bar{\lambda}}{\lambda-\mu^*}\right]. \tag{3.22}$$

This is an analytic formula for T_c that is semiquantitative and has no fitting parameters. Furthermore, ω_0 has a definite meaning and so does μ^*, since ω_0 is the maximum frequency in $\alpha^2F(\omega)$. If we assume that $\omega_0/\nu\gg 1$ for all important ν in the spectral density, then

$$\bar{\lambda}\cong\lambda\ln\left[\frac{\omega_0}{\omega_{\ln}}\right] \tag{3.23}$$

and

$$k_BT_c\cong 1.13\omega_0\exp\left[-\frac{1+\lambda}{\lambda-\mu^*}\right]\exp\left[-\frac{\lambda}{\lambda-\mu^*}\ln\left[\frac{\omega_0}{\omega_{\ln}}\right]\right]. \tag{3.24}$$

If we should further replace $\lambda-\mu^*$ in the second exponential by λ, which is reasonable when λ is much larger that μ^*, we arrive at

$$k_BT_c=1.13\omega_{\ln}\exp\left[-\frac{1+\lambda}{\lambda-\mu^*}\right], \tag{3.25}$$

which is a simplified form of the Allen-Dynes equation.

D. Relation between the real- and the imaginary-axis equations

Before turning to the zero-temperature Eliashberg equations on the real-frequency axis and a discussion of

superconducting tunneling, we shall discuss the relationship between the real- and the imaginary-axis equations.

First, the real-frequency-axis equations (3.1) and (3.2) can be obtained from the imaginary-axis equations (2.1) and (2.2) by formal analytic continuation, and the two sets of equations are fully equivalent provided the cutoff ω_c is infinite. For a finite cutoff, one must remember that a sharp cutoff on the real axis does not analytically continue to a sharp cutoff on the imaginary axis and vice versa. This problem was discussed at length by Leavens and Fenton (1980). Still, it is conventional to use a sharp cutoff in both cases, and so there is a small difference between the two formulations. What is often done when one is using tunneling-derived data for $\alpha^2F(\nu)$ in the imaginary-axis formulation is that the Coulomb pseudopotential is readjusted to get the exact experimental T_c value.

Another method of relating the real- and the imaginary-axis solution of the gap equation that has often been employed in particular calculations is to obtain the real-axis gap and renormalization by analytically continuing the Matsubara $\Delta(i\omega_n)$ and $Z(i\omega_n)$, given by Eqs. (2.1) and (2.2), to the real axis by means of Padé approximants [Vidberg and Serene (1977)]. The N-point Padé approximant to a complex function $u(z)$ of the complex variable z, whose N values u_i $(i=1,\ldots,N)$ are given at N complex points z_i $(i=1,\ldots,N)$, is defined as a continued fraction:

$$C_N(z)=\cfrac{a_1}{1+\cfrac{a_2(z-z_1)}{1+\cfrac{a_3(z-z_2)}{\vdots\\ 1+\cfrac{a_n(z-z_{n-1})}{1}}}} , \tag{3.26}$$

such that

$$C_N(z_i)=u_i , \quad i=1,\ldots,N . \tag{3.27}$$

The coefficients a_i are then given by the recursion

$$a_i=g_i(z_i) , \quad g_1(z_i)=u_i , \quad i=1,\ldots,N , \tag{3.28}$$

$$g_p(z)=\frac{g_{p-1}(z_{p-1})-g_{p-1}(z)}{(z-z_{p-1})g_{p-1}(z)} , \quad p\geq 2 . \tag{3.29}$$

It can be shown that

$$C_N(z)=\frac{A_N(z)}{B_N(z)} , \tag{3.30}$$

where A_N and B_N are polynomials given by the recursion

$$A_{n+1}(z)=A_n(z)+(z-z_n)a_{n+1}A_{n-1}(z) , \quad n=1,2,\ldots,N-1 , \tag{3.31}$$

$$B_{n+1}(z)=B_n(z)+(z-z_n)a_{n+1}B_{n-1}(z) , \quad n=1,2,\ldots,N-1 ,$$

and

$$A_0=0 , \quad A_1=a_1 , \quad B_0=B_1=1 . \tag{3.32}$$

Vidberg and Serene (1977) have tested this method on several general cases and have applied it to the problem of obtaining the real-axis solutions $\Delta(\omega)$ and $Z_S(\omega)$ from the imaginary solutions $\Delta(i\omega_n)$ and $Z_S(i\omega_n)$ at the Matsubara frequencies. The main conclusions of their analysis are as follows:

(1) In order to get a good approximation to a function structured in the interval $[0,\bar{\omega}]$ on the real axis, one should use a sufficient number of input points from the interval $[0,i\omega']$ on the imaginary axis where $i\omega'$ belongs to the range of the imaginary axis where the function attains its asymptotic form (usually $i\omega'$ is several times $i\bar{\omega}$).

(2) The number of digits in the known values of the function u_i $(i=1,\ldots,N)$ is crucial for obtaining an accurate analytic continuation.

(3) Overall agreement between the $\Delta(\omega)$ and $Z_S(\omega)$ obtained by means of the N-point Padé approximant and those tabulated by Rowell *et al.* (1970) is good, being excellent in the low-frequency range (from zero up to several meV) and somewhat less satisfactory in the phonon region.

It is usually only the zero-temperature solutions that are analytically continued in this way. Leavens and Ritchie (1984, 1985) have discussed the case of finite T and, in particular, T near T_c, which is somewhat more complicated. Similar results were also given by Blaschke and Blocksdorf (1982) in the course of their discussion of optical properties in strong-coupling theory. In all cases, the phonon structure is not accurately represented by the numerical work, although, for many purposes, this is not an important limitation, particularly when dealing with quantities that involve integrals over the quasiparticle density of states or other related quantities.

A new and better method of analytic continuation from imaginary to real axis has been introduced recently by Marsiglio, Schossmann, and Carbotte (1988). Their final equations for the renormalized frequency $\tilde{\omega}(\omega)$ and pairing function $\phi(\omega)$ are [here $\tilde{\omega}(z)\equiv zZ(z)$]

$$\tilde{\omega}(\omega)=\omega+i\pi T\sum_{m=1}^{\infty}\frac{\tilde{\omega}(i\omega_m)}{[\tilde{\omega}^2(i\omega_m)+\phi^2(i\omega_m)]^{1/2}}[\lambda(\omega-i\omega_m)-\lambda(\omega+i\omega_m)]$$

$$+i\pi\int_{-\infty}^{\infty}dz\frac{\tilde{\omega}(\omega-z)}{[\tilde{\omega}^2(\omega-z)-\phi^2(\omega-z)]^{1/2}}\alpha^2F(z)[n(z)+f(z-\omega)] , \tag{3.33}$$

$$\phi(\omega)=i\pi T\sum_{m=1}^{\infty}\frac{\phi(i\omega_m)}{[\tilde{\omega}^2(i\omega_m)+\phi^2(i\omega_m)]^{1/2}}[\lambda(\omega-i\omega_m)+\lambda(\omega+i\omega_m)-2\mu^*\theta(\omega_c-|\omega_m|]$$
$$+i\pi\int_{-\infty}^{\infty}dz\frac{\phi(\omega-z)}{[\tilde{\omega}^2(\omega-z)-\phi^2(\omega-z)]^{1/2}}\alpha^2F(z)[n(z)+f(z-\omega)]\ . \tag{3.34}$$

These equations give solutions for the real-axis gap and renormalization that are essentially identical to those obtained from the solution of the real-axis equations even in the phonon region. Results for the quasiparticle density of states in Pb are shown in Fig. 13 and are barely discernible (few parts per thousand) from the corresponding results obtained from the real-axis equations (3.1) and (3.2) (with a smeared cutoff in μ^*, as discussed by Marsiglio, Schossmann, and Carbotte (1988). The phonon structure near 5 and 10 meV is clearly identifiable in the quasiparticle density of states given by

$$\frac{N(\omega)}{N(0)}=\mathrm{Re}\left[\frac{\omega}{\sqrt{\omega^2-\Delta^2(\omega,T)}}\right], \tag{3.35}$$

where $N(0)$ is the single-spin electronic density of states at the Fermi energy. In the inset of Fig. 13, we show results when a bin structure is used for defining $\alpha^2F(\omega)$. Oscillations in the density of states are faithfully reproduced in the numerical work, indicating the accuracy of the method. This new method for solving for the real-axis gap function is about two orders of magnitude faster than the conventional method and does not involve any principal-part integrals with singular integrands. Numerically, it is therefore much superior to the older method, and we recommend use of (3.3) and (3.34) in conjunction with (2.1) and (2.2) over (3.1) and (3.2), and over the Vidberg-Serene continued-fraction method.

E. The zero-temperature limit and tunneling

The zero-temperature version of the Eliashberg equations plays an essential role in tunneling inversion. The equations are obtained as the zero-temperature limit of Eqs. (3.1) and (3.2) and are

$$\Delta(\omega)Z_S(\omega)=\int_0^{\omega_c}d\omega'\mathrm{Re}\left[\frac{\Delta(\omega')}{\sqrt{\omega'^2-\Delta^2(\omega')}}\right]\int_0^{\infty}d\nu\,\alpha^2F(\nu)\left[\frac{1}{\omega+\omega'+\nu+i0^+}-\frac{1}{\omega-\omega'-\nu+i0^+}\right]$$
$$-\mu\int_0^{\omega_c}d\omega'\mathrm{Re}\left[\frac{\Delta(\omega')}{\sqrt{\omega'^2-\Delta^2(\omega')}}\right] \tag{3.36}$$

and

$$[1-Z_S(\omega)]\omega=\int_0^{\infty}d\omega'\mathrm{Re}\left[\frac{\omega'}{\sqrt{\omega'^2-\Delta^2(\omega')}}\right]\int_0^{\infty}d\nu\,\alpha^2F(\nu)\left[\frac{1}{\omega+\omega'+\nu+i0^+}+\frac{1}{\omega-\omega'-\nu+i0^+}\right]. \tag{3.37}$$

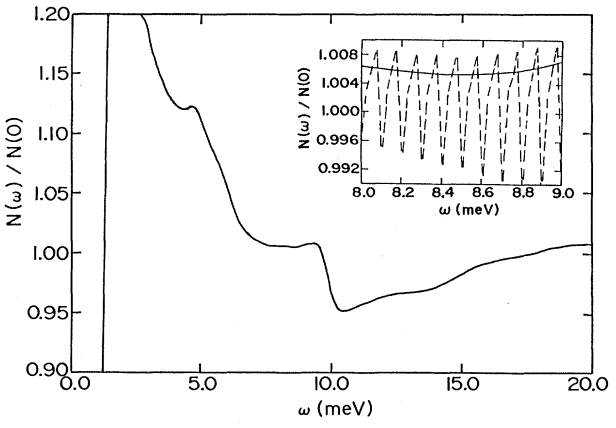

FIG. 13. Frequency dependence of the quasiparticle density of states in Pb calculated by the analytic continuation technique based on Eqs. (3.33) and (3.34). On the scale of the figure, the results are indistinguishable from those generated by the real-axis equations (at zero temperature) (3.36) and (3.37). The dashed curve in the inset shows the oscillations of the density of states if the $\alpha^2F(\omega)$ spectrum is treated as a set of δ functions with spacing $\Delta\omega=0.1$ meV.

For given microscopic parameters $\alpha^2F(\nu)$ and μ, one can calculate the quasiparticle density of states $N(\omega)/N(0)$ given by (3.35) and from it the current (I)–voltage (V) characteristics of a tunneling junction. For a normal-metal–insulator–superconductor junction (NIS), the formula for I versus V is [Meservey and Schwartz (1969)]

$$I_S(V)\propto\int d\omega\,\mathrm{Re}\left[\frac{|\omega|}{\sqrt{\omega^2-\Delta^2(\omega)}}\right][f(\omega)-f(\omega+V)]\ ; \tag{3.38}$$

at zero temperature, the derivative of the thermal factors in (3.38) reduces to a delta function, so that we get

$$\left[\frac{dI}{dV}\right]_S\Big/\left[\frac{dI}{dV}\right]_N=\mathrm{Re}\left[\frac{|V|}{\sqrt{V^2-\Delta^2(V)}}\right], \tag{3.39}$$

where S and N denote "superconducting" and "normal state," respectively. We have already seen in Fig. 13 that this last function contains a sharp picture of $\alpha^2F(\nu)$. McMillan and Rowell (1965, 1969) have invented a technique to go from a knowledge of the measured quasiparticle density of states

$$N_m(V) \equiv \left[\frac{dI}{dV}\right]_S \Big/ \left[\frac{dI}{dV}\right]_N \tag{3.40}$$

(where the subscript m denotes "measured") to $\alpha^2F(\nu)$ and μ (or μ^*, if you wish). The procedure followed is simple. A first guess is made for the two quantities, namely, $\alpha_0^2F(\nu)$ and μ_0^*. Equations (3.36) and (3.37) are solved numerically to get $\Delta(\omega)$ and from it an initial calculated value of the density of quasiparticle states $N_c^0(\omega)/N(0)$, which is given by (3.35). Here the subscript c stands for "calculated" and the superscript 0 for a first choice. In addition, the functional derivative $\delta N_c^0(V)/\delta\alpha^2F(\nu)$, which gives the infinitesimal response of $N_c^0(V)$ to a change in $\alpha^2F(\nu)$, is computed. This is used to make a second guess for $\alpha^2F(\nu)$ through the equation

$$\delta\alpha^2F(\nu) = \int dV \left[\frac{\delta N_c^0(V)}{\delta\alpha^2F(\nu)}\right]^{-1} [N_m(V) - N_c^0(V)] \; . \tag{3.41}$$

The new spectral density is

$$\alpha_1^2F(\nu) = \alpha_0^2F(\nu) + \delta\alpha^2F(\nu) \; . \tag{3.42}$$

The procedure is continued until convergence is reached. A unique $\alpha^2F(\nu)$ and μ^* result, and they are referred to as the measured microscopic parameters for that particular material. Results obtained in this way for Pb are shown in Fig. 14 (dotted curve).

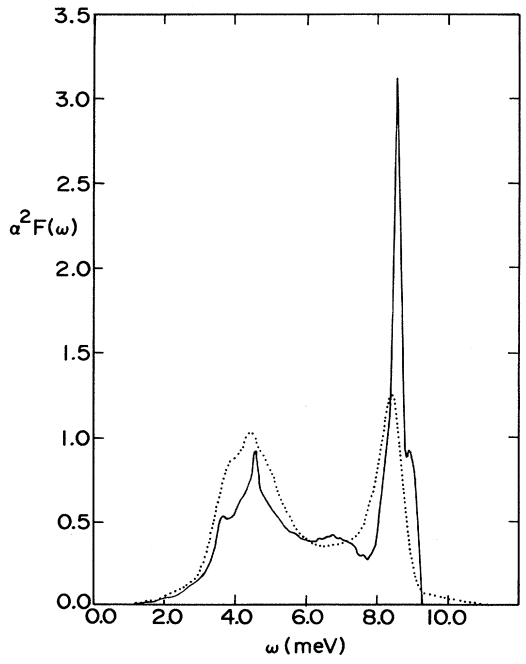

FIG. 14. Electron-phonon spectral density $\alpha^2F(\omega)$ measured in tunneling experiments (dotted curve) compared with that which is calculated from first principles (solid curve).

The inversion procedure just described requires data only up to the voltage that corresponds to the maximum phonon energy in $\alpha^2F(\nu)$ plus the zero-temperature gap value. As a first test of the Eliashberg equations, one can use the measured spectral density and the zero-temperature equations, (3.36) and (3.37), to predict the quasiparticle density of states at higher voltages in the multiphonon region. When this is done and the theoretical results are compared with experiment, McMillan and Rowell (1969) get, for the case of Pb, the excellent agreement shown in Fig. 15. This remarkable figure constitutes strong evidence for the validity of the Eliashberg equations in the conventional superconductors. Many inversions have now been carried out for a variety of systems, including many A15 compounds. A tabulation of earlier data is given by Rowell, McMillan, and Dynes (1970).

It has turned out that not all data can be treated as easily as that for Pb. In some cases it has proved very difficult to produce good-quality junctions and often a proximity layer will have formed between the superconductor and the oxide barrier. In this case the interpretation of data is more difficult, but Arnold and other researchers [Wolf and Zasadzinski (1974); Arnold (1978); Wolf *et al.* (1979); Arnold *et al.* (1978, 1980); Wolf and Arnold (1982)] have devised a new inversion method in which the proximity layer is explicitly accounted for by introducing appropriate modifications of the underlying mathematical equations. However, it is necessary to introduce a fitting parameter, as the proximity layer is not well characterized. This introduces some uncertainties in the inversion procedure, which, although it is somewhat less satisfactory, has, nevertheless, proved useful in many cases.

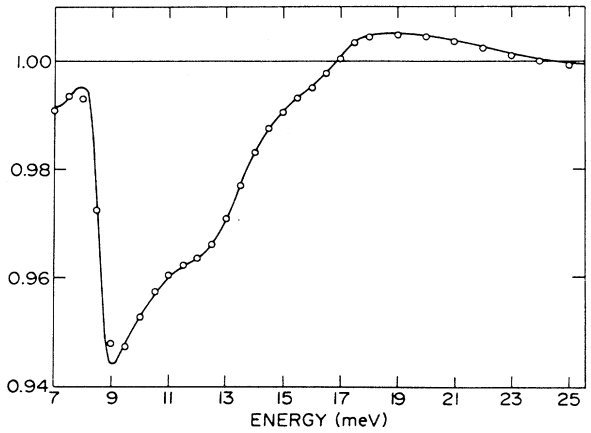

FIG. 15. Predicted (solid curve) normalized density of states in Pb as a function of energy ω compared with measured values (open dots) as a function of energy measured from the gap edge. The measured density of states divided by the BCS density of states above 11 meV was not used in the fitting procedure that produced $\alpha^2F(\omega)$, and a comparison of theory and experiment in the multiple-phonon region is a valid test of the theory [McMillan and Rowell (1969)].

Once an $\alpha^2F(\nu)$ is known from tunneling inversion, a second test of the validity of the Eliashberg equations can be carried out. One can calculate from the finite-temperature Eliashberg equations on the imaginary axis, (2.1) and (2.2), a variety of superconducting properties and compare with experiment. In general, the degree of agreement with experiment obtained is remarkable, as we will see in detail in Sec. V. In fact, at this point, it is probably the experiments that lag behind.

F. Calculation of the spectral density function

A third test involves first-principle calculations of the electron-phonon spectral density $\alpha^2F(\nu)$ which require knowledge of the electronic wave functions, the phonon spectrum, and the electron-phonon matrix elements between two single-particle Bloch states. It is beyond the scope of this review to give a detailed description of such work, and the reader is referred to the book of Grimvall (1981) for a comprehensive presentation. It will be sufficient here to give some of the highlights. The general equation for the electron-phonon spectral density $\alpha^2F(\nu)$ that enters the Eliashberg equations is [Carbotte and Dynes (1968); Carbotte (1969); Dynes *et al.* (1969); Leung *et al.* (1976a, 1976b)]

$$\alpha^2F(\nu)=\left[\frac{\Omega_a}{(2\pi)^3}\right]^2\frac{1}{N(0)\hbar}\times\sum_j\int d^3\mathbf{k}\,\delta(\epsilon_\mathbf{k})\times\int d^3\mathbf{k}'\delta(\epsilon_{\mathbf{k}'})|g_{\mathbf{k}\mathbf{k}'j}|^2\delta(\nu-\omega_j(\mathbf{k}'-\mathbf{k}))\,, \tag{3.43}$$

where Ω_a is the atomic volume, $\epsilon_\mathbf{k}$ is the energy of the Bloch state $\psi_\mathbf{k}$ with band index implied in the momentum label $\mathbf{k}$, j is a phonon branch index with phonon frequency $\omega_j(\mathbf{k}'-\mathbf{k})$, and $g_{\mathbf{k}\mathbf{k}'j}$ is the electron-phonon matrix element. The two Dirac delta functions of energy limit the integrations over momentum to the Fermi surface, and the Fermi energy has been taken to be zero. Finally, in the notation of Eq. (3.43), the single-spin density of states is

$$N(0)=\frac{\Omega_a}{(2\pi)^3}\int d^3\mathbf{k}\,\delta(\epsilon_\mathbf{k})=\frac{\Omega_a}{(2\pi)^3}\int_{S_F}\frac{dS_\mathbf{k}}{|\hbar v_\mathbf{k}|} \tag{3.44a}$$

where, because the integration is over the Fermi surface only, $dS_\mathbf{k}$ is an element of Fermi surface area and $v_\mathbf{k}$ is the Fermi velocity. The electron-phonon matrix element is related to the matrix element of the gradient of the crystal potential and the phonons. It is

$$g_{\mathbf{k}\mathbf{k}'j}=\langle\psi_\mathbf{k}|\epsilon^j(\mathbf{k}-\mathbf{k}')\cdot\nabla V|\psi_{\mathbf{k}'}\rangle\left[\frac{\hbar}{2M\omega_j(\mathbf{k}-\mathbf{k}')}\right]^{1/2}, \tag{3.44b}$$

where M is the ion mass, V is the crystal potential, and $\epsilon^j(\mathbf{k})$ is the polarization vector for the $(j\mathbf{k})$th phonon mode. We note that $g^2_{\mathbf{k}\mathbf{k}'j}$ goes like $1/\sqrt{M}$, and, of course, $\omega_j(\mathbf{k}'-\mathbf{k})$ in Eq. (3.43) goes like $1/\sqrt{M}$. This means that the delta function in the definition of $\alpha^2F(\omega)/\sqrt{M}$ goes like $\sqrt{M}$ times a delta function independent of ω and independent of mass; Eq. (2.54) follows. For a compound with atoms of different masses M_j we can refer each to some reference mass M through $M_j=\alpha_jM$ with α_j some appropriate number. In this case $g^2_{\mathbf{k}\mathbf{k}'j}$ again goes like the scaling mass M to power minus one-half, as does $\omega_j(\mathbf{k}'-\mathbf{k})$, and Eq. (2.54) also holds with no change.

Tomlinson and Carbotte (1977) have computed (3.43) for Pb from first principles. They use a pseudopotential [Appapillai and Williams (1973); Anderson and Gold (1963)] to characterize the electron-ion potential and multiple plane waves for the corresponding Bloch states. The phonons are taken from a Born–von Kármán fit to the phonon-dispersion curves measured by coherent inelastic neutron scattering [Brockhouse *et al.* (1962); Stedman *et al.* (1967); Kotov *et al.* (1968a, 1968b); Cowley (1974)]. In Fig. 14, the theoretical results obtained (solid curve) are compared with the measured tunneling spectral density (dotted curve). There is a great deal of agreement between these two spectral densities as to shape, although there certainly are minor disagreements in detail. Moreover, the theoretical value obtained for the electron-phonon mass-renormalization parameter λ is 1.32, to be compared with 1.55 from tunneling. At present, we assign the difference between these two quantities (which is significant) to inaccuracies in the calculations. Having said this, it is clear that the measured $\alpha^2F(\omega)$ is very closely related to the phonon frequency distribution and reflects well its shape. We discuss this important point next.

G. Comparison with the phonon distribution

Some of the discrepancy seen in Fig. 14 between calculated and measured spectral density can be traced to deficiencies in the Born–von Kármán model used to specify the phonons. Because the phonon-dispersion curves are highly structured in Pb [Cowley (1974)], long-range force constants are required in order to get a good fit in a harmonic analysis. It has been found, in fact, that a fit to only a few high-symmetry directions [Dynes *et al.* (1968)] is not sufficient to produce a reliable phonon frequency distribution $F(\omega)$ from the derived Born–von Kármán fit. This is illustrated in Fig. 16, compiled from various sources by Rowell and Dynes (1970). The uppermost curve is the phonon frequency distribution $F(\omega)$ for Pb calculated by Gilat (1965) from a fit to only high-symmetry measured phonon-dispersion curves [Cowley (1974)]. Dynes *et al.* (1968) have noted that the van Hove singularities present in this curve, that are in poorest agreement with the tunneling results (shown as the solid curve in the frame second from the top), correspond to off-symmetry regions in the Brillouin zone not

sampled in the fit. The dashed curve in the second frame is a result of a direct sampling of all measured phonons on and off high symmetry by Stedman *et al.* (1967). This greatly improves the agreement with tunneling. The shapes of the two curves are close except for a small shift of the upper longitudinal peaks. The dashed line in the lowermost frame labeled as Roy and Brockhouse (1970) was obtained by these authors through incoherent inelastic neutron scattering on a polycrystal sample of Pb. It is compared with the solid curve, which is the tunneling result for $\alpha^2F(\omega)$ folded with the resolution of their spectrometer. The agreement is excellent, and we can conclude that the tunneling-derived $\alpha^2F(\omega)$ agrees well with the measured phonon frequency distribution $F(\omega)$ in Pb and, by implication, with the shape obtained from first-principle calculations of $\alpha^2F(\omega)$, as these are based on the measured phonons. Further evidence that this is so is given in Fig. 17. In the lower frame, we show a comparison of tunneling results (solid curve) for $\alpha^2F(\omega)$ in

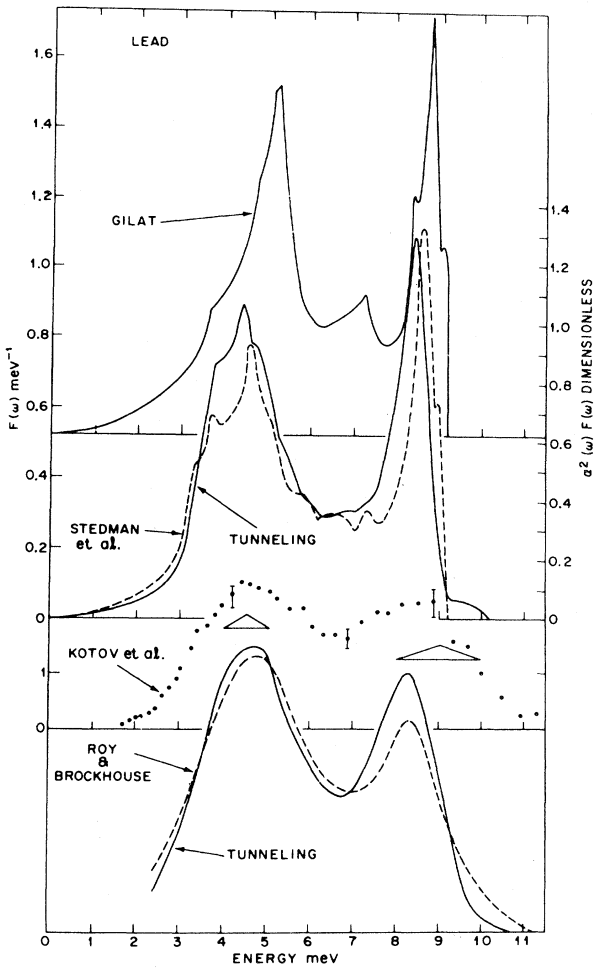

FIG. 16. Phonon frequency distribution for Pb, upper frame, as derived by Gilat (1965) through a Born–von Kármán analysis of the measured high-symmetry phonon-dispersion curves from coherent inelastic neutron scattering. The second frame gives the phonon frequency distribution (dashed curve) determined by Stedman *et al.* (1967) through a sampling of phonon energies throughout the Brillouin zone by inelastic neutron scattering and its comparison with the tunneling-derived $\alpha^2F(\omega)$. The second to last frame is data on the phonon frequency distribution obtained directly from inelastic incoherent neutron scattering on polycrystalline Pb by Kolov *et al.* (1968); the last frame is a comparison of the tunneling $\alpha^2F(\omega)$ smeared by the instrument resolution of the neutron spectrometer (solid curve) compared with polycrystalline results for $F(\omega)$ by Roy and Brockhouse (1970). From Rowell and Dynes (1970).

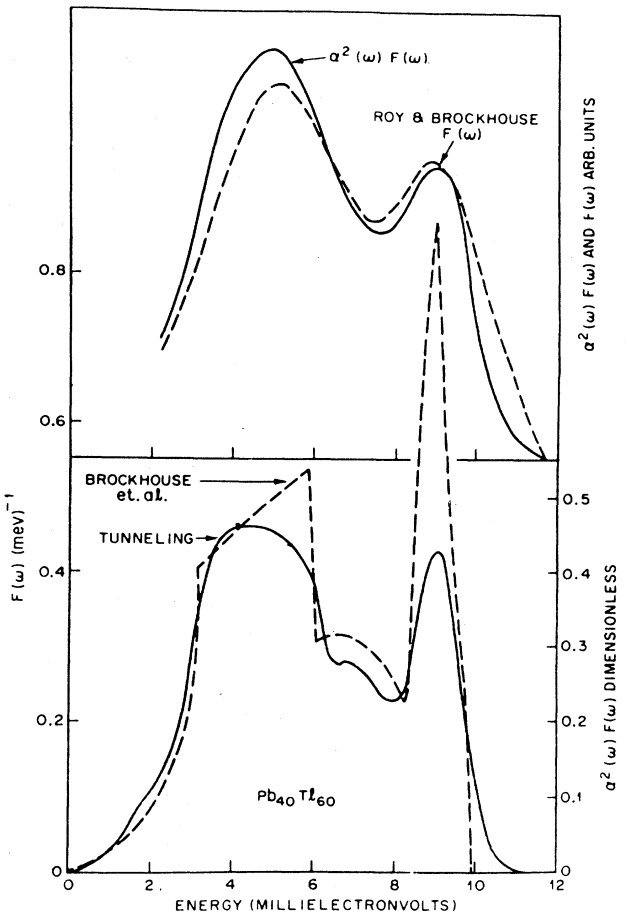

FIG. 17. Electron-phonon spectral density $\alpha^2F(\omega)$ (solid curve, upper frame) for $Pb_{0.40}Tl_{0.60}$, determined from tunneling experiments and convoluted by instrument resolution of the neutron spectrometer, compared with the neutron results for the phonon frequency distribution $F(\omega)$ (dashed curve) measured by Roy and Brockhouse (1970) by incoherent inelastic neutron scattering. The lower frame shows the tunneling results (solid curve) compared with the phonon frequency distribution (dashed curve) determined from a Born–von Kármán analysis of the phonon-dispersion curves in $Pb_{0.40}Tl_{0.60}$ by Brockhouse *et al.* (1968).

$Pb_{0.4}Tl_{0.6}$, which we compare with the phonon frequency distribution (dashed curve) obtained for the same system through a Born–von Kármán fit to high-symmetry phonon-dispersion curves measured by inelastic coherent neutron scattering by Brockhouse *et al.* (1968). Dynes *et al.* (1969) have also calculated $\alpha^2F(\omega)$ in a one-plane-wave pseudopotential model for this alloy and find no significant change in shape from $F(\omega)$. The degree of agreement between the tunneling-derived $\alpha^2F(\omega)$ and the phonon frequency distribution is very good. This is not surprising, since the phonon-dispersion curves for this alloy are smooth and a fit only to high-symmetry phonons can be expected to give a good representation of the phonons throughout the Brillouin zone. We note that the position and width of the two prominent peaks in Fig. 17 agree and that the main difference is that $F(\omega)$ shows sharp van Hove singularities while the tunneling result does not. This is partially an artifact because the phonon lifetime effects present in the alloy are left out of any Born–von Kármán analysis, which necessarily assumes sharp phonons [Rowell and Dynes (1970)]. But inelastic incoherent neutron scattering on polycrystalline samples gives $F(\omega)$ directly, which, in principle, includes lifetime effects. This is shown in the upper frame of Fig. 17 as the dashed line and is compared with the tunneling $\alpha^2F(\omega)$ (solid curve) folded into the resolution function of the neutron spectrometer. The agreement is very good. On the basis of these results, it has become conventional to compare neutron results for $F(\omega)$ directly with tunneling results for $\alpha^2F(\omega)$.

That $\alpha^2F(\omega)$ turns out to look nearly the same as the frequency distribution $F(\omega)$ is not very surprising since the frequency distribution is given by a formula that is not so different from Eq. (3.43) for $\alpha^2F(\omega)$. It is worth contrasting the two. A known prescription for $F(\omega)$ is

$$F(\omega)=\frac{1}{N}\sum_{\mathbf{k}j}\delta(\omega-\omega_j(\mathbf{k})) \tag{3.45}$$

with N, the number of ions in the system; j, the phonon branch index; and $\mathbf{k}$, the momentum ranging over the first Brillouin zone (FBZ). Thus each phonon mode enters (3.45) once and is given equal weighting. The same delta function that puts phonons into bins according to energy ω in (3.45) also appears in (3.43). One difference between these two formulas is that for $\alpha^2F(\omega)$ each phonon $\omega_j(\mathbf{k}-\mathbf{k}')$ is weighted by the appropriate strength of the electron-phonon interaction $|g_{\mathbf{k}\mathbf{k}'j}|^2$ rather than by one. Furthermore, in (3.43), the phase space over which the label $\mathbf{k}-\mathbf{k}'$ in the phonon variable ω_j varies is controlled by electronic variables, namely, by the momentum transfer for electron scattering from $\psi_{\mathbf{k}}$ to $\psi_{\mathbf{k}'}$. But as initial and final electron states are each averaged over the Fermi surface, $\mathbf{k}-\mathbf{k}'$ will, in general, range over several Brillouin zones and each phonon mode will be sampled several times. Thus the main difference between $\alpha^2F(\omega)$ and $F(\omega)$ is that each phonon is weighted in a slightly different way, and so it is not surprising that these two functions are nearly proportional to each other. The proportionality is, however, not exact as can be seen in Fig.18. What is shown in this figure is the ratio $\alpha^2F(\omega)/F(\omega)$ denoted by $\alpha^2(\omega)$ calculated by Tomlinson and Carbotte (1976) for the case of Pb. While some uncertainty in $\alpha^2(\omega)$ may arise because these authors used a Born–von Kármán model to specifiy the phonons, this is probably not very serious for the ratio of $\alpha^2F(\omega)$ to $F(\omega)$. Besides some small, almost random wiggles that are not of interest, we note in Fig. 18 a gradual increase in the coupling of the electrons to the phonons as ω increases. The lower-energy end corresponds mainly to coupling to transverse phonons while the high end deals mainly with longitudinal phonons. While the variation in $\alpha^2(\omega)$ is certainly significant, it is not sufficient to profoundly affect the shape of $\alpha^2F(\omega)$ relative to $F(\omega)$.

A comparison of tunneling results on $\alpha^2F(\omega)$ for Nb_3Sn and inelastic incoherent neutron-scattering results for the generalized phonon frequency distribution $G(\omega)$ is given in Fig. 19 where the ratio of $\alpha^2F(\omega)/G(\omega)$ is also shown [dashed line; Schweiss *et al.* (1976)]. It is important to realize that for an alloy system with atoms of differing Fermi scattering length which describes the interaction between the incident neutron and the scattering nucleus, $G(\omega)$ can be somewhat different from $F(\omega)$, but we shall ignore this here. We see that the effective $\alpha^2(\omega)$ (dashed curve) obtained for Nb_3Sn in this way is quite different from that obtained for Pb. It is largest at low phonon energies, dropping significantly across the main peak at intermediate energies and increasing slightly over the small high-energy hump. Thus $\alpha^2(\omega)$ is not independent of ω, but, to a first approximation, it is probably justifiable to ignore this effect, particularly when it enters quantities that depend on an integration of $\alpha^2F(\omega)$ over all frequencies. In this case it is more the overall shape and strength of $\alpha^2F(\omega)$ that matters, and other details are less important.

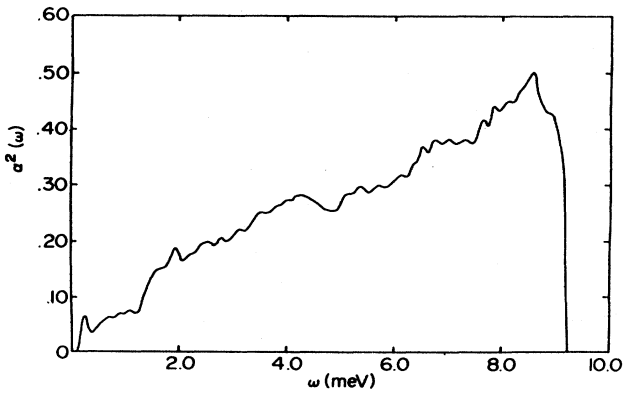

FIG. 18. Calculated $\alpha^2(\omega)$ for Pb using a multiple-plane-wave electronic structure and the measured phonon-dispersion curves.

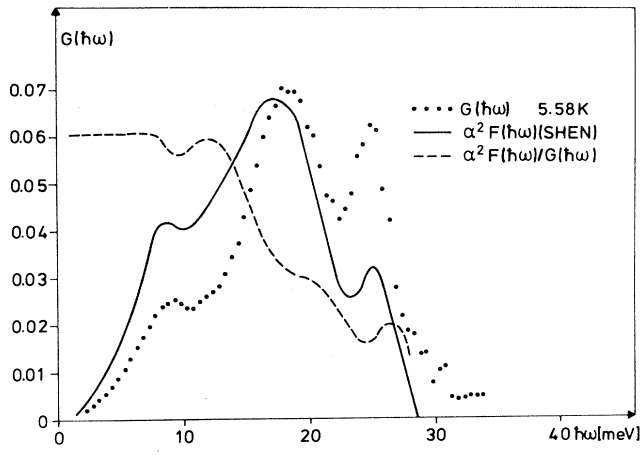

FIG. 19. Measured incoherent inelastic neutron-scattering general frequency distribution for Nb_3Sn (solid dots), as a function of energy $\hbar\omega$, compared with the electron-phonon spectral density measured in tunneling experiments (solid curve). The ratio $\alpha^2(\hbar\omega)\equiv\alpha^2F(\hbar\omega)/G(\hbar\omega)$ is shown by the dashed curve [from Schweiss *et al.* (1976)].

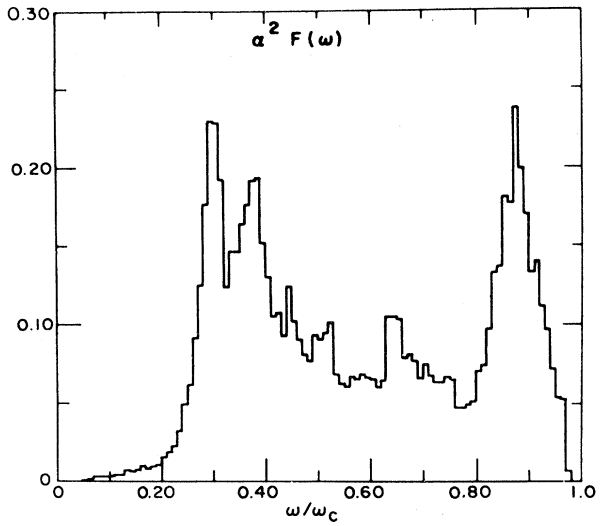

FIG. 20. Calculated isotropic $\alpha^2F(\omega)$ function for Zn as a function of reduced frequency ω/ω_c with $\omega_c=4.178\times10^{13}$ rad/sec, the maximum phonon frequency in the crystal. Multiple plane waves with a fitted pseudopotential and measured phonons were employed [Tomlinson and Swihart (1979)].

H. More about the calculations of $\alpha^2F(\omega)$

Returning to first-principle calculations of $\alpha^2F(\omega)$, the only other multiple-plane-wave calculations in the *s-p* metals besides Pb (which include a distorted, nonspherical Fermi surface) with which we are familiar and for which a full $\alpha^2F(\omega)$ spectrum is displayed, are the calculations of Leung *et al.* (1976a, 1976b) for Al and Tomlinson and Swihart (1979) for Zn. In Fig. 20, we reproduce the $\alpha^2F(\omega)$ for Zn calculated by these authors. The corresponding mass-enhancement parameter is $\lambda=0.334$. Tomlinson and Swihart (1979) also quote a second value of 0.36 obtained from a different treatment of the pseudopotential. These values are to be compared with the previous values of 0.425 by Truant and Carbotte (1973) and 0.42 by Allen and Cohen (1969), both obtained using a spherical Fermi surface and a single-plane-wave approximation for the pseudowavefunction. It is clear that one-plane-wave calculations are not very accurate, and we will not describe such work in detail here except to point out that the first such calculations appear to be due to Carbotte and Dynes (1968) for Na, K, Al, and Pb. For more information on such work, which is extensive, we refer the reader to the book by Grimvall (1981).

Before turning to $\alpha^2F(\omega)$ calculations in the transition metals, some alloys, and the refractory and the A15 compounds, we need to expand somewhat on the theory of $\alpha^2F(\omega)$ and related quantities. So far, we have introduced four important moments of $\alpha^2F(\omega)$, namely, λ [formula (2.5)], A [the area under $\alpha^2F(\omega)$], $\omega_{\ln}$ [formula (2.46)], and $\bar{\lambda}$ [formula (3.18)]. The first moment of $\alpha^2f(\omega)$ is also important because it depends only on electronic quantities, as can easily be seen by substitution of (3.44b) into (3.43) and integrating to get

$$\int_0^\infty \alpha^2F(\omega)\omega\,d\omega = \left[\frac{\Omega_a}{(2\pi)^3}\right]^2\frac{1}{N(0)}\int d^3\mathbf{k}\,\delta(\epsilon_\mathbf{k})\int d^3\mathbf{k}'\delta(\epsilon_{\mathbf{k}'})\times|\langle\psi_\mathbf{k}|\nabla V|\psi_{\mathbf{k}'}\rangle|^2\frac{1}{2M}\equiv\frac{\eta}{2M}\ . \tag{3.46}$$

The McMillan-Hopfield parameter [Grimvall (1981)] denoted by η is defined by the last identity in (3.46). We can define an average of the square of the phonon frequencies by

$$\langle\omega^2\rangle\equiv\frac{2}{\lambda}\int_0^\infty\alpha^2F(\omega)\omega\,d\omega \tag{3.47}$$

and so conclude that

$$\lambda=\frac{\eta}{M\langle\omega^2\rangle}\ . \tag{3.48}$$

There are many calculations of η in the literature from which λ is estimated through (3.48). This requires a guess for $\langle\omega^2\rangle$ which is usually taken from a consideration of phonon data alone. The accuracy of such a procedure is not clear, although it should be reasonable since $F(\omega)$ and $\alpha^2F(\omega)$ are not so different [Rainer (1986)]. Here we describe only calculations that avoid this approximation. While several such calculations proceed to a direct evaluation of (3.43) based on band-structure cal-

culations and the gradient of the electron-ion potential, others employ a related formula first given by Allen (1972, 1974, 1975, 1980). The inverse lifetime of a phonon ($\mathbf{k}j$) of frequency $\omega_j(\mathbf{k})$ due to the electron-ion interaction is given by

$$\gamma_j(\mathbf{q},\omega)=\frac{\Omega_a}{(2\pi)^2}\int d^3\mathbf{k}\int d^3\mathbf{k}'\delta(\epsilon_{\mathbf{k}})\delta(\epsilon_{\mathbf{k}'}) \times\delta(\mathbf{k}-\mathbf{k}'-\mathbf{q})\omega|g_{\mathbf{k}\mathbf{k}'j}|^2 \tag{3.49a}$$

and is related to the spectral density through

$$\alpha^2F(\omega)=\frac{\Omega_a}{2\pi N(0)(2\pi)^3} \times\int d^3\mathbf{q}\sum_j\frac{\gamma(\mathbf{q},\omega_j(\mathbf{q}))}{\hbar\omega_j(\mathbf{q})}\delta(\omega-\omega_j(\mathbf{q}))\ . \tag{3.49b}$$

Thus $\alpha^2F(\omega)$ can be calculated from a knowledge of phonon quantities alone. This procedure was followed by Butler *et al.* (1977) in a calculation of phonon properties for Nb, as well as giving a comparison with experiment. Further details are found in the paper of Butler *et al.* (1979). The results of their calculated lifetimes, based on full band-structure results for Nb, are presented in Fig. 21 for two high-symmetry directions, $[\zeta,0,0]$ and $[\zeta,\zeta,0]$ for transverse (dashed and dotted curves) and longitudinal (solid curve) branches. A comparison with experiment is also given. The spectral density obtained in this way from formula (3.49b) is presented in Fig. 22 (solid histogram) and is compared with early tunneling results by Robinson and Rowell (1972; solid curve). The agreement between the two curves is not good, but it was improved in later tunneling experiments as to shape. The high-frequency peak, however, remains attenuated in all tunneling work. As for absolute magnitude, it is to be noted that the theoretical calculations [Butler *et al.* (1977)] give a λ value of 1.22, which is considerably larger than the best tunneling value to date which is 1.01 given by Arnold *et al.* (1980). The difference between these two numbers may well be representative of the accuracy of present first-principle calculations. There have, in fact, been several other independent first-principle calculations for $\alpha^2F(\omega)$ in Nb differing mainly in the computational scheme used for the band structure and electron-ion matrix element. Harmon and Sinha (1976) quote a $\lambda=1.87$ and, in a later calculation (1977), 1.58. Butler *et al.* (1979) in extended calculations quote $\lambda=1.12$. Peter *et al.* (1977) give a smaller value of $\lambda=0.86$ and Weber (1984a), 0.9. Finally, Glötzel *et al.* (1979) have attempted to give a critical assessment of some of the errors that might be expected in such calculations and find for Nb that $\lambda=1.3$ [Rainer (1986)]. It is clear that while such calculations generally confirm the idea that the electron-phonon interaction is largely resopnsible for the superconductivity in this material and, presumably, in the other transition metals, it is not possible to calculate an accurate value of T_c yet or, if you like, λ, although it is safe to say that its magnitude is close to 1.0. Glötzel *et al.* (1979) also give values of λ for other metals: 1.2 for V, 0.9 for Ta, 0.4 for Mo, and 0.5 for Pd. On the basis of similar full calculations of $\alpha^2F(\omega)$, Rietschel and Winter (1979) obtained 1.04 for V

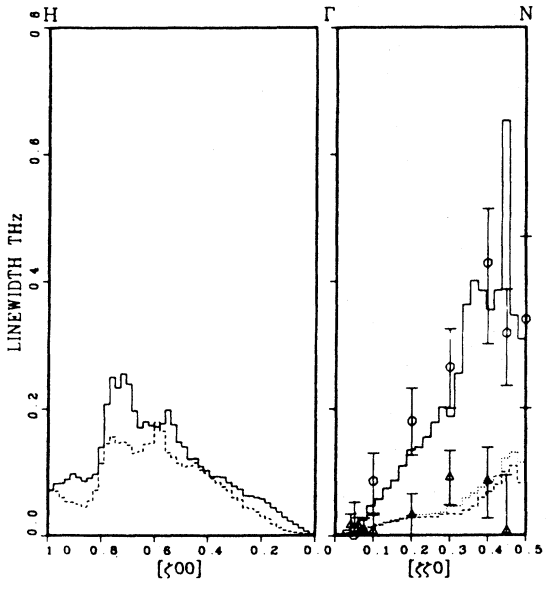

FIG. 21. Phonon linewidths in Nb. The histograms indicate calculated linewidths (full width at half-maximum). The solid histograms indicate longitudinal modes and the dashed and dotted histograms indicate transverse modes. The circles and triangles are experimental mode linewidths [Butler *et al.* (1977)].

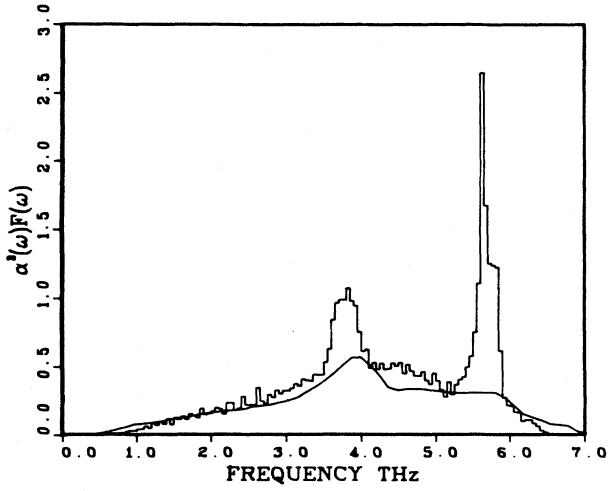

FIG. 22. Calculated (histogram) and experimental (smooth curve) spectral density $\alpha^2F(\omega)$ for Nb. The calculated spectral function should be broadened somewhat, since the δ function in Eq. (3.49b) should really be a Lorentzian of half-width $\gamma_i(\mathbf{q})$ [Butler *et al.* (1977)].

and Pinski *et al.* (1978) get 0.4 and 0.41 for Mo and Pd, respectively. The relatively large value of λ of order 0.4–0.5 found in these calculations for Pd is worth commenting on because Pd is not observed to be a superconductor. It is, however, known to have a significantly enhanced spin susceptibility. It is argued that it is the paramagnons that suppress T_c in this case. Pinski *et al.* (1978) give arguments for a mass renormalization due to spin fluctuations of $\lambda_{SF} \cong 0.34$ in Pd. This large value is interesting but remains to be confirmed.

Before turning to calculations of $\alpha^2F(\omega)$ for the A15 compounds, we describe an interesting application of formula (3.49a) for phonons. This prescription comes from the Fermi "golden rule" for electron scattering from the Fermi-surface state $\psi_{\mathbf{k}}$ to a state $\psi_{\mathbf{k}'}$ of energy $\hbar\omega_j(\mathbf{k}-\mathbf{k}')$ above the Fermi surface through the absorption of a phonon. But in the superconducting state, at zero temperature all electrons are bound in a condensate, and an energy 2Δ (twice the superconducting energy gap) needs to be supplied before energy conservation can be fulfilled. Hence a phonon with energy $\omega < 2\Delta$ will have no contribution to its lifetime from the electron-phonon interaction. Thus the corresponding neutron group should be sharper at $T=0$ than it is at a temperature that is greater than the critical temperature. This has been observed by Axe and Shirane (1973) in Nb_3Sn. In Fig. 23 we show neutron counts as a function of energy for the $[\zeta\zeta 0]T_1$ phonon in Nb_3Sn with $\zeta = 0.18$. The phonon energy $\hbar\omega_j$ is around 4.0 meV, which is less than $2\Delta \cong 7.0$ meV. At $T=6$ K, which is much less than the superconducting critical temperature of approximately 18 K, the phonon line shape is narrow (open circles) compared with the $T=26$ K case (solid dots). Axe and Shirane argue that the remaining linewidth at low T is within instrument resolution and that the difference between the high- and

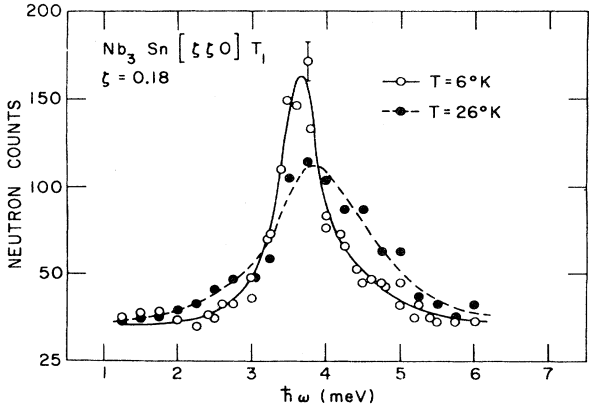

FIG. 23. Widths of low-energy $[\zeta\zeta 0]T_1$ acoustic phonons broaden appreciably at temperatures near T_c, the superconducting transition temperature. This figure shows the same phonon profile above and below $T_c \cong 18.0$ K [Axe and Shirane (1973)].

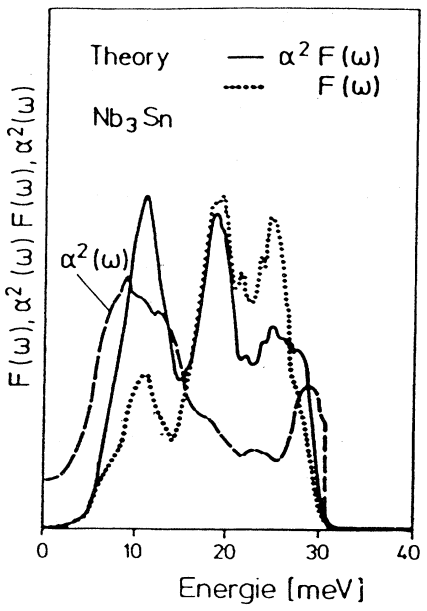

FIG. 24. Calculated electron-phonon spectral density $\alpha^2F(\omega)$ (solid curve) for Nb_3Sn compared with calculated phonon frequency distribution $F(\omega)$ (dotted curve). Also shown is the calculated result for $\alpha^2(\omega)$ as a function of ω (long dashed curve) [Weber (1984a)].

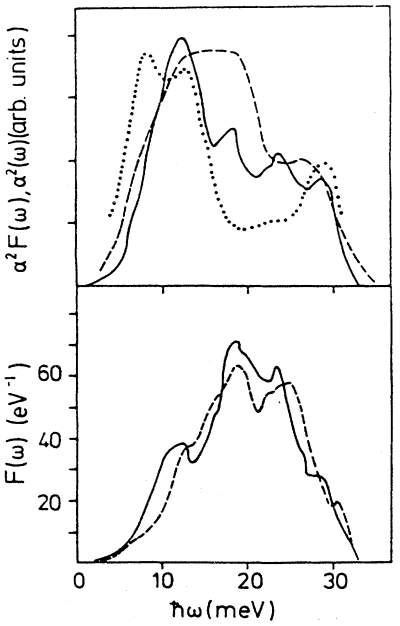

FIG. 25. Eliashberg function $\alpha^2F(\omega)$ and phonon density of states $F(\omega)$ for Nb_3Ge. The theoretical results are given by solid lines; the dashed lines for $\alpha^2F(\omega)$ and $F(\omega)$ are data. The dotted line represents the theoretical coupling function $\alpha^2(\omega)$ [Weber (1984)].

low-T results measures the electron-phonon contribution to the lifetime for this phonon.

Weber (1984a, and 1984b) has done extensive and detailed calculations of the electron-phonon spectral density for the A15 compounds. His results for Nb_3Sn are reproduced in Fig. 24. What is shown is $\alpha^2F(\omega)$ (solid curve), the phonon frequency distribution on $F(\omega)$ (dotted curve), and the ratio $\alpha^2F(\omega)/F(\omega)$, which is $\alpha^2(\omega)$. The results for the frequency dependence of $\alpha^2F(\omega)$ are quite different from those presented in Fig. 19, which involved no calculations. On the other hand, the calculated λ value is 1.5, which is not far off the measured value of 1.5–1.7 [Shen (1972)]. A similar situation holds for Nb_3Ge, and Weber's results are summarized in the upper frame of Fig. 25. In the lower frame we show a comparison between the tunneling-derived results (dashed line) for $\alpha^2F(\omega)$ by Kihlstrom and Geballe (1981) and the phonon frequency distribution measured by incoherent inelastic neutron scattering by Müller *et al.* (1982). A good deal of agreement is clearly evident between these two functions. The agreement with theory is not as good and the λ value obtained somewhat large at $\lambda=1.9$.

We mention two more calculations. Rietschel *et al.* (1980) have calculated spectral densities for several refractory compounds, namely, TiN, SnN, VN, and NbN with T_c's of 5.5, 10.0, 8.6, and 17.3, respectively. Their results are shown in Fig. 26, and the values obtained for λ are 0.45, 0.60, 1.54, and 1.23, respectively. These data cannot be compared with experiment at this time, but Rietschel *et al.* (1980) make the interesting point that spin fluctuations must limit the T_c value in at least VN. They also argue that this may be a much more general occurrence in materials with a spin-enhanced susceptibility. Finally, we simply mention that Schell *et al.* (1980) have presented similar calculations of $\alpha^2F(\omega)$ in some transition-metal hexaborides.

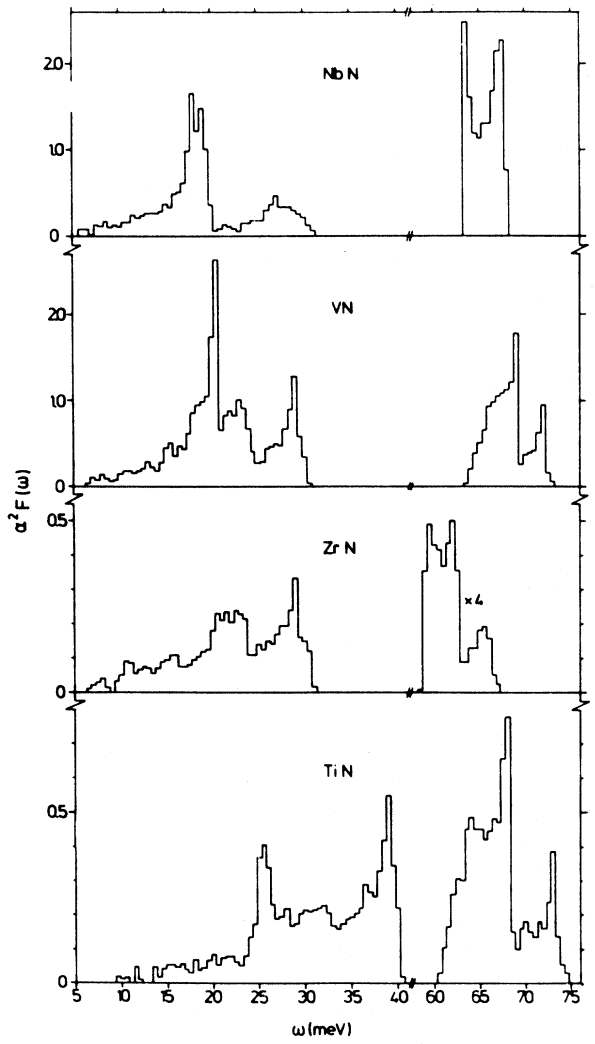

FIG. 26. Eliashberg function $\alpha^2F(\omega)$ for TiN, ZrN, VN, and NbN as calculated from Eq. (3.43). For ZrN the optical part has been reduced before plotting and must be multiplied by 4 [from Rietschel *et al.* (1980)].

I. Inversion for a joint phonon-exciton mechanism

Before leaving this section, we describe work on tunneling inversion when a high-energy mechanism is present in addition to a phonon mechanism. This may have some relevance for some of the high-T_c oxides like La-Sr-Cu-O and also $BaPb_{0.75}Bi_{0.25}O_3$ and $Ba_{0.6}K_{0.4}BiO_3$

Phonon structure as large in size as in Pb has been observed in tunnel junctions of $Ba(Pb,Bi)O_3$ [Batlogg *et al.* (1982)], which has a critical temperature of about 12.0 K. An attempt to invert the data so as to recover microscopic parameters failed Batlogg *et al.* (1982). No details are given of this failure. Presumably, a negative effective Coulomb repulsion parameter μ^* resulted, and the effective parameters did not reproduce well the initial data.

There is as yet no consensus as to the mechanism that is responsible for the superconductivity of the high-T_c oxides [Wolf and Kresin (1987)]. One possibility that is being explored is that it is a combined phonon-plus-excitonic mechanism [Marsiglio, Akis, and Carbotte (1987b, 1988); Marsiglio and Carbotte (1987b, 1988a)]. In this picture, La-Sr-Cu-O would have a significant phonon contribution and an attendant isotope effect as measured, while Y-Ba-Cu-O would be mainly excitonic with no or almost zero isotope effect. We wish to consider now the quasiparticle density of states for a combined phonon-and-exciton model. We also wish to invert the data assuming a pure phonon system so as to understand what the signature of the exciton peak might be when such a procedure is applied in the analyses of experiments.

To calculate the density of quasiparticle states normalized to the single-spin electronic density of states at the

Fermi energy [$N(0)$] which is given by Eq. (3.35), we need the complex frequency-dependent gap $\Delta(\omega)$ which follows from the zero-temperature Eliashberg equations (3.36) and (3.37) on the real-frequency axis. The kernel in these equations is now denoted by $g(\Omega)$, where $g(\Omega)$ is the sum of the usual electron-phonon spectral density denoted by $\alpha^2F(\Omega)$ and an exciton contribution $P(\Omega)$, presumably at higher frequencies. Given $g(\Omega)$ and the Coulomb pseudopotential μ^* with a fixed cutoff ω_c, we can calculate the quasiparticle density of states $N(\omega)$—a quantity that is measured in tunneling experiments. Conversely, given $N(\omega)$, we can recover, through an inversion procedure, the kernel $g(\Omega)$ and μ^*. In what follows, we shall invert $N(\omega)$ using the method of Galkin *et al.* (1979) as implemented by Mitrović and Carbotte (1981c, 1982).

The method of Galkin *et al.* (1979) used the previously given Eq. (3.39) for the normalized tunneling conductance, which we repeat here for convenience using a slightly different notation,

$$\frac{(dI/dV)_S}{(dI/dV)_N}\equiv\sigma(\omega)=\mathrm{Re}\left[\frac{|\omega|}{\sqrt{\omega^2-\Delta^2(\omega+i0^+)}}\right] \tag{3.50}$$

with ω representing the voltage. In addition, the dispersion relation

$$\mathrm{Im}\left[\frac{\omega}{\sqrt{\omega^2-\Delta^2(\omega+i0^+)}}\right]=\frac{2\omega}{\pi}P\int_{\Delta_0}^{+\infty}\frac{\sigma(\omega')-\sigma_{\mathrm{BCS}}(\omega')}{\omega^2-\omega'^2}d\omega' \tag{3.51}$$

holds. These two equations can be used to determine $\Delta(\omega)$ from the experimentally measured $\sigma(\omega)$. We note that this procedure does not require the use of the Eliashberg equations.

In the next step of the inversion procedure, one has to solve the equation

$$\begin{bmatrix}b_1\\b_2\\\vdots\end{bmatrix}=\begin{bmatrix}c_1&0&0&\cdots\\c_2&c_1&0&\\\vdots&&&\end{bmatrix}\begin{bmatrix}a_1\\a_2\\\vdots\end{bmatrix} \tag{3.52}$$

for the vector (a), where for the set of equally spaced frequencies

$$0=\Omega_0<\Omega_1<\Omega_2<\cdots$$

[see Eqs. (3.36) and (3.37) for the origin of these equations]

$$\begin{aligned}a_i&=\alpha^2F(\Omega)_{\mathrm{eff}}\,,\quad \Omega_{i-1}\le\Omega\le\Omega_i\,,\\ b_i&=\frac{1}{\pi}\mathrm{Im}[\Delta(\Delta_0+\Omega_i)Z(\Delta_0+\Omega_i)]\,,\\ c_i&=\int_{\Omega_{i-1}}^{\Omega_i}d\omega'\mathrm{Re}\left[\frac{\Delta(\Delta_0+\omega')}{[(\Delta_0+\omega')^2-\Delta^2(\Delta_0+\omega')]^{1/2}}\right],\end{aligned} \tag{3.53}$$

where $i=1,2,\ldots$ with

$$Z(\Delta_0+\omega)=1-\frac{1}{\Delta_0+\omega}\int_0^{+\infty}d\omega'\mathrm{Re}\left[\frac{\Delta_0+\omega'}{[(\Delta_0+\omega')^2-\Delta^2(\Delta_0+\omega')]^{1/2}}\right]\times\int_0^{+\infty}d\Omega\,\alpha^2(\Omega)F(\Omega)_{\mathrm{eff}}\left[\frac{1}{\omega'+\omega+\Omega+2\Delta_0+i\delta}-\frac{1}{\omega'-\omega+\Omega-i\delta}\right]. \tag{3.54}$$

In these equations Δ_0 is the gap edge at zero temperature $\mathrm{Re}[\Delta(\omega=\Delta_0)]=\Delta_0$. Equations (3.52) and (3.53) can be obtained by taking the imaginary part of Eq. (3.36) with $P(\Omega)=0$ and assuming that $\alpha^2F(\Omega)_{\mathrm{eff}}$ is known. A guess is made for $\alpha^2F(\Omega)_{\mathrm{eff}}$ and Z is calculated from (3.54). The resulting function together with the known $\Delta(\omega)$ determines matrices (b) and (c) via (3.53). Equation (3.52) is solved for the vector (a), which gives $\alpha^2F(\Omega)_{\mathrm{eff}}$, and the procedure is repeated until a fully converged $\alpha^2F(\Omega)_{\mathrm{eff}}$ is obtained. With this inversion procedure, the Coulomb repulsion parameter $\mu^*(\omega_c)$ does not come in.

In Fig. 27, we show our input spectrum for $g(\Omega)$. For the lower frequency distribution, we use the tunneling-derived electron-phonon spectral density obtained for pure Pb but reduced by a factor of 0.83, so that the mass-renormalization value is $\lambda_{\mathrm{ep}}=1.28$. The high-frequency Lorentzian peak is meant to simulate an excitonic contribution and has a mass-enhancement factor of $\lambda_{\mathrm{ex}}=0.67$. For these parameters the zero-temperature gap edge $\Delta_0\cong7.3$ meV. The quasiparticle density of states that is obtained in this way is shown in Fig. 28 (solid curve) in the low-energy region. If the data in this region are inverted without reference to the excitonic structure that appears at high energy, we recover very nearly the input electron-phonon spectral density $\alpha^2F(\Omega)$ divided by the renormalization factor $(1+\lambda_{\mathrm{ex}})$. This was expected from some previous work [Daams, Mitrović, and Carbotte (1981); Zarate and Carbotte (1984)]. The first signature of the effect of the exciton peak is that this efective phonon spectral density

$$\alpha^2_{\mathrm{eff}}F(\Omega)\cong\frac{\alpha^2F(\Omega)}{1+\lambda_{\mathrm{ex}}} \tag{3.55}$$

is too small to be consistent with a gap edge (Δ_0) value of ~7.3 meV, and, in fact, a negative effective Coulomb pseudopotential μ^*_{eff} (-0.176) is required to reproduce

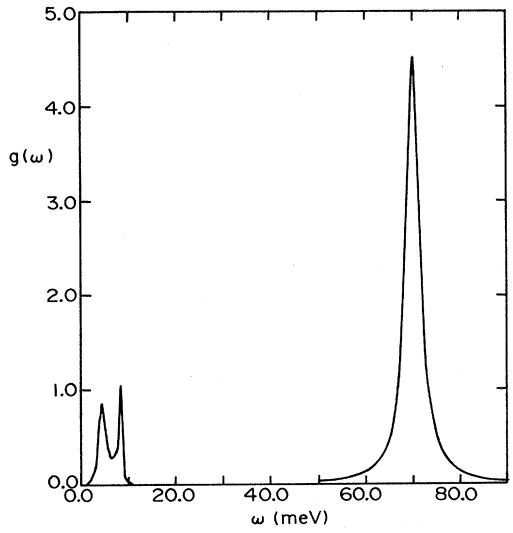

FIG. 27. Eliashberg spectral density $g(\omega)$ used in this work. It is made up of the sum of an electron-phonon contribution $\alpha^2F(\omega)$ at low energy and an excitonic part $P(\omega)$ at higher energy centered on 70 meV (Lorentzian peak).

this value of Δ_0. This negative value of μ^*_{eff} of course, simulates the presence of the excitonic peak at a higher energy, which was not used in the inversion. Another important signature is that the effective kernels cannot reproduce exactly the original quasiparticle density of states, as is shown in the dashed curve of Fig. 28. While it overlaps the solid curve, there are some differences, and we must conclude that no effective phonon kernel plus negative μ^* can ever reproduce exactly the effect of a phonon-plus-exciton kernel. We can therefore take the failure of the inversion procedure as outlined here as indirect evidence of an additional high-energy mechanism adding on to a phonon contribution. This second mechanism need not be excitonic in origin. It need only be at higher energies and describable, in a first approximation, by some high-energy peak in the Eliashberg equations.

The effective electron-phonon mass renormalization corresponding to the spectral density (3.55) is small, equal approximately to 0.77, and is, simply, $\lambda_{ep}/(1+\lambda_{ex})$. On its own with $\mu^*=0$, it would give a small gap edge and a small amount of phonon structure. On the other hand, the original phonon kernel plus exciton leads to a large gap Δ_0 and considerable structure in the phonon region. That this is the case can be seen when Figs. 29 and

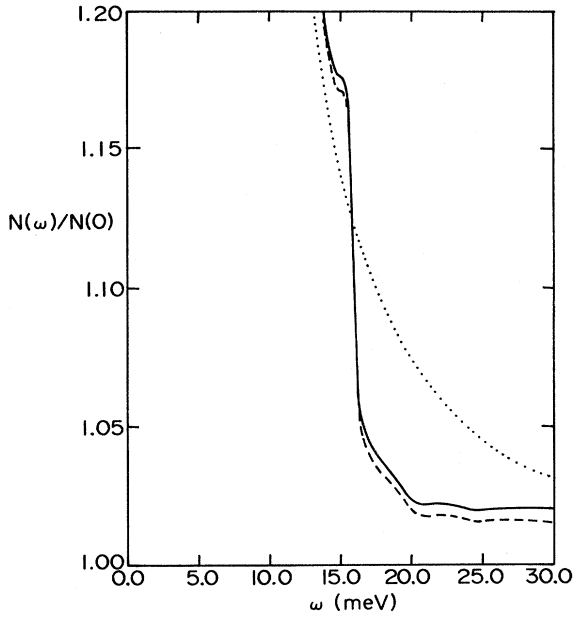

FIG. 28. Quasiparticle density of states (solid curve) obtained from the combined phonon and exciton spectrum of Fig. 27. For $\mu^*=0.1$, we get a gap edge of 7.27 meV. Superimposed are results (dashed line) obtained from the effective Eliashberg kernels ($\lambda^{\text{eff}}_{ep}\cong 0.77$ and $\mu^*_{\text{eff}}\cong -0.176$) derived by inversion of the solid curve. The effective kernels do not reproduce the density of states exactly. The dotted curve is the BCS density of states, included for reference.

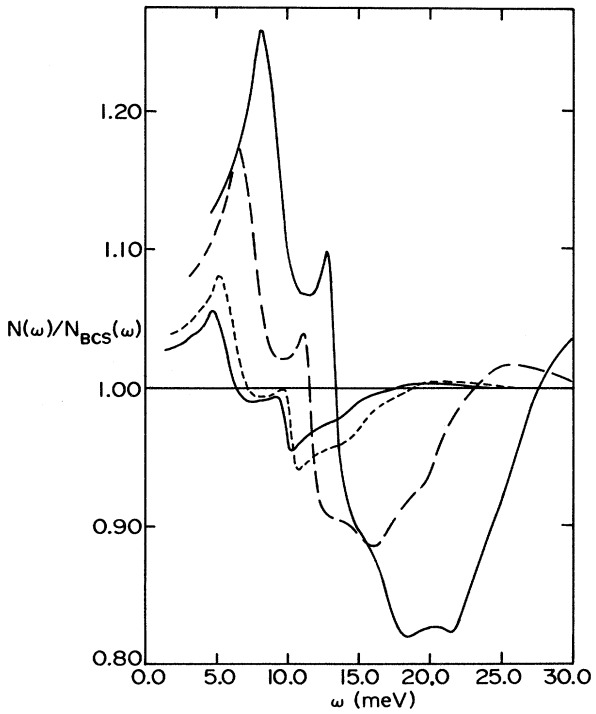

FIG. 29. Ratio of the quasiparticle density of states $N(\omega)$ to its BCS value $N_{\text{BCS}}(\omega)$ for various systems. In all cases $\mu^*\cong 0.08$ and the Pb electron-phonon spectral density is used, but with a multiplicative factor of B included so as to increase or decrease the coupling. The curves exhibit more structure as B increases with $B=0.83$, 1.00, 2.83, and 3.83, and the gap edge Δ_0 is, respectively, 1.25, 1.63, 3.02, and 4.57 meV.

30 are compared.

In Fig. 29, we show results of several runs using, in all cases, a Pb spectral shape with $\mu^* \cong 0.08$. Only the phonon region is shown and what is plotted in $N(\omega)$ divided by the BCS density of states

$$\frac{N_{\rm BCS}(\omega)}{N(0)} = {\rm Re}\left[\frac{\omega}{\sqrt{\omega^2-\Delta_0^2}}\right], \tag{3.56}$$

a quantity that involves only the gap edge. The various curves shown start at their respective gap edges Δ_0 and are for $B=0.83$, $B=1.00$, $B=2.83$, and $B=3.83$ in order of increasing size. Here B is a factor multiplying the original Pb $\alpha^2F(\Omega)$ so as to increase or decrease its value. The gap edges are, respectively, 1.25, 1.63, 3.02, and 4.57 meV and correspond to ever increasing electron-phonon spectral density. These curves are to be compared with the curve in Fig. 30, which applies to the case of phonon plus exciton that we have previously described. It has a $\Delta_0=7.27$ meV for a $\mu^*=0.1$. It is clear that the amount of structure obtained in the phonon region is much larger than that obtained for the same $\alpha^2F(\Omega)$ along (i.e., without an additional exciton peak) and very much larger than for $\alpha^2_{\rm eff}F(\Omega)$. It is only slightly smaller than the $B=2.83$ case. As first pointed out by Kus and Carbotte (1979) within the context of hydrogen in aluminum, a high-energy peak in the Eliashberg kernel, which goes unrecognized in a tunneling experiment, effectively enhances the structure in the phonon region at lower energy and could lead one to think that the phonon kernel is larger than it actually is.

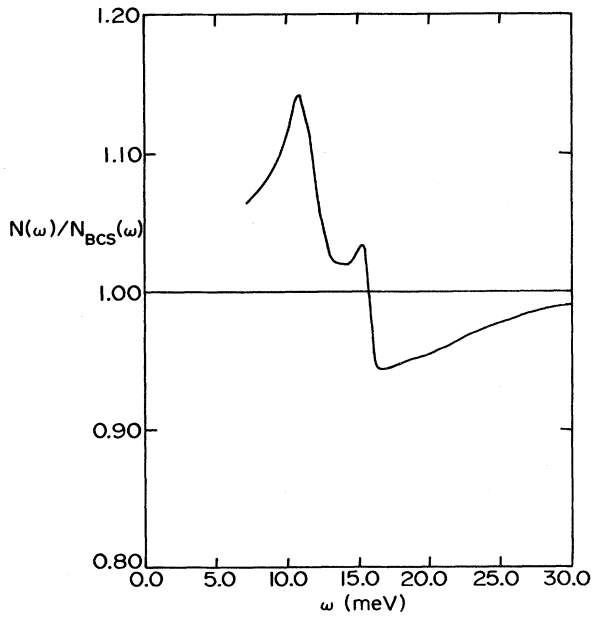

FIG. 30. Ratio of the quasiparticle density of states $N(\omega)$ to its BCS value $N_{\rm BCS}(\omega)$ for the combined phonon-plus-exciton spectrum of Fig. 27. This case corresponds to $B=0.83$ and has a gap edge of $\Delta_0=7.27$ meV for $\mu^*=0.01$. The amount of structure obtained is much larger than that for the corresponding $B=0.83$ case of Fig. 29.

IV. THE ENERGY GAP AT ZERO TEMPERATURE

A. Gap for specific systems and comparison with experiment

An important check on the validity of the Eliashberg equations for phonon superconductors is the calculation of superconducting properties from tunneling-derived microscopic parameters $\alpha^2F(\omega)$ and μ^* and comparison with experiment. One such quantity is the energy gap. Mitrović, Zarate, and Carbotte (1984) have carried out such calculations for many superconductors. The sources for the spectra used are specified in Table I and the results given in Table III. In all cases, the imaginary-axis Eliashberg equations (2.1) and (2.2) were used with the μ^* parameter fit to get the measured T_c. It can be seen from the table that such fitted values are slightly different from those given by tunneling. This is as expected, since a sharp cutoff on the real axis is not completely equivalent to a sharp cutoff on the imaginary axis [Leavens and Fenton (1980)]. Furthermore, μ^* depends on the cutoff frequency (ω_c) used. This frequency is not always quoted in tunneling inversion work, although this is not expected to affect the value of $\alpha^2F(\omega)$. In almost all cases considered in Table III, we have used 3 times the maximum frequency in the spectral density. Given in Table III are the theoretical and experimental gap values as well as the percent difference between these two quantities. The agreement is very good in almost all cases and is at the level of a few percent. A notable exception is Nb_3Sn, for which we have no explanation except perhaps that the measured value has been underestimated. Usually, the larger the gap value obtained in a tunneling experiment, the higher the quality of the data. We note, also, that all the values quoted in Table III were obtained using the analytic continuation technique of Vidberg and Serene (1977) described in the previous section, which allows us to go from the imaginary to the real frequency axis. The gap edge Δ_0 is determined from the complex real-axis gap at zero temperature through the equation $\Delta_0={\rm Re}[\Delta(\omega=\Delta_0, T=0)]$. On the whole, Table III is a striking confirmation of the validity of Eliashberg theory and of the electron-phonon mechanism.

Mitrović, Zarate, and Carbotte (1984) derived an approximate formula for the ratio $2\Delta_0/k_BT_c$ valid in the strong-coupling regime. The form they suggest, which is derived in Appendix B, is the same as that given earlier by Geilikman and Kresin [1965, 1966; Geilikman *et al.* (1975)] but with different numerical factors. Contrary to the previous work, the characteristic phonon energy that enters the new formula is well defined and is $\omega_{\ln}$ given

first by Allen and Dynes (1975) in the context of improved McMillan-type equations. The method of derivation employed by Mitrović, Zarate, and Carbotte (1984) appears to be very different from that used by Geilikman and Kresin (1965, 1966), so that, in a sense, the calculations are complementary. The final form obtained is [Eq. (B41)]

$$\frac{2\Delta_0}{k_B T_c}=3.53\left[1+12.5\left[\frac{T_c}{\omega_{\ln}}\right]^2 \ln\left[\frac{\omega_{\ln}}{2T_c}\right]\right], \qquad (4.1)$$

where the numerical factors 12.5 and 2 were chosen to fit as well as is possible all the numerical data on real materials. This is illustrated in Fig. 31 where the solid dots are the calculated values of Table IV. In the table, we give the calculated T_c values, which are also the experimental numbers. All calculations were done for a cutoff frequency of 6 times the maximum phonon energy and the μ^* fit to T_c using a sharp cutoff on the imaginary axis. The difference in μ^* between Tables III and IV reflects the different cutoffs. In addition, λ, $\omega_{\ln}$, A, and $\omega_{\max}$ are entered in columns 4 to 7, respectively; the strong-coupling index $T_c/\omega_{\ln}$ in column 8; and the values of $2\Delta_0/k_B T_c$, in column 9. These data correspond to the solid dots of Fig. 31. The deviations off the dashed trend curve are due to details of $\alpha^2F(\omega)$ that are not captured by a single parameter $T_c/\omega_{\ln}$. We note that the BCS value results for $T_c/\omega_{\ln}\to 0$, and that the conventional strong-coupling region extends up to $T_c/\omega_{\ln}\cong 0.25$.

It is of some interest to understand a little better why

TABLE III. Comparison of calculated and experimental gap edge.

System	μ^*_{tunn}	μ^*_{fitted}	Δ_0^{expt} (meV)	Δ_0^{calc} (meV)	$\frac{\Delta_0^{\text{calc}}-\Delta_0^{\text{expt}}}{\Delta_0^{\text{expt}}}$
Al		0.1472		0.18	
Sn	0.11	0.1143	0.606	0.599	−1.1
Nb_3Sn	0.15	0.1575	3.1	3.53	+13.9
Nb (Robinson)	0.11	0.1158	1.46	1.57	+7.5
Nb (Butler)		0.2735		1.53	
Nb (Arnold)	0.16	0.1854	1.51	1.54	+2
V	0.15	0.19	0.8	0.85	+6
$Nb_{0.75}Zr_{0.25}$	0.10±0.02	0.1808	1.9	1.93	+1.6
Ta	0.11	0.1169	0.72	0.71	−1.4
In	0.125	0.1130	0.541	0.556	+2.8
$In_{0.9}Tl_{0.1}$	0.12	0.1271	0.530	0.540	+1.9
$In_{0.73}Tl_{0.27}$	0.13	0.1358	0.57	0.564	−1.0
$In_{0.67}Tl_{0.33}$	0.13	0.1314	0.54	0.543	+0.6
$In_{0.57}Tl_{0.43}$	0.14	0.1387	0.42	0.426	+1.4
$In_{0.50}Tl_{0.50}$	0.13	0.1377	0.41	0.41	0.0
$Pb_{0.8}Tl_{0.2}$	0.122	0.1239	1.28	1.33	+3.9
$In_{0.27}Tl_{0.73}$	0.11	0.1164	0.64	0.64	0.0
$In_{0.17}Tl_{0.83}$	0.12	0.1188	0.535	0.545	+1.9
$In_{0.07}Tl_{0.93}$	0.13	0.1311	0.45	0.46	+2.2
Tl	0.135	0.1281	0.366	0.382	+4.0
$Pb_{0.4}Tl_{0.6}$	0.113	0.1149	0.805	0.822	+2.1
$Pb_{0.6}Tl_{0.4}$	0.126	0.1262	1.08	1.11	+2.8
Pb	0.131	0.1446	1.40	1.40	0.0
$Pb_{0.9}Bi_{0.10}$	0.095	0.1120	1.54	1.55	+0.6
$Pb_{0.8}Bi_{0.2}$	0.111	0.1127	1.61	1.67	+3.7
$Pb_{0.7}Bi_{0.3}$	0.11	0.1154	1.77	1.82	+2.8
$Pb_{0.65}Bi_{0.35}$	0.111	0.0996	1.84	1.98	+7.6
$Pb_{0.60}Tl_{0.02}Bi_{0.02}$	0.137	0.1538	1.50	1.49	−0.7
$Tl_{0.90}Bi_{0.10}$	0.119	0.1114	0.354	0.374	+5.6
Hg	0.11	0.1197	0.83	0.83	0.0
Amorphous Bi	0.105	0.0917	1.21	1.30	+7.4
Amorphous $Pb_{0.50}Bi_{0.50}$	0.14	0.1338	1.51	1.57	+4.0
Amorphous $Pb_{0.75}Bi_{0.25}$	0.14	0.1340	1.48	1.53	+3.4
Amorphous Ga	0.17	0.1632	1.68	1.74	+3.6

some materials fall off the main-trend curve in Fig. 31. Coombes and Carbotte (1986a) have given a detailed analysis of these deviations. To be specific, they consider the case of Pb for which $T_c/\omega_{\ln}=0.128$. To get some feeling for the dependence, in this case, of $2\Delta_0/k_BT_c$ on shape of the spectral density, they scale several model base spectra $\alpha_0^2F(\omega)$ to get $\alpha^2F(\omega)^*=B\alpha_0^2F(b\omega)$ with B and b constants, as described in Sec. II. In this way, they can start with the spectrum for any given material (X) and get the Pb T_c value, as well as $T_c/\omega_{\ln}$ value, by adjusting the two constants B and b. Once this is done, they can recalculate the gap-to-critical-temperature ratio and see how it compares with that for pure Pb. Such rescaled spectra based on Sn and In are shown in Fig. 1. Results for $2\Delta_0/k_BT_c$ are given in the inset of Fig. 31. We see that this ratio is, indeed, dependent not only on $T_c/\omega_{\ln}$ value, but also on the shape of $\alpha^2F(\omega)^*$. The differences are not very large, however. Larger differences can, of course, be found if more extreme model spectra are used instead of real-material shapes.

B. Functional derivatives

The functional derivative of the gap edge Δ_0 as a function of $\alpha^2F(\omega)$ gives information on the relative importance of different phonon modes on Δ_0. Such derivatives can be computed directly by augmenting a given base $\alpha^2F(\omega)$ spectrum by an infinitesimal delta function at a particular frequency ω, as was done by Mitrović *et al.* (1980). Some of their results are reproduced in Fig. 32 where we plot $\delta\ln\Delta_0/\delta\alpha^2F(\Omega)$ against Ω/Δ_0 for Tl (dot-dashed), Nb (dotted), Pb (dashed), and Nb_3Sn (solid). These are to be compared with $\delta\ln T_c/\delta\alpha^2F(\Omega)$ for the same materials given in Fig. 33. The shape of the functional derivative curves for Δ_0 are very similar to those

TABLE IV. Superconducting properties of conventional materials.

Material	T_c (meV)	$\mu^*(N=6)$	λ	$\omega_{\ln}$ (meV)	Area (meV)	$\omega_{\max}$ (meV)	$T_c/\omega_{\ln}$	$\frac{2\Delta_0}{k_BT_c}$
Al	0.1017	0.147	0.43	25.50	5.74	41.4	0.004	3.535
V	0.4621	0.223	0.80	14.78	6.76	33.1	0.031	3.675
Ta	0.3862	0.121	0.69	11.06	4.18	20.9	0.035	3.673
Sn	0.3233	0.116	0.72	8.40	3.42	18.8	0.038	3.705
Tl	0.2034	0.132	0.80	4.45	2.00	10.9	0.046	3.753
$Tl_{0.9}Bi_{0.1}$	0.1983	0.113	0.78	4.15	1.86	10.5	0.048	3.769
In	0.2931	0.116	0.81	5.83	2.74	15.8	0.050	3.791
Nb (Butler)	0.7931	0.373	1.22	13.88	9.35	26.9	0.057	3.876
Nb (Arnold)	0.7931	0.186	1.01	12.83	7.25	28.3	0.062	3.883
V_3Si_1	1.4741	0.142	1.00	21.11	11.80	49.3	0.070	3.933
V_3Si (Kihl.)	1.4132	0.139	1.00	19.88	10.76	44.5	0.071	3.935
Nb (Rowell)	0.7931	0.118	0.98	10.69	6.29	28.5	0.074	3.964
Mo	0.7586	0.071	0.90	9.95	5.47	33.0	0.076	3.968
$Pb_{0.4}Tl_{0.6}$	0.3966	0.115	1.15	4.17	2.74	11.0	0.095	4.134
La	0.4340	0.040	0.98	4.37	2.56	15.0	0.099	4.104
V_3Ga	1.2931	0.090	1.14	12.54	8.56	37.0	0.103	4.179
Nb_3Al (2)	1.2070	0.082	1.20	10.66	7.51	35.7	0.113	4.248
Nb_3Ge (2)	1.7240	0.238	1.60	15.17	13.34	31.3	0.114	4.364
$Pb_{0.6}Tl_{0.4}$	0.5086	0.125	1.38	4.27	3.35	10.9	0.119	4.352
Pb	0.6198	0.144	1.55	4.83	4.03	11.0	0.128	4.497
Nb_3Al (3)	1.6121	0.225	1.70	12.52	12.72	35.7	0.129	4.461
$Pb_{0.8}Tl_{0.2}$	0.5862	0.121	1.53	4.32	3.71	10.9	0.136	4.505
Hg	0.3612	0.124	1.62	2.47	2.64	14.3	0.146	4.591
Nb_3Sn	1.5603	0.156	1.70	10.68	10.69	28.7	0.146	4.567
$Pb_{0.9}Bi_{0.1}$	0.6595	0.105	1.66	4.33	3.98	9.9	0.152	4.674
Nb_3Al (1)	1.4138	0.127	1.70	9.06	9.32	35.7	0.156	4.617
Nb_3Ge (1)	1.7240	0.088	1.60	10.80	10.33	34.3	0.160	4.601
$Pb_{0.8}Bi_{0.2}$	0.6853	0.111	1.88	3.99	4.21	11.0	0.172	4.843
$Pb_{0.7}Bi_{0.3}$	0.7284	0.109	2.01	4.01	4.46	10.4	0.182	4.968
$Pb_{0.65}Bi_{0.35}$	0.7716	0.091	2.13	3.85	4.60	10.1	0.200	5.081
$Pb_{0.5}Bi_{0.5}$	0.6026	0.136	3.00	1.88	4.30	13.1	0.320	5.194
Ga	0.7379	0.174	2.25	3.04	6.15	27.0	0.243	4.722
$Pb_{0.75}Bi_{0.25}$	0.5957	0.136	2.76	2.07	4.20	10.4	0.288	5.119
Bi	0.5267	0.091	2.45	1.64	3.53	14.0	0.320	4.916

for T_c. In general, however, they fall slightly above in magnitude, and the peak is at a somewhat lower frequency. A rule of thumb is

$$2\Omega^*(\Delta_0)\sim\Omega^*(T_c)\sim 7\ k_B T_c\ , \tag{4.2}$$

where $\Omega^*(\Delta_0)$ is the optimum frequency for Δ_0 and $\Omega^*(T_c)$ for T_c.

From a knowledge of the functional derivative given in Figs. 32 and 33, we can construct the functional derivative of the dimensionless ratio $2\Delta_0/k_B T_c$ through the formula

$$\frac{\delta(2\Delta_0/k_B T_c)}{\delta\alpha^2F(\Omega)}=\frac{2\Delta_0}{k_B T_c}\left[\frac{\delta\ln\Delta_0}{\delta\alpha^2F(\Omega)}-\frac{\delta\ln T_c}{\delta\alpha^2F(\Omega)}\right]. \tag{4.3}$$

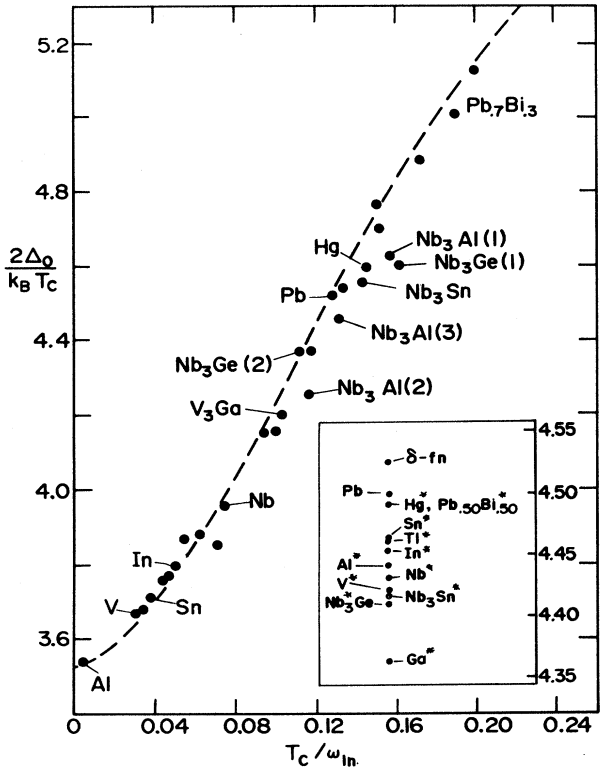

FIG. 31. Ratio $2\Delta_0/k_B T_c$ vs $T_c/\omega_{\ln}$. The solid dots represent the accurate results from the full numerical solutions of the Eliashberg equations. Experiment tends to agree to within 10 percent. In increasing order of $T_c/\omega_{\ln}$, the dots correspond to the following systems: Al, V, Ta, Sn, Tl, $Tl_{0.9}Bi_{0.1}$, In, Nb (Butler), Nb (Arnold), V_3Si (1), V_3Si (Kihl), Nb (Rowell), Mo, $Pb_{0.4}Tl_{0.6}$, La, V_3Ga, $Nb_3Al(2)$, Nb_3Ge (2), $Pb_{0.6}Tl_{0.4}$, Pb, Nb_3Al (3), $Pb_{0.8}Tl_{0.2}$, Hg, Nb_3Sn, $Pb_{0.9}Bi_{0.1}$, Nb_3Al (1), Nb_3Ge (1), $Pb_{0.8}Bi_{0.2}$, $Pb_{0.7}Bi_{0.3}$, and $Pb_{0.65}Bi_{0.35}$. The drawn curve corresponds to $2\Delta_0/k_B T_c=3.53[1+12.5(T_c/\omega_{\ln})^2\ln(\omega_{\ln}/2T_c)]$. The insert shows results for different $\alpha^2F(\omega)$ spectra as defined in the text. They all correspond to the same value of T_c and of $\omega_{\ln}$ as Pb.

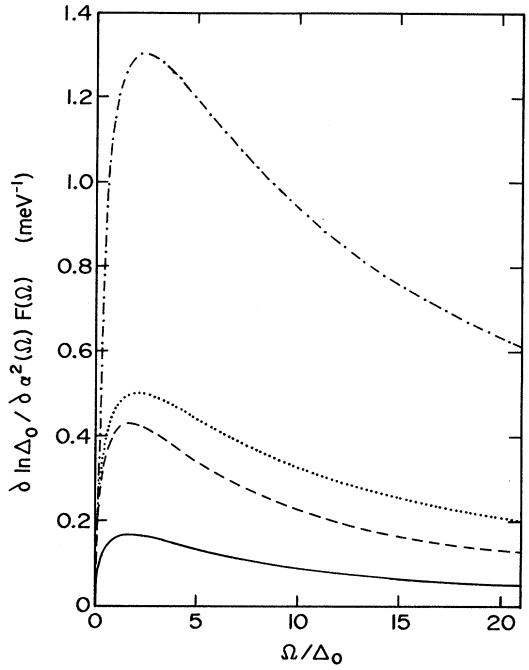

FIG. 32. Functional derivative of the gap edge at zero temperature Δ_0 normalized to Δ_0, i.e., $\delta\ln\Delta_0/\delta\alpha^2F(\Omega)$ as a function of Ω/Δ_0 for Nb_3Sn (solid curve), Pb (dashed curve), Nb (dotted curve), and Ta (dot-dashed curve).

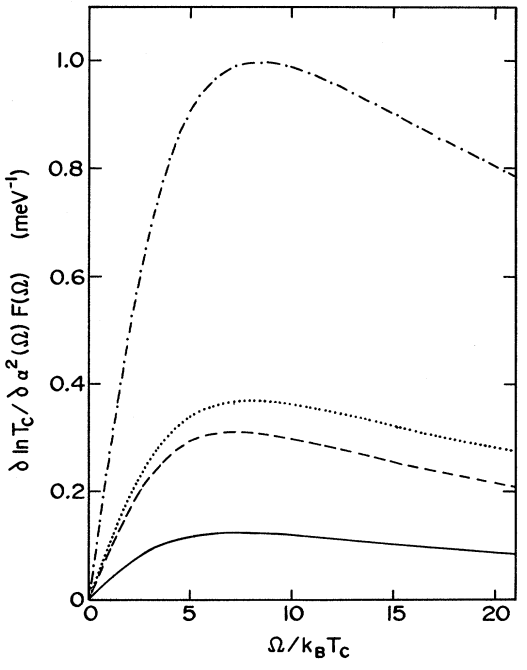

FIG. 33. Functional derivative of the critical temperature T_c normalized to T_c, i.e., $\delta\ln T_c/\delta\alpha^2F(\Omega)$ as a function of $\Omega/k_B T_c$ for Nb_3Sn (solid curve), Pb (dashed curve), Nb (dotted curve), Ta (dot-dashed curve).

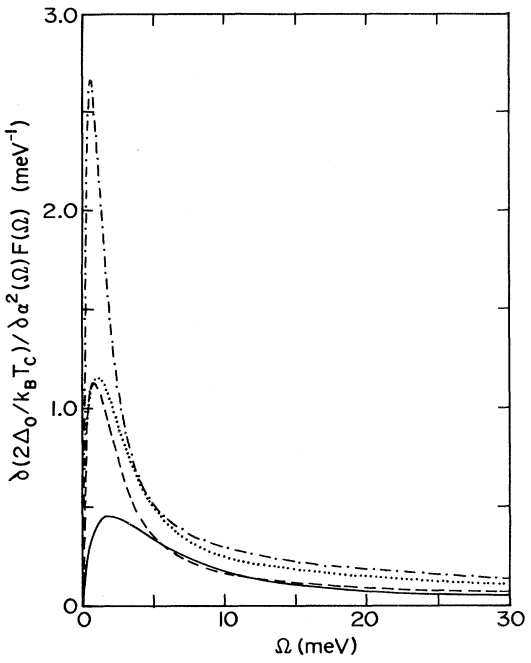

FIG. 34. Functional derivative of the dimensionless ratio of the gap to critical temperature with respect to $\alpha^2F(\Omega)$, i.e., $\delta[2\Delta_0/k_BT_c]/\delta\alpha^2F(\Omega)$ as a function of Ω for Nb_3Sn (solid curve), Pb (dashed curve), Nb (dotted curve), and Ta (dot-dashed curve).

Results for the same four materials as described in Figs. 32 and 33 are given in Fig. 34. We see that this functional derivative is largest for the weakest coupling material Ta and that, in all cases, it peaks at lower energy than either the functional derivative of Δ_0 or T_c. As well, the peak is much sharper and the rule of thumb for the frequency at maximum is now

$$6\Omega^*(2\Delta_0/k_BT_c)\sim 8k_BT_c\ . \tag{4.4}$$

To maximize this ratio for a given area under $\alpha^2F(\Omega)$, we would need to place the entire spectrum at rather low energies. In fact, we shall analyze this in detail later on in this section. First, though, we wish to describe work by Coombes and Carbotte (1987), who have proposed a more elegant method for getting the functional derivative of the gap. They used Padé approximants to analytically continue directly the infinitesimal part of the gap.

C. Formal theory

Introducing $\overline{\Delta}_n\equiv\Delta(i\omega_n)/|\omega_n|$ into Eqs. (2.1) and (2.2) and substituting the second equation into the first gives $[\lambda(n-m)\equiv\lambda(i\omega_n-i\omega_m)]$

$$\overline{\Delta}_n\left[\omega_n+\pi T\sum_m\lambda(n-m)\frac{1}{\sqrt{1+\overline{\Delta}_m^2}}\right]=\pi T\sum_m[\lambda(n-m)-\mu^*]\frac{\overline{\Delta}_m}{\sqrt{1+\overline{\Delta}_m^2}}\ . \tag{4.5}$$

For the rest of the mathematical manipulations of this section, which are rather tedious, we shall denote $\alpha^2F(\Omega)\equiv G(\Omega)$. Besides a dependence on temperature, Eq. (4.5) depends explicitly on $G(\Omega)$ through the λ's. Denoting this explicit variation by $\delta\overline{\Delta}_n/\delta G(\Omega)$, we find the equation

$$\sum_m H_{n,m}\frac{\delta\overline{\Delta}_m}{\delta G(\Omega)}=h_n \tag{4.6}$$

with

$$H_{n,m}=\delta_{n,m}\left[\frac{\omega_n}{\pi T}+\sum_{m'=1}^{N_c}[\lambda(n-m')-\lambda(n+m'-1)]\frac{1}{\sqrt{1+\overline{\Delta}_{m'}^2}}\right]-\overline{\Delta}_n[\lambda(n-m)-\lambda(n+m-1)]\frac{\overline{\Delta}_m}{(1+\overline{\Delta}_m^2)^{3/2}}-[\lambda(n-m)+\lambda(n+m-1)-2\mu^*]\frac{1}{(1+\overline{\Delta}_m^2)^{3/2}} \tag{4.7}$$

and

$$h_n=\sum_{m=1}^{N_c}\frac{2\Omega}{\Omega^2+(2\pi T)^2(n-m)^2}\frac{-\overline{\Delta}_n+\overline{\Delta}_m}{\sqrt{1+\overline{\Delta}_m^2}}+\sum_{m=1}^{N_c}\frac{2\Omega}{\Omega^2+(2\pi T)^2(n+m-1)^2}\frac{\overline{\Delta}_n+\overline{\Delta}_m}{\sqrt{1+\overline{\Delta}_m^2}}\ . \tag{4.8}$$

This last quantity is completely known from the solution of (4.5); and so Eq. (4.6) is now explicit. But $\overline{\Delta}_n$ is also an explicit function of temperature $T=tT_c$, with t the reduced temperature that we take as fixed. The full variation of $\overline{\Delta}_n$ is given by

$$\frac{\delta\overline{\Delta}_n}{\delta G(\Omega)}=\frac{\delta\overline{\Delta}_n}{\delta G(\Omega)}+\frac{\partial\overline{\Delta}_n}{\partial T}t\frac{\delta T_c}{\delta G(\Omega)}\ , \tag{4.9}$$

where $\partial\overline{\Delta}_n/\partial T$ satisfies the equation

$$\sum_m H_{n,m}T\frac{\partial\overline{\Delta}_m}{\partial T}=g_n \tag{4.10}$$

with

$$g_n=\sum_m[\Delta\lambda(n-m)-\Delta\lambda(n+m-1)]\frac{\overline{\Delta}_n}{\sqrt{1+\overline{\Delta}_m^2}} -\sum_m[\Delta\lambda(n-m)+\Delta\lambda(n+m-1)]\frac{\overline{\Delta}_m}{\sqrt{1+\overline{\Delta}_m^2}} , \tag{4.11}$$

where

$$\Delta\lambda(l)=4\int_0^\infty d\Omega\frac{\alpha^2F(\Omega)\Omega}{[\Omega^2+(2\pi T)^2l^2]^2}(2\pi T)^2l^2 . \tag{4.12}$$

Thus our final equation is

$$\frac{\delta\overline{\Delta}_n}{\delta G(\Omega)}=\sum_m H^{-1}_{n,m}\left[h_m+g_m\frac{1}{T_c}\frac{\delta T_c}{\delta G(\Omega)}\right] . \tag{4.13}$$

From a knowledge of $\delta\overline{\Delta}_n/\delta G(\Omega)$ and $\overline{\Delta}_n$, we want to construct $\Delta(\omega,T)$ on the real axis and $\delta\Delta(\omega,T)/\delta G(\Omega)$. This can be done by analytic continuation using Padé approximants as described in the previous section.

First, we note that the $\overline{\Delta}_n$'s used in our numerical work are related to the Δ_n's by $\overline{\Delta}_n\omega_n=\Delta_n$ for positive n with the analytic continuation of Δ_n being $\Delta(\omega,T)$. Thus we have

$$\frac{\delta\Delta_n}{\delta G(\Omega)}=\omega_n\frac{\delta\overline{\Delta}_n}{\delta G(\Omega)}+\frac{\Delta_n}{T_c}\frac{\delta T_c}{\delta G(\Omega)} . \tag{4.14}$$

The Matsubara gaps for the system with the added piece $\epsilon\delta(\Omega-\omega_0)$ are denoted by $\Delta'(i\omega_n')$ and related to those with $\epsilon=0$ by the equation

$$\Delta'(i\omega_n')=\Delta(i\omega_n)+\epsilon\frac{\delta\Delta(i\omega_n)}{\delta G(\Omega)} . \tag{4.15}$$

For t constant, T' and T are related by the ratio $(\delta T_c+T_c)/T_c=1+\delta T_c/T_c$ with $\delta T_c=\epsilon[\delta T_c/\delta G(\Omega)]$, so that we can write

$$\Delta'(i\omega_n)=\Delta(i\omega_n/(1+\delta T_c/T_c))+\epsilon\frac{\delta\Delta(i\omega_n)}{\delta G(\Omega)} . \tag{4.16}$$

Both sides of Eq. (4.16) can now be analytically continued to get

$$\Delta'(\omega,T)=\Delta\left[\omega\left[1-\frac{\delta T_c}{T_c}\right],T\right]+\epsilon\mathcal{A}\left[\frac{\delta\Delta(i\omega_n)}{\delta G(\Omega)}\right] , \tag{4.17}$$

where the last term stands for analytical continuation using, in our case, Padé approximants. We get, on expanding (4.17),

$$\Delta'(\omega,T)=\Delta(\omega,T)-\omega\frac{\partial\Delta(\omega,T)}{\partial\omega}\frac{\delta T_c}{T_c}+\epsilon\mathcal{A}\left[\frac{\delta\Delta(i\omega_n)}{\delta G(\Omega)}\right] . \tag{4.18}$$

For a fixed value of ω, this last equation tells us that on rearranging terms

$$\frac{\delta\Delta(\omega,T)}{\delta G(\Omega)}=\mathcal{A}\left[\frac{\delta\Delta(i\omega_n)}{\delta G(\Omega)}\right]-\omega\frac{\partial\Delta(\omega,T)}{\partial\omega}\frac{1}{T_c}\frac{\delta T_c}{\delta G(\Omega)} \tag{4.19}$$

In addition, the gap $\Delta_0'=\Delta_0+\epsilon[\delta\Delta_0/\delta G(\Omega)]$ is obtained from the equation

$$\Delta_0'=\mathrm{Re}\Delta'(\omega=\Delta_0',T)\equiv\Delta_1'(\omega=\Delta_0',T) , \tag{4.20}$$

which leads to

$$\frac{\delta\Delta_0}{\delta G(\Omega)}=\lim_{\epsilon\to0}\frac{\Delta'(\Delta_0')-\Delta(\Delta_0)}{\epsilon}=\frac{\mathcal{A}_1\left[\frac{\delta\Delta(i\omega_n)}{\delta G(\Omega)}\right]\Big|_{\Delta_0}-\Delta_0\frac{\partial\Delta_1(\omega,T)}{\partial\omega}\Big|_{\Delta_0}\frac{1}{T_c}\frac{\delta T_c}{\delta G(\Omega)}}{1-\frac{\partial\Delta_1(\omega,T)}{\partial\omega}\Big|_{\Delta_0}} , \tag{4.21}$$

where $\mathcal{A}_1$ is the real part of the analytic continuation $\mathcal{A}$ and Δ_1 is the real part of the gap. This last formula can be evaluated directly in our programs, which gives us $\mathcal{A}[\delta\Delta(i\omega_n)/\delta G(\Omega)]$ and $\Delta(\omega,T)$ through Padé approximants techniques. While formula (4.21) is the most useful for our work, it can be rewritten in another way that is sometimes more useful for discussion. Substituting (4.19) into (4.21) leads to

$$\frac{\delta\Delta_0}{\delta G(\Omega)}=\frac{\frac{\delta\Delta_1(\omega,T)}{\delta G(\omega)}\Big|_{\Delta_0}}{1-\frac{\partial\Delta_1(\omega,T)}{\partial\omega}\Big|_{\Delta_0}} . \tag{4.22}$$

Assuming constant t, we can rewrite

$$\frac{\delta\Delta_1(\omega,T)}{\delta G(\Omega)}=\frac{\delta\Delta_1(\omega,T)}{\delta G(\Omega)}+\frac{\partial\Delta_1}{\partial T}t\frac{\delta T_c}{\delta G(\Omega)} \tag{4.23}$$

so that

$$\frac{\delta\Delta_0}{\delta G(\Omega)}=\frac{\frac{\delta\Delta_1(\omega,T)}{\delta G(\Omega)}\Big|_{\Delta_0}+T\frac{\partial\Delta_1(\omega,T)}{\partial T}\Big|_{\Delta_0}\frac{1}{T_c}\frac{\delta T_c}{\delta g(\Omega)}}{1-\frac{\partial\Delta_1(\omega,T)}{\partial\omega}\Big|_{\Delta_0}} . \tag{4.24}$$

This last formula involves the temperature derivative of the real gap $\partial\Delta_1(\omega,T)/\partial T$, which is not evaluated directly here. If we assume that it is finite, however, we see

from (4.24) that it is not needed, because the second term drops out as $T\to 0$, since it contains an explicit factor of temperature. This leaves us with the formula

$$\frac{\delta\Delta_0}{\delta G(\Omega)}=\frac{\left.\frac{\delta\Delta_1(\omega,T)}{\delta G(\Omega)}\right|_{\Delta_0}}{1-\left.\frac{\partial\Delta_1(\omega,T)}{\partial\omega}\right|_{\Delta_0}}\ ,\quad T\to 0\ . \tag{4.25}$$

Thus, at low temperature, it does not matter whether we keep T or t constant as we would expect. Our numerical work confirms that as well and suggests that working with $t=0.1$ is good enough.

Application of the above technique to the calculation of the functional derivative of the gap edge gives essentially the same results as the direct technique of Mitrović *et al.* (1980) and verifies that both approaches have been properly implemented on the computer.

D. Optimization of the gap

The shape of the functional derivative of Δ_0 shown in Fig. 32 suggests that for a given area under $\alpha^2F(\omega)$ we can maximize the value of the gap edge by using a delta function spectral density $\alpha^2F(\omega)=A\delta(\omega-\Omega_E)$ centered at the Einstein frequency Ω_E. For such a model spectrum we have already shown in Sec. II that $\Delta(i\omega_n)=Af_n(T/A,\Omega_E/A,\mu^*)$, where f_n is a universal function. This implies that the gap edge at zero temperature satisfies

$$\Delta_0=Ag(\bar{\Omega}_E,\mu^*) \tag{4.26}$$

with g a universal function independent of material parameters except for the dimensionless frequency

$$\bar{\Omega}_E\equiv\Omega_E/A\ .$$

We have solved for $g(\bar{\Omega}_E,\mu^*)\equiv\Delta_0/A$ for three values of μ^*, namely, 0.0, 0.1, and 0.227. In all cases, $g(\bar{\Omega}_E,\mu^*)$ is found to exhibit a maximum at some definite optimum frequency $\bar{\Omega}_E^*$ that varies with μ^*. In fact, the shape of $g(\bar{\Omega}_E,\mu^*)$ reflects well the functional derivative curve of Fig. 32. The behavior obtained by Carbotte *et al.* (1986) is shown in Fig. 35, where Δ_0 is plotted as a function of Ω_E and λ_E on the left- and right-hand picture, respectively. All calculations are for $A=10.672$ meV (the Nb_3Sn value), and only the region near the maximum is plotted with a dense set of points.

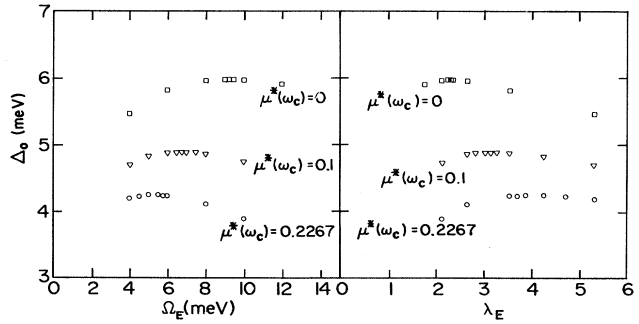

FIG. 35. Gap edge at zero temperature Δ_0 in meV as a function of Einstein frequency Ω_E in meV for various values of μ^*: □, $\mu^*=0.0$; ∇, $\mu^*=0.1$; and ○, $\mu^*=0.2267$ (left-hand frame) and as a function of $\lambda_E\equiv 2A/\Omega_E$ (right-hand frame). The curves are universal and the base $\alpha^2F(\Omega)=A\delta(\Omega-\Omega_E)$.

TABLE V. Variation of $b(\mu^*)$ and $c(\mu^*)$ with Coulomb pseudopotential. The quantities $b(\mu^*)$ and $c(\mu^*)$ give, respectively, the value of Δ_0/A and Ω_E/A at maximum.

	$\mu^*=0$	$\mu^*=0.1$	$\mu^*=0.2267$
$b(\mu^*)$	0.56	0.46	0.40
$c(\mu^*)$	0.87	0.63	0.52

The maximum observed in Fig. 35 for each of the three values of μ^* considered represents the maximum value for the ratio of the gap to A that can be achieved for any shape of $\alpha^2F(\Omega)$, since the peak must occur when the phonon energy in the base delta function is placed at the maximum of its own functional derivative $\delta\Delta_0/\delta\alpha^2F(\Omega)$. If we determine this value of $\bar{\Omega}_E^*$, we conclude that

$$\Delta_0^*=Ag(\bar{\Omega}_E^*,\mu^*)\equiv Ab(\mu^*)\ , \tag{4.27}$$

since $\bar{\Omega}_E^*$ is a well-defined dimensionless number denoted by $c(\mu^*)$ in Table V. In Table V, we show the results obtained for $b(\mu^*)$, and we note that $b(\mu^*)$ is reduced as μ^* increases. For any other spectrum with the same μ^* and A, we expect

$$\Delta_0\le Ab(\mu^*)=\Delta_0^*\ . \tag{4.28}$$

The previously mentioned results of Mitrović, Zarate, and Carbotte (1984) on Δ_0 for a large number of materials, given in Table III, can be used to test the validity of the inequality (4.28). This is shown in Fig. 36 by the line $b(\mu^*)$ versus μ^*, along with the Δ_0/A for the many superconductors previously discussed. The solid dots, unidentified individually, are for PbTlBi alloys; the crosses are for the InTl alloys. We note that the inequality (4.28) on the gap is well satisfied. The system falling closest to the $b(\mu^*)$ versus μ^* curve is the alloy $Pb_{0.65}Bi_{0.35}$ for which $\mu^*=0.0996$ and $\Delta_0/A=0.43$. This is to be compared with the value of $b(\mu^*=0.1)$ given in Table V, which is 0.46. The difference with $Pb_{0.65}Bi_{0.35}$ is only 10 percent. This shows that some real materials can very nearly exhibit the maximum possible gap value for their particular spectral weight A.

With the discovery of superconductivity with temperatures as high as 125 K in the copper oxides, it is worthwhile considering what value the dimensionless ratio $2\Delta_0/k_BT_c$ might take, should we go beyond the conventional strong-coupling regime for $T_c/\omega_{\ln}$, which ends

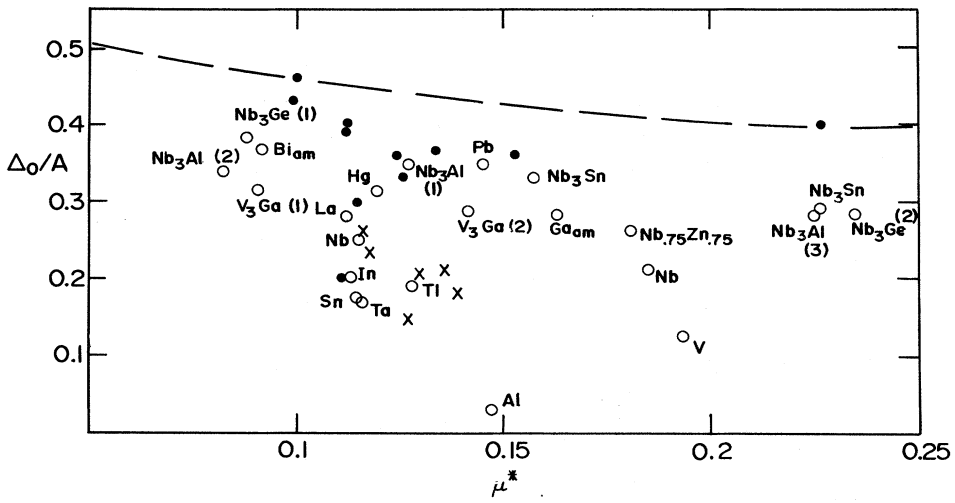

FIG. 36. Maximum value of Δ_0/A as a function of μ^* (dashed curve through solid dots). The data for the various materials are from full numerical solutions of the Eliashberg equations based on tunneling data for the spectral density.

around $T_c/\omega_{\ln} \lesssim 0.25$. This was done by Marsiglio *et al.* (1987a). These authors consider two possible spectra for $\alpha^2F(\Omega)$. They take Pb and the spectral shape calculated by Weber (1987a, 1987b) for La-Sr-Cu-O, which is shown in Fig. 37. The scaling described in Sec. II allows us to reach any value of T_c and $T_c/\omega_{\ln}$ we wish through adjustment of the two parameters B and b in the form $B\alpha_0^2F(b\omega)$. When this is done and $2\Delta_0/k_BT_c$ is calculated, we obtain the curve shown in Fig. 38. We see that $2\Delta_0/k_BT_c$ simply rises with increasing coupling, although it does have some dependence on spectral shape. At $T_c/\omega_{\ln}=1.4$, the Pb based curve (dotted) has reached a value greater than 10 while the La-Sr-Cu-O based one (solid) is less than 9. Both also show some signs of saturation at higher values of $T_c/\omega_{\ln}$.

From the shape of the functional derivative of $2\Delta_0/k_BT_c$ shown previously in Fig. 34 for a few select materials, we would expect that, for a given spectral weight A, the optimum shape for $\alpha^2F(\Omega)$ that maximizes this ratio is a delta function placed at some low frequency

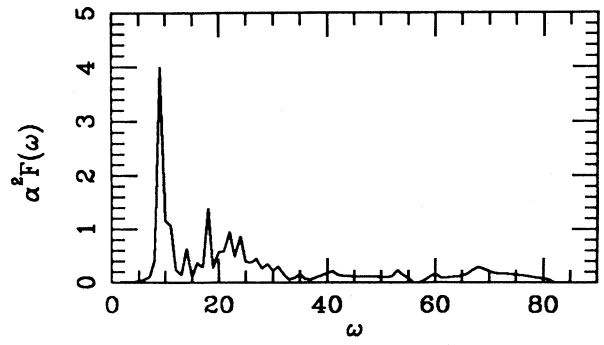

FIG. 37. Calculated electron-phonon spectral density $\alpha^2F(\omega)$ for $La_{1.85}Sr_{0.15}CuO_4$ from the work of Weber (1987a, 1987b).

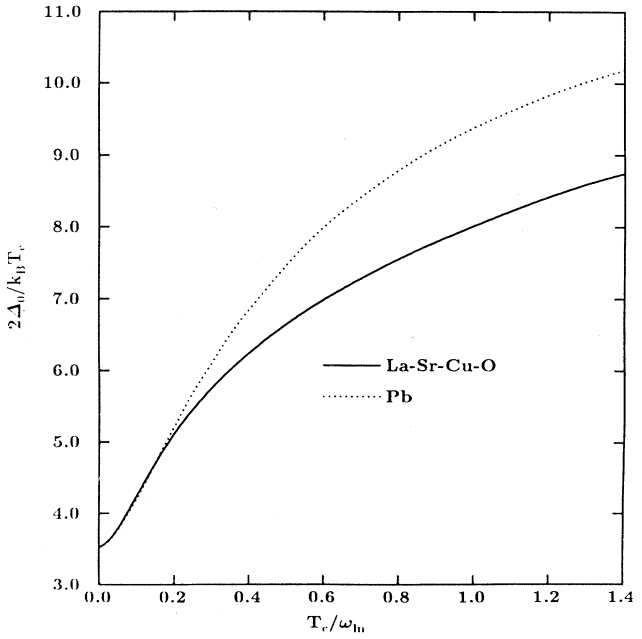

FIG. 38. Gap ratio $2\Delta_0/k_BT_c$ vs $T_c/\omega_{\ln}$ for two spectral-function shapes, that of Pb and LSCO. In the very strong coupling regime, $2\Delta_0/k_BT_c$ continues to rise above the BCS value, and the shape dependence is more pronounced. However, the qualitative feature of increasing $2\Delta_0/k_BT_c$ seems to be shape independent.

corresponding to the maximum in its own functional derivative. Use of a delta-function spectrum indeed shows that $2\Delta_0/k_BT_c$ keeps rising as $\lambda\to\infty$, and numerical work indicates that the limit of $\Omega_E\to 0$ for fixed A is about 13 [Carbotte (1987b)]. The maximum value turns out also to be the asymptotic limit. Some insight into this interesting result can be obtained from functional derivative considerations. At the maximum, we would expect the functional derivative of the base delta function to be negative definite and exactly zero right at the position of the frequency in the base delta function. This would prove that adding weight to the base delta function changes nothing, while taking weight from it and placing it anywhere else reduces $2\Delta_0/k_BT_c$ so that the delta function indeed maximizes this quantity. But our numerical work shows that the maximum occurs for $\omega_E\to 0$ in the base function. Because of numerical problems, we could not calculate the functional derivative right at $\omega_E=0$, but we could calculate such a quantity for smaller and smaller values of ω_E and analyze the trend. In Fig. 39 we show functional derivative results for $\omega_E/T_c=4.7$, $\omega_E/T_c=1.8$, and $\omega_E/T_c=0.75$ base functions. It is clear that the progression of these curves is towards a negative definite curve with maximum equal to zero at $\omega=0$ as the base Einstein frequency is lowered towards zero.

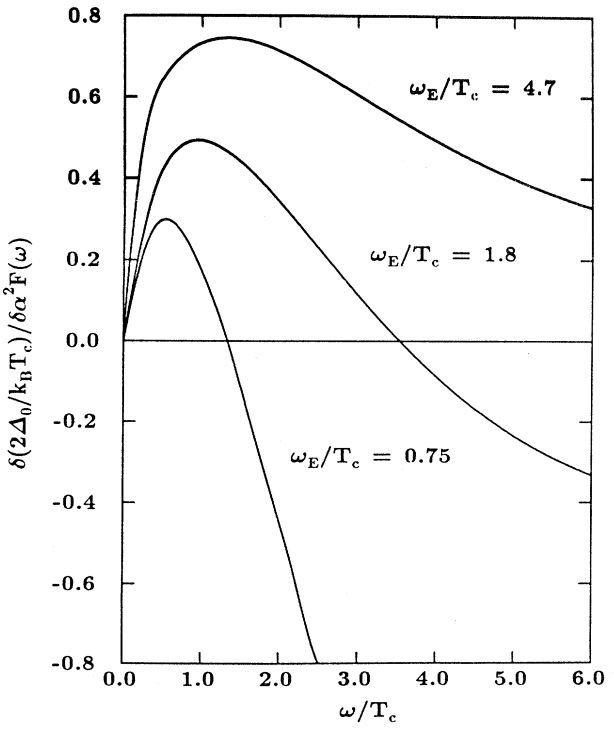

FIG. 39. Functional derivative of the dimensionless ratio of gap to critical temperature $2\Delta_0/k_BT_c$ with electron-phonon spectral density $\alpha^2F(\omega)$, $\delta(2\Delta_0/k_BT_c)/\delta\alpha^2F(\omega)$, as a function of ω/T_c for three different delta-function base spectra identified by the Einstein frequency of the base $\alpha^2F(\omega)=A\delta(\omega-\omega_E)$.

E. Asymptotic limit

Additional insight can be obtained from approximate analytic results. In principle, in the asymptotic limit, the universal equation (2.28) gives the gap at zero temperature as well as the critical temperature, and both asymptotically go like $\sqrt{A\Omega_E}$ or $\sqrt{\lambda}\,\Omega_E$. We have already established that in exact numerical calculations $T_c\simeq 0.26\sqrt{A\omega_E}$. In a single-Matsubara-gap approximation, as described by Allen and Dynes (1975) and as we shall show later, the approximate result would instead have been $T_c=(1/\pi\sqrt{2})\sqrt{A\omega_E}$. To get an equivalent approximate equation for the gap edge, it is convenient to return to Eqs. (2.1) and (2.2) and take the zero-temperature limit to get

$$Z(\omega)\Delta(\omega)=\frac{1}{2}\int_{-\infty}^{+\infty}d\omega'\frac{2\Omega_E A}{\Omega_E^2+(\omega-\omega')^2}\frac{\Delta(\omega')}{\sqrt{\omega'^2+\Delta^2(\omega')}}\ , \tag{4.29}$$

$$Z(\omega)=1+\frac{1}{2\omega}\int_{-\infty}^{+\infty}d\omega'\frac{2\Omega_E A}{\Omega_E^2+(\omega-\omega')^2}\frac{\omega'}{\sqrt{\omega'^2+\Delta^2(\omega')}}\ . \tag{4.30}$$

Detailed numerical solutions of (3.33) and (3.34) by Marsiglio (1988) indicate that in the very strong coupling limit ($\lambda\to\infty$) a reasonable model for the gap is ($\omega>0$)

$$\Delta(\omega)=\begin{cases}\Delta_0 & \text{for } \omega<2\Delta_0\ , \\ 0 & \text{for } \omega>2\Delta_0\ .\end{cases} \tag{4.31, 4.32}$$

Making use of this model in Eqs. (4.29) and (4.30), we obtain

$$Z(\omega\sim 0)=1+2A\frac{d}{d\Omega_E}[\Omega_E^2J(\Omega_E)]+\frac{A\Omega_E}{2\Delta_0^2} \tag{4.33}$$

and

$$\Delta_0Z(\omega\sim 0)=2A\Omega_E\Delta_0J(\Omega_E) \tag{4.34}$$

with

$$J(\Omega_E)=\int_0^{2\Delta_0}\frac{d\omega'}{\omega'^2+\Omega_E^2}\frac{1}{\sqrt{\omega'^2+\Delta_0^2}}$$

$$\cong\frac{1}{\Omega_E\Delta_0}\left[\frac{\pi}{2}-\frac{\sqrt{5}}{2}\frac{\Omega_E}{\Delta_0}\right]\ . \tag{4.35}$$

Substitution of (4.35) into (4.33) and (4.34) and combining these last two relationships gives

$$\Delta_0\cong 1.3\sqrt{A\Omega_E}\ . \tag{4.36}$$

When use is made of the approximate result

$$k_BT_c=\frac{1}{\pi\sqrt{2}}\sqrt{A\Omega_E}\ ,$$

we finally arrive at the asymptotic value of [Carbotte

(1987b); Kresin (1987); Dolgov *et al.* (1988)]

$$\frac{2\Delta_0}{k_B T_c} \cong 11.6 \ , \tag{4.37}$$

which is not very far off the rigorous numerical result of 13. No boson-exchange superconductor, for which the isotropic Eliashberg equations apply, can have a gap edge larger than this value.

F. Jump at Δ_0 in I-V characteristics

To end this section, we consider the jump at the energy-gap voltage in the quasiparticle current of a superconducting tunneling junction. The ratio of the jump to its weak-coupling limit, which we denote by J_R, is given by [Harris *et al.* (1976)]

$$J_R = \left[1+\frac{1}{2}\frac{d\Delta_1(\omega)}{d\omega}\bigg|_{\Delta_0}\right]^2 , \tag{4.38}$$

where $\Delta_1(\omega)\equiv \mathrm{Re}\Delta(\omega)$, with $\Delta(\omega)$ the gap on the real-frequency axis and the gap edge Δ_0 given by $\Delta_0=\Delta_1(\omega=\Delta_0)$. They have calculated this quantity for a few select superconductors. Coombes and Carbotte (1986b) have given more extensive results. Both sets of results are plotted in Fig. 40. The solid dots are the results of Coombes and Carbotte (1986b), and the crosses are those of Harris *et al.* (1976). The dashed curve is a visual fit through the points. It is seen to fit the data very well, indicating an important correlation between J_R and the strong-coupling parameter $T_c/\omega_{\ln}$. Harris *et al.* (1976) have pointed out a similar correlation with the $\lambda-\mu^*$ value, which Coombes and Carbotte (1986b) confirm. As the very strong coupling regime is also of interest, we plot in Fig. 41 results for a delta-function

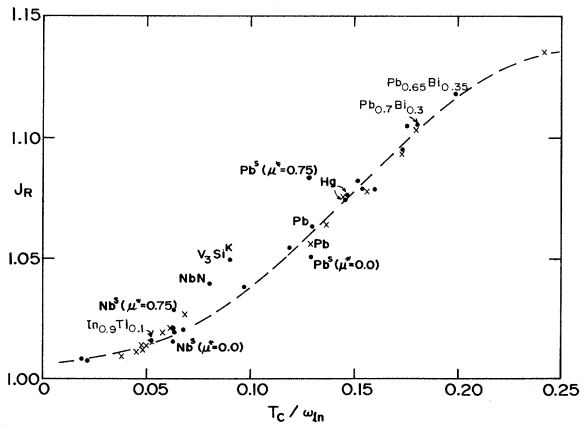

FIG. 40. Calculated values of J_R (dots) and the data of Harris *et al.* (1976) (crosses) plotted vs the strong-coupling parameter $T_c/\omega_{\ln}$. The dashed line is empirical and does not represent any theory.

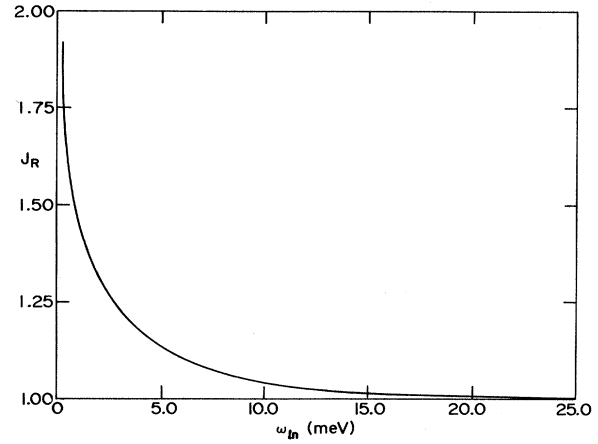

FIG. 41. J_R calculated for δ-function spectra of constant area vs the frequency $\omega_{\ln}$ (in meV).

spectrum as a function of $\omega_{\ln}=\omega_E$, where ω_E is the Einstein frequency. We see that, in this case, J_R can get very large as $\omega_E\to 0$. We note that the numerical calculations had to be terminated at a small but finite value of ω_E because of insufficient computer accuracy. To understand this increase a little better, Coombes and Carbotte (1987) have also calculated the functional derivative of J_R, making use of the formalism developed previously in this sec-

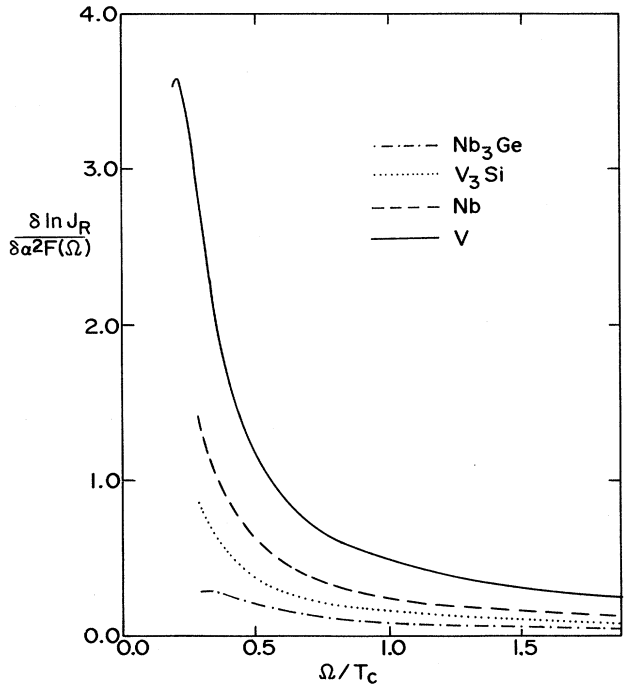

FIG. 42. $\delta \ln J_R/\delta\alpha^2F(\Omega)$ vs Ω/T_c for V (solid line), Nb (dashed line), V_3Si (dotted line), and Nb_3Ge (dot-dashed line).

tion. The quantity of interest is

$$\frac{\delta J_R}{\delta G(\Omega)} = J_R^{1/2} \frac{\delta}{\delta G(\Omega)} \left[\left. \frac{d\Delta_1(\omega)}{d\omega} \right|_{\omega=\Delta_0} \right] . \tag{4.39}$$

To find the functional derivative of

$$\left. \frac{d\Delta_1(\omega)}{d\omega} \right|_{\omega=\Delta_0} ,$$

we need to return to Eq. (4.18) and take the derivative with respect to ω of the real part of the gap evaluate at Δ_0' and expand to first order in ϵ to get

$$\begin{aligned} \frac{\delta}{\delta G(\Omega)} \left[\left. \frac{d\Delta_1(\omega)}{d\omega} \right|_{\Delta_0} \right] = & \left[\frac{d}{d\omega} \mathcal{A}_1 \left[\frac{\delta\Delta(i\omega_n)}{\delta G(\Omega)} \right] \right]_{\Delta_0} + \left. \frac{d^2\Delta_1(\omega)}{d\omega^2} \right|_{\Delta_0} \left. \frac{\delta\Delta_0}{\delta G(\Omega)} \right|_{\Omega_0} \\ & - \left[\left. \frac{d\Delta_1(\omega)}{d\omega} \right|_{\Delta_0} + \Delta_0 \left. \frac{d^2\Delta_1(\omega)}{d\omega^2} \right|_{\Delta_0} \right] \frac{1}{T_c} \left. \frac{\delta T_c}{\delta G(\Omega)} \right|_{\Omega_0} . \end{aligned} \tag{4.40}$$

Results based on this last formula are given in Fig. 42 as a function of Ω/T_c for V (solid line), Nb (dashed line), V_3Si (dotted line), and Nb_3Ge (dot-dashed line). It is seen that in all cases the functional derivative increases rapidly as Ω/T_c is decreased and that, for the lowest temperature at which it was possible to converge our programs, signs of a turnover toward 0 at $\omega=0$ are visible. This form for the functional derivative is consistent with the results shown in Fig. 41.

V. THERMODYNAMICS FOR SPECIFIC MATERIALS

A. Comparison with experiment for Pb and Nb

The thermodynamics of a strong-coupling superconductor follows from the numerical solutions of Eqs. (2.1) and (2.2) with appropriate microscopic parameters. The free-energy difference ΔF between superconducting (F^S) and normal (F^N) state is given by the formula of Bardeen and Stephen (1964)

$$\frac{\Delta F}{N(0)} = -\pi T \sum_n \left[\sqrt{\omega_n^2 + \Delta^2(i\omega_n)} - |\omega_n| \right] \times \left[Z^S(i\omega_n) - Z^N(i\omega_n) \frac{|\omega_n|}{\sqrt{\omega_n^2 + \Delta^2(i\omega_n)}} \right] , \tag{5.1}$$

where $Z^N(i\omega_n)$ is the renormalization function for the normal state. It is given by Eq. (2.2) with $\Delta(i\omega_m)$ set equal to zero on the right-hand side.

All thermodynamic properties follow from a knowledge of ΔF. In particular, the specific-heat difference is

$$\Delta C(T) = -T \frac{d^2\Delta F}{dT^2} , \tag{5.2}$$

and the thermodynamic critical magnetic field is

$$H_c(T) = \sqrt{-8\pi\Delta F} . \tag{5.3}$$

Finally, the deviation function for the critical magnetic field, which is used to describe its temperature dependence, is defined as

$$D(t) \equiv \frac{H_c(T)}{H_c(0)} - (1-t^2) . \tag{5.4}$$

Dimensionless BCS ratios, which are associated with the thermodynamics and which are often quoted, are the normalized jump in the specific heat at T_c, $\Delta C(T_c)/(\gamma T_c)$, the ratio $\gamma T_c^2/H_c^2(0)$, the slope of the specific heat at T_c,

$$\left[\frac{d\Delta C(T)}{dT} \right]_{T_c} \frac{1}{\gamma} ,$$

and the minimum in the deviation function. These quantities have the value 1.43, 0.168, 3.77, and -0.037, respectively, for a weak-coupling system, but are quite different for actual electron-phonon systems.

Extensive calculations of thermodynamic properties of specific superconductors, for which $\alpha^2F(\omega)$ is known from tunneling, have been carried out by Daams and Carbotte (1981) and the results compared with experiment. In Table VI, we reproduce some of their results for Pb and Nb. Similar results can be found in their paper for Hg, Sn, Tl, and Al. Additional results exist for the Tl-Pb-Bi [Daams *et al.* (1978)] alloy series; for Nb [Daams and Carbotte (1980b)], where the effect of various choices of $\alpha^2F(\omega)$ is examined in detail; for Nb, including a possible contribution from paramagnons [Baquero *et al.* (1981)]; for $Nb_{0.75}Zr_{0.25}$ [Mitrović and Carbotte (1981a)]; for Ta [Baquero and Carbotte (1983)]; and for V [Daams *et al.* (1984)], including an investigation of the effects of paramagnons.

From Table VI where the thermodynamic quantities $C_{es}/(\gamma T_c)$, $\gamma T_c^2/H_c^2(0)$ and the extrema values of $D(t)$ are quoted and compared with experiment, it is seen that good agreement is achieved although there is more variation from one experiment to the next than one might like. Despite this uncertainty, it is clear that BCS theory does not apply, while Eliashberg theory does. The other quantities entered—$H_c(0)$, $\Delta C(T_c)$, and $-\partial H_c(T)/\partial T)_{T_c}$—are all dependent on the electronic density of states at

the Fermi energy $N(0)$, which enters linearly in formula (5.1) for the free-energy difference. This quantity is determined from the measured Sommerfeld constant γ [Gladstone *et al.* (1969)] and the tunneling-derived mass-enhancement parameter according to the formula

$$\gamma=\tfrac{2}{3}\pi^2 k_B^2 N(0)(1+\lambda)\ , \tag{5.5}$$

where k_B is the Boltzmann constant usually taken to be 1. It is seen that when $N(0)$ is derived from γ, good agreement with experiment is obtained for all three quantities quoted above, namely, the zero-temperature critical magnetic field, its slope at T_c, as well as the specific-heat jump at T_c. The theoretical results for Pb are based on the spectrum given in the tabulation by Rowell *et al.* (1970) as discussed in Table I. Two sets of theoretical results are given for the case of Nb. They are Nb(R), based on the tunneling-derived spectrum of Robinson and Rowell (1972), and Nb(B), based on the calculated spectrum of Butler *et al.* (1977). As seen in a previous sec-

TABLE VI. The experiments are classified according to type (magnetization or calorimetric). The numbers in parentheses were obtained indirectly from plots or other data. The entries under $D(t)$ are the extrema of $D(t)$. The γ used for the theoretical work was taken from a compilation of Gladstone *et al.* (1969). $N(0)$ was then deduced from γ and the $\lambda(0)$ of the $\alpha^2F(\omega)$.

	T_c K	H_c G	γ mJ/mol K^2	$\Delta C_v(T_c)$ mJ/mol K	$-(\partial H_c/\partial T)_{T_c}$ G/K	$C_{es}/\gamma T_c$	$\gamma T_c^2/H_c^2$	$D(t)$	Ref.
				Pb experiment					
Cal	7.19	(803)	3.00	59	(240)	3.71	(0.134)	0.025	a
Cal	(7.19)	(803)	(3.13)	58	(236)	(3.67)	(0.140)		b
Cal	(7.19)	(803)	(3.13)	53	(227)	(3.36)	(0.140)		c
Mag	7.18	803	3.06	58	238	(3.69)	(0.137)	0.024	d
Mag	7.20	803	3.13	60	237	(3.66)	(0.140)	0.021	e
Mag	7.18	803	(3.13)	(57)	237	(3.57)	(0.140)		f
				Theory					
BCS						2.43	0.168	−0.037	
Isotropic (tunneling, $\omega_c=66$)	7.19	818	3.13	61	247	3.70	0.132	0.025	
$N(0)=0.86\times10^{19}$ meV^{-1}cm^{-3}, molar volume$=17.9$ cm^3									
				Nb experiment					
Mag	9.20	1960	7.15				(0.146)		g
Mag	9.25	1993	7.90	147	(430)	(3.01)	(0.158)	$^{-0.003}_{+0.003}$	h
Mag	9.20	1980	7.88	127	(401)	(2.75)	(0.158)		i
Cal	9.17	1944	7.53,7.95	140	415	3.03,2.92	(0.155)	−0.027	j
Cal	9.19	1994	7.80	(134)	412	2.87	(0.153)	$^{-0.012}_{+0.005}$	k
Cal	9.18		7.72	(144)	427	(3.03)			l
Cal	9.26	2061	7.80	140	419	(2.94)	(0.146)	$^{-0.015}_{+0.003}$	m
Cal	8.70	2000	8.47	153	453	3.07	(0.148)		n
Cal	9.28	2014	7.82	139	417	2.91	0.154	$^{-0.008}_{+0.0004}$	o
Cal	9.23	(1975)	7.80	(135)	(413)	(2.87)	(0.158)	$^{-0.007}_{+0.002}$	p
Cal	9.18	2038	7.74	(134)	413	(2.88)	(0.157)		q
Cal	9.09		7.53	(131)	(409)				r
				Theory					
BCS						2.43	0.168	−0.037	
Isotropic spectrum									
Nb(R)	9.20	2007	7.80	141	422	2.96	0.151	$^{-0.008}_{+0.002}$	
Nb(B)	9.25	1992	7.80	139	418	2.91	0.155	$^{-0.009}_{+0.002}$	
$N(0)=4.64\times10^{19}$ meV^{-1}cm^{-3}, molar volume$=10.8$ cm^3									

[a]Neighbor *et al.* (1967).
[b]Shiffman *et al.* (1963).
[c]Clement and Quinnell (1952).
[d]Decker *et al.* (1958).
[e]Chanin and Torre (1972).
[f]Rohrer (1960).
[g]Stromberg and Swenson (1962).
[h]Finnemore *et al.* (1966).
[i]French (1968).
[j]Chou *et al.* (1958).
[k]Leupold and Boorse (1964).
[l]Ishikawa and Toth (1971).
[m]Novotny and Meincke (1975).
[n]Brown *et al.* (1953).
[o]Ferreira da Silva *et al.* (1969).
[p]Ohtsuka and Kimura (1971).
[q]Corsan and Cook (1969).
[r]Hershfeld *et al.* (1962).

tion, these spectra differ significantly from one another in detail, but we now see that they give basically the same thermodynamics. Yet another more recent Nb spectrum will be presented later in relation to a comparison between the thermodynamics of $Nb_{0.75}Zr_{0.25}$ with Nb [Wolf and Noer (1979)].

B. Critical-field deviation function

The results obtained by Daams and Carbotte (1981) for the critical-field deviation function $D(t)$ are shown in Fig. 43 for Pb, Hg, Nb, In, Tl, Sn, Ta, and Al (denoted as BCS) in order of decreasing deviation from BCS. They can be compared with the experimental results compiled by Swihart [(1962); Rickayzen (1965); Daams (1979)], which we reproduced in Fig. 44. The qualitative and near quantitative agreement obtained between theory and experiment is very good and leaves no doubt that an electron-phonon mechanism is operative and that Eliashberg theory is remarkably exact while BCS theory cannot be used for quantitative comparison with experiment. Similar theoretical results of Daams and Carbotte (1981) for the electronic specific heat in the superconducting state $C_{es}(T)/(\gamma T)$ are presented for the same systems as in Fig. 43, namely, Pb, Hg, Nb, In, Tl, Ta, Sn, and Al in Fig. 45 [Swihart *et al.* (1965)]. Since calculated $D(t)$'s

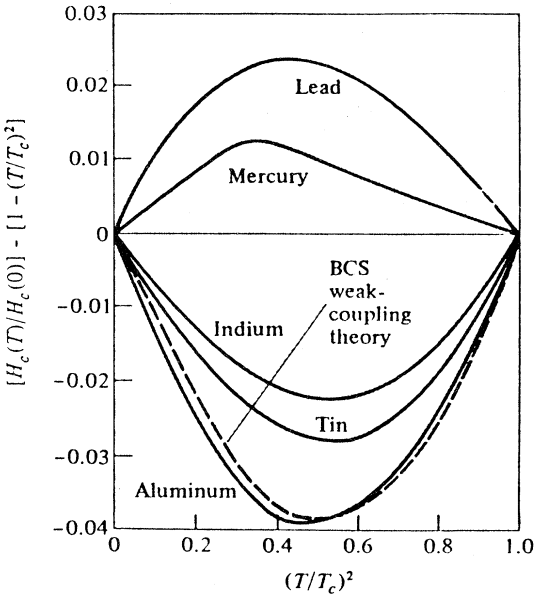

FIG. 44. Experimental results for the thermodynamic critical magnetic field as compiled by Swihart (1962).

agree well with experiment, these also do. In fact, the specific-heat difference between superconducting and normal state for Pb, measured by Chanin and Torre (1972), is given in Fig. 46. These results fall almost exactly on the theoretical results shown in Fig. 47, which are very different from BCS. If the two figures had been su-

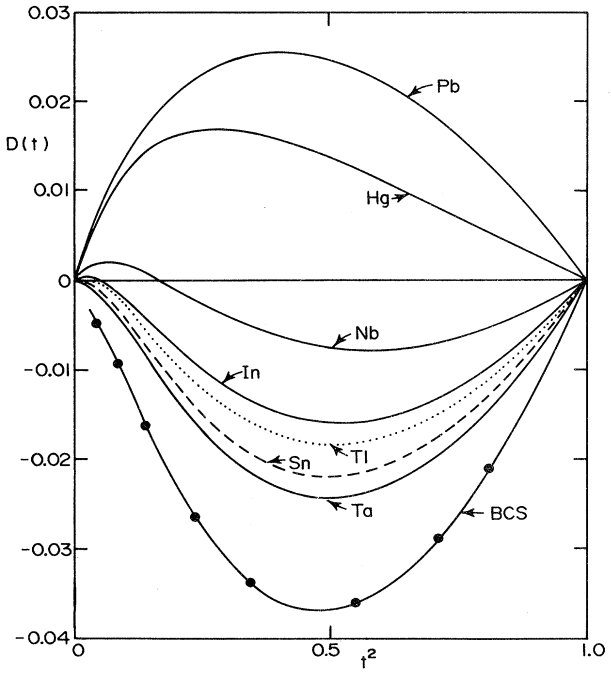

FIG. 43. Thermodynamic critical magnetic-field deviation function $D(t)$ as a function of the square of the reduced temperature t for various materials as calculated in Eliashberg theory. The lowest solid curve is the BCS result, while the solid circles are the results of full Eliashberg calculations for Al.

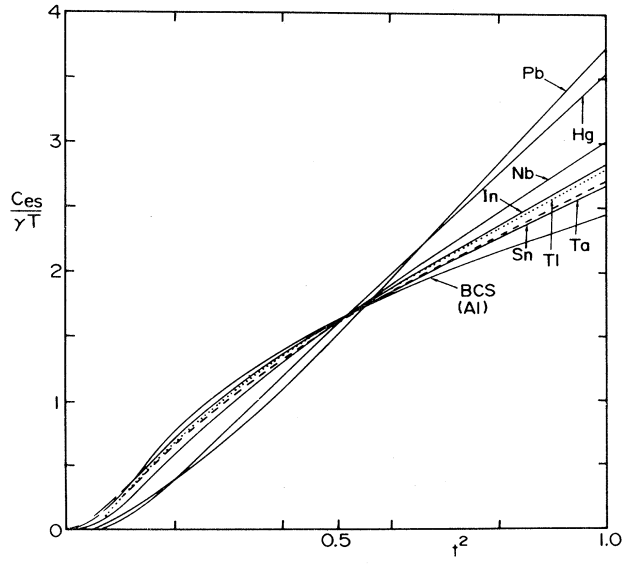

FIG. 45. Calculated (with Eliashberg theory) electronic specific heat in the superconducting state normalized to γT (the normal state) with γ Sommerfeld constant, as a function of the square of the reduced temperature for several materials.

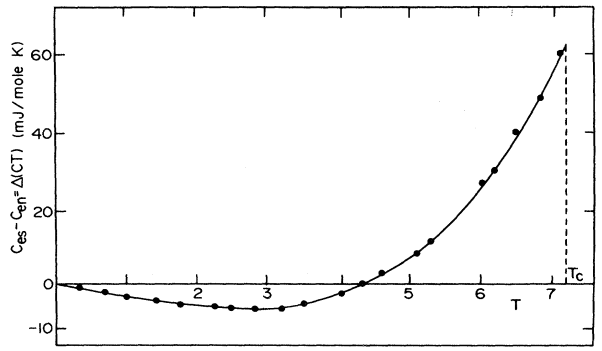

FIG. 46. Measured electronic specific-heat difference $C_{es}-C_{en}$ (in mJ/mol K) of Pb as a function of temperature T.

perimposed, the theoretical curve would not have been distinguishable from the solid curve put through the experimental points to guide the eye. As an example, and to be more specific, the slope at T_c normalized to the jump

$$\frac{T_c}{\Delta C(T_c)}\frac{d\Delta C(T)}{dT}\bigg|_{T_c}=4.6 \tag{5.6}$$

for both theory and experiment, while in BCS theory it is 2.64.

The select results presented so far, which include ordinary s-p metals as well as transition metals, were given to illustrate the excellent agreement that can be achieved between experiment and the results of Eliashberg theory which, in general, are quite different from BCS. Other examples would have done equally well, and the reader is referred to the paper of Daams and Carbotte (1981) as well as others [Daams and Carbotte (1980a, 1980b); Baquero *et al.* (1981); Mitrović and Carbotte (1981); Baquero and Carbotte (1983); Daams *et al.* (1984)] for further details. We next turn to alloys and then to the A15 compounds.

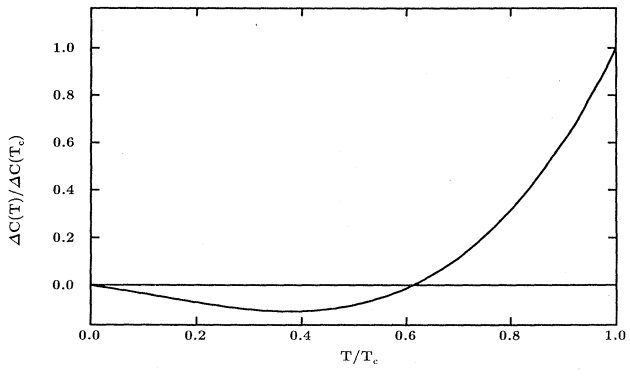

FIG. 47. Calculated electronic specific-heat difference between superconducting and normal state, normalized to its value at T_c, as a function of reduced temperature T/T_c. The calculations are for Pb and result from full numerical evaluation of the free-energy formula in Eliashberg theory with the tunneling-derived electron-phonon spectral density.

C. Some alloys

For the alloy $Pb_{0.9}Bi_{0.1}$, tunneling inversion gives a $\lambda=1.66$ compared with 1.55 for pure Pb and a T_c of 7.65 compared with 7.19. This indicates a trend towards stronger coupling, which is verified in our calculations of $2\Delta_0/k_BT_c$. We obtain 4.67 for $Pb_{0.9}Bi_{0.1}$ [Daams *et al.* (1979)], to be compared with 4.50 for Pb, in agreement with experiment. Consistent with this are the experiments by Park *et al.* (1974), which give results for $D(t)$ that look very much like the Pb curve (Fig. 44) but which peak at a somewhat higher value of $D(t)$, namely, 0.3 rather than 0.26. Calculations give 0.29, which is a little lower, but the shape is essentially the same as measured. A similar good agreement was obtained by Niel *et al.* (1985) in $In_{0.90}Tl_{0.10}$. Thus alloys of s-p metals are also well described by Eliashberg theory.

Tunneling results are also available for the alloy $Nb_{0.75}Zr_{0.25}$ [Wolf and Noer (1979)]. They show much more pronounced softening effects over Nb than does $Pb_{0.9}Bi_{0.1}$ when compared with Pb. The spectrum for this alloy is compared with Nb in Fig. 48 [Mitrović and Carbotte (1981)] and some derived parameters are given in Table VII. The Nb spectrum used here is probably the

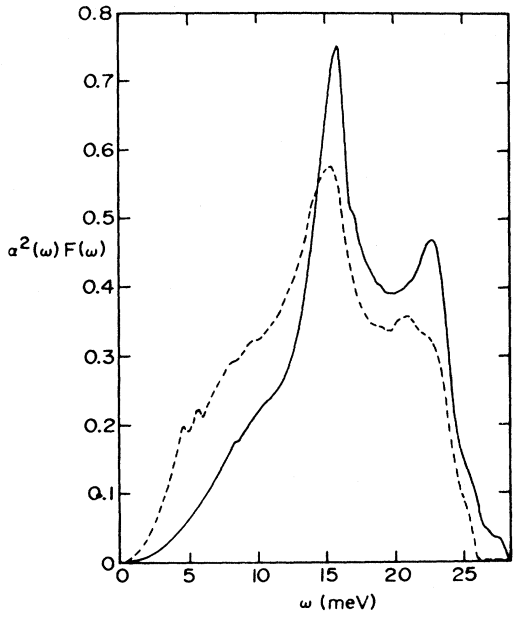

FIG. 48. Comparison of the electron-phonon spectral density $\alpha^2F(\omega)$ for $Nb_{0.75}Zr_{0.25}$ (dashed curve) with that for Nb (solid curve) according to Wolf and Noer (1979).

TABLE VII. Comparison of some microscopic parameters for $Nb_{0.75}Zr_{0.25}$ and Nb.

	$Nb_{0.75}Zn_{0.25}$	Nb
$\lambda=2\int_0^\infty \frac{\alpha^2(\omega)F(\omega)}{\omega}d\omega$	1.311	1.009
$A=\int_0^\infty \alpha^2(\omega)F(\omega)d\omega$ (meV)	7.425	7.247
ω_0, maximum phonon energy in $\alpha^2(\omega)F(\omega)$ (meV)	26.0	28.3
ω_{0c}, cutoff in Matsubara sums (meV)	156.0	169.7
μ^*, Coulomb pseudopotential	0.1808	0.1854
T_c critical temperature (meV)	0.922	0.7945
T_c (K)	10.8	9.22

best tunneling-derived value to date. The most important feature of these results is the considerable shift in $\alpha^2F(\omega)$ towards higher weight at lower energy observed with alloying. A measure of the extent of this softening is given by λ which, we note from Table VII, increases by 30% despite the fact that the area A under $\alpha^2F(\omega)$ increases by only 2.5 percent. This softening in spectrum leads to more pronounced strong-coupling effects in the thermodynamic properties of $Nb_{0.75}Zr_{0.25}$ compared with Nb as calculated by Mitrović and Carbotte (1981). This is seen in Table VIII for thermodynamic quantities that are all found to move significantly towards larger deviations from BCS values when $Nb_{0.75}Zr_{0.25}$ is compared with Nb. The calculations of Mitrović and Carbotte (1981) seem to have stimulated new, more accurate experiments in both Nb and $Nb_{0.75}Zr_{0.25}$ by Junod *et al.* (1986). Their experimental data are entered in Table VIII, and it is seen that the agreement with theory is almost exact. This is important, since some of the older data reported in Table VI did show bothersome differences from one paper to the other. When new more accurate data are taken, the agreement between theory and experiment is seen to improve and is excellent.

Finally, the gap-to-critical-temperature ratio based on the spectra of Wolf and Noer (1979) gives 4.19 for $Nb_{0.75}Zr_{0.25}$ and 3.88 for Nb, to be compared with the experimental result of 4.12 and 3.86 by Wolf and Noer (1979) and 4.18 and 3.89 by Junod *et al.* (1986). The agreement is very good. One can easily understand why Δ_0 is more affected than T_c by the softening of $\alpha^2F(\omega)$ (seen in Fig. 48) on going from Nb to $Nb_{0.75}Zr_{0.25}$. We have already given functional derivatives for T_c, Δ_0, and $2\Delta_0/k_BT_c$ with respect to $\alpha^2F(\omega)$ in previous sections. The results from Nb are presented in Figs. 49(a) and 49(b). The functional derivative $\delta\Delta_0/\delta\alpha^2F(\omega)$ compared with $\delta T_c/\delta\alpha^2F(\omega)$ peaks at lower energy ($\sim 4k_BT_c$) and

$$\Delta_0^{-1}\delta\Delta_0/\delta\alpha^2F(\omega)\geq T_c^{-1}\delta T_c/\delta\alpha^2F(\omega)\ ,$$

which results in a non-negative $\delta(2\Delta_0/k_BT_c)/\delta\alpha^2F(\omega)$ that peaks at $\sim 8k_BT_c/6$. Thus it is seen that the shift towards lower energy of spectral weight in $\alpha^2F(\omega)$ to the region below ~ 10 meV in going from Nb to $Nb_{0.75}Zr_{0.25}$ will increase Δ_0, T_c, and also $2\Delta_0/k_BT_c$. The Coulomb

TABLE VIII. Thermodynamic properties.

	$Nb_{0.75}Zr_{0.25}$		Nb	
	Theory	Exp.	Theory	Exp.
$H_c(0)$, critical field at $T=0$ (Oe)	2571.0	2490	2002.0	2020
$\Delta C(T_c)$, specified heat jump at T_c (mJ/mol K)	213.0	215.0	138.0	138.0
$-(dH_c/dT)_{T_c}$ (G/K)	478.0	480.0	415.0	415.0
Minimum $D(t)$ deviation function			−0.0101	−0.011
At $t=T/T_c$			0.542	0.55
Maximum $D(t)$ deviation function	0.0070	0.008	0.0013	0.001
At $t=T/T_c$	0.184	0.23	0.051	0.047
$C_{es}(T_c)/(\gamma T_c)$, ratio of electronic specific heat at T_c in superconducting and normal states	3.22	3.23	2.91	2.91
$\gamma T_c/H_c^2(0)$, ratio of specific heat in normal state to square of zero-temperature critical field	0.143	0.143	0.153	0.153

repulsion parameter μ^* also changes slightly from ~ 0.185 for Nb to ~ 0.181 for $Nb_{0.75}Zr_{0.25}$, but this is a small effect. From the values of $T_c^{-1}\partial T_c/\partial\mu^* \simeq -4.2$, $\Delta_0^{-1}\partial\Delta_0/\partial\mu^* \simeq -4.8$, and $\partial \ln(2\Delta_0/k_B T_c)/\partial\mu^* \simeq -0.6$ for Nb, we estimate the changes in T_c, Δ_0, and $2\Delta_0/k_B T_c$ due to the change in μ^* to be $\delta(T_c)\approx 0.15$ K, $\delta(\Delta_0)\simeq 0.03$ meV, and $\delta(2\Delta_0/k_B T_c)\simeq 0.06$. These changes are small compared to the total changes $\delta_{tot}(T_c)=1.58$ K, $\delta_{tot}(\Delta_0)=0.39$ meV, and $\delta_{tot}(2\Delta_0/k_B T_c)=0.27$. Therefore most of the shift in going from Nb to $Nb_{0.75}Zr_{0.25}$ is due to shift of the electron-phonon spectral weight to the more favorable frequency region as indicated by the functional derivatives.

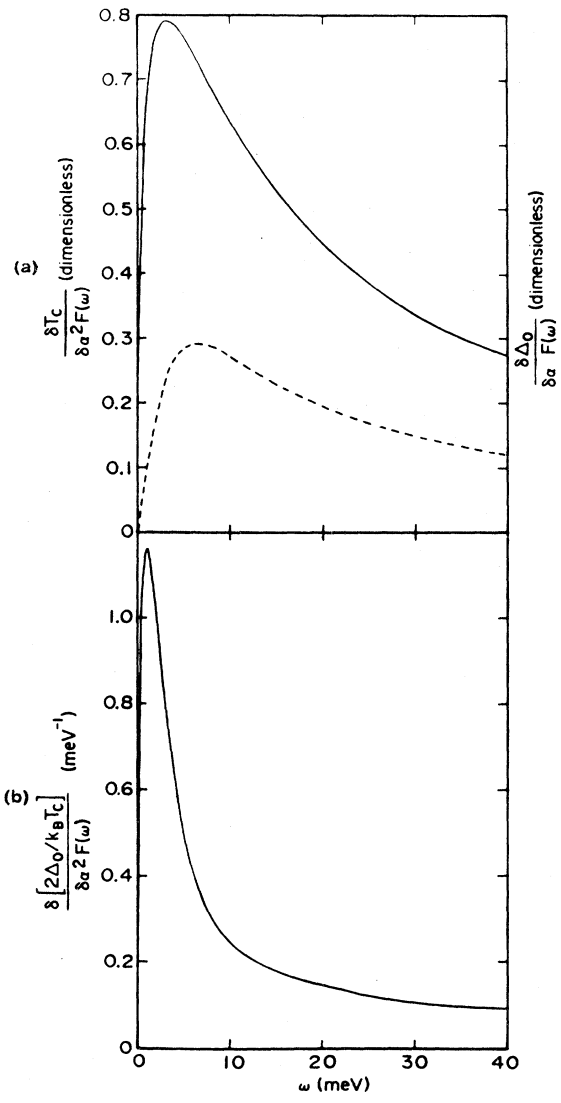

FIG. 49. (a) the functional derivative of T_c (dashed curve) and of the gap Δ_0 (solid curve) with respect to $\alpha^2F(\omega)$ for Nb. (b) the functional derivative of the dimensionless ratio $2\Delta_0/k_B T_c$ with respect to $\alpha^2F(\omega)$ for Nb.

D. V_3Si, comparison with experiment

We turn next to a discussion of the thermodynamic properties of the A15 compounds. It will be sufficient for our purposes to consider in detail only the case of V_3Si. Similar agreement is found in the other A15's. We begin with two non-tunneling-derived models for $\alpha^2F(\omega)$. The first, which we shall later see is not far from the tunneling-derived spectrum, is taken to be a constant "c" times the measured [Schweiss *et al.* (1970)] generalized phonon density of states $G(\omega)$ in V_3Si at $T=77$ K obtained from incoherent inelastic neutron scattering. The constant c is taken in such a way that the resulting mass renormalization $\lambda=1$, so $\alpha^2F_1(\omega)=cG(\omega)$. The second spectrum is $\alpha^2F_2(\omega)\equiv\alpha^2_{tr}F(\omega)$ with $\alpha^2_{tr}F(\omega)$ determined from far-infrared-absorption experiments (McKnight, Bean, and Perkowitz, 1979; McKnight, Perkowitz, *et al.* 1979). In this case, λ is equal to 1.29. We need to stress that $\alpha^2_{tr}F(\omega)$, which controls transport properties, is different from $\alpha^2F(\omega)$ and that it is used here mainly to illustrate that thermodynamic properties are sensitive to some of the details of $\alpha^2F(\omega)$, so that we cannot use just any arbitrary spectrum. This will be discussed in more detail later.

The two spectra α^2_1F (solid curve) and α^2_2F (dotted curve) are compared in Fig. 50 and are seen to be quite different. These differences are also reflected in Table IX where some typical parameters for the two spectra are given in the first four rows. In particular, we note that spectrum 1 is much harder than spectrum 2, as can be seen by the values of the average phonon energy $\langle\omega\rangle$ and $\langle\omega^2\rangle^{1/2}$. They will lead to very different thermodynam-

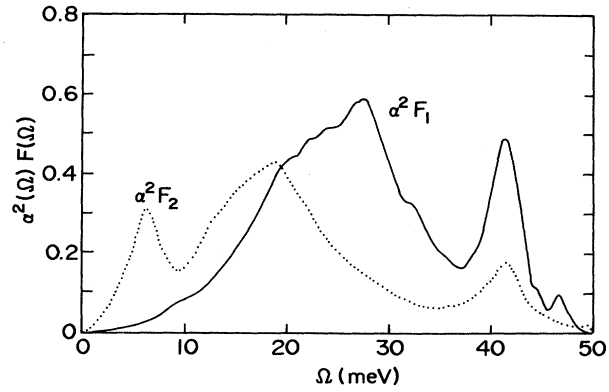

FIG. 50. Comparison of two model electron-phonon spectral densities for V_3Si. The first model $\alpha^2F_1(\omega)$ (solid curve) involves a constant times the measured phonon frequency distribution determined by incoherent inelastic neutron scattering. The second model $\alpha^2F_2(\omega)$ (dotted curve) involves the transport electron-phonon spectral density measured in optical measurements.

ics. In Fig. 51 we present the results of our calculation of the deviation functions $D(t)$ for the two spectra together with the experimental results [Muto *et al.* (1979)]; in Fig. 52, we show a similar comparison for the specific heat $\ln(C_{es}/\gamma T_c)$. In Table IX, we give calculated and experimental values for some characteristic thermodynamic parameters.

Obviously, the results obtained from the spectrum based on the neutron experiments with $\lambda=1$ give a fit to the experimental values of thermodynamic quantities, which is of the same quality as that found for the *s-p* and transition metals. At the same time, the thermodynamic properties calculated on the basis of the second spectrum ($\lambda=1.29$) correspond to a superconductor that is considerably more strongly coupled than V_3Si and is unacceptable. Moreover, the latter spectrum requires an unusually small Coulomb repulsion parameter; i.e., $\mu^*(\omega_c)=0.05$, in order to obtain the experimental value of T_c. It can safely be ruled out as the possible candidate for the $\alpha^2F(\omega)$ in V_3Si.

The results presented so far do not depend on the numerical value for the electronic density of states. Since the results for dimensionless ratios based on the first spectrum give good agreement with the experiments, it makes sense to attempt to fit the value of $N(0)$ to the experimental result for some particular thermodynamic quantity dependent on $N(0)$. Calculated values for other quantities, also dependent on $N(0)$, can then be compared with the experiment. In addition, the value of $N(0)$ extracted in such a way can be compared with the values inferred from other independent experimental quantities or obtained in band-structure calculations. We have fit $N(0)$ to the zero-temperature thermodynamic critical field $H_c(0)=6.43$ kOe [Muto *et al.* (1979)], and the value obtained for $N(0)=13.64\times10^{19}$ states/(meV cm^3 spin). When we compare calculated thermodynamic parameters for this value of $N(0)$ with the experimental results [Brock (1969); Knapp *et al.* (1975)], in all cases, the agreement is within a few percent.

The results presented so far clearly suggest that the $\alpha^2F(\omega)$ spectrum, based on the measured $G(\omega)$ at $T=77$ K and with $\lambda=1$, is able to account for the thermodynamic properties of V_3Si within the usual Eliashberg theory of superconductivity, while the $\alpha^2_{tr}F(\Omega)$ inferred from the far-infrared-absorption measurements cannot. Thus, from this point on, we shall not refer to the results obtained on the basis of the latter spectrum.

The calculated value for the ratio $2\Delta_0/k_BT_c$ is in excellent agreement with the value ~3.8 obtained in the re-

TABLE IX. Summary of some typical parameters for the two-model spectra of electron-phonon interaction in V_3Si and comparison of calculated values for several thermodynamic quantities with experimental results. Tunneling results are also included.

	Spectrum 1	Spectrum 2	Experiment	Tunneling
$\lambda=2\int_0^{+\infty}d\Omega\,\alpha^2(\Omega)F(\Omega)/\Omega$	1	1.29		0.902
$A=\int_0^{+\infty}d\Omega\,\alpha^2(\Omega)F(\Omega)$	11.99 meV	8.63 meV		9.55 meV
$\langle\omega\rangle=2A/\lambda$	23.96 meV	13.38 meV		10.6 meV
$\langle\omega^2\rangle^{1/2}=\left[2\int_0^{+\infty}d\Omega\,\Omega\alpha^2(\Omega)F(\Omega)/\lambda\right]^{1/2}$	25.78 meV	16.45 meV		
Ω_{max} maximum phonon energy in α^2F	50 meV	50 meV		42 meV
ω_c cutoff energy in Matsbuara sums	250 meV	250 meV		254 meV
$\mu^*(\omega_c)$ Coulomb repulsion parameter	0.15	0.05		0.102
T_c superconducting critical temperature	17.1 K	16.63 K	14.5–17.1 k[a]	15.4 K
$-\frac{1}{H_c(0)}\left[\frac{dH_c(T)}{dT}\right]_{T_c}T_c$, parameter for which the BCS theory gives the value 1.74	1.95	2.44	1.97[b]	1.93
$\gamma\left[\frac{T_c}{H_c(0)}\right]^2$ parameter for which BCS theory gives the value 0.168	0.151	0.142	0.153[b]	0.151
$\Delta C/(\gamma T_c)$ ratio of jump in specific heat at T_c to the normal-state electronic specific heat at T_c; BCS value is 1.43	2.01	2.25	2.01[b]	1.97
$2\Delta_0/k_BT_c$; BCS value is 3.53	3.85	4.33	3.76±0.1[c] 3.8[d] 3.8[e] 3.4–3.6[f]	3.89

[a]Roberts (1976).
[b]Muto *et al.* (1979).
[c]McKnight, Bean, and Perkowitz (1979); McKnight, Perkowitz *et al.* (1979).
[d]Hauser *et al.* (1966).
[e]Moore *et al.* (1977).
[f]Moore *et al.* (1979).

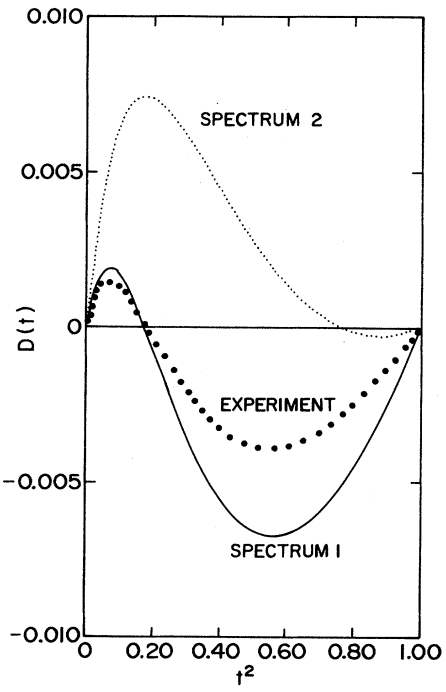

FIG. 51. Thermodynamic critical-field deviation function $D(t)$ as a function of the square of the reduced temperature t. The solid dots are experimental results, while the solid curve represents the predictions of Eliashberg theory based on model spectrum $\alpha^2F_1(\omega)$. The dotted curve is the result for similar calculations based on the model $\alpha^2F_2(\omega)$.

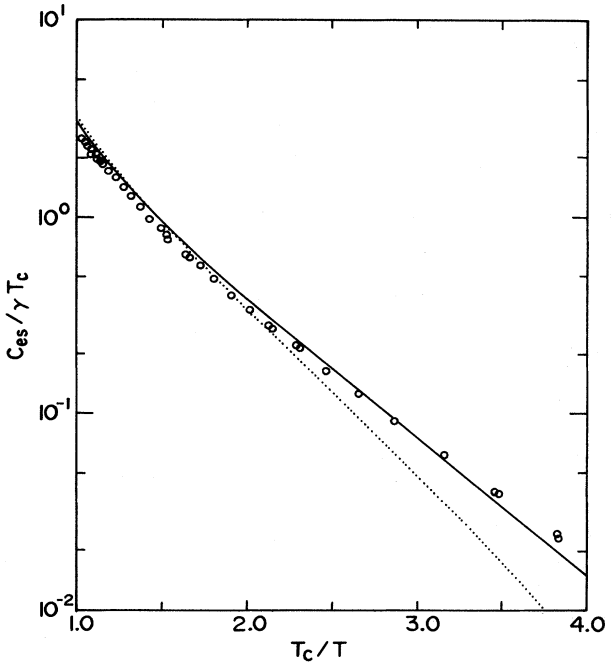

FIG. 52. Comparison of theory and experimental (empty circles) results for the electronic specific heat C_{es} in the superconducting state normalized to the normal-state value at T_c (γT_c) as a function of T_c/T. The solid curve is the result of full Eliashberg calculations based on model $\alpha^2F_1(\omega)$, while the dotted curve involves, instead, $\alpha^2F_2(\omega)$.

cent far-infrared measurements [McKnight, Bean, and Perkowitz (1979); McKnight, Perkowitz, *et al.* (1979)] as well as in the older tunneling results [Hauser *et al* (1966); Moore *et al.* (1977)]. More recent tunneling experiments [Moore *et al.* (1979)] give the value $2\Delta_0/k_BT_c \sim 3.5$, but there were indications that the bulk value for Δ_0 was underestimated. On the basis of the functional derivatives $\delta T_c/\delta\alpha^2F(\Omega)$, $\delta\Delta_0/\delta\alpha^2F(\Omega)$, and $\delta(2\Delta_0/k_BT_c)/\delta\alpha^2F(\Omega)$, which are non-negative peaked functions with the peak frequencies $\Omega^*(T_c)\sim 8k_BT_c$, $\Omega^*(\Delta_0)\sim 2\Delta_0$, and $\Omega^*(2\Delta_0/k_BT_c)\sim\Delta_0/3$, respectively, we can conclude that $\alpha^2F(\Omega)$ in V_3Si cannot have significantly more weight at lower frequencies and less weight at higher frequencies than our model (solid curve in Fig. 50), since that would increase the value of the ratio $2\Delta_0/k_BT_c$ above the observed upper limit of 3.8. This is borne out in the tunneling experiment of Kihlstrom (1985). His derived spectrum has a $\lambda=0.9$ and is quite close to $\alpha_1^2F(\omega)$ except for a slight shift toward lower frequency of the lower-energy peak in the spectral density and some attenuation of the high-energy peak. Results of thermodynamic calculations [Mitrović and Carbotte (1986)] for this spectrum are given in Table IX (last column) and are seen to be close to those of spectrum 1.

It is instructive to compare the value of $N(0)=13.64\times10^{19}$ states/(spin meV cm^3), obtained by fitting the calculated zero-temperature thermodynamic critical field to the experimental value, with other values of $N(0)$ in V_3Si available in the literature. Muto *et al.* (1979) have obtained from their experiments the value 28.27×10^{19} states/(meV cm^3 spin) for the fully dressed electronic density of states $N^*(0)=N(0)(1+\lambda)$, where we assumed that $N(0)$ contains the renormalization by the Coulomb interactions [Heine *et al.* (1966)]. If we take $\lambda=1$, this would give $N(0)=14.14\times10^{19}$ states/(meV cm^3 spin), in good agreement ($\sim$5 percent) with our value. Testardi and Mattheiss (1978) give the experimental value 14.25×10^{19} states/(spin meV cm^3) for nearly stoichiometric V_3Si, again in excellent agreement with our value for $N(0)$. However, the band-structure calculations give for $N(0)$ in stoichiometric V_3Si a value that is about one-half of the above-quoted numbers. Mattheiss *et al.* (1978) calculated $N(0)=5.70\times10^{19}$ states/(meV cm^3 spin). Self-consistent augmented plane-wave (APW) calculations by Klein *et al.* (1978, 1980) give the similar result $N(0)=6.99\times10^{19}$ states/(meV cm^3 spin). Using a linear combination of muffin-tin orbitals, the self-consistent band-structure calculations of Arbman and Jarlborg (1978) give an even smaller value $N(0)\sim4.2\times10^{19}$ states/(meV cm^3 spin).

Testardi and Mattheiss (1978) have offered an explanation for the large discrepancy in the values of calculated $N(0)$ and the one inferred from the experiments in V_3Si in terms of the rapid variation in $N(E)$ around the Fermi level. They assume that actual samples correspond to $V_{3-x}Si$ with small $x>0$. Then by assuming the rigid-band model they conclude that the resulting shift (of about 35 meV) in the position of the Fermi level in

$V_{2.94}Si$ compared to its value in V_3Si leads to a large increase in $N(0)$.

To end, it should be mentioned that the experimental γ value ~ 70 mJ/(mol K^2) has been obtained by analyzing the normal-state specific heat using the formula $C(T)=\gamma T+\beta T^3+\alpha T^5$ (plus the requirement that at T_c, the entropy in the normal state is equal to that in the superconducting state). This procedure is, perhaps, more appropriate for complicated solids such as V_3Si, which cannot be described by a Debye model ($\alpha=0$). An analysis of the specific-heat data, on the basis of $C(T)=\gamma T+\beta T^3$ only, usually gives a smaller value for γ, between 55 and 62 mJ/(mol K^2) [Muto *et al.* (1979)].

Other results for the thermodynamics in the A15 compounds are discussed by Mitrović, Schachinger, and Carbotte (1984), and comparison with experiment is made whenever possible. Good agreement is found. In some cases different spectra are examined for a particular material so as to get some feeling for the dependence of the result obtained on choice of spectral density. Preliminary results using a model $\alpha^2F(\omega)$ based on the phonon frequency distribution in the Chevrel phase compounds have also been obtained [Schachinger, Zarate, *et al.* (1986)]. In this case, no tunneling results exist as yet. A general conclusion of all this is that Eliashberg theory with an electron-phonon kernel applies equally well to the A15 compounds and probably to the Chevrel phases.

E. Approximate analytic formulas

So far, we have presented limited theoretical results and have compared with experiment in specific cases so as to illustrate the kind of agreement that can be achieved between Eliashberg theory, with a tunneling-derived spectral density, and experimental data. On the whole, the agreement is very good and constitutes strong evidence for Eliashberg theory with an electron-phonon mechanism. We wish now to give additional theoretical results for many more materials. We shall do this in the context of approximate equations for strong-coupling corrections of the kind already discussed for the gap-to-critical-temperature ratio and shall not compare further with experiment. Such formulas contain the single strong-coupling parameter $T_c/\omega_{\ln}$ [Kresin and Parkhomenko (1974, 1975); Marsiglio and Carbotte (1986)]. The gap is modeled by

$$\Delta(\omega_n)=\begin{cases}\Delta_0(T), & |\omega_n|<\omega_0\ ,\\ 0, & |\omega_n|>\omega_0\ ,\end{cases} \tag{5.7a}$$

and

$$Z(\omega_n)=\begin{cases}Z_0(T), & |\omega_n|<\omega_0\ ,\\ 1, & |\omega_n|>\omega_0\ .\end{cases} \tag{5.7b}$$

Here, ω_0 represents roughly a few times the maximum phonon frequency in the system. For self-consistency, we would require $\lambda(i\omega_n-i\omega_m)$ to be independent of n. This would reduce to the $\lambda^{\theta\theta}$ approximation. Instead, we evaluate Eqs. (2.1) and (2.2) at $n=1$. Thus Δ_1 is the constant gap in Eq. (5.7a). The procedure is outlined in Appendix B. Essential to the approximations used is the requirement $T_c/\omega_{\ln}\ll 1$. We have also assumed that ω_0 is sufficiently large that $\omega_{\ln}/\omega_0\ll 1$. Expansions near T_c give

$$\frac{\Delta C(T)}{\gamma T_c}=f+(1-t)g\ , \tag{5.8}$$

where

$$f\equiv\frac{\Delta C(T_c)}{\gamma T_c}=1.43\left[1+53\left[\frac{T_c}{\omega_{\ln}}\right]^2\ln\left[\frac{\omega_{\ln}}{3T_c}\right]\right] \tag{5.9}$$

and

$$g=-3.77\left[1+117\left[\frac{T_c}{\omega_{\ln}}\right]^2\left[\frac{\omega_{\ln}}{2.9T_c}\right]\right] \tag{5.10}$$

TABLE X. Superconducting properties: thermodynamic properties.

Material	$T_c/\omega_{\ln}$	$\frac{\gamma T_c^2}{H_c^2(0)}$	$\frac{\Delta C(T_c)}{\gamma_0 T_c}$	$h_c(0)$
Al	0.004	0.168	1.43	0.576
V	0.031	0.162	1.63	0.550
Ta	0.035	0.162	1.63	0.550
Sn	0.038	0.160	1.68	0.544
Tl	0.046	0.158	1.74	0.538
$Tl_{0.9}Bi_{0.1}$	0.048	0.157	1.76	0.536
In	0.050	0.156	1.79	0.533
Nb (Butler)	0.057	0.153	1.94	0.517
Nb (Arnold)	0.062	0.153	1.92	0.521
V_3Si_{-1}	0.070	0.150	1.99	0.515
V_3Si (Kihl.)	0.071	0.150	2.02	0.512
Nb (Rowell)	0.074	0.150	1.97	0.518
Mo	0.076	0.150	1.98	0.518
$Pb_{0.4}Tl_{0.6}$	0.095	0.144	2.24	0.497
La	0.099	0.145	2.14	0.506
V_3Ga	0.103	0.143	2.24	0.499
Nb_3Al (2)	0.113	0.141	2.33	0.492
Nb_3Ge (2)	0.114	0.137	2.61	0.471
$Pb_{0.6}Tl_{0.4}$	0.119	0.137	2.52	0.479
Pb	0.128	0.132	2.77	0.466
Nb_3Al (3)	0.129	0.137	2.54	0.479
$Pb_{0.8}Tl_{0.2}$	0.136	0.134	2.69	0.470
Hg	0.146	0.134	2.49	0.488
Nb_3Sn	0.146	0.134	2.64	0.474
$Pb_{0.9}Bi_{0.1}$	0.152	0.130	2.86	0.463
Nb_3Al (1)	0.156	0.134	2.61	0.477
Nb_3Ge (1)	0.160	0.134	2.59	0.479
$Pb_{0.8}Bi_{0.2}$	0.172	0.127	2.92	0.462
$Pb_{0.7}Bi_{0.3}$	0.182	0.125	3.01	0.460
$Pb_{0.65}Bi_{0.35}$	0.200	0.125	2.98	0.462
$Pb_{0.5}Bi_{0.5}$	0.320	0.147	2.16	0.500
Ga	0.243	0.150	2.04	0.509
$Pb_{0.75}Bi_{0.25}$	0.288	0.143	2.27	0.494
Bi	0.320	0.153	2.03	0.506

[see also Swihart (1963); Marsiglio and Carbotte (1986)]. The general form of these equations is not new and has been derived and used previously [Geilikman and Kresin (1965, 1966); Masharov (1974a, 1974b); Kresin and Parkhomenko (1974, 1975)]. What is new is our use of the specific characteristic phonon energy $\omega_{\ln}$ in Eqs. (5.8) to (5.10) and the suggested specific numerical coefficients to go along with our choice of average phonon energy. These numerical coefficients are fit to the numerous numerical results listed in Table X; and so, Eqs. (5.9) and (5.10), as well as other such equations to be introduced later, represent well the data on real materials. The derived equations are plotted in Figs. 53 and 54 along with the numerical data. For clarity, experimental data have been omitted, although the Eliashberg theory results are found to be generally accurate to within 10 percent. We note that there is some scatter in the exact numerical results, especially among the A15 compounds and Hg. In the case of Hg, there is a very-low-frequency peak in the $\alpha^2F(\omega)$ spectrum, so that the assumption $\omega \gg T_c$ for all important ω has broken down. In addition, we note that the results from amorphous materials have not been plotted. They are not at all well described by Eqs. (5.8)–(5.10). They are included in Table X, where it is seen that their values for $T_c/\omega_{\ln}$ are near 0.3. This value is beyond the limit of validity of Eqs. (5.9) and (5.10), and of others that will be presented later. More importantly, however, the spectral shapes of $\alpha^2F(\omega)$ for these materials is such that they are not even approximately described by an Einstein spectrum with frequency $\omega_E = \omega_{\ln}$ of the material. The opposite tends to be true for the crystalline materials. Coombes and Carbotte (1986a, 1988) have analyzed in detail the dependence of the results on the shape of the spectral density. Some of the

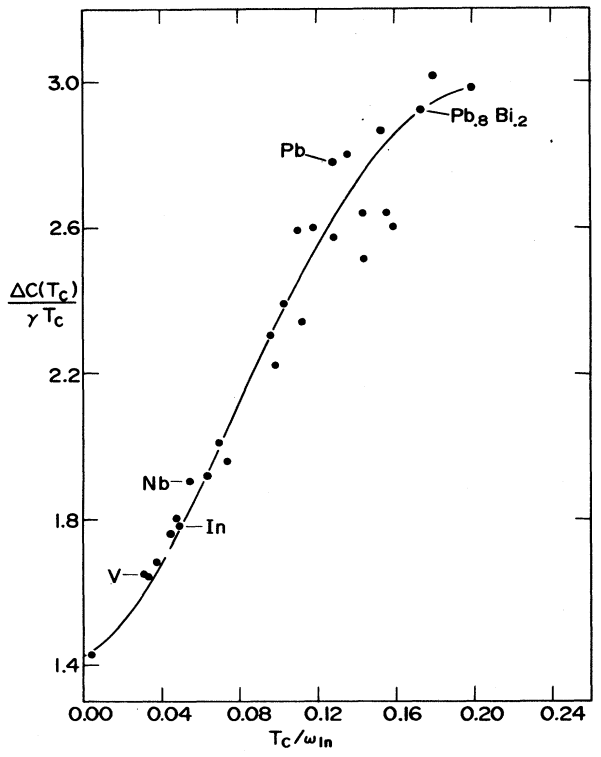

FIG. 53. Specific-heat-jump ratio $f \equiv \Delta C(T_c)/(\gamma T_c)$ vs $T_c/\omega_{\ln}$. The dots represent the accurate results from the full numerical solutions of the Eliashberg equations. Experiment tends to agree to within 10 percent. In increasing order of $T_c/\omega_{\ln}$, the dots correspond to the following systems: Al, V, Ta, Sn, Tl, $Tl_{0.9}Bi_{0.1}$, In, Nb (Butler), Nb (Arnold), $V_3Si(1)$, V_3Si (Kihl.), Nb (Rowell), Mo, $Pb_{0.4}Tl_{0.6}$, La, V_3Ga, $Nb_3Al(2)$, $Nb_3Ge(2)$, $Pb_{0.6}Tl_{0.4}$, Pb, Nb_3Al (3), $Pb_{0.8}Tl_{0.2}$, Hg, Nb_3Sn, $Pb_{0.9}Bi_{0.1}$, $Nb_3Al(1)$, $Nb_3Ge(1)$, $Pb_{0.8}Bi_{0.2}$, $Pb_{0.7}Bi_{0.3}$, and $Pb_{0.65}Bi_{0.35}$. The drawn curve corresponds to $\Delta C(T_c)/\gamma T_c = 1.43[1+53(T_c/\omega_{\ln})^2\ln(\omega_{\ln}/3T_c)]$.

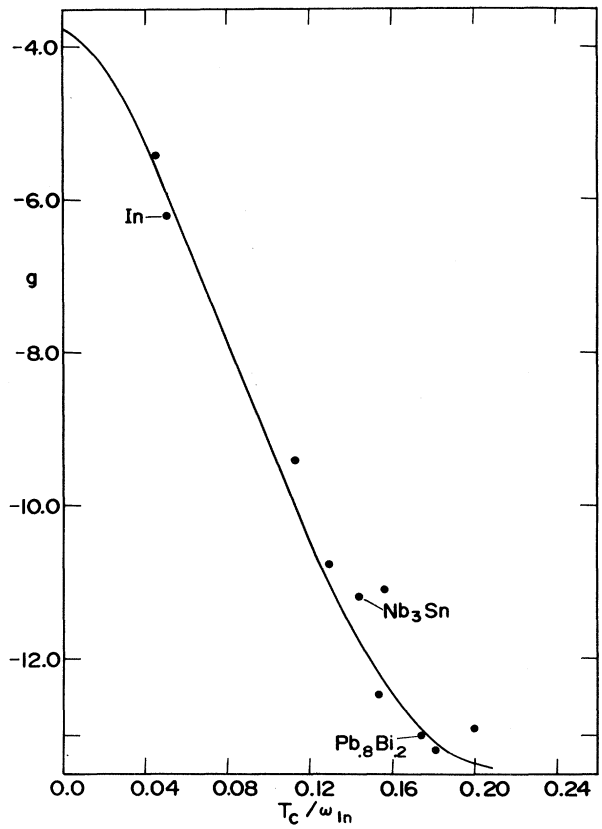

FIG. 54. Negative specific-heat slope g at T_c vs $T_c/\omega_{\ln}$ for a selected number of systems. Dots correspond to the results extracted from numerical solutions for $D(t) \equiv H_c(T)/H_c(0) - (1-t^2)$ vs t, using the Eliashberg equations. In increasing order of $T_c/\omega_{\ln}$, the dots correspond to Tl, In, $Nb_3Al(2)$, Nb_3Sn, $Pb_{0.9}Bi_{0.1}$, $Nb_3Al(1)$, $Pb_{0.8}Bi_{0.2}$, $Pb_{0.7}Bi_{0.3}$, and $Pb_{0.65}Bi_{0.35}$. The drawn curve corresponds to $g = -3.77[1 + 117(T_c/\omega_{\ln})^2\ln(\omega_{\ln}/2.9T_c)]$. The fit is remarkably good, considering the constraints on the coefficients.

scatter is also due to variations in μ^*. In any event, the point of these equations is to describe the general trend of superconducting properties as a function of strong coupling. The result is a continual increase of both f and the absolute value of g as $T_c/\omega_{\ln}$ increases from 0 (BCS) to 0.20. We note that there are signs of saturation in the curves around $T_c/\omega_{\ln}\cong 0.2$, and, in fact, it will later be seen that as the coupling is increased further, $\Delta C(T_c)/(\gamma T_c)$, for example, will eventually decrease to values below 1.43.

The physical reason behind the increase in $\Delta C(T_c)/(\gamma T_c)$ can be traced to the gap opening up more rapidly just below T_c as the coupling strength is increased. The specific-heat jump, which is a measure of steepness of the ascent of the gap, will increase as well. The subsequent decline alluded to in the previous paragraph is not physical; it is a result of having used γ instead of the Grimvall (1968, 1969) $\gamma(T_c)$.

Also derived in Appendix B are equations for two more commonly used ratios:

$$\frac{\gamma T_c^2}{H_c^2(0)}=0.168\left[1-12.2\left[\frac{T_c}{\omega_{\ln}}\right]^2\ln\left[\frac{\omega_{\ln}}{3T_c}\right]\right] \quad (5.11)$$

and

$$\frac{H_c(0)}{\left.\frac{dH_c(T)}{dT}\right|_{T_c} T_c}=h_c(0)=0.576\left[1-13.4\left[\frac{T_c}{\omega_{\ln}}\right]^2\ln\left[\frac{\omega_{\ln}}{3.5T_c}\right]\right]. \quad (5.12)$$

These equations, along with numerical data for many real materials, are plotted in Figs. 55 and 56. The first ratio is rather well described by Eq. (5.11). The second exhibits considerably more scatter. Both show indications of saturation. The important point, however, is that the trend for realistic spectral shapes is well described by these formulas. Moreover, the deviation from BCS behavior is relatively small (~20 percent) in $h_c(0)$, as compared to $2\Delta_0/k_BT_c$.

Tunneling junctions are sometimes difficult to fabricate; hence, for some materials, an $\alpha^2F(\omega)$ spectrum does not exist. Moreover, for the same reason, the gap edge is unknown as well. Hence over the years many formulas [Toxen (1965); Padamsee *et al.* (1973); Stewart (1979);

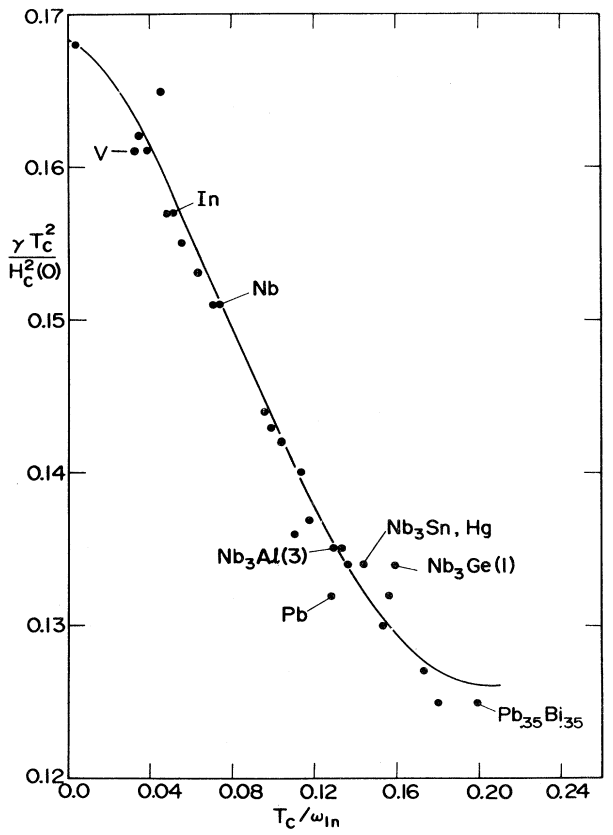

FIG. 55. Ratio $\gamma T_c^2/H_c^2(0)$ vs $T_c/\omega_{\ln}$ (see Fig. 53 for identification of materials). The curve corresponds to $\gamma T_c^2/H_c^2(0)=0.168[1-12.2(T_c/\omega_{\ln})^2\ln(\omega_{\ln}/3T_c)]$.

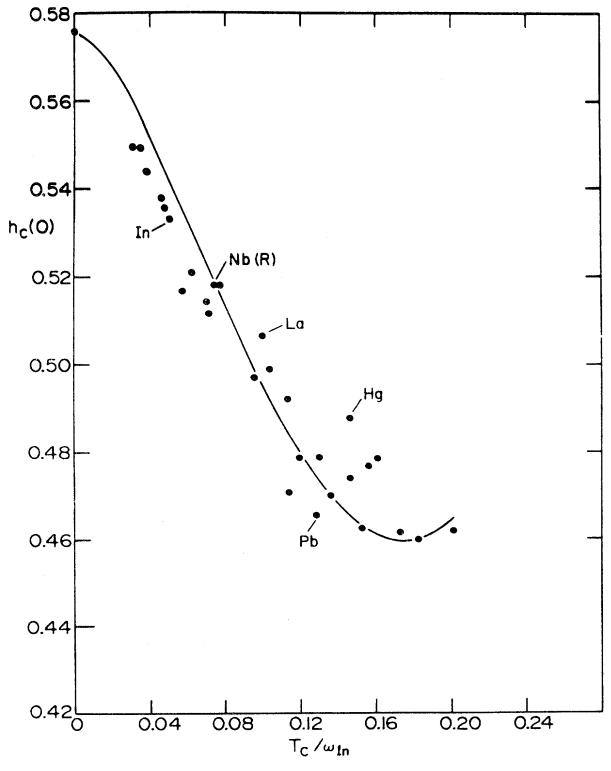

FIG. 56. Ratio $h_c(0)$ vs $T_c/\omega_{\ln}$ (see Fig. 53 for identification of materials). The curve corresponds to $h_c(0)=0.576[1-13.4(T_c/\omega_{\ln})^2\ln(\omega_{\ln}/3.5T_c)]$.

and Marsiglio, Coombes, and Carbotte (1987)] have been developed, which estimate the gap edge given thermodynamic properties, since these are often more easily measured. These formulas are usually not reliable, as discussed recently by Marsiglio, Coombes, and Carbotte (1987). The formulas in the previous section, however, allow much more accurate determinations. The parameter $T_c/\omega_{\ln}$ is still unknown, but it can be determined through one measurement, for example, of the specific-heat jump, from Eq. (5.9). Equation (4.1) then allows for an accurate determination of the gap ratio, $2\Delta_0/k_BT_c$. In Fig. 57, we plot $\Delta C/\gamma T_c$ versus $2\Delta_0/k_BT_c$ for many crystalline spectra. The solid curve is determined through Eqs. (5.9) and (4.1). Once again, amorphous materials tend to ruin the simple relation somewhat. What is clear, however, is that with little error the specific-heat jump of a material uniquely determines the gap ratio, provided the material is crystalline, and has a value of $T_c/\omega_{\ln} \lesssim 0.2$. Similar remarks hold for the other properties discussed.

While the solid curves of Figs. 53 and 57 certainly represent well the trend in the data up to $T_c/\omega_{\ln} \cong 0.24$, a range which covers conventional superconductors, some solid points do fall off the curve. This means that in these cases the quantity considered is not completely determined by the single strong-coupling parameter $T_c/\omega_{\ln}$ and depends on further details of the spectral density. Full numerical calculations are required in such cases in order to get quantitative answers. As they did in the case of the ratio $2\Delta_0/k_BT_c$, which we previously discussed, Coombes and Carbotte (1986a) have studied these deviations in detail for thermodynamic properties. They use model spectra based on real materials, but each is rescaled to get the same T_c and $T_c/\omega_{\ln}$ as Pb. With these spectra labeled with an asterisk, they recalculate the thermodynamics, which would not change if shape were unimportant and $T_c/\omega_{\ln}$ were the only significant parameter characterizing the spectrum. In Fig. 58, we repeat our result for $\Delta C(T_c)/(\gamma T_c)$, but in the inset we show how this ratio changes in the case of Pb when various shapes are considered, namely, a delta function, Pb, Al, Tl, Nb, Sn, In, Hg, Nb_3Sn, $Pb_{0.5}Bi_{0.5}$, and amorphous Ga. It is seen that $\Delta C(T_c)/(\gamma T_c)$ can range from approximately 3.0 to 2.0 depending on shape. Therefore shape dependence beyond that captured by $\omega_{\ln}$ does come

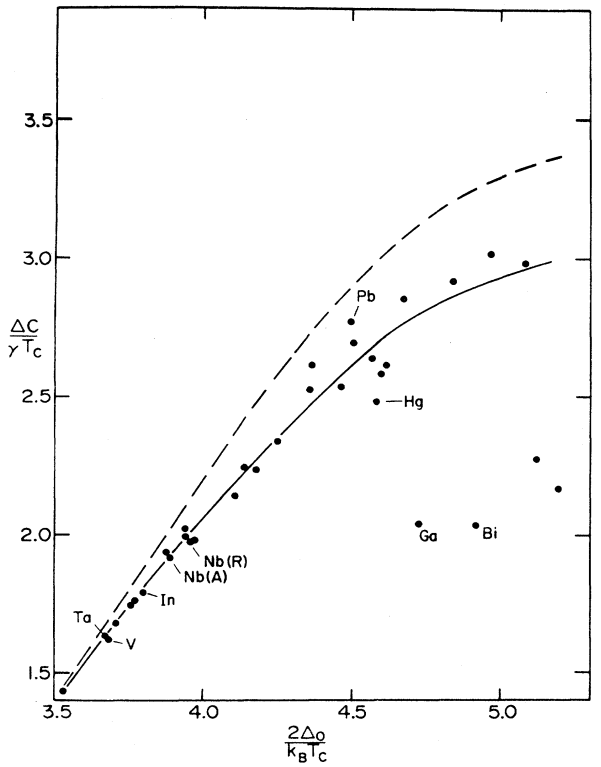

FIG. 57. Ratio $\Delta C/(\gamma T_c)$ vs $2\Delta_0/k_BT_c$. There is an almost unique relationship between these two quantities for crystalline materials. The amorphous materials ruin this universality. The solid line corresponds to solutions based on Eqs. (5.8) and (4.1) and, of course, represents the numerical data quite well. The dashed line represents solutions for Einstein spectra with $\mu^*=0$.

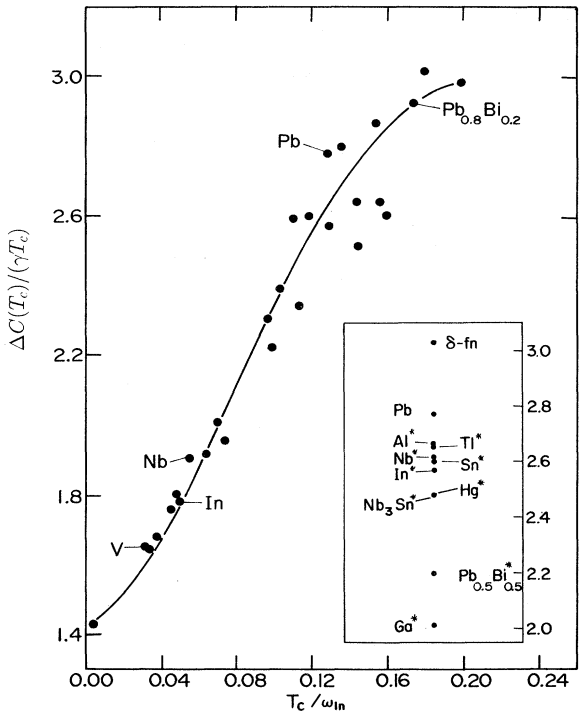

FIG. 58. Normalized specific-heat jump at T_c, $\Delta C(T_c)/(\gamma T_c)$ as a function of $T_c/\omega_{\ln}$. The insert shows results for $\Delta C(T_c)/(\gamma T_c)$ using model-shifted spectra for the real metals indicated. More specifically, $\alpha_M^2F(\omega)=B\alpha_0^2F(b\omega)$ where $\alpha_0^2F(\omega)$ refers to a specific material. The constants B and b have been chosen in every case to get the same value of T_c and of $\omega_{\ln}$ as apply to Pb.

into play. Results for other thermodynamic indices, as well as for more extreme shapes than those shown here, can be found in the work of Coombes and Carbotte (1988), to which the reader is referred.

F. Very strong coupling regime

So far, we have been interested exclusively in superconductors for which $T_c/\omega_{\ln} \lesssim 0.24$. In view of the existence of the high-T_c oxides, it is of some interest to extend the range of $T_c/\omega_{\ln}$ considered to much higher values. To accomplish this, we return to the scaling $\alpha_M^2 F(\omega) = B\alpha_0^2 F(b\omega)$. For definiteness, we take for base spectrum (denoted by a subscript zero) the spectral density that was calculated by Weber (1987a, 1987b) for La-Sr-Cu-O and change B to get different values of $T_c/\omega_{\ln}$ ranging through the very strong coupling regime up to $T_c/\omega_{\ln}=1.4$. Results [Marsiglio *et al.* (1987a)] are given in Fig. 59 for $\Delta C(T_c)/(\gamma T_c)$ against $T_c/\omega_{\ln}$. It is seen from this figure that as $T_c/\omega_{\ln}$ increases from 0, the normalized jump also increases from its BCS value of 1.43 and that a maximum is reached (solid curve) around $T_c/\omega_{\ln}\approx 0.2$, which is near the end of the conventional strong-coupling region shown in Fig. 53. After the maximum there is a steady decline towards lower values; at $T_c/\omega_{\ln}=1.4$ the curve has fallen way below 1.43. This is an unexpected feature that can be taken as characteristic of the very strong coupling regime.

One may well wonder if the shape of the curve obtained for the variation of $\Delta C(T_c)/(\gamma T_c)$ with coupling strength is sensitive to the shape of the spectrum used. To check on this point, we show on the same figure (59) additional results based on the tunneling-derived Pb spectrum (dotted curve). While the maximum in the curve is now at slightly higher $T_c/\omega_{\ln}$ value and larger in magnitude, the two curves are qualitatively similar. Akis and Carbotte (1989a) have given a more detailed analysis of this shape dependence and conclude that while shape can be important, the main features of our results are not changed.

Besides the normalized specific-heat jump at the critical temperature that we have just discussed, other quantities are of some interest. The dimensionless ratio $\gamma T_c^2/H_c^2(0)$ is often discussed. Results are shown in Fig. 60. The solid line applies, as before, to the La-Sr-Cu-O base spectrum, while the dotted line is for Pb. For this quantity the results of the two models are closer than those found for the specific-heat jump. As $T_c/\omega_{\ln}\to 0$, the value of $\gamma T_c^2/H_c^2(0)\to 0.168$ (the BCS value). As $T_c/\omega_{\ln}$ increases, the ratio decreases, has a minimum near $T_c/\omega_{\ln}\approx 0.2$ to 0.3, and then starts rising towards values that can be as large as 0.4 for $T_c/\omega_{\ln}=1.6$. Again we note that all the conventional superconductors fall in the small region before the minimum. Furthermore, we stress that in the very strong coupling regime, Eliashberg theory predicts a behavior for this ratio that is quite different from what is found in the conventional case. This should serve as a clear signature of a large electron-boson spectral density at low frequency.

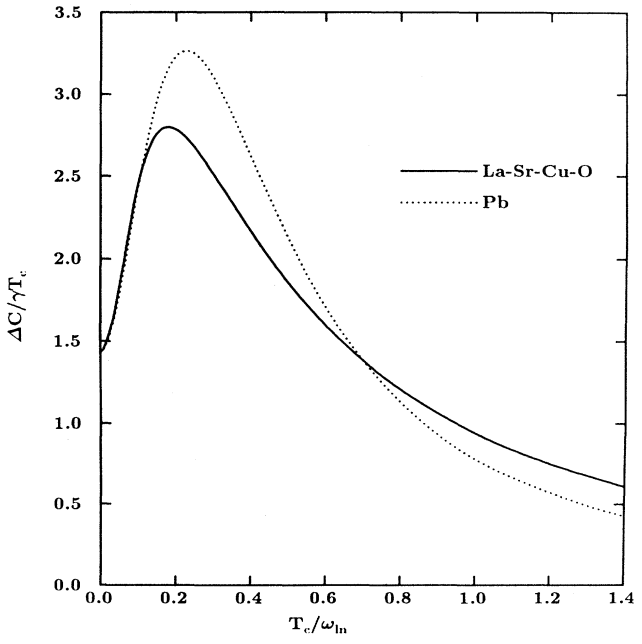

FIG. 59. $\Delta C(T_c)/(\gamma T_c)$ vs $T_c/\omega_{\ln}$. As $T_c/\omega_{\ln}$ increases beyond the conventional regime ($T_c/\omega_{\ln}\sim 0.25$), the normalized jump decreases to values lower than the BCS value.

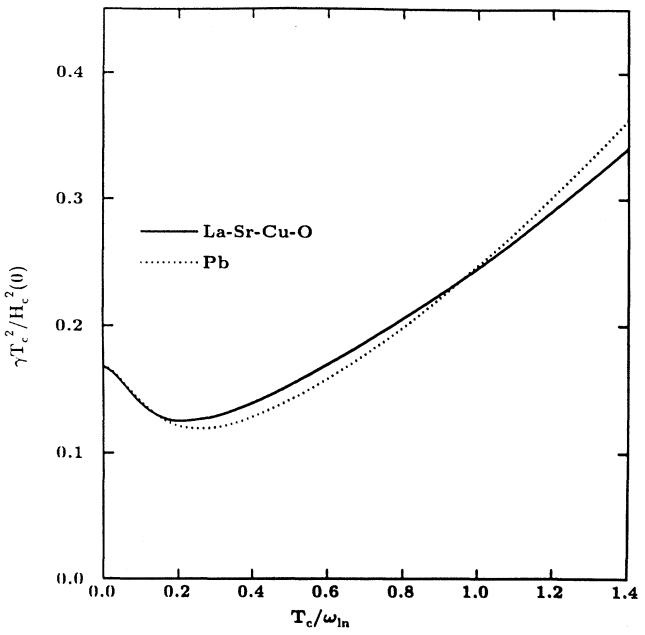

FIG 60. $\gamma T_c^2/H_c^2(0)$ vs $T_c/\omega_{\ln}$ in the very strong coupling regime. The trend has reversed, as it did for the jump, and values above that of BCS are found in this regime.

In addition to the zero-temperature critical magnetic field, we can consider its finite temperature counterpart and introduce the deviation function $D(t)$ [formula (5.4)]. In Fig. 61, we show results for the maximum or minimum (or both) value of this function versus $T_c/\omega_{\ln}$. For values $\lesssim 0.2$, the deviation function is positive definite (the conventional strong-coupling regime), but as $T_c/\omega_{\ln}$ is increased beyond this range, the maximum in $D(t)$ peaks and then begins to drop. Eventually, both a maximum and a minimum are present [S-shaped curve for $D(t)$] and finally, there is only a minimum with $D(t)$ negative definite. We note that in the very strong coupling limit, the minimum of $D(t)$ can be very much smaller than the BCS value of -0.037.

Another quantity of interest is the slope of the normalized specific heat at T_c, namely, $(d\Delta C/dT)_{T_c}/\gamma$, which we show in Fig. 62 [Akis and Carbotte (1989b)]. It starts at the BCS value of 3.77 achieved for $T_c/\omega_{\ln}=0$ and then rises towards a maximum, which falls around the end of the strong-coupling region. The absolute value of the maximum depends significantly on the shape of the based spectrum, while its position as a function of $T_c/\omega_{\ln}$ is much less sensitive. The solid curve for the La-Sr-Cu-O spectrum peaks at about 11, to be compared with nearly 17 for a delta function [dashed curve; Akis and Carbotte (1989a)]. As the coupling is increased further, the slope drops and can fall below its BCS weak-coupling value, as

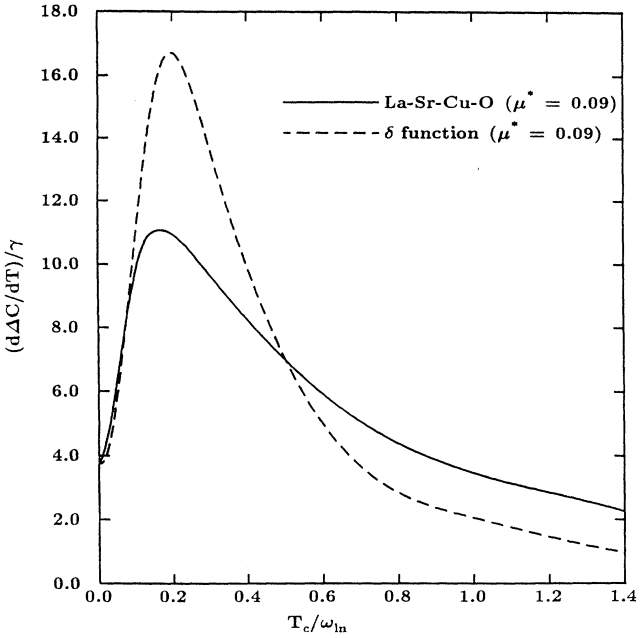

FIG. 62. Specific-heat slope at T_c, $T_c[d\Delta C(T)/dT)_{T_c}]$, normalized to γT_c as a function of the strong-coupling parameter $T_c/\omega_{\ln}$. The solid curve applies to a La-Sr-Cu-O base spectrum, while the dashed curve is for a delta-function model.

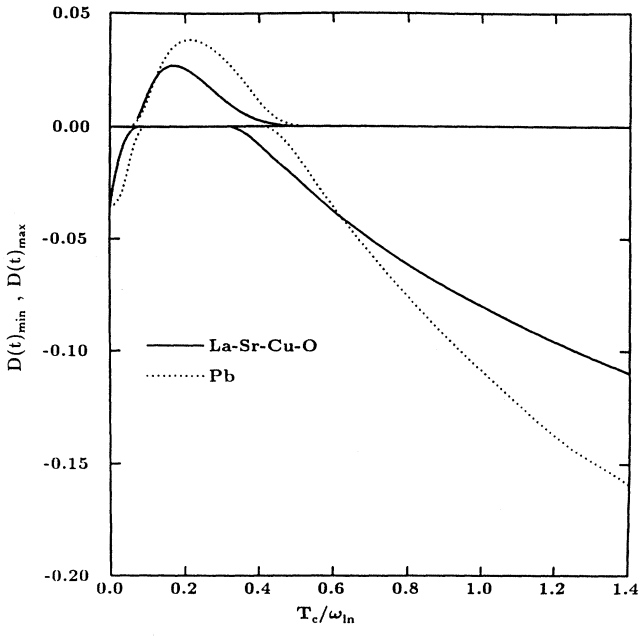

FIG. 61. The maximum or minimum (or both when it is S shaped) of the critical magnetic-field deviation function vs $T_c/\omega_{\ln}$. In the very strong coupling regime, the curve becomes negative definite with minimum values that exceed the BCS value in absolute terms.

was found for the normalized specific-heat jump. It is of interest also to consider the slope normalized to the jump, as this ratio is independent of the Sommerfeld constant γ, a quantity that is sometimes not well known, particularly in the new oxide superconductors. This ratio, which is given in Fig. 63, for a La-Sr-Su-O (solid line) and a delta function (dashed line) base spectral shape as a function of coupling strength, also exhibits a maximum around the end of the strong-coupling range and then drops at higher values of $T_c/\omega_{\ln}$. For the largest value shown, $T_c/\omega_{\ln}=1.2$, it is, however, still larger than the $T_c/\omega_{\ln}=0$ limit, which is 2.66.

The results of Fig. 37 for $2\Delta_0/k_BT_c$ are in striking contrast to those of Figs. 59 to 63. In the very strong coupling regime, Eliashberg theory predicts a large $2\Delta_0/k_BT_c$ of the order of 10 or more while at the same time $\Delta C(T_c)/(\gamma T_c)$ is much smaller than the BCS value of 1.43, as is the slope of the specific-heat difference at T_c, $[d\Delta C(t)/dt]_{t=1}/\gamma$. $\gamma T_c^2/H_c^2(0)$ is larger than 0.168. In addition, $D(t)$ is negative definite with a minimum value much less than -0.037. These predictions are very different from the pattern of behavior predicted and observed in conventional strong-coupling systems.

To end this discussion of the very strong coupling regime, it is of interest to show the value of λ that corresponds to the results presented in Figs. 59–63. This is given in Fig. 64 where the solid line is the λ versus $T_c/\omega_{\ln}$ curve obtained on the basis of the La-Sr-Cu-O

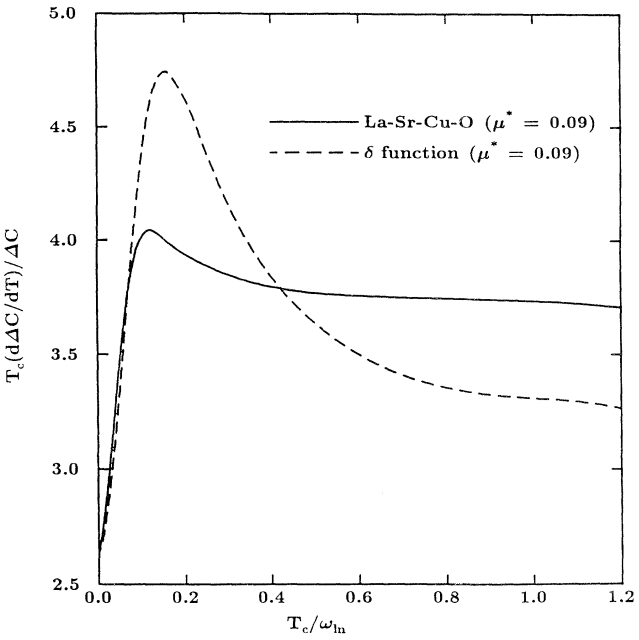

FIG. 63. Specific-heat slope at T_c, $[d\Delta C(T)/dT)_{T_c}]T_c$ normalized to the jump $\Delta C(T_c)$ as a function of the strong-coupling parameter T_c/ω_{ln}. The solid curve applies to a La-Sr-Cu-O base spectrum, while the dashed curve is for a delta-function model.

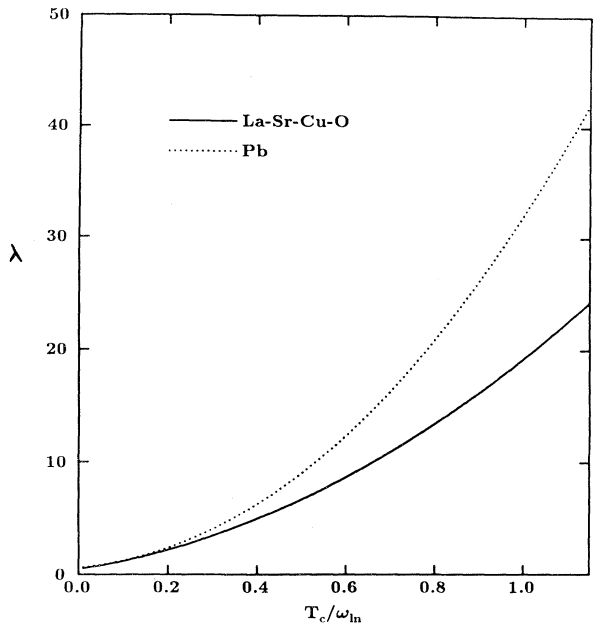

FIG. 64. λ vs T_c/ω_{ln} for La-Sr-Cu-O (solid curve) and Pb (dotted curve) shaped spectra, with $\mu^*=0.1$.

spectrum; the dotted curve is based on Pb. We see that large values of λ are implied. No attempt has been made to see if such values are compatible with lattice stability. They probably are not. Of course, the bosons involved need not be phonons. No specific choice is implied in much of the work described, even though shapes are used for the spectral density that are characteristic of lattice vibrations. This was done only for convenience.

VI. THERMODYNAMICS: SOME FORMAL RESULTS AND APPLICATIONS

A. Functional derivatives

To obtain the functional derivative of the critical-field deviation function or of the specific heat, we need the functional derivative of the free-energy difference between superconducting and normal state. The use of the Bardeen-Stephen (1964) formula is not a very convenient way to accomplish this, because it is not zero under variations of either $\Delta(i\omega_n)$ or $Z(i\omega_n)$, and these variations would need to be taken into account. Rainer and Bergmann (1974) noted that this difficulty could be bypassed by using instead the Wada (1964) formula given by

$$\frac{\Delta F}{N(0)}=-2\pi T\sum_n \omega_n\left[\frac{\tilde{\omega}(i\omega_n)}{\sqrt{\tilde{\omega}^2(i\omega_n)+\tilde{\Delta}^2(i\omega_n)}}-\mathrm{sgn}(\omega_n)\right]$$
$$-(\pi T)^2\sum_{n,m}\left[\left[\frac{\tilde{\omega}(i\omega_n)}{\sqrt{\tilde{\omega}^2(i\omega_n)+\tilde{\Delta}^2(i\omega_n)}}\frac{\tilde{\omega}(i\omega_m)}{\sqrt{\tilde{\omega}^2(i\omega_m)+\tilde{\Delta}^2(i\omega_m)}}-\mathrm{sgn}(\omega_n\omega_m)\right]\lambda(i\omega_n-i\omega_m)\right.$$
$$+\frac{\tilde{\Delta}(i\omega_n)}{\sqrt{\tilde{\omega}^2(i\omega_n)+\tilde{\Delta}^2(i\omega_n)}}\frac{\tilde{\Delta}(i\omega_m)}{\sqrt{\tilde{\omega}^2(i\omega_m)+\tilde{\Delta}^2(i\omega_m)}}$$
$$\left.\times[\lambda(i\omega_n-i\omega_m)-\mu^*\theta(\omega_c-|\omega_m|)\theta(\omega_c-|\omega_n|)]\right], \tag{6.1}$$

where $\tilde{\Delta}(i\omega_n)=\Delta(i\omega_n)\tilde{\omega}(i\omega_n)/\omega_n$ and $\tilde{\omega}(i\omega_n)=\omega_n Z(i\omega_n)$. Taking variations with respect to $\tilde{\Delta}$ or $\tilde{\omega}$ and setting each

equal to zero gives, respectively, the Eliashberg equations (2.1) and (2.2).

The total variation of the free-energy difference with $\alpha^2F(\omega)$ is then given by [Marsiglio *et al.* (1986)]

$$\frac{\delta\Delta F}{\delta\alpha^2F(\omega)}=\sum_{n,m}\frac{\partial\Delta F}{\partial\lambda(i\omega_n-i\omega_m)}\frac{\delta\lambda(i\omega_n-i\omega_m)}{\delta\alpha^2F(\omega)}+t\frac{\partial\Delta F}{\partial T}\frac{\delta T_c}{\delta\alpha^2F(\omega)}\ , \tag{6.2}$$

where the additional term enters because it is t and not T that is considered to be constant with respect to changes in $\alpha^2F(\omega)$. The derivative of the free energy with temperature alone is given by

$$\frac{\partial\Delta F}{\partial T}=\sum_{n,m}\frac{\partial\Delta F}{\partial\lambda(i\omega_n-i\omega_m)}\frac{\partial\lambda(i\omega_n-i\omega_m)}{\partial T}+\frac{2\Delta F}{T}\ . \tag{6.3}$$

The first term in (6.2) which represents the explicit variation of ΔF with respect to variations in $\alpha^2F(\omega)$ and which we denote by $\delta\Delta F/\delta\alpha^2F(\omega)$, can be obtained directly from (6.1), to get

$$\frac{1}{N(0)}\frac{\delta\Delta F}{\delta\alpha^2F(\omega)}=-(\pi T)^2\sum_{n,m}\left[\left[\frac{\tilde{\omega}(i\omega_n)}{\sqrt{\tilde{\omega}^2(i\omega_n)+\tilde{\Delta}^2(i\omega_n)}}\frac{\tilde{\omega}(i\omega_m)}{\sqrt{\tilde{\omega}^2(i\omega_m)+\tilde{\Delta}^2(i\omega_m)}}+\frac{\tilde{\Delta}(i\omega_n)}{\sqrt{\tilde{\omega}^2(i\omega_n)+\tilde{\Delta}^2(i\omega_n)}}\frac{\tilde{\Delta}(i\omega_m)}{\sqrt{\tilde{\omega}^2(i\omega_m)+\tilde{\Delta}^2(i\omega_m)}}-\mathrm{sgn}(\omega_n\omega_m)\right]\frac{2\omega}{\omega^2+(\omega_n-\omega_m)^2}\right] \tag{6.4}$$

and

$$\frac{1}{N(0)}\frac{\partial\Delta F}{\partial T}=\frac{2\Delta F}{T}-(\pi T)^2\sum_{n,m}\left[\left[\frac{\tilde{\omega}(i\omega_n)}{\sqrt{\tilde{\omega}^2(i\omega_n)+\tilde{\Delta}^2(i\omega_n)}}\frac{\tilde{\omega}(i\omega_m)}{\sqrt{\tilde{\omega}^2(i\omega_m)+\tilde{\Delta}^2(i\omega_m)}}+\frac{\tilde{\Delta}(i\omega_n)}{\sqrt{\tilde{\omega}^2(i\omega_n)+\tilde{\Delta}^2(i\omega_n)}}\frac{\tilde{\Delta}(i\omega_m)}{\sqrt{\tilde{\omega}^2(i\omega_m)+\tilde{\Delta}^2(i\omega_m)}}-\mathrm{sgn}(\omega_n\omega_m)\right]\times\frac{-4}{T}\int_0^\infty\frac{(\omega_n-\omega_m)^2\omega'\alpha^2F(\omega')d\omega'}{[\omega'^2+(\omega_n-\omega_m)^2]^2}\right]\ . \tag{6.5}$$

The functional derivative of the deviation function $D(t)$ [Daams and Carbotte (1978)] is related to the functional derivative of the critical magnetic field $H_c(T)$ which follows from that for ΔF because $\Delta F=-H_c^2(T)/8\pi$. We have

$$\frac{\delta D(t)}{\delta\alpha^2F(\omega)}=\frac{H_c(T)}{H_c(0)}\frac{\delta}{\delta\alpha^2F(\omega)}\ln\left[\frac{H_c(T)}{H_c(0)}\right] \tag{6.6}$$

with

$$\frac{\delta H_c(T)}{\delta\alpha^2F(\omega)}=\frac{-4\pi}{H_c(T)}\frac{\delta\Delta F}{\delta\alpha^2F(\omega)}\ . \tag{6.7}$$

In Eqs. (6.6) and (6.7), the explicit variation with $\alpha^2F(\omega)$ could have been taken instead of the total variation. In addition,

$$\frac{\partial H_c(T)}{\partial T}=\frac{-4\pi}{H_c(T)}\frac{\partial\Delta F}{\partial T}\ , \tag{6.8}$$

which is needed to go from explicit variation on $\alpha^2F(\omega)$ to total variation.

Results for the functional derivative [Daams and Carbotte (1978)] of $D(t)$ based on a Pb spectrum are shown in Fig. 65 for three values of reduced temperature, namely, $t=0.15$ (solid curve), $t=0.6$ (dashed curve), and $t=0.96$ (dashed-double-dotted curve). While the amplitudes of these curves are dependent on the value of reduced temperature employed, the shape is not. The high-frequency modes have only a small effect on $D(t)$ because the functional derivative is small. It is positive so that such modes tend to increase $D(t)$ slightly above the BCS result. By comparison, the modes around (very roughly) $5T_c$ have a much larger effect as they fall near or at the maximum in the functional derivative curves. At still lower frequencies, the functional derivative is negative, indicating that $D(t)$ is reduced by such low-

energy modes. Thus various frequency ranges in $\alpha^2F(\omega)$ can affect $D(t)$ in very different ways. These functional derivatives will become very useful shortly when we examine the effect of hydrostatic pressure on $D(t)$ and discuss the idea of optimum spectra.

Returning to the functional derivative of the specific heat and noting that t is to be kept constant when taking variations with $\alpha^2F(\omega)$ we have [Marsiglio *et al.* (1986)]

$$\frac{1}{\gamma}\frac{\delta[\Delta C(T)/T_c]}{\delta\alpha^2F(\omega)}=\frac{N(0)}{\gamma}\frac{T}{T_c}\frac{d^2}{dT^2}\left\{(\pi T)^2\sum_{n,m}\left[\frac{\tilde{\omega}(i\omega_n)}{\sqrt{\tilde{\omega}^2(i\omega_n)+\tilde{\Delta}^2(i\omega_n)}}\frac{\tilde{\omega}(i\omega_m)}{\sqrt{\tilde{\omega}^2(i\omega_m)+\tilde{\Delta}^2(i\omega_m)}}\right.\right.$$
$$\left.-\mathrm{sgn}(\omega_n\omega_m)+\frac{\tilde{\Delta}(i\omega_n)}{\sqrt{\tilde{\omega}^2(i\omega_n)+\tilde{\Delta}^2(i\omega_n)}}\frac{\tilde{\Delta}(i\omega_m)}{\sqrt{\tilde{\omega}^2(i\omega_m)+\tilde{\Delta}^2(i\omega_m)}}\right]$$
$$\left.\times\left[\frac{2\omega}{\omega^2+(\omega_n-\omega_m)^2}-\frac{2}{T_c}(\omega_n-\omega_m)^2\frac{\delta T_c}{\delta\alpha^2F(\omega)}\int\frac{2\omega'\alpha^2F(\omega')d\omega'}{[\omega'^2+(\omega_n-\omega_m)^2]^2}\right]\right\}. \tag{6.9}$$

The functional derivative indicated in (6.9) is not the only one of interest. In this equation, we are normalizing to γ, which is $\frac{2}{3}\pi^2k_B^2N(0)(1+\lambda)$. This is, strictly speaking, only valid at low T. When the electron-boson interaction is large, we could use instead the temperature-dependent Sommerfeld constant $\gamma(T)$ given by Grimvall (1981). It is

$$\gamma(T)=\gamma\left\{1+\frac{1}{1+\lambda}\int_0^\infty 2\frac{d\omega}{\omega}\alpha^2F(\omega)\left[Z\left[\frac{T}{\omega}\right]-1\right]\right\}. \tag{6.10}$$

The kernel $Z(x)$ can be written in terms of a universal function introduced by Grimvall (1981) or, more simply and suitably for our purposes, by the approximation [Kresin and Zaitsev (1978a, 1978b)]

$$Z(x)\approx\Phi(9x^2),$$
$$\Phi(u)=\frac{1+2.6u+16u^2}{1+65u^3}-1.6\frac{u^3+4.1u^2}{u^4+9(u^3+1)}. \tag{6.11}$$

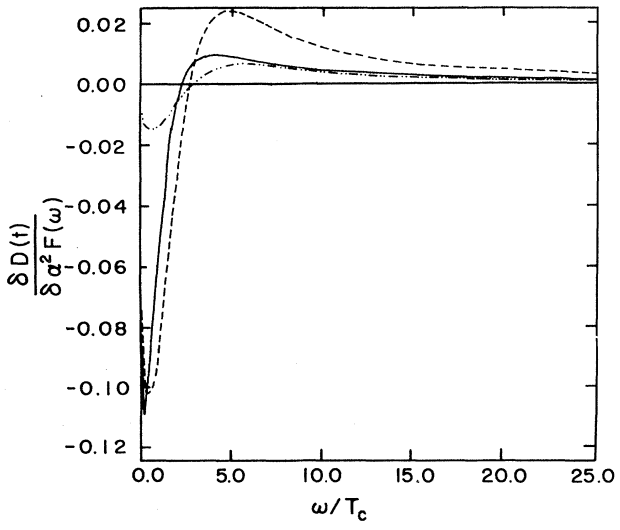

FIG. 65. Functional derivative $\delta D(t)/\delta\alpha^2F(\omega)$ as a function of frequency ω/T_c for Pb at three temperatures: (solid curve) $t=0.15$, (dashed curve) $t=0.6$, and (dashed-double-dotted curve) $t=0.96$.

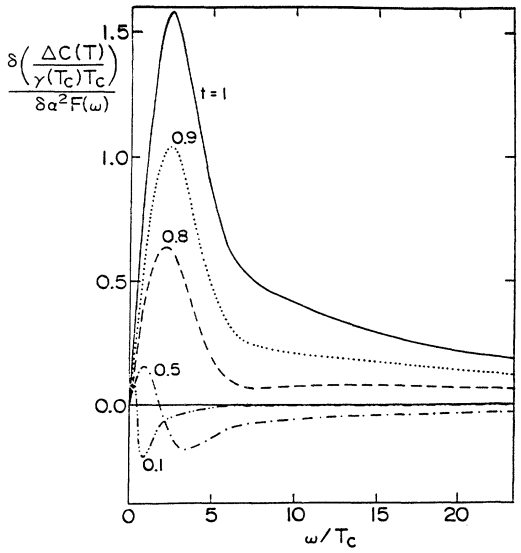

FIG. 66. Functional derivative of the specific-heat difference, $\delta[\Delta C(T)/\gamma T_c]/\delta\alpha^2F(\omega)$, for Pb as a function of reduced frequency. The maximum at T_c occurs at $\omega^*\simeq 3.5\ T_c$, in agreement with the weak-coupling result. As $\omega\to 0$ or ∞, the derivative approaches zero, indicating that low- and high-frequency phonons are ineffective in altering the specific-heat jump. As the temperature is lowered, the functional derivative becomes negative for the frequency range of interest. The curves shown correspond to $t=1$ (——), $t=0.9$ (· · · ·), $t=0.8$ (— — —), $t=0.5$ (—·—·—·), and $t=0.1$ (–··–).

We note that for $T=0$, Z becomes 1 and $\gamma(T=0)$ reduces to the more familiar equation for γ. If we designate $\gamma_c \equiv \gamma(T_c)$, we get

$$I(T) \equiv \frac{1}{\gamma_c} \frac{\delta[\Delta C(T)/T_c]}{\delta\alpha^2 F(\omega)} \tag{6.12}$$

and that

$$\frac{1}{\gamma_c T_c} \frac{\delta \Delta C(t)}{\delta\alpha^2 F(\omega)} = I(T) + \frac{1}{T_c} \frac{\Delta C(T)}{\gamma_c T_c} \frac{\delta T_c}{\delta\alpha^2 F(\omega)}$$

and

$$\frac{\delta}{\delta\alpha^2 F(\omega)} \left[\frac{\Delta C(t)}{\gamma_c T_c} \right] = I(T) - \frac{1}{\gamma_c} \frac{\Delta C(t)}{\gamma_c T_c} \left[\frac{\delta\gamma(T_c)}{\delta\alpha^2 F(\omega)} + \frac{\partial\gamma(T)}{\partial T} \bigg|_{T_c} \frac{\delta T_c}{\delta\alpha^2 F(\omega)} \right] . \tag{6.13}$$

Much simpler but approximate results for this functional derivative have been obtained in a $\lambda^{\theta\theta}$ model by Marsiglio and Carbotte (1985).

Results for $\delta(\Delta C(t)/\gamma_c T_c)/\delta\alpha^2 F(\omega)$ based on the complete equations given in this section are found in Fig. 66 [Marsiglio *et al.* (1986)] for several values of the reduced temperature t. At $t=1$, the functional derivative is positive definite and exhibits a single peak at an optimum frequency and goes to zero for both $\omega \to 0$ and $\omega \to \infty$. As the reduced temperature t is lowered, the peak shifts to lower energy and drops in amplitude. At sufficiently low t, part of the curve becomes negative and a much more complex behavior is observed, particularly in the small ω region.

B. Application of functional derivatives to Pb under pressure

There are many possible uses that can be made of these functional derivatives. Here we describe their application to the problem of shifts in thermodynamic and other properties of Pb under hydrostatic pressure P as described by Daams and Carbotte (1978). These authors consider a model for the change in $\alpha^2 F(\omega)$ under hydrostatic pressure based on the $p=0$ tunneling results. Under pressure, the transverse phonon peak at lower energy is shifted according to the measured value

$$\frac{d \ln\omega_t}{dp} = 7.49 \times 10^{-6} \text{ bar}^{-1} , \tag{6.14}$$

and the high-energy longitudinal phonon peak according to

$$\frac{d \ln\omega_l}{dp} = 5.8 \times 10^{-6} \text{ bar}^{-1} . \tag{6.15}$$

Both values are obtained from an extrapolation to pure Pb of data by Hansen *et al.* (1973) for PbIn alloys. No further adjustment in shape is made. Finally, the scale on the spectral density is altered to get the experimentally determined value of

$$\frac{d \ln\lambda}{dp} = -6.185 \times 10^{-6} \text{ bar}^{-1} \tag{6.16}$$

for the change in λ with pressure.

From Eq. (6.16) we get that λ at 2960 bars is 1.5195, to be compared with 1.5477 at zero pressure. At the same time, the area under $\alpha^2 F(\omega)$ is hardly changed, going to 4.063 from 4.032, as indicated in Table XI. To get the measured reduction of T_c to 7.088 K for $p=2960$ bars, we need to additionally change μ^* from 0.150 63 at zero pressure to 0.158 01 at 2960 bars. Having done this, there remain no further adjustable parameters and explicit predictions for the change in thermodynamic and other properties with pressure follow.

Before proceeding to a discussion of the implied changes in $H_c(0)$ and $D(t)$, it is important to note that most of the change in T_c is coming from the change in μ^*. Since $\partial T_c/\partial\mu^* = -1.11$ meV in Pb, a change in μ^* of 0.007 38 gives a decrease in T_c of 0.095 K, which is almost the entire measured change. This implies that the changes in $\alpha^2 F(\omega)$ in going from 0 to 2960 bars hardly affect T_c. This can be understood with reference to Fig. 67 where we have superimposed on the same plot the change $\Delta\alpha^2(\omega)F(\omega)$ versus ω and $\delta T_c/\delta\alpha^2 F(\omega)$ (dashed curve). It is clear that a great deal of cancellation occurs in the overlap integral.

$$\Delta T_c = \int_0^\infty \Delta\alpha^2(\omega) F(\omega) \frac{\delta T_c}{\delta\alpha^2 F(\omega)} d\omega \tag{6.17}$$

for ΔT_c, and the integral (6.17) comes out to be nearly zero (0.01 K).

On the other hand, the cancellation that occurs in the overlap integral for the change in $H_c(0)$ will not be as large as that for ΔT_c because the maximum in $\delta H_c(0)/\delta\alpha^2 F(\omega)$ (solid curve in Fig. 67) is at lower frequencies. From the change in $\alpha^2(\omega)F(\omega)$ alone we get a change of -8 Oe in $H_c(0)$. The change due to μ^* can be obtained from

$$\frac{\partial H_c(0)}{\partial\mu^*} = -1602 \text{ Oe}$$

for Pb at zero pressure and is -11.8 Oe, which is equally important to the change induced by the shift in spectral

TABLE XI. Parameters for Pb under pressure.

	Pb($p=0$)		Pb($p=2960$ bars)
λ	1.5477	$\Delta\lambda$	-0.0282
A	4.032 meV	ΔA	$+0.004$
μ^*	0.150 63	$\Delta\mu^*$	$+0.007\,38$

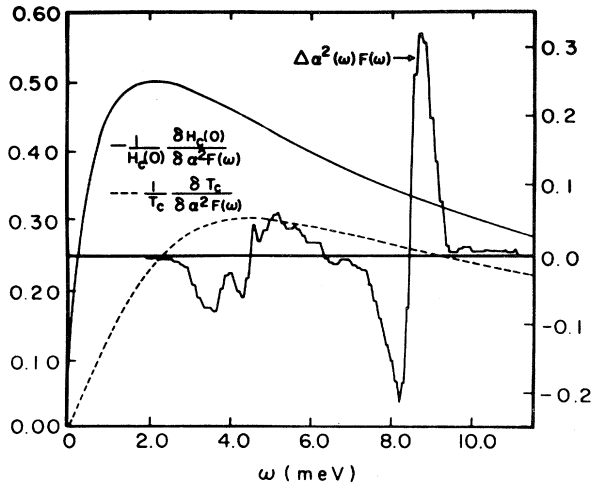

FIG. 67. Right scale applies to the change in the spectrum weight $\Delta\alpha^2F(\omega)$ due to pressure. The left scale applies to $(1/T_c)[\delta T_c/\delta\alpha^2F(\omega)]$ (dashed curve) and $1/H_c(0)$ $\delta H_c(0)/\delta\alpha^2F(\omega)$ (solid curve). The horizontal scale is the frequency in meV.

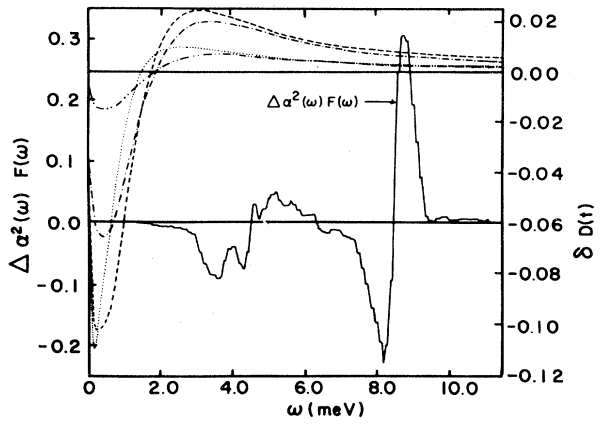

FIG. 68. Left scale applies to the change in the spectral density $\Delta\alpha^2F(\omega)$ under pressure. The right scale is for the functional derivative $\delta D(t)/\delta\alpha^2F(\omega)$ denoted simply by $\delta D(t)$ as a function of frequency ω in meV for four temperatures: $t=0.15$ (dotted), $t=0.6$ (dashed), $t=0.8$ (dot dashed), and $t=0.96$ (dashed double dotted).

density. The total value of $H_c(0)$ is 781 Oe at 2960 bars, to be compared with an experimental value of 778 Oe [Daams and Carbotte (1978)].

To get the change in $D(t)$, we need to work out

$$\int_0^\infty \Delta\alpha^2(\omega)F(\omega)\frac{\delta D(t)}{\delta\alpha^2F(\omega)}d\omega \tag{6.18}$$

at the temperature of interest and add in

$$\frac{\partial D(t)}{\partial\mu^*}\Delta\mu^*. \tag{6.19}$$

In Fig. 68 we have superimposed on the same plot $\Delta\alpha^2(\omega)F(\omega)$ and the functional derivative $\delta D(t)/\delta\alpha^2F(\omega)$ for four temperatures. We note that the low-frequency minima in these curves play no role as $\Delta\alpha^2(\omega)F(\omega)$ is nearly negligible in that range of frequencies. At higher frequencies there is clearly a great deal of cancellation in the overlap integral (6.18), indicating that the change in $D(t)$ is not related to any prominent change in $\alpha^2(\omega)F(\omega)$. To obtain the full change in $D(t)$, we need to add on the effect of changes in μ^*. Daams and Carbotte, however, find that it is the changes in $\alpha^2(\omega)F(\omega)$ that produce the most important decrease in $D(t)$, with the additional decrease due to μ^* being of lesser importance. The change in $D(t)$ measured by Alterovitz and Mapother (1975) is somewhat larger than the total calculated value. What is more important here is that the data are well understood from functional-derivative considerations, and the above discussion illustrates well the power of the technique.

C. Application to specific-heat jump

We now turn to the idea of the existence of an optimum spectrum for thermodynamic properties, which follows from a consideration of functional derivatives. In Fig. 69, we show results for

$$(1+\lambda)T_c\frac{\delta}{\delta\alpha^2F(\omega)}\left[\frac{\Delta C(T_c)}{\gamma T_c}\right] \tag{6.20}$$

in the case of Pb (solid curve). It is seen that this functional derivative diverges toward $-\infty$ at low ω. This divergence can be traced to our use of γ in Eq. (6.20)

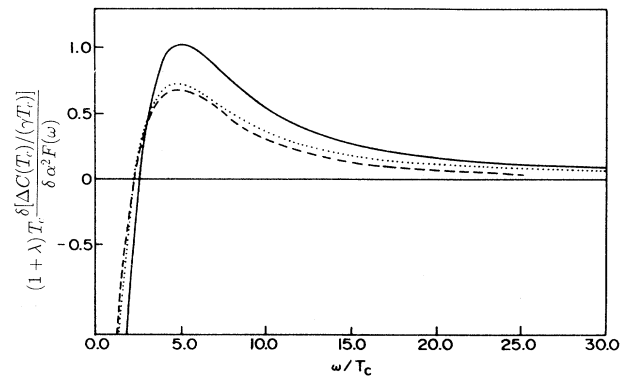

FIG. 69. Functional derivative of the specific-heat jump at T_c normalized to γT_c. What is given is $(1+\gamma)T_c\delta[\Delta C(T_c)/\gamma T_c]/\delta\alpha^2F(\omega)$ vs ω/T_c. The solid curve is for Pb, the dotted line for Al, and the dashed line for any weak-coupling superconductor in a two-square-well model.

since $\delta\gamma/\delta\alpha^2F(\omega)\sim 1/\omega$. If, instead, γ_c had been used, the functional derivative would go smoothly to zero as seen in Fig. 66. At higher frequencies, around $\omega/T_c\simeq 5$, a positive maximum occurs and then the functional derivative slowly decays towards zero as $\omega\rightarrow\infty$. We have tried many other realistic tunneling-derived spectra and find, in all cases, the same shape for the functional derivative. For example, the dotted line was calculated using the Al spectrum given by Leung *et al.* (1976a, 1976b). It is very close to the dashed line, which was calculated using a two-square-well model for $\lambda(n-m)$. Details of the two-square-well-model results can be found in the work of Marsiglio and Carbotte (1985). In this simplified model, no assumption is made about the shape of the spectral density, except that all important phonon frequencies should be much greater than several k_BT_c's. This is the usual BCS limit and applies to all weak-coupling systems.

From the above we conclude that the shape of $\delta[\Delta C(T_c)/(\gamma T_c)]/\delta\alpha^2F(\omega)$ is fairly universal for realistic values of $\alpha^2F(\omega)$ (i.e., actual measured shapes for real materials). This leads to the idea that in order to increase $\Delta C(T_c)/(\gamma T_c)$ for a given $\alpha^2F(\omega)$, we should take weight from some frequency where the functional derivative is smaller than its value at maximum, and transfer it to the optimum frequency, keeping the total area under $\alpha^2F(\omega)$ constant. This suggests that to maximize $\Delta C(T_c)/(\gamma T_c)$, for a given value of $A=\int_0^\infty\alpha^2F(\omega)d\omega$, we should use a delta function with all its weight placed at the same Einstein frequency ω_E [Blezius and Carbotte (1987)].

D. Optimum spectrum for jump

For a delta-function spectrum, the scaled equations (2.45) and (2.46) hold, from which we can conclude that $\Delta(i\omega_n)/A$ is a function only of $\bar{\omega}_E\equiv\omega_E/A$ and $\bar{T}\equiv T/A$, as is $Z(i\omega_n)$. Reference to the free-energy formula yields immediately that [Blezius and Carbotte (1987, 1988)]

$$|\Delta F|=N(0)A^2g(\bar{\omega}_E,\bar{T})\ , \tag{6.21}$$

where g is an appropriate function related to the free-energy. Thus the specific-heat difference between superconducting and normal state is

$$\Delta C(T)=-T\frac{d^2\Delta F(T)}{dT^2}=-\bar{T}AN(0)\frac{d^2g(\bar{\omega}_E,\bar{T})}{d\bar{T}^2} \tag{6.22}$$

and, therefore,

$$\frac{\Delta C(T)}{\gamma T_c}=\frac{-3t}{2\pi^2k_B^2(1+2/\bar{\omega}_E)}\frac{d^2g(\bar{\omega}_E,\bar{T})}{d\bar{T}^2}\ . \tag{6.23}$$

But $T_c=Af(\bar{\omega}_E,\mu^*)$ so that we can finally write

$$\frac{\Delta C(T_c)}{\gamma T_c}\equiv\mathcal{G}(\omega_E/T_c,\mu^*,t)\ , \tag{6.24}$$

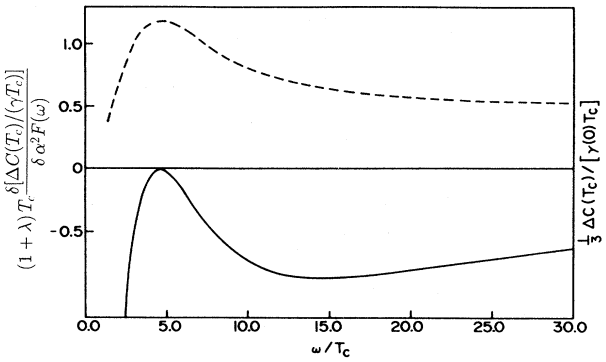

FIG. 70. Value of $\frac{1}{3}\Delta C(T_c)/[\gamma(0)T_c]$ (right-hand label) for an Einstein spectrum as a function of ω_E/T_c (dashed curve), where ω_E is the position of the phonon frequency. The results are independent of the value used for the area (A) under the delta function. The μ^* value was 0.051. The functional derivative $\delta[\Delta C(T_c)/(\gamma T_c)]/\delta\alpha^2F(\omega)$ multiplied by $(1+\lambda)T_c$ (left-hand label) for the case of a delta-function spectrum $\alpha^2F(\omega)=A\delta(\omega-\omega_E^*)$, where ω_E^* is the frequency of the maximum in the dashed curve. It is negative definite and exactly zero at the frequency ω_E^* of the optimum spectra. This indicates a local maximum

where the function $\mathcal{G}$ is related to g, with t the reduced temperature $t=T/T_c$, which is independent of A. In particular, the specific-heat jump depends only on ω_E/T_c for a specific choice of Coulomb pseudopotential μ^*.

In Fig. 70 we show results of calculations for the normalized jump in the case of a delta-function base spectrum centered at ω_E as a function of ω_E/T_c (dashed curve) for $\mu^*=0.051$. What is plotted is

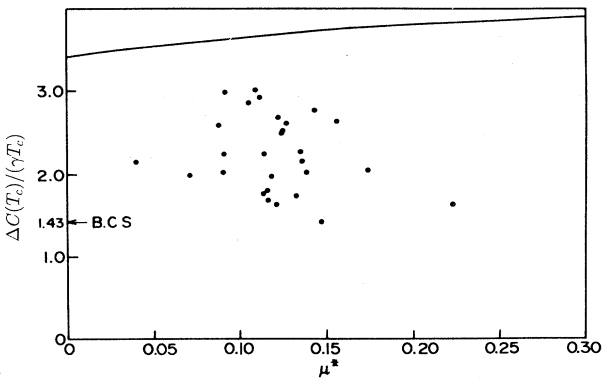

FIG. 71. Maximum possible value for $[\Delta C(T_c)/\gamma T_c]$ as a function of μ^*. The solid dots represent theoretical values for the following materials in order of decreasing value of $\Delta C(T_c)/[\gamma T_c]$: $Pb_{0.7}Bi_{0.3}$, $Pb_{0.65}Bi_{0.35}$, $Pb_{0.8}Bi_{0.2}$, $Pb_{0.9}Bi_{0.1}$, Pb, $Pb_{0.8}Tl_{0.2}$, Nb_3Sn, Nb_3Al, Nb_3Ge, $Pb_{0.6}Tl_{0.4}$, Hg, $Pb_{0.75}Bi_{0.25}$, $Pb_{0.4}Tl_{0.6}$, V_3Ga, $Pb_{0.5}Bi_{0.5}$, La, Ga (amorphous), Bi (amorphous), V_3Si, Mo (amorphous), Nb, In, $Tl_{0.9}Bi_{0.1}$, Tl, Sn, Ta, V, Al (BCS).

$\frac{1}{3}\Delta C(T_c)/(\gamma T_c)$. We see that, on lowering the position of the Einstein frequency in the delta function, the normalized jump increases steadily until a maximum of 3.57 is reached at the optimum frequency for $\bar{\omega}_E^*=4.55$, after which it drops rather rapidly towards very small values as ω_E goes toward zero. This curve proves that, for a delta function, there is an optimum frequency that maximizes the specific-heat jump and that the maximum in this quantity is 3.57 (for $\mu^*=0.051$) and is independent of A. We can use functional derivatives to prove that any other shape will lower $\Delta C(T_c)/(\gamma T_c)$. Returning to Fig. 70, the solid curve is

$$(1+\lambda)T_c\delta[\Delta C(T_c)/(\gamma T_c)]/\delta\alpha^2F(\omega)$$

(left-hand label) for a model delta function $\alpha^2F(\omega)=A\,\delta(\omega-\omega_E^*)$, with ω_E^* the frequency giving the maximum of the dashed curve. It is clear from the figure that the new functional derivative, which applies for the delta-function base centered at $\bar{\omega}_E^*=4.55$, is now very different from those found for realistic $\omega^2F(\omega)$ spectra. It is negative definite with value zero right at ω_E^*. This proves that a delta function at ω_E^* gives a local maximum. Removal of some weight from the delta function at ω_E^* and placing it at any other frequency reduces the specific-heat jump. Our experience with realistic spectra would lead us to believe that this is, in fact, an absolute maximum. In Fig. 71 we show as the solid line the maximum value of $\Delta C(T_c)/(\gamma T_c)$ obained for different choices of μ^*. On the same figure, we have shown (dark points) values for the same quantity obtained with realistic spectra. They all fall below our theoretical local maximum, indicating that for physical systems, the solid line is, indeed, an absolute maximum.

E. Specific-heat slope at T_c

The functional derivative of the specific-heat slope at T_c

$$\frac{\delta}{\delta\alpha^2F(\omega)}\left[\left.\frac{d\Delta C(T)}{dT}\right|_{T_c}\Big/\gamma\right] \tag{6.25}$$

and of the normalized slope

$$\frac{\delta}{\delta\alpha^2F(\omega)}\left[\left.T_c\frac{d\Delta C(T)}{dT}\right|_{T_c}\Big/\Delta C(T_c)\right] \tag{6.26}$$

can easily be related to the equations introduced previously. As an example,

$$\frac{\delta}{\delta\alpha^2F(\omega)}\left[\left.T_c\frac{d\Delta C(T)}{dT}\right|_{t=1}\Big/\gamma\right]$$

$$=\left.\frac{d\Delta C(T)}{dT}\right|_{t=1}\frac{1}{\gamma}\frac{\delta T_c}{\delta\alpha^2F(\omega)}+\frac{T_c}{\gamma}\left[\frac{d}{dT}\left[\frac{\delta\Delta C(T)}{\delta\alpha^2F(\omega)}\right]\right]_{t=1}-\frac{T_c}{\gamma^2}\left.\frac{d\Delta C(T)}{dT}\right|_{t=1}\frac{\delta\gamma}{\delta\alpha^2F(\omega)}\,. \tag{6.27}$$

Considerations of the shape of the functional derivatives similar to those just described have led Akis and Carbotte [(1989a); Akis *et al.* (1989)] to the idea of a maximum slope as well as a maximum normalized slope. These are shown as a function of μ^* in Figs. 72 and 73, respectively. The solid line gives the predicted maximum while the solid dots apply to the real systems indicated in the caption.

F. Critical field and deviation function

In Fig. 74 we present results for the functional derivative of $H_c(0)$ in the case of Pb (solid line) and Al [dotted line; Blezius and Carbotte (1988)]. What is plotted is the normalized quantity $[(1+\lambda)T_c/H_c(0)]\delta H_c(0)/\delta\alpha^2F(\omega)$ against normalized phonon energy ω/T_c. We note that both curves are positive definite, exhibit a maximum for ω/T_c around 4 (3.4 for Pb and 4.5 for Al), and go smoothly to zero as $\omega\to 0$ and $\omega\to\infty$. Similar curves for other materials, i.e., base spectra, are all found to exhibit the same features and, in particular, to exhibit a most effective frequency. This suggests once more that for a given $\alpha^2F(\omega)$, we can increase the value of $H_c(0)/\sqrt{2N(0)}$ by transferring weight from some arbitrary boson energy to the most effective frequency indicated in the functional derivative. For a fixed weight under the spectral density A, a delta-function shape should maximize $H_c(0)/\sqrt{2N(0)}$. In this case, $H_c(0)/[\sqrt{2N(0)}\,A]$ depends only on ω_E/A or ω_E/T_c and the value of μ^* used. Moreover, as the Einstein oscillator frequency ω_E is changed, we get a curve that mimics closely the shape of the functional derivative curve as is shown in the dot-dashed curve of Fig. 74 that gives $\frac{1}{500}$ $H_c(0)/[\sqrt{2N(0)}\,A]$ as a function of ω_E/T_c. The maximum in this curve gives an upper bound on $H_c(0)/(\sqrt{2N(0)}\,A)$, and the frequency maximum (ω_E^*) gives the optimum boson energy for a delta-function base function. It is $\omega_E^*=3.5T_c$.

We can verify that our delta-function model gives a local maximum in function space by working out the functional derivative of $H_c(0)$ with respect to $\alpha^2F(\omega)$ for the case function $A\,\delta(\omega-\omega_E^*)$. This functional derivative is given by the dashed curve in Fig. 74. This curve peaks exactly at $\omega_E^*=3.5T_c$, which is precisely the frequency in the delta-function base spectra density. Taking weight out of the delta-function base and placing it at any other

frequency $\omega \neq \omega_E^*$ will therefore decrease $H_c(0)/[\sqrt{2N(0)}\,A]$.

In Fig. 75 we have plotted our theoretical maximum for $H_c(0)/[\sqrt{2N(0)}\,A]$ (solid curve) as a functon of μ^* [Blezius and Carbotte (1988)]. On the same figure we have also placed results for many real materials (solid dots) as identified in the caption. All real systems fall below the optimum curve, as they must. We turn next to a discussion of the critical magnetic-field derivation function. The form of the functional derivative, given in Fig. 65 suggests that we can maximize the value of $D(t)$ at a fixed reduced temperature by shifting weight in $\alpha^2F(\omega)$ from ω to the most effective boson energy ω/T_c defined by the maximum in $\delta D(t)/\delta\alpha^2F(\omega)$. For a delta-function spectral density, $D(t)$ is completely independent of A and a function only of ω_E/T_c for a fixed value of μ^*. This is illustrated in Fig. 76 where we plot the maximum in $D(t)$ (dashed curve) as a function of ω_E/T_c. At sufficiently small and large frequencies, no maximum occurs in $D(t)$. It exhibits a minimum rather than a maximum and so only a limited frequency region is relevant. It is clear that as the Einstein frequency in the base function is varied, an optimum Einstein frequency

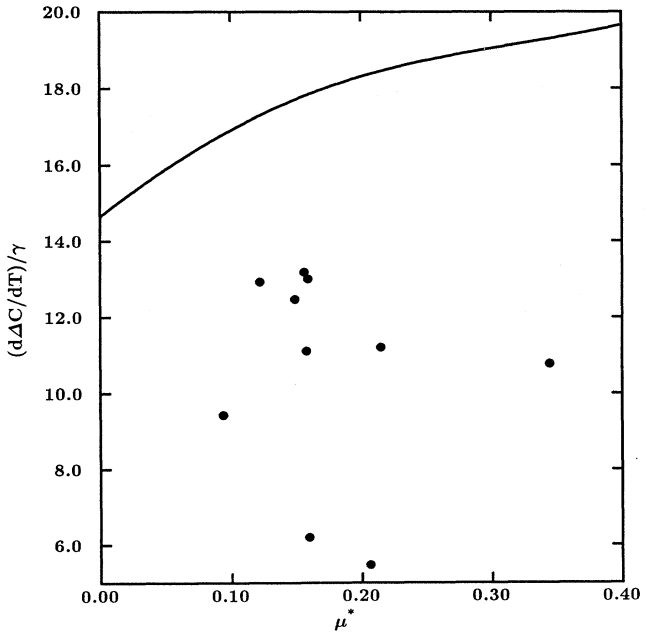

FIG. 72. Maximum value for the specific-heat slope at T_c normalized to γT_c, namely, $(1/\gamma)[d\Delta C(T)/dT]_{T_c}$, as a function of Coulomb pseudopotential μ^* (solid curve). The solid dots represent theoretical values for the following materials in order of decreasing value of $[d\Delta C(T)/dT]_{T_c}/\gamma$. $Pb_{0.7}Bi_{0.3}$, $Pb_{0.8}Bi_{0.2}$, $Pb_{0.65}Bi_{0.35}$, $Pb_{0.9}Bi_{0.1}$, Nb_3Sn, Nb_3Al (1), Nb_3Al (3), Nb_3 Al (2), In, Tl.

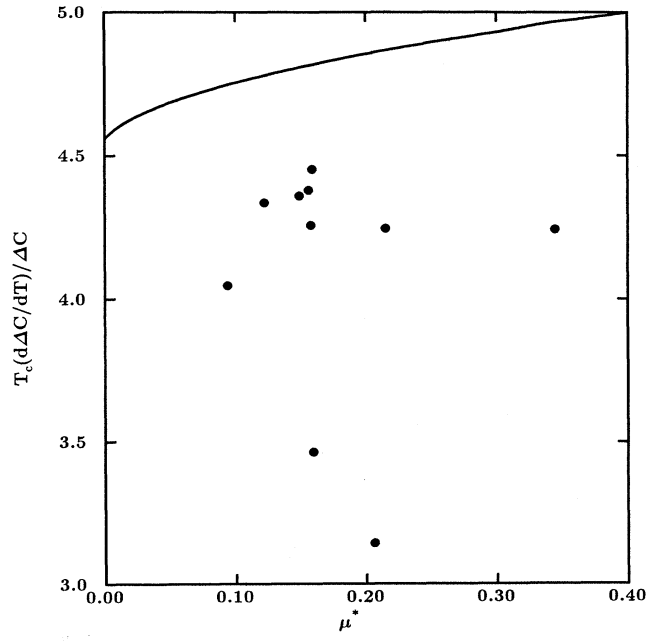

FIG. 73. Maximum value for the normalized specific-heat slope at T_c, $[T_c/\Delta C(T_c)][d\Delta C(T)/dT]_{T_c}$, as a function of Coulomb pseudopotential μ^* (solid curve). The solid dots represent theoretical values for the following materials in order of decreasing value of $T_c[d\Delta C(T)/dT]_{T_c}/\Delta C(T_c)$: $Pb_{0.8}Bi_{0.2}$, $Pb_{0.7}Bi_{0.3}$, $Pb_{0.9}Bi_{0.1}$, $Pb_{0.65}Bi_{0.35}$, Nb_3Al (1), Nb_3Sn, Nb_3Al (3), Nb_3Al (2), In, Tl.

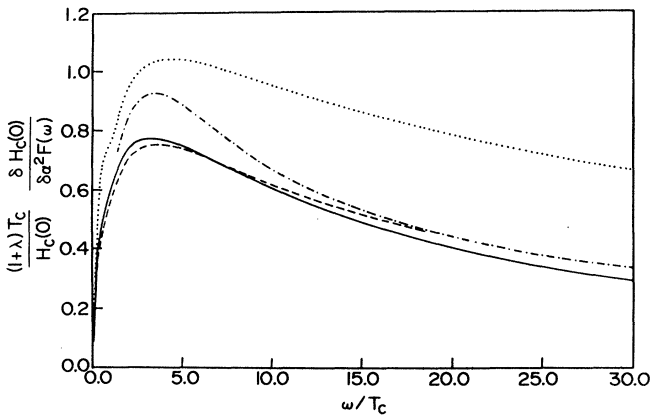

FIG. 74. Functional derivative of the thermodynamic critical field $H_c(T)$ at zero temperature ($T=0$) as a function of frequency ω normalized to the critical temperature T_c, for Pb (——) and Al (· · · ·), a strong- and weak-coupling superconductor, respectively. The dashed curve (— — —) is the functional derivative for the optimum Einstein spectrum. The dot-dashed curve (—·—·—·) is $\frac{1}{500}H_c(0)/[2N(0)]^{1/2}A$, which is dimensionless and independent of electron density of states $N(0)$ at the Fermi energy and of the area A under the spectral density as a function of the frequency ω_E of the Einstein oscillator in the model delta-function spectral density.

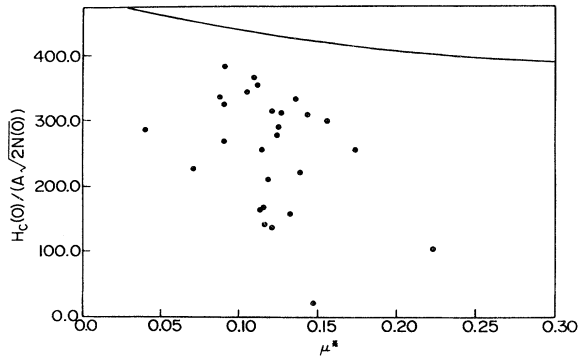

FIG. 75. Maximum possible value of $H_c(0)/[2N(0)]^{1/2}A$ as a function of μ^*. The solid dots are the theoretical values for the following materials in order of decreasing $H_c(0)/[2N(0)]^{1/2}A$: $Pb_{0.65}Bi_{0.35}$, $Pb_{0.7}Bi_{0.3}$, $Pb_{0.8}Bi_{0.2}$, $Pb_{0.9}Bi_{0.1}$, Nb_3Ge, $Pb_{0.5}Bi_{0.5}$, $Pb_{0.75}Bi_{0.25}$, Bi (amorphous), $Pb_{0.8}Tl_{0.2}$, Nb_3Al, Pb, Nb_3Sn, $Pb_{0.6}Tl_{0.4}$, La, Hg, V_3Ga, $Pb_{0.4}Tl_{0.6}$, Ga (amorphous), Mo (amorphous), V_3Si, Nb, Tl, In, $Tl_{0.9}Bi_{0.1}$, Sn, Ta, V, Al (BCS).

$\omega_E^*=4.8T_c$ exists for which the maximum $D(t)$ values, as a function of t, which, as it turns out, occurs for $t=0.65$, is itself a maximum. If we work out the functional derivative $\delta D(t)/\delta\alpha^2F(\omega)$ for the optimum base function obtained, i.e., for $A\delta(\omega-\omega_E^*)$, we get the dotted curve of Fig. 76, which is quite remarkable. It is negative definite and exhibits a zero at a frequency that is exactly the frequency of the base spectrum, namely, ω_E^*. This proves that $A\delta(\omega-\omega_E^*)$ gives a local maximum for $D(t)$.

In Fig. 77 we plot our theoretical results for $D(t)$ at maximum as a function of Coulomb pseudopotential μ^* (solid curve). On the same figure are shown (solid dots) results for real materials. None come very close to our theoretical maximum. For details of the systems used, see the caption and refer to the discussion following Fig. 75 that deals with $H_c(0)[\sqrt{2N(0)}\,A]$ instead of with $D(t)$.

Another dimensionless thermodynamic ratio that is often introduced and discussed is $\gamma T_c^2/H_c^2(0)$ [Blezius and Carbotte (1988)]. In BCS theory, this would be a universal number equal to 0.168. To understand how this quantity varies with details of the electron-boson spectral density, we first work out its functional derivative. In Fig. 78 we show results for the normalized quantity

$$(1+\lambda)T_c\frac{\delta}{\delta\alpha^2F(\omega)}[\gamma T_c^2/H_c^2(0)]$$

as a function of the normalized frequency ω/T_c. The solid curve is for Pb and is seen to have a negative minimum at some intermediate frequency $\omega/T_c=3.9$. While at higher frequency it remains negative and tends to zero as $\omega\to\infty$, at lower frequencies it cuts through the horizontal axis at $\omega/T_c=2.1$ and then diverges as $1/\omega$ for $\omega\to\infty$, which reflects the presence of the factor γ in $\gamma T_c^2/H_c^2(0)$. Shown also on the same figure are results for Al (dotted curve). The shape displayed is similar to that for Pb, but the minimum is larger in absolute value and occurs at $\omega/T_c=3.5$ with zero at $\omega/T_c=1.8$. It is clear that in the region of the minimum an infinitesimal change in the spectral density reduces $\gamma T_c^2/H_c^2(0)$ more in the weak-coupling case of Al than in strong-coupling

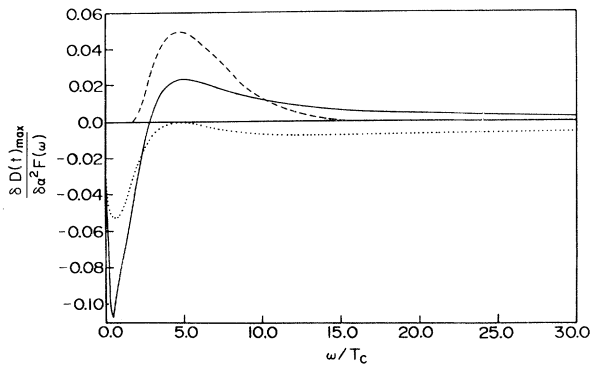

FIG. 76. Functional derivative of the thermodynamic critical magnetic-field deviation function $D(t)$ at the temperature corresponding to its maximum value for Pb as a function of frequency normalized to the critical temperature (solid curve). The functional derivative for the optimum Einstein spectrum is also shown (dotted curve), as is the maximum value in $D(t)$ for an Einstein spectral density $\alpha^2F(\omega)=A\delta(\omega-\omega_E)$ as a function of ω_E/T_c (dashed curve). It is independent of A, and at sufficiently large and small ω_E no maximum occurs in $D(t)$, which is then negative definite.

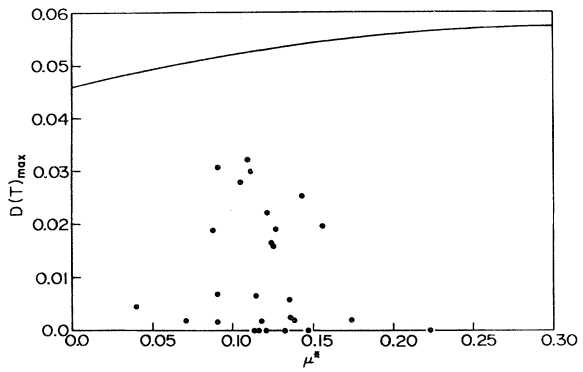

FIG. 77. Maximum possible value of the magnetic deviation function as a function of μ^*. The solid dots are the theoretical values for different materials, in order of decreasing value of $D(t)$: $Pb_{0.7}Bi_{0.3}$, $Pb_{0.65}Bi_{0.35}$, $Pb_{0.8}Bi_{0.2}$, $Pb_{0.9}Bi_{0.1}$, Pb, $Pb_{0.8}Tl_{0.2}$, Nb_3Sn, Nb_3Al, Nb_3Ge, Hg, $Pb_{0.6}Tl_{0.4}$, V_3Ga, $Pb_{0.4}Tl_{0.6}$, $Pb_{0.75}Bi_{0.25}$, La, $Pb_{0.5}Bi_{0.5}$, Ga (amorphous), V_3Si, Mo (amorphous), Nb, Bi (amorphous), In, $Tl_{0.9}Bi_{0.1}$, Tl, Sn, Ta, V, Al (BCS).

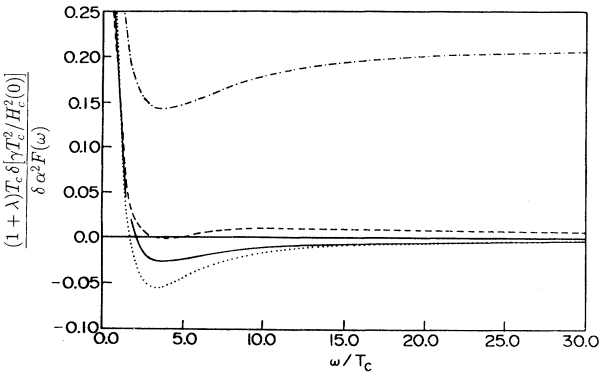

FIG. 78. Functional derivative of the squared ratio of the critical temperature to zero-temperature critical magnetic field $H_c(0)$ multiplied by the Sommerfeld constant γ as a function of frequency normalized to the critical temperature, for Pb (——) and Al (· · · ·), a strong- and weak-coupling superconductor, respectively. The same derivative for the optimum Einstein spectrum is also shown (— — —), as is $(4\pi/10)\gamma[T_c/H_c(0)]^2$ (—·—·—·) for an Einstein spectral density $\alpha^2F(\omega)=A\delta(\omega-\omega_E)$ as a function of ω_E/T_c. It is independent of A.

Pb. This is not unexpected since in weak coupling T_c is exponentially dependent on λ while for strong coupling the dependence is much weaker.

The dot-dashed line of Fig. 78 is our result for a delta-function spectrum $A\delta(\omega-\omega_E)$ as a function of ω_E/T_c. What is plotted is $(4\pi/10)\gamma T_c^2/H_c^2(0)$. As expected, this quantity follows closely the shape found for the functional derivative and does exhibit a clear minimum at a definite frequency ω_E^* equal to $3.9T_c$. As before, the minimum is independent of A, the area under the spectral density. With this base spectrum $A\delta(\omega-\omega_E^*)$, we have calculated the functional derivative and have found the dashed curve of Fig. 78. We note the functional derivative is now positive definite for all frequencies and exhibits a zero at exactly the frequency $\omega=\omega_E^*$—the Einstein frequency in the base delta function. Taking weight out of the base delta function to place it at any other frequency $\omega\neq\omega_E^*$ will increase $\gamma T_c^2/H_c^2(0)$.

In Fig. 79 we show results for the minimum $\gamma T_c^2/H_c^2(0)$ (solid curve) as a function of μ^* [Blezius and Carbotte (1988)]. Again, on the same plot, we show results of Eliashberg calculations (solid dots) based on tunneling values of $\alpha^2F(\omega)$ for many real electron-phonon superconductors. They all fall above our minimum, confirming our functional derivative arguments.

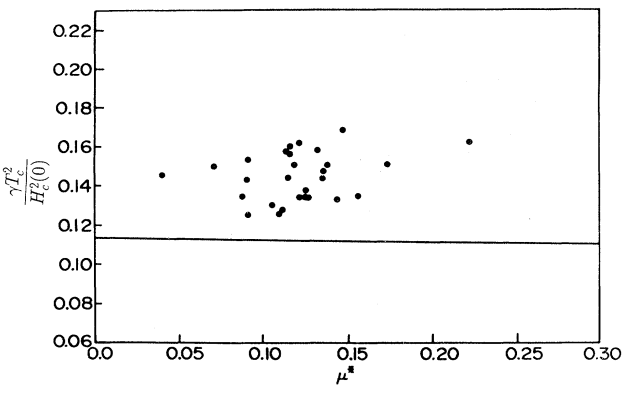

FIG. 79. Minimum possible value of $\gamma[T_c/H_c(0)]^2$ as a function of μ^*. The solid dots are the theoretical values for the following materials in order of increasing value of $\gamma(0)/[T_c/H_c(0)]^2$: $Pb_{0.65}Bi_{0.35}$, $Pb_{0.7}Bi_{0.3}$, $Pb_{0.8}Bi_{0.2}$, $Pb_{0.9}Bi_{0.1}$, Pb, $Pb_{0.8}Tl_{0.2}$, Nb_3Al, Hg, Nb_3Sn, Nb_3Ge, $Pb_{0.6}Tl_{0.4}$, V_3Ga, $Pb_{0.75}Bi_{0.25}$, $Pb_{0.4}Tl_{0.6}$, La, $Pb_{0.5}Bi_{0.5}$, Mo (amorphous), Nb, V_3Si, Ga (amorphous), Bi (amorphous), In, $Tl_{0.9}Bi_{0.1}$, Tl, Sn, Ta, V, Al (BCS).

G. Asymptotic limit

We turn next to the asymptotic limit $\lambda\to\infty$ for thermodynamic properties. To calculate this asymptotic limit, we need to know the free-energy difference between superconducting and normal state $\Delta F(t)$, which is given by the Bardeen-Stephen formula (5.1); we repeat it here for convenience in a slightly different form. It is

$$\frac{\Delta F}{N(0)}=-2\pi T\sum_{n=1}^{\infty}\omega_n\left[Z^S(i\omega_n)-\frac{Z^N(i\omega_n)}{\sqrt{1+\Delta^2(i\omega_n)/\omega_n^2}}\right]\times\left(\sqrt{1+\Delta^2(i\omega_n)/\omega_n^2}-1\right). \quad (6.28)$$

From Eq. (2.28) it is clear that each of the two square-root factors in (6.28) is independent of λ since it depends only on the normalized dimensionless quantity $\bar{\Delta}(i\bar{\omega}_n)$ and on $\bar{\omega}_n$. Further, the superconducting-state renormalization factor Z^S can be written as [Marsiglio *et al.* (1989)].

$$Z^S(i\omega_n)=1+\frac{\pi\bar{T}}{\sqrt{\bar{\omega}_n^2+\bar{\Delta}^2(i\bar{\omega}_n)}}\lambda+\frac{\pi\bar{T}}{\bar{\omega}_n}\sum_{m\neq n}\frac{2}{(\bar{\omega}_n-\bar{\omega}_m)^2}\frac{\bar{\omega}_m}{\sqrt{\bar{\omega}_m^2+\bar{\Delta}^2(i\bar{\omega}_m)}}, \quad (6.29)$$

which depends on λ only in the second term, as does Z^N, which is obtained from (6.29) by setting $\bar{\Delta}(i\bar{\omega}_m)$ equal to zero in the last two terms on the right-hand side. On inserting (6.29) into (6.28), it is clear that the λ dependence in both Z^S and Z^N cancel, so that the expression in the first large square bracket of (6.28) is material independent. Thus the free energy scales like T_c^2 because of the presence of an overall factor of T^2; so,

$$-\frac{\Delta F}{N(0)}=\frac{A^2}{\lambda}g(t)\equiv\tfrac{1}{4}\lambda\omega_E^2g(t), \quad (6.30)$$

where $g(t)$ is a universal function of reduced temperature T/T_c. This function, independent of any material parameters, can be calculated from the universal equation (2.28) for $\bar{\Delta}(i\bar{\omega}_m)$ and from the free-energy difference (6.28). The material-dependent parameter λ, which still appears explicitly in both Z^S and Z^N, cancels in the combination needed in this formula.

The thermodynamic critical magnetic field $H_c(T)$ follows from $\Delta F(t)$, as does the specific-heat difference $\Delta C(T)$. We have

$$H_c(T)=\sqrt{-8\pi\Delta F} \text{ and } \Delta C(T)=-T\frac{d^2\Delta F}{dT^2}\ , \tag{6.31}$$

so that the universal quantity $g(t)$ as a function of reduced temperature (t) gives both $H_c(t)$ and $\Delta C(t)$. The results of our numerical calculations are given in Fig. 80. Instead of $g(t)$ itself, we have chosen to plot $h_c(t)$, the reduced thermodynamic critical magnetic field given by Marsiglio *et al* (1989), as

$$h_c(t)=\frac{H_c(t)}{\left|\frac{dH_c(t)}{dt}\right|_{t=1}}=\frac{\sqrt{g(t)}}{\left|\frac{d\sqrt{g(t)}}{dt}\right|_{t=1}} \tag{6.32}$$

which is simply the square root of the universal function g normalized to its slope at $t=1$. The asymptotic-limit field $h_c(t)$ is given as the solid curve of Fig. 80. It looks very different from its behavior in BCS theory, in which case $h_c(t)$ has a negative curvature at all temperatures and at $t=0$, $h_c(0)=0.576$. By contrast, in the asymptotic limit, $h_c(t)$ exhibits a large region of near linear dependence below $t=1$ and then shows the opposite curvature bending upward as t decreases; it is still rising rapidly at $t=0.008$. This is the lowest reduced temperature we could handle in our numerical work, due to computer time limitations. Consequently, we do not have information on its zero-temperature behavior, because our work is valid only for

$$\sqrt{\lambda}\,t\gg 1\ , \tag{6.33}$$

which precludes $t=0$. Equation (6.33) follows from our initial approximation $\omega_E \ll 2\pi T$. We can rewrite $H_c(t)$ in the form

$$H_c(t)=\sqrt{2\pi N(0)}\,\lambda\left[\frac{1}{\sqrt{\lambda}\,t}th_c(t)\right]\left|\frac{d\sqrt{g(t)}}{dt}\right|_{t=1}\omega_E \tag{6.34}$$

and find that its $t\to 0$ behavior is not singular because condition (6.33) requires that $1/(\sqrt{\lambda}\,t)\ll 1$. In addition, we note that $th_c(t)$ shown in Fig. 80 (dotted curve) is well behaved even for $t\to 0$. Thus the expression in the square bracket of Eq. (6.34) is also well behaved in the range $\sqrt{\lambda}\,t\gg 1$. What we need to remember is that λ must go to ∞ before t goes to zero for the condition $\sqrt{\lambda}\,t\gg 1$ to be satisfied.

Our results for $h_c(t)$ or $th_c(t)$ cover the entire temperature dependence of the free-energy difference and so the specific heat follows as well [formula (6.31)]. Evaluation of the jump in $\Delta C(T)$ at T_c and of its slope gives, respectively.

$$\frac{\Delta C(T_c)}{\gamma T_c}=\frac{19.9}{\lambda} \tag{6.35}$$

and

$$\frac{d}{dt}\frac{\Delta C(t)}{\gamma T_c}\bigg|_{t=1}=\frac{39.2}{\lambda}\ . \tag{6.36}$$

While both the normalized jump and slope go to zero as $\lambda\to\infty$, their ratio remains constant. It is equal to 1.96, which is to be compared with a BCS value of 2.64.

It is interesting to get rough estimates for the two quantities (6.35) and (6.36) using a single-Masubara-gap approximation, that is assuming $\Delta(1)=\Delta(T)$ and all other gaps to be zero. In this case, Eq. (2.1) gives, after noting the symmetries $\Delta(-n)=\Delta(n+1)$ and $\omega_{-n}=-\omega_{n+1}(\mu^*\equiv 0)$,

$$\Delta(n)Z(n)=\pi T\sum_{m=1}^{\infty}[\lambda(m-n)+\lambda(m+n-1)]\times\frac{\Delta(m)}{\sqrt{\omega_m^2+\Delta^2(m)}}\ ; \tag{6.37}$$

and so

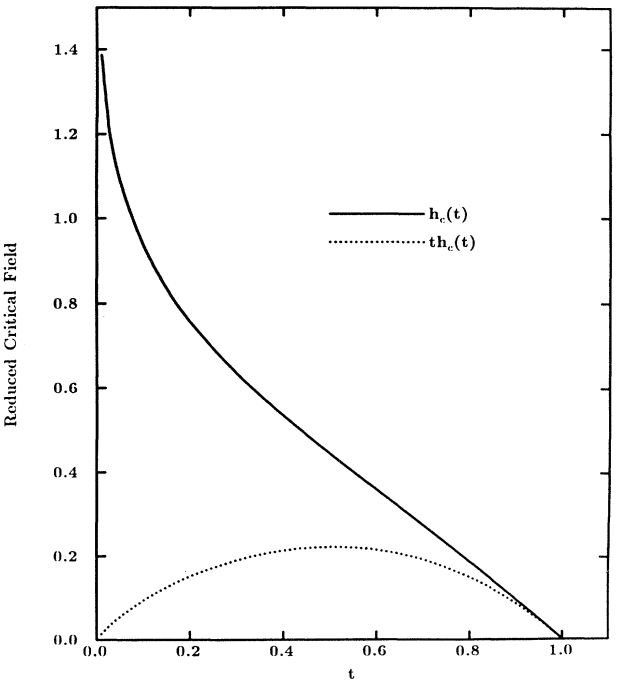

FIG. 80. Reduced thermodynamic critical magnetic field $h_c(t)$ (solid curve) in the asymptotic limit. The dotted curve is $th_c(t)$, which is well behaved in the $t\to 0$ limit.

$$\Delta(T)Z(1)=(\pi T)[\lambda(0)+\lambda(1)]\frac{\Delta(T)}{\sqrt{(\pi T)^2+\Delta^2(T)}} \tag{6.38}$$

Equation (2.2) requires a little more care. We can write it as

$$Z(n)=1+\frac{\pi T}{\omega_n}\sum_{m=1}^{\infty}[\lambda(m-n)-\lambda(m+n-1)]\times\frac{\omega_m}{\sqrt{\omega_m^2+\Delta^2(m)}} \tag{6.39}$$

$$=1+\frac{\pi T}{\omega_n}\sum_{m=1}^{\infty}[\lambda(m-n)-\lambda(m+n-1)]\times\left[1-\frac{1}{2}\left[\frac{\Delta(m)}{\omega_m}\right]^2+\frac{3}{8}\left[\frac{\Delta(m)}{\omega_m}\right]^4-\cdots\right] . \tag{6.40}$$

The sum over m in the first term of the last curly bracket in Eq. (6.40) must be carried out to infinity. It makes a contribution of

$$\frac{\pi T}{\omega_n}\left[\lambda(0)+2\sum_{m'=1}^{n-1}\lambda(m')\right] ; \tag{6.41}$$

and so since (6.41) equals $\lambda(0)$ for $n=1$,

$$Z(1)=1+\lambda(1)+\frac{[\lambda(0)-\lambda(1)]\pi T}{\sqrt{(\pi T)^2+\Delta^2(T)}} , \tag{6.42}$$

where we have reconstructed the square root from the expansion in (6.40) after taking out the constant term. Taking $\mu^*=0$ for simplicity and combining (6.42) and (6.38) gives an equation for the gap,

$$(\pi T)\frac{\lambda(0)+\lambda(1)}{\sqrt{(\pi T)^2+\Delta^2(T)}}=1+\lambda(1)+\frac{[\lambda(0)-\lambda(1)]\pi T}{\sqrt{(\pi T)^2+\Delta^2(T)}} . \tag{6.43}$$

As we expect from our discussion in Sec. II on asymptotic limits for the critical temperature, $\lambda(0)$ drops out of Eq. (6.43), which can be rewritten as

$$\sqrt{(\pi T)^2+\Delta^2(T)}=\frac{2\pi T\lambda(1)}{1+\lambda(1)} . \tag{6.44}$$

The critical temperature follows from (6.44) with $T=T_c$ and $\Delta(T)=0$. Reference to (2.27) gives $\lambda(1)=2/(2\pi\bar{T})^2$ with $\bar{T}\equiv T/\sqrt{A\omega_E}$, and so we get

$$1=\frac{2}{(2\pi\bar{T}_c)^2} \quad \text{or} \quad T_c=\frac{1}{\sqrt{2}\,\pi}\sqrt{A\omega_E} , \tag{6.45}$$

a result already referred to in Sec. II.

In the one-Matsubara-gap model, the sum over n in formula (6.28) for the free-energy difference $\Delta F/N(0)$ can be cut off at $n=1$, as can be seen easily on expanding the square root in the second bracket and noting the cancellation of the unit terms with all remaining terms proportional to powers of $\Delta^2(n)$. On substituting (6.42) into this equation, we get to order Δ^6

$$\frac{\Delta F}{N(0)}=-\frac{(\pi T)^2}{2}[1+\lambda(1)]\left[\frac{\Delta(T)}{\pi T}\right]^4\left[1-\left[\frac{\Delta(T)}{\pi T}\right]^2\right] . \tag{6.46}$$

To obtain the gap to second order in $(1-t)$, we return to (6.44) and expand the square root to second order to get

$$1+\frac{1}{2}\left[\frac{\Delta(T)}{\pi T}\right]^2-\frac{1}{2}\left[\frac{1}{2}\left[\frac{\Delta(T)}{\pi T}\right]^2\right]^2=\frac{2}{1+t^2} , \tag{6.47}$$

where use was made of (6.45). On expanding the right-hand side, we get

$$\frac{1}{2}\left[\frac{\Delta(T)}{\pi T}\right]^2-\frac{1}{2}\left[\frac{1}{2}\left[\frac{\Delta(T)}{\pi T}\right]^2\right]^2=(1-t)+\frac{1}{2}(1-t)^2 , \tag{6.48}$$

from which we conclude that to lowest order

$$\left[\frac{\Delta(T)}{\pi T_c}\right]^2=2(1-t) . \tag{6.49}$$

Substituting (6.49) back into the gap equation (6.48) gives to second order

$$\left[\frac{\Delta(T)}{\pi T_c}\right]^2=2(1-t)[1+(1-t)] \tag{6.50}$$

or

$$\Delta(T)=\sqrt{A\omega_E}\sqrt{1-t}\,[1-\tfrac{1}{2}(1-t)] . \tag{6.51}$$

Equation (6.50) needs to be substituted into (6.46) to get the free-energy difference, which is

$$\frac{\Delta F}{N(0)}=-\frac{(\pi T_c)^2}{2}2[1-(1-t)]\left[\frac{\Delta(T)}{\pi T_c}\right]^4\times\left[1-\left[\frac{\Delta(T)}{\pi T_c}\right]^2\right] \tag{6.52}$$

and works out to be

$$\frac{\Delta F}{N(0)}=-4(\pi T_c)^2[1-(1-t)](1-t)^2 , \tag{6.53}$$

from which it follows that

$$\frac{\Delta C(T_c)}{\gamma T_c}=\frac{12}{\lambda} \quad \text{and} \quad \frac{d}{dt}\left[\frac{\Delta C(t)}{\gamma T_c}\right]\Bigg|_{t=1}=\frac{48}{\lambda} . \tag{6.54}$$

These rough values compare well with the exact results (6.35) and (6.36).

VII. THE UPPER CRITICAL MAGNETIC FIELD

A. General formulas

Schossmann and Schachinger (1986) have given formulas from which the upper critical magnetic field $H_{c2}(T)$ can be computed if the electron-phonon spectral density and Coulomb pseudopotential are known for a particular material. The formulas are valid for any impurity concentration described by $t^+=1/2\pi\tau$ with τ the scattering time. In the weak-coupling limit, the equations of Schossmann and Schachinger (1986) reduce to a renormalized form of the BCS theory of Helfand and Werthamer (1964, 1966) and of Werthamer *et al.* [(1966); see also Abrikosov (1957a, 1957b) and Gork'ov (1959a, 1959b)]. In the dirty limit, they reduce to well-known formulas used by Rainer and Bergmann (1974) in extensive calculations of the critical magnetic field for real materials in that limit [see also Werthamer and McMillan (1967)].

The equations derived by Schossmann and Schachinger (1986) from which the second critical magnetic field $H_{c2}(T)$ follows at any temperature T and for any impurity content are

$$\tilde{\Delta}(i\omega_n)=\pi T\sum_m \frac{[\lambda(n-m)-\mu^*]\tilde{\Delta}(i\omega_m)}{\chi^{-1}[\tilde{\omega}(i\omega_m)]-\pi t^+} \tag{7.1a}$$

with

$$\tilde{\omega}(i\omega_n)=\omega_n+\pi T\sum_m \lambda(n-m)\mathrm{sgn}\omega_m+\pi t^+\mathrm{sgn}\omega_n \ . \tag{7.1b}$$

Neglecting Pauli limiting, the factor $\chi(\tilde{\omega}(i\omega_n))$ in Eq. (7.1a) is

$$\chi(\tilde{\omega}(i\omega_n))=\frac{2}{\sqrt{\alpha}}\int_0^\infty dq\, e^{-q^2}\tan^{-1}\left[\frac{\sqrt{\alpha}\,q}{|\tilde{\omega}(i\omega_n)|}\right] . \tag{7.1c}$$

The eigenvalue α operating in the definition of χ is related to H_{c2}:

$$\alpha(T)=\tfrac{1}{2}eH_{c2}(T)v_F^2 \tag{7.1d}$$

with e the charge on the electron and v_F the electron Fermi velocity.

To include Pauli limiting, we only need to replace the factor $|\tilde{\omega}(i\omega_n)|$, which enters the argument of the inverse tangent in (7.1c), by

$$|\tilde{\omega}(i\omega_n)|+i\mu_B H\,\mathrm{sgn}\tilde{\omega}_n \ ,$$

where H is the external magnetic field and μ_B is the Bohr magneton. This replacement, while simple, has the effect of making the Matsubara gaps $\tilde{\Delta}(i\omega_n)$ in Eq. (7.1a) complex.

B. Reduction to BCS

To reduce these equations to a form similar to those derived by Werthamer *et al.* (1966) on the basis of BCS theory, we need to apply the standard two-square-well model for the n and m dependence of $\lambda(n-m)$ with cutoff at N_c. In this approximation, $\tilde{\omega}_n=\omega_n(1+\lambda)+\pi t^+\mathrm{sgn}\omega_n$ and Eq. (7.1a) reduces, with Pauli limiting included, to the form

$$1=2\pi T\sum_{m=0}^{N_c}(\lambda-\mu^*)\mathrm{Re}\{[\chi^{-1}(\tilde{\omega}_m)-\pi t^+]^{-1}\} \ . \tag{7.2}$$

It is convenient to introduce into (7.2) the renormalized quantities

$$H^*=H/(1+\lambda)T_c \ , \tag{7.3a}$$

$$v_F^*=v_F/\sqrt{(1+\lambda)T_c} \ , \tag{7.3b}$$

$$(t^+)^*=t^+/(1+\lambda)T_c \ , \tag{7.3c}$$

and obtain the universal relationship

$$\frac{1+\lambda}{\lambda-\mu^*}=2\pi t\sum_{m=0}^{N_c}\mathrm{Re}\{[\bar{\chi}^{-1}(\tilde{\omega}_n)-\pi(t^+)^*]^{-1}\} \tag{7.4a}$$

with

$$\bar{\chi}(\tilde{\omega}_m)=\frac{2}{\sqrt{\alpha^*}}\int_0^\infty dq\, e^{-q^2}\tan^{-1}\times\left[\frac{q\sqrt{\alpha^*}}{(2m+1)\pi t+\pi(t^+)^*+i\mu_B H^*}\right] \tag{7.4b}$$

with $\alpha^*=\frac{1}{2}eH^*v_F^{*2}$ and $t=T/T_c$. To complete the set of equations for H_{c2}, we note that the critical temperature is given by

$$\frac{1+\lambda}{\lambda-\mu^*}=\ln(1.13\omega_c/T_c) \ . \tag{7.4c}$$

Equations (7.4) have the same formal structure as those given by WHH (Werthamer, Helfand, Hohenberg) theory. Our equations differ from the BCS limit, because they involve renormalizations in α^*, v_F^*, H^*, and $(t^+)^*$. In particular, it is important to note that the band-splitting term in (7.4b) is given by $i\mu_B H^*$ and is, therefore, renormalized by a factor of $(1+\lambda)^{-1}$ over its value in BCS theory. For a fixed value of the external magnetic field, this factor can greatly reduce the effect of Pauli limiting. It was noted in the extensive calculations of Orlando *et al.* (1979) for Nb_3Sn and V_3Si that such a renormalization factor greatly reduces the need to introduce spin-orbit coupling, which traditionally is needed to reduce the strong effect of Pauli limiting. In the work of Orlando *et al.* (1979), a free-energy argument is advanced on the basis of which they suggest the $i\mu_B H$ term should be reduced by $\sqrt{1+\lambda}$ instead of the full $1+\lambda$ found here. Thus, in a complete theory, the effect of Pauli limiting is reduced even further over the semiphenomenological approach of Orlando *et al.* [see Orlando and Beasley (1981)]. We shall return to this point later.

C. Comparison with experiment in Nb

To begin our discussion of comparison with experiment, we shall start with the case of Nb with 0.3 percent N and a T_c of 9.112 K [Schachinger, Prohammer, Seidl, and Weber (1988)]. In Fig. 81, we compare theory with experimental results (solid squares). No Pauli limiting is included, and the best fit to the data is the solid curve, which is computed on the basis of the strong-coupling equations (7.1) with $\alpha^2F(\omega)$ taken from Robinson and Rowell (1972). The value of mass renormalization, $\lambda=0.983$, and the Fermi velocity, $v_F=0.5\times10^6$ m/s, were fitted to the initial slope of $H_{c2}(T)$ at T_c for an impurity content of $t^+=0.76$ meV. The agreement is good and can be improved further if anisotropy is included in the theory, as described by Prohammer and Schachinger (1987) and used in Schachinger, Prohammer, Seidl, and Weber (1988).

For comparison, we include results of three other calculations. In the first two calculations, the Fermi velocity is kept fixed, as is the T_c. In a first calculation, the WHH theory is used without renormalization $(1+\lambda)$, and this yields the dotted curve, which falls way below the data. Of course, we really should have worked with renormalized quantities as in Eqs. (7.4). If this is done, the medium dashed curve results, and the fit to the data is now much better, although still not at all as good as for the full calculations. Thus differences remain between full Eliashberg theory [Eqs. (7.1)] and the renormalized version of WHH [Eq. (7.4)]. The remaining differences can be reduced further if, in renormalized WHH, we treat v_F as an adjustable parameter and make a new fit to the data. This gives the long dashed curve of Fig. 81, which is now close to the solid curve and to the data. The new Fermi velocity is now 0.478×10^6 m/s, which is only slightly reduced from 0.5×10^6 m/s. These values compare favorably with the band-structure result 0.62×10^6 m/s given by Mattheiss (1970), but are a little low. A fit to a theory that includes anisotropy [Weber and Schachinger (1988)] and therefore falls outside the scope of this review gives 0.57×10^6 m/s [Schachinger, Prohammer, Seidl, and Weber (1988)]. Our conclusions from the above consideration is that strong-coupling theory gives somewhat different results from renormalized WHH, but that in Nb the differences are small if the Fermi velocity is treated as an adjustable parameter and interpreted as a renormalized quantity. When Pauli limiting is needed, however, WHH theory requires modification of the band-splitting term by, at the very least, $(1+\lambda)^{-1}$, as we now explore further.

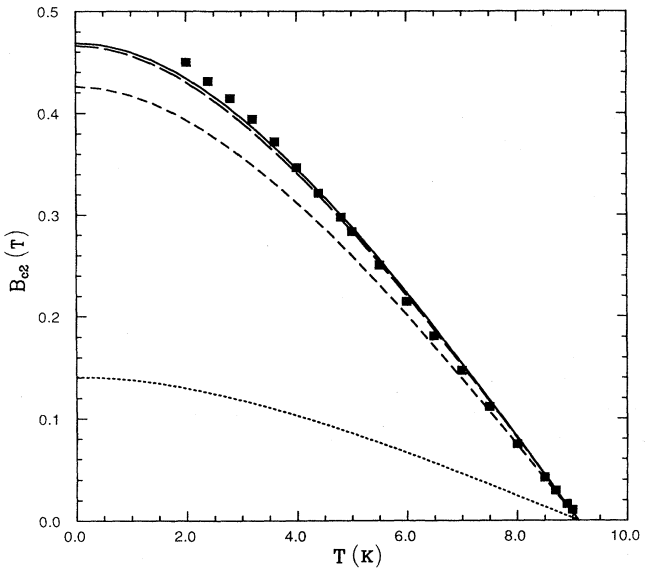

FIG. 81. Comparison with experiment (solid squares) of the upper critical field $H_{c2}(T)$ in Nb with 0.3 percent N. The solid curve is obtained from a numerical solution of the full equations (7.1) based on a tunneling-derived electron-phonon spectral density. The other curves are based on the simpler equations (7.4). For the dotted curve, the same Fermi velocity is used but no renormalization $(1+\lambda)$ introduced, so that this is the prediction of a pure WHH (BCS) theory. The medium dashed curve is computed in the same way, but the $(1+\lambda)$ factors are all included so that the full renormalized WHH equations are used. Finally, the long dashed curve is obtained from the renormalized WHH equations with Fermi velocity fitted to the initial slope. The agreement with experiment is not quite as good as for the full Eliashberg equations, but it is not very different.

D. Inclusion of Pauli limiting

Returning to Eqs. (7.4) for the renormalized WHH equations, we see that they are universal, provided renormalized quantities are used. For a fixed impurity content $(t^+)^*$, they are unique for a given value of v_F^*. If, instead of v_F^*, we consider the slope of the renormalized upper critical field at T_c, namely,

$$\left.\frac{dH_{c2}(T)}{dT}\right|_{T=T_c}\frac{1}{1+\lambda}\equiv\dot{H}_{c2}/[(1+\lambda)T_c]\ ,$$

we get a single curve for $H_{c2}(0)/[(1+\lambda)T_c]$ as a function of $\dot{H}_{c2}/[(1+\lambda)T_c]$, which applies to all BCS superconductors including Pauli limiting. These curves are shown as the solid and dashed lines in Fig. 82 for the clean and dirty limit, respectively. If Pauli limiting is ignored, $H_{c2}(0)/[(1+\lambda)T_c]$ is simply proportional to the slope $[dH_{c2}(t)/dt]_{t=1}/[(1+\lambda)T_c]$. This relationship corresponds to the two straight lines, solid (clean) and dashed (dirty), of Fig. 82 with slope 0.73 and 0.69, respectively. This figure is very important since, given a value of the slope at T_c, we can estimate the corresponding effect of Pauli limiting. Without the electron-phonon renormalization factor $(1+\lambda)$ included in such an analysis, we see that the effect of Pauli limiting is much exaggerated,

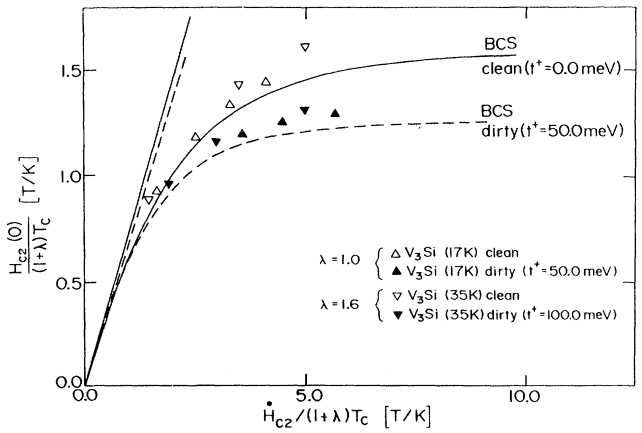

FIG. 82. Normalized zero-temperature upper critical field $H_{c2}(0)/[(1+\lambda)T_c]$ as a function of the normalized initial slope at T_c, $[dH_{c2}(t)/dt]_{t=1}/[(1+\lambda)T_c]$. The solid and dashed curves were obtained using a renormalized BCS theory including Pauli limiting and apply, respectively, to the clean and dirty ($t^+=50.0$ meV) limits. The straight lines result when Pauli limiting is neglected. The upward- and downward-pointing open (clean limit) and solid (dirty limit) triangles are results of full strong-coupling calculations for V_3Si with $\lambda=1.0$ and a fictitious system with $T_c=35.0$ K having the same shape $\alpha^2F(\Omega)$ as that for V_3Si, but with $\lambda=1.6$.

since we fall further to the right on the horizontal axis.

It is of some interest to reduce the renormalized WHH formulas (7.4) in the dirty and clean limit. In the dirty limit ($t^+\to\infty$), we can rewrite

$$\bar{\chi}^{-1}(\tilde{\omega}_m)=[(2m+1)\pi t+\pi(t^+)^*+i\mu_B H^*]\times\left[1+\frac{\alpha^*}{3\pi^2(t^{+*})^2}\right] \tag{7.5a}$$

and get

$$\frac{1+\lambda}{\lambda-\mu^*}=2\pi t\sum_{m=0}^{N_c}\mathrm{Re}\left\{\left[(2m+1)\pi t+i\mu_B H^*+\frac{\alpha^*}{3\pi(t^+)^*}\right]^{-1}\right\}, \tag{7.5b}$$

which gives

$$\frac{1+\lambda}{\lambda-\mu^*}=\mathrm{Re}\left[\psi\left(\frac{\omega_c}{2\pi T}+\frac{i\mu_B H^*}{2\pi t}+\frac{\alpha^*}{6\pi^2 t(t^+)^*}\right)-\psi\left(0.5+\frac{i\mu_B H^*}{2\pi t}+\frac{\alpha^*}{6\pi^2 t(t^+)^*}\right)\right], \tag{7.5c}$$

where $\psi(x)$ denotes the digamma function. By assuming ω_c to be very large, one can approximate the first digamma function in (7.5c) by $\ln(\omega_c/2\pi T)$. Furthermore, using the T_c equation, we find

$$-\ln(1.13\times 2\pi t)=\mathrm{Re}\psi\left[0.5+\frac{i\mu_B H^*_{c2}}{2\pi t}+\frac{\alpha^*}{6\pi^2 t(t^+)^*}\right]. \tag{7.5d}$$

In the limit when the reduced temperature is small, (7.5d) has the solution

$$H^*_{c2}=\frac{1}{1.13}\{(ev_F^{*2})^2/[6\pi(t^+)^*]^2+\mu_B^2\}^{-1/2}, \tag{7.5e}$$

and the initial slope is found by differentiating (7.5d) with respect to t:

$$\dot{H}^*_{c2}=\left.\frac{dH^*_{c2}}{dt}\right|_{t=1}=-\frac{24(t^+)^*}{ev_F^{*2}}, \tag{7.5f}$$

which can be inserted into (7.5e) to give

$$H^*_{c2}=[(0.695\dot{H}^*_{c2})^{-2}+(H^*_{c2,P})^{-2}]^{-1/2}. \tag{7.5g}$$

The extreme Pauli follows for infinite slope $\dot{H}^*_{c2}\to\infty$:

$$H^*_{c2,P}=\frac{1}{1.13\mu_B}\quad\text{or}\quad 1.32\ \text{T/K}, \tag{7.5h}$$

which is slightly different from the Clogston value obtained from free-energy considerations. In that approach, we set the band-splitting energy equal to the BCS condensation energy

$$\mu_B^2 H^2_{c2,P}N(0)=\tfrac{1}{2}N(0)(1+\lambda)(1.76)^2T_c^2, \tag{7.5i}$$

where $N(0)$ is the single-spin electronic density of states at the Fermi energy. This leads to

$$\frac{H_{c2,P}}{\sqrt{1+\lambda}\,T_c}=\frac{1.76}{\sqrt{2}}\frac{1}{\mu_B}=\frac{1.24}{\mu_B}, \tag{7.5j}$$

as given by Orlando *et al.* (1979) and without a $1+\lambda$ correction by Decroux *et al.* (1982). We see clearly that free-energy arguments cannot be used to get the correct numerical factor in such relationships or the right λ renormalization.

In the clean limit the situation is more complicated mathematically, but Schossmann and Carbotte (1989) have been able to establish that Eq. (7.5h) holds as well. While the factor $(1+\lambda)^{-1}$ greatly deemphasizes the effect of Pauli limiting and reduces the need to introduce spin-orbit scattering, it is important to study strong-coupling effects beyond this factor.

In order to estimate strong-coupling corrections beyond the $1+\lambda$ rescaling that appear in the modified BCS results, we calculated the reduced upper critical magnetic field $H^*_{c2}=H_{c2}/[(1+\lambda)T_c]$ as a function of the reduced initial slope $\dot{H}^*_{c2}=\dot{H}_{c2}/[(1+\lambda)T_c]$ for several cases. As was shown in the previous section, there is only one such curve in BCS, given a fixed reduced impurity concentration $t^+/[(1+\lambda)T_c]$. This is no longer the case when realistic values for $\alpha^2F(\omega)$ are taken into account. In Fig. 82, we show some of our results based on the full strong-coupling equations (7.1a) to (7.1c). In one

calculation (triangular symbols pointing up), we have used the electron-phonon spectral density $\alpha^2F(\omega)$ determined by Kihlstrom (1985) for V_3Si from tunneling data. The value of λ is 1.0, and we chose μ^* to give a $T_c=17.0$ K for this value of λ. This corresponds fairly closely to a sample studied by Orlando *et al.* (1979) with a fairly low residual resistivity of 5.2 $\mu\Omega$ cm at 20 K, an estimated mean free path of 95 Å and an electromagnetic coherence length of 56 Å. In Fig. 82, two cases are considered. The first is the clean-limit results with $t^+=0.0$ meV (open triangles), which are seen to fall above the BCS clean-limit curve but not by very much. In this case, strong-coupling corrections beyond the very essential factor of $1+\lambda$, are not very pronounced. The same remarks apply to the solid triangles describing the dirty limit. To get larger corrections, we have arbitrarily increased the area under the spectral density $\alpha^2F(\omega)$ of V_3Si by multiplication by a constant amount to increase the corresponding λ from 1.0 to 1.6 and, at the same time, to raise T_c to 35 K, which is not very different from the critical temperature found in $La_{1.85}Sr_{0.15}CuO_4$ (a high-T_c oxide superconductor). The clean-limit results are the open triangles pointing downward in Fig. 82. We see that, in this case, the deviations from BCS are much more significant than for V_3Si itself. This shows clearly that, in some cases at least, it is necessary to perform a full strong-coupling calculation based on Eqs. (7.1a) to (7.1c) in order to get an accurate value for $H_{c2}(0)/[(1+\lambda)T_c]$. Additional results for dirty samples (solid downward triangles) are also given in Fig. 82 and compared to the BCS $t^+=50.0$ meV curve. Again, significant corrections can arise, and this should be kept in mind in the analyses of data.

Finally, we return to the solid and dashed lines in Fig. 82, giving $H_{c2}(0)/[(1+\lambda)T_c]$ as a function of the initial slope at T_c, $\dot{H}_{c2}(t=1)/(1+\lambda)T_c$. These straight lines apply, respectively, to the clean and dirty limits in BCS when Pauli limiting (band splitting) is ignored. The bending over of solid and dashed curves away from these straight lines gives the effect of band splitting. In the work of Orlando *et al.* (1979), they quote for $\mu_0H'_{c2}(T_c)$ in V_3Si a value of 2.0 T/K. If we divide by $1+\lambda$, we get for the horizontal variable a value $\mu_0\dot{H}_{c2}(t=1)/(1+\lambda)T_c\cong 1.0$ T/K, which indicates the Pauli limiting is not a large effect in V_3Si. This conclusion was also reached by Schossmann and Schachinger (1986) on the basis of detailed numerical considerations. In our case, we need only realize that in this region the solid and dashed curves do not differ very much from the corresponding straight lines. If the $(1+\lambda)$ factor is ignored, a very different conclusion is reached.

We now return to the complete equations (7.1) for H_{c2} without Pauli limiting and begin a derivation of strong-coupling corrections.

E. Reduction to analytic form

We first study the dirty limit for which πt^+ becomes very large. This limit was considered extensively by Rainer and Bergmann (1974). We obtain it here from Eq. (7.1). Noting that, in this limit, Eq. (7.1b) becomes dominated by πt^+, we can assume that $|\tilde{\omega}(i\omega_n)|\gg 1$ and can expand the inverse tangent in (7.1c). Retaining only the first two terms gives

$$\chi^{-1}(\tilde{\omega}(i\omega_n))-\pi t^+\cong|\tilde{\omega}_0(i\omega_n)|+\frac{1}{3}\frac{\alpha}{|\tilde{\omega}(i\omega_n)|}\ , \tag{7.6a}$$

where $\tilde{\omega}_0(i\omega_n)$ is given by (7.1b) without the πt^+ term. In Eq. (7.6a), it is justified to replace $|\tilde{\omega}(i\omega_n)|$ in the denominator of the last term by πt^+, which gives the familiar form

$$\tilde{\Delta}(i\omega_n)=\pi T\sum_m[\lambda(n-m)-\mu^*]\frac{\tilde{\Delta}(i\omega_m)}{|\tilde{\omega}_0(i\omega_m)|+\rho^{\rm di}}\ . \tag{7.6b}$$

The new parameter $\rho^{\rm di}$ is

$$\rho^{\rm di}=\frac{1}{3}\frac{\alpha^{\rm di}}{\pi t^+}=\tfrac{1}{3}v_F^2\tau eH_{c2}^{\rm di}(T)\equiv DeH_{c2}^{\rm di}(T)\ , \tag{7.7}$$

where reference has been made to (7.1d) and the diffusion constant $D\equiv\frac{1}{3}v_F^2\tau$ has been introduced. Numerical solutions of (7.6) have already been obtained for many materials by Rainer and Bergmann. Our own more extensive solutions will be presented shortly in graphical form. Before doing this, we wish to derive approximate formulas for H_{c2} that go beyond BCS theory and include a first correction for strong coupling characterized by the single strong-coupling parameter $T_c/\omega_{\ln}$. The necessary algebra is found in Appendix B.

Equation (B54) gives the slope of the critical magnetic field at T_c and reads

$$T_c|\rho^{\rm di'}(T_c)|=\frac{4T_c}{\pi}(1+\lambda)\left[1+\frac{2T_c}{\lambda}d+4\left[\frac{T_c}{\lambda}\right]^2d^2+\frac{(\pi T_c)^2}{\lambda}[2a(T_c)-\tfrac{8}{3}b]\right]\ . \tag{7.8}$$

In (7.8) we can approximate

$$a(T_c)\cong\frac{\alpha_1}{\omega_{\ln}^2}\lambda\ln\left[\frac{1.13\omega_{\ln}}{k_BT_c}\right]\ ,$$

$$b\cong\frac{\alpha_2}{\omega_{\ln}^2}\lambda,\ \text{and}\ d\cong\alpha_4\lambda/\omega_{\ln}\ .$$

Here we think of α_1, α_2, and α_4 as numbers to be fit to results of exact numerical solutions of the full equations (7.1a) to (7.1d) for a large number of known superconductors (tabulated in Table XII). Such a fit is necessary so as to compensate for the errors inevitably made in reducing the exact equations, which are very complicated, to the simple form (7.8). In this way, we obtain for the slope of H_{c2} at $T=T_c$ the final equation

$$|H_{c2}^{di'}(T_c)|=\frac{4(1+\lambda)}{\pi eD}\left[1+5.0\left[\frac{T_c}{\omega_{ln}}\right]-9.3\left[\frac{T_c}{\omega_{ln}}\right]^2\ln\left[\frac{\omega_{ln}}{T_c}\right]\right]. \quad (7.9)$$

For $T_c/\omega_{ln}=0$, we recover the BCS result renormalized by $(1+\lambda)$. Next, we consider the second critical magnetic field at zero temperature, which is given approximately by Eq. (B57) and is

$$\rho^{di}(0)=\frac{\pi T_c}{2e^{\gamma}}(1+\lambda)\left[1+\frac{\pi}{4e^{\gamma}}\frac{\pi T_c}{\lambda}d+\frac{3}{2}\left[\frac{\pi}{4e^{\gamma}}\right]^2\left[\frac{\pi T_c}{\lambda}\right]^2 d^2+\frac{(\pi T_c)^2}{\lambda}\left[\frac{4e^{2\gamma}-1}{4e^{2\gamma}}a(T_c)-\tfrac{4}{3}b\right]\right] \quad (7.10)$$

with $\gamma\simeq 0.577$ the Euler constant. Substituting for b,d, and $a(T_c)$, as before, we obtain, after fitting to exact data

$$H_{c2}^{di}(0)=\frac{\pi T_c(1+\lambda)}{2e^{\gamma}(eD)}\left[1+3.3\left[\frac{T_c}{\omega_{ln}}\right]-4.8\left[\frac{T_c}{\omega_{ln}}\right]^2\ln\left[\frac{\omega_{ln}}{T_c}\right]\right]. \quad (7.11)$$

The BCS limit results when $T_c/\omega_{ln}=0$ and is renormalized by the $(1+\lambda)$ factor. The reduced critical field at zero temperature is defined by

$$h_{c2}^{di}(0)\equiv\frac{H_{c2}^{di}(0)}{T_c\left|\frac{dH_{c2}^{di}}{dT}\right|_{T_c}}=0.69\left[1-1.5\frac{T_c}{\omega_{ln}}+2.0\left[\frac{T_c}{\omega_{ln}}\right]^2\ln\left[\frac{\omega_{ln}}{0.8T_c}\right]\right], \quad (7.12)$$

TABLE XII. Superconducting properties: upper critical field.

Material	T_c/ω_{ln}	$\mu^*(N=6)$	$h_{c2}(0,0)$	$h_{c2}(0,100)$	$k(0,0)$	$k(0,100)$
Al	0.004	0.000	0.727	0.690	1.26	1.20
V	0.031	0.219	0.725	0.667	1.32	1.21
Ta	0.035	0.119	0.725	0.666	1.32	1.21
Sn	0.038	0.114	0.725	0.662	1.33	1.22
Tl	0.046	0.130	0.726	0.658	1.35	1.22
$Tl_{0.9}Bi_{0.1}$	0.048	0.112	0.727	0.659	1.36	1.23
In	0.050	0.114	0.727	0.657	1.36	1.23
Nb (Butler)	0.057	0.363	0.724	0.648	1.40	1.25
Nb (Arnold)	0.062	0.182	0.728	0.652	1.40	1.25
V_3Si_1	0.070	0.140	0.729	0.651	1.42	1.26
V_3Si (Kihl.)	0.071	0.136	0.727	0.646	1.42	1.26
Nb (Rowell)	0.074	0.116	0.737	0.659	1.42	1.27
Mo	0.076	0.069	0.737	0.659	1.42	1.27
$Pb_{0.4}Tl_{0.6}$	0.095	0.112	0.739	0.647	1.49	1.30
La	0.099	0.039	0.743	0.657	1.47	1.30
V_3Ga	0.103	0.088	0.746	0.658	1.50	1.32
Nb_3Al (2)	0.113	0.080	0.748	0.656	1.52	1.33
Nb_3Ge (2)	0.114	0.231	0.743	0.643	1.58	1.36
$Pb_{0.6}Tl_{0.4}$	0.119	0.122	0.750	0.649	1.57	1.35
Pb	0.128	0.139	0.756	0.643	1.62	1.38
Nb_3Al (3)	0.129	0.219	0.760	0.664	1.59	1.39
$Pb_{0.8}Tl_{0.2}$	0.136	0.118	0.760	0.652	1.62	1.39
Hg	0.146	0.123	0.791	0.690	1.62	1.41
Nb_3Sn	0.146	0.151	0.769	0.670	1.62	1.41
$Pb_{0.9}Bi_{0.1}$	0.152	0.101	0.777	0.661	1.68	1.43
Nb_3Al (1)	0.156	0.124	0.777	0.679	1.63	1.42
Nb_3Ge (1)	0.160	0.085	0.774	0.679	1.62	1.42
$Pb_{0.8}Bi_{0.2}$	0.172	0.108	0.796	0.679	1.72	1.47
$Pb_{0.7}Bi_{0.3}$	0.182	0.105	0.813	0.691	1.77	1.50
$Pb_{0.65}Bi_{0.35}$	0.200	0.087	0.827	0.709	1.79	1.53
$Pb_{0.5}Bi_{0.5}$	0.320	0.133	0.800	0.793	1.60	1.59
Ga	0.243	0.171	0.763	0.745	1.50	1.46
$Pb_{0.75}Bi_{0.25}$	0.288	0.132	0.803	0.774	1.62	1.57
Bi	0.320	0.089	0.762	0.767	1.51	1.52

where the numerical coefficients have been refitted to the data rather than obtained directly from the values quoted in (7.9) and (7.11). This increased the accuracy of the fit for $h_{c2}^{di}(0)$ to the exact numerical results obtained from the full equation (7.6) for a large number of real superconductors for which the spectral density is known. The data (solid dots) and our fit (solid line) are shown in Fig. 83 (see Table XII). We see that the fit is not very good and that no single curve will describe all the data. In fact, the dotted curve given by

$$h_{c2}^{di}(0)=0.69\left[1-\frac{T_c}{\omega_{ln}}-3.2\left[\frac{T_c}{\omega_{ln}}\right]^2\ln\left[\frac{\omega_{ln}}{30T_c}\right]\right] \tag{7.13}$$

is different from (7.12) and represents an almost equally good fit. To get really accurate values of $h_{c2}^{di}(0)$ it is clear that full numerical calculations based on (7.6) are required. The differences from BCS are, however, never large, and the derived formulas (7.12) and (7.13) do give the general trend observed in Fig. 83.

For the clean limit near T_c Eq. (B62) gives

$$T_c|H_{c2}^{cl'}(T_c)|=\frac{24}{7\zeta(3)}\frac{(\pi T_c)^2}{ev_F^2}(1+\lambda)^2\left\{1+\frac{(\pi T_c)^2}{\lambda}\left[\left[2+\frac{4}{7\zeta(3)}\right]a(T_c)-\tfrac{8}{3}b\right]\right\}, \tag{7.14}$$

which can be put in the form

$$T_c|H_{c2}^{cl'}(T_c)|=\frac{24}{7\zeta(3)}\frac{(\pi T_c)^2}{(ev_F^2)}(1+\lambda)^2\left[1+1.8\left[\frac{T_c}{\omega_{ln}}\right]-1.1\left[\frac{T_c}{\omega_{ln}}\right]^2\ln\left[\frac{\omega_{ln}}{0.05T_c}\right]\right] \tag{7.15}$$

where, to get a good fit to the numerical data for the many materials considered, it was necessary to introduce, on a purely phenomenological basis, the additional linear term of weight $1.8T_c/\omega_{ln}$. Such a formula was first derived by Masharov (1974a, 1974b), who obtained, however, very different values for the numerical coefficients, and the characteristic boson energy entering his work was not well defined. Here it is the Allen-Dynes characteristic value ω_{ln}.

At zero temperature Eq. (B65) applies, and we have

$$\alpha(0)=\left[\frac{\pi}{2}\right]^2 e^{-\gamma+2}T_c^2(1+\lambda)^2\left[1+\frac{\pi^2}{2}e^{-\gamma}T_c\frac{d}{\lambda}+\frac{\pi^2}{4}e^{-2\gamma}\left[\pi T_c\frac{d}{\lambda}\right]^2+\frac{2(\pi T_c)^2}{\lambda}\left\{\left[1-\frac{e^{-2\gamma}}{4}\right]a(T_c)-\frac{4}{3}b\right\}\right], \tag{7.16}$$

which, after fitting to data, takes on the form

$$H_{c2}^{cl}(0)=\left[\frac{\pi}{2}\right]^2 e^{-\gamma+2}\frac{2T_c^2(1+\lambda)^2}{(ev_F^2)}\left[1+1.44\left[\frac{T_c}{\omega_{ln}}\right]+a_7\left[\frac{T_c}{\omega_{ln}}\right]^2\ln\left[\frac{\omega_{ln}}{b_4T_c}\right]\right] \tag{7.17}$$

where the coefficient a_7 is nearly zero, so b_4 is irrelevant. From Eqs. (7.15) and (7.17) and a new fit to the data for $h_{c2}^{cl}(0)$, we obtain

$$h_{c2}^{cl}(0)=0.727\left[1-2.7\left[\frac{T_c}{\omega_{ln}}\right]^2\ln\left[\frac{\omega_{ln}}{20T_c}\right]\right], \tag{7.18}$$

where no linear term is needed. The fit for $h_{c2}^{cl}(0)$ is shown in Fig. 84 and is seen to be quite good. Formula (7.18) is almost quantitative in giving $h_{c2}^{cl}(0)$ for all the systems computed here (solid dots). Such a formula can therefore be used with confidence in analysis of data.

F. Ginzburg-Landau parameter

The Ginzburg-Landau parameter $\kappa_1(T,t^+)$ for temperature T and impurity concentration described by t^+ is related to H_{c2} and to the thermodynamic critical field H_c. The familiar formula is

$$\kappa_1(T,t^+)=\frac{1}{\sqrt{2}}\frac{H_{c2}(T,t^+)}{H_c(T)}. \tag{7.19}$$

We note that the thermodynamic critical field does not depend explicitly on t^+ for an isotropic superconductor. $H_c(T)$ has been computed at $T=0$ and at $T=T_c$ in Sec. V, and simple formulas of the same form as those derived here have been obtained so that the similar forms also apply to κ_1.

In Fig. 85, we show our results for $k(T=0,\ t^+=100.0$ meV) obtained for many materials (solid dots) through complete numerical evaluation of (7.1). Also shown is our fit (solid line), which is described by the formula

$$k(0,100)=1.2\left[1+2.3\left[\frac{T_c}{\omega_{ln}}\right]^2\ln\left[\frac{\omega_{ln}}{0.2T_c}\right]\right]. \tag{7.20}$$

Here $k(T,t^+)\equiv\kappa_1(T,t^+)/\kappa_1(T_c,t^+)$. The fit is satisfactory. In particular, the only odd point is for Ga, which is amorphous. It clearly follows a different law than the one indicated in Eq. (7.20).

In Fig. 86 we show additional results for the Ginzburg-Landau parameter at zero temperature, but now in the clean limit. The solid curve is given by

$$k(0,0)=1.26\left[1+12\left[\frac{T_c}{\omega_{\ln}}\right]^2\ln\left[\frac{\omega_{\ln}}{2T_c}\right]\right] \tag{7.21}$$

and fits the data on real materials (solid dots) reasonably well, although there are some fluctuations off the curve. The overall trend is, however, well captured by our two-parameter fit (7.21).

The various approximate relations derived here and in the previous work on thermodynamic properties imply that, to a good approximation, specific relationships exist in Eliashberg theory between the various quantities considered. For example, in Sec. IV, we have already seen that the ratio of the zero-temperature gap edge to the critical temperature is given by [Eq. (4.1)]

$$\frac{2\Delta_0}{k_BT_c}=3.53\left[1+12.5\left[\frac{T_c}{\omega_{\ln}}\right]^2\ln\left[\frac{\omega_{\ln}}{2T_c}\right]\right]. \tag{7.22}$$

Comparison of Eqs. (7.21) and (7.22) leads to the relationship

$$\frac{2\Delta_0}{k_BT_c}=2.9k(0,0)-0.13 \tag{7.23}$$

between $k(0,0)$ and $2\Delta_0/k_BT_c$. The fit of the numerical data on real materials to this law is shown in Fig. 87. The agreement is very good. Many other such relationships are implied although they are, in general, somewhat more complicated and will not be exhibited explicitly.

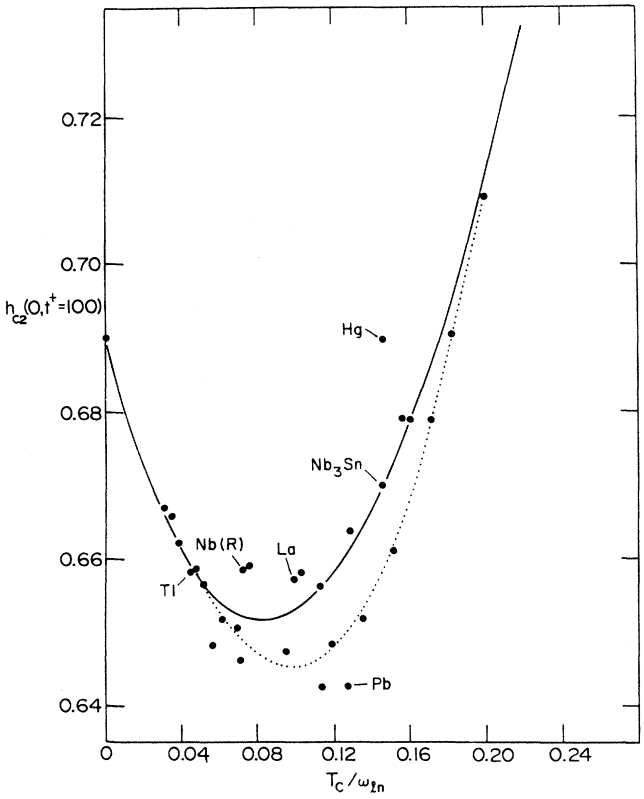

FIG. 83. Reduced quantity $h_{c2}^{\rm di}(0)\cong h_{c2}(0,t^+=100\ \text{meV})$ vs $T_c/\omega_{\ln}$. In increasing order of $T_c/\omega_{\ln}$, the solid dots correspond to the systems for Al, V, Ta, Sn, Tl, $Tl_{0.9}Bi_{0.1}$, In, Nb (Butler), Nb (Arnold), V_3Si (1), V_3Si (Kihl.), Nb (Rowell), Mo, $Pb_{0.4}Tl_{0.6}$, La, V_3Ga, Nb_3Al (2), Nb_3Ge (2) $Pb_{0.6}Tl_{0.4}$, Pb, Nb_3Al (3), $Pb_{0.8}Tl_{0.2}$, Hg, Nb_3Sn, $Pb_{0.9}Bi_{0.1}$, $Nb_3Al(1)$, $Nb_3Ge(1)$, $Pb_{0.8}Bi_{0.2}$, $Pb_{0.7}Bi_{0.3}$, and $Pb_{0.65}Bi_{0.35}$. See Table XII for details. Two curves are drawn: The solid one corresponds to $h_{c2}^{\rm di}(0)=0.69)$ $[1-1.5\,T_c/\omega_{\ln}+2.0(T_c/\omega_{\ln})^2\ln(\omega_{\ln}/0.8T_c)]$. The dotted curve corresponds to $h_{c2}^{\rm di}(0)=0.69$ $[1-T_c/\omega_{\ln}+3.2(T_c/\omega_{\ln})^2\ln(\omega_{\ln}/30T_c)]$. Note that the corrections from BCS are small. Moreover, the variation in possible parameters used in the fits indicates that the scatter in the data is much too large to be described by a single curve. It is clear, however, that there is a small decrease initially, followed by corrections that are positive with respect to the BCS value.

G. Very strong coupling limit

So far, we have only considered the conventional strong-coupling regime for the upper critical field, which ends around $T_c/\omega_{\ln}\lesssim 0.25$. We next want to consider

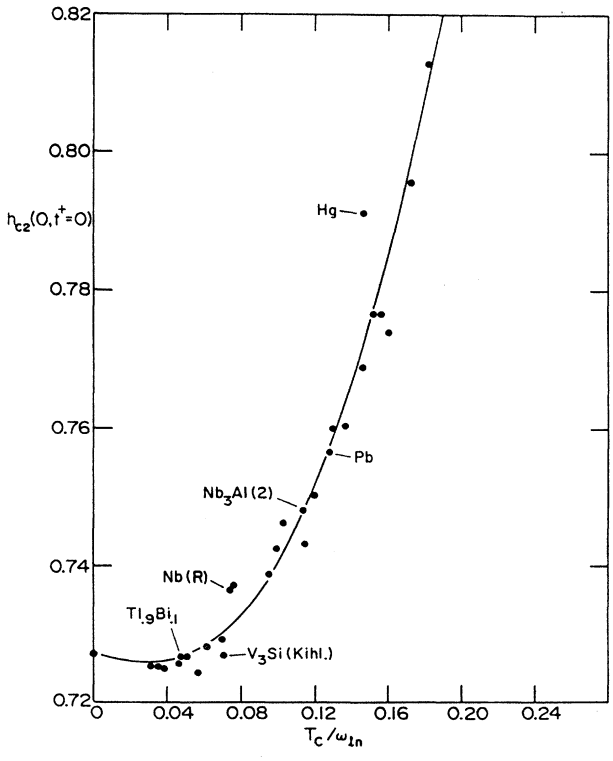

FIG. 84. Reduced ratio $h_{c2}^{\rm cl}(0)$ vs $T_c/\omega_{\ln}$. See caption of Fig. 83 and Table XII for more detailed identification of materials (solid dots). The curve corresponds to $h_{c2}^{\rm cl}(0)=0.727[1-2.7(T_c/\omega_{\ln})^2\ln(\omega_{\ln}/20T_c)]$. There is a very tiny initial decrease from BCS as $T_c/\omega_{\ln}$ is increased above 0.

the very strong coupling region defined by larger values of the strong-coupling index $T_c/\omega_{\ln}$. We start by defining a strong-coupling correction factor for $H_{c2}(T)$ by Marsiglio and Carbotte (1987a, 1988b),

$$H_{c2}(T,t^+)\equiv\eta_{H_{c2}}(T,t^+)H_{c2}^{\rm BCS}(T,t^+)\ , \tag{7.24}$$

where the impurity parameter t^+ has been made explicit. We are interested first in $\eta_{H_{c2}}(T,t^+)$ at $T=0$ and $T=T_c$ and for $t^+=0$ (clean limit) and t^+ equal to some high impurity concentration (dirty limit). It is sufficient to take $t^+=100.0$ meV. Results for $\eta_{H_{c2}}$ are given in Fig. 88 as a function of coupling strength $T_c/\omega_{\ln}$ for two different base spectra, namely, La-Sr-Cu-O and Pb. Figure 88(a) applies to a La-Sr-Cu-O spectrum and shows $\eta_{H_{c2}}(T,t^+)$ for $T=T_c$ and $T=0$ and $t^+=0.0$ in one case (clean limit) and $t^+=100.0$ meV in the other (dirty limit). The differences between these two cases are not large, particularly for $\eta_{H_{c2}}$ at T_c. We note, also, that because $\eta_{H_{c2}}$ measures deviations from BCS, which corresponds to $T_c/\omega_{\ln}\to 0$, the correction factor $\eta_{H_{c2}}$ will tend towards 1 in this limit for any temperature or impurity concentration. As $T_c/\omega_{\ln}$ increases, $\eta_{H_{c2}}$ first increases, and for small values of $T_c/\omega_{\ln}$ a $(T_c/\omega_{\ln})^2\ln(\omega_{\ln}/bT_c)$ expansion applies with b a constant. This is the conventional strong-coupling regime previously described. Most known electron-phonon superconductors fall in this range. As $T_c/\omega_{\ln}$ goes beyond roughly 0.25, the situation changes. The coefficient $\eta_{H_{c2}}$ first exhibits a maximum and then starts to drop. By the time $T_c/\omega_{\ln}$ is of order 1, the value of $\eta_{H_{c2}}$ has dropped to well below 1; this surprising result could not have been guessed from an extrapolation of what is known in the conventional case for which $\eta_{H_{c2}}$ is always greater than 1 [Marsiglio and Carbotte (1987a)]. Thus the very strong coupling regime is distinct from the conventional regime and also from BCS.

To be sure that the results of Fig. 88(a) are not strongly dependent on the base spectrum used, we have carried out additional calculations using the Pb $\alpha^2F(\omega)$ as the base electron-phonon spectral density instead of that for $La_{1.85}Sr_{0.15}CuO_4$. These additional results are presented in Fig. 88(b). It is clear that the differences between the Pb-based results and those based on $La_{1.85}Sr_{0.15}CuO_4$ are

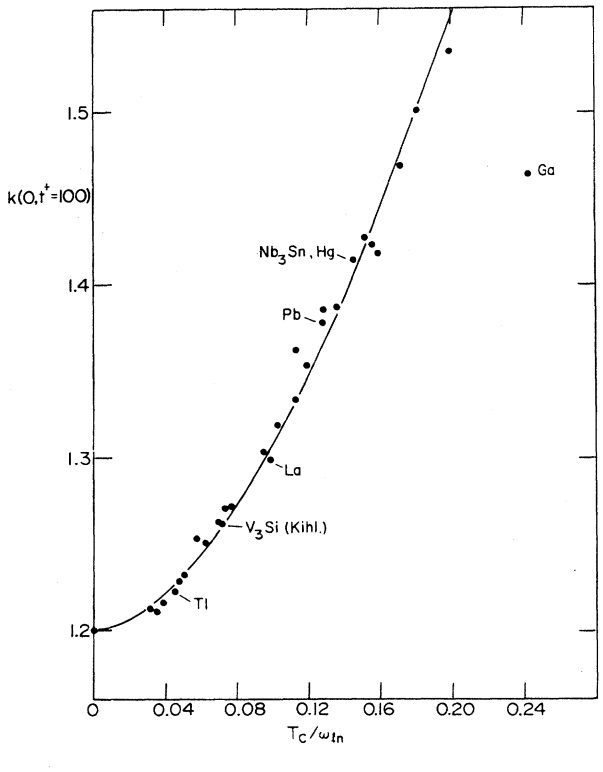

FIG. 85. Ratio $k(0,t^+=100$ meV) vs $T_c/\omega_{\ln}$. See caption to Fig. 83 and Table XII for detailed identification of materials (solid dots). The curve corresponds to $k(0,100)=1.2$ $[1+2.3(T_c/\omega_{\ln})^2\ln(\omega_{\ln}/0.2T_c)]$. A linear term is not needed for a good fit.

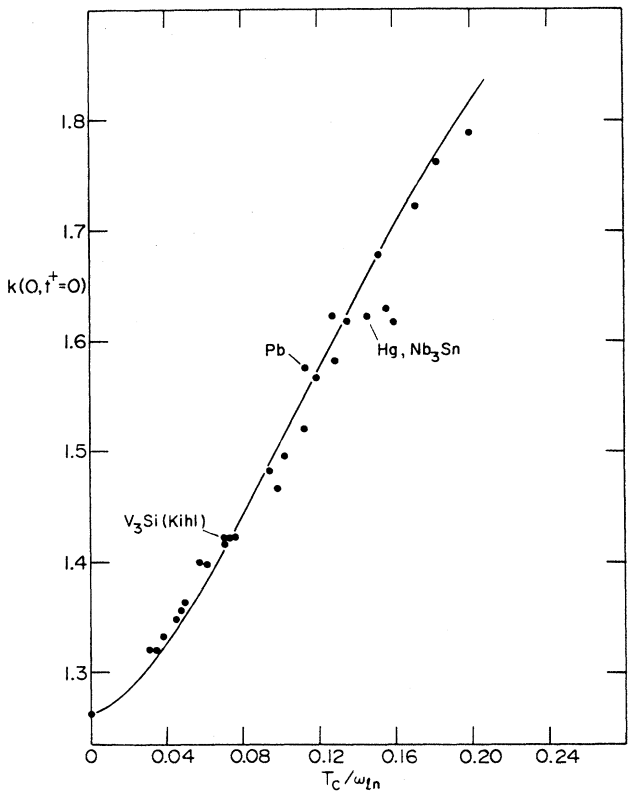

FIG. 86. Ratio $k(0,t^+=0$ meV) vs $T_c/\omega_{\ln}$. See caption to Fig. 83 and Table XII for detailed identification of materials (solid dots). The curve corresponds to $k(0,0)=1.26$ $[1+12(T_c/\omega_{\ln})^2\ln(\omega_{\ln}/2T_c)]$.

never great. While acknowledging that there are indeed small quantitative differences that come from the very different shapes of the two base spectra, we can safely conclude that shape is not an essential feature in determining the qualitative behavior of $\eta_{H_{c2}}$ as a function of $T_c/\omega_{\ln}$. Thus we expect that any reasonably shaped spectral density that corresponds to a value $T_c/\omega_{\ln}\cong 1$ will give a value of $\eta_{H_{c2}}$, of order 0.2.

In Fig. 89 we show results for the reduced temperature ($t\equiv T/T_c$) dependence of the normalized upper critical field $h_{c2}(t,t^+)$ defined by [a generalization of (7.12)]

$$h_{c2}(T,t^+)\equiv\frac{H_{c2}(T,t^+)}{T_c\left|\left[\frac{dH_{c2}(t^+,T)}{dT}\right]_{T_c}\right|}\ . \tag{7.25}$$

The normalization with the slope of H_{c2} at the critical temperature T_c means that h_{c2} itself is independent of the choice of Fermi velocity and therefore depends only on a $\alpha^2F(\omega)$ and the value used for μ^*.

In Fig. 89, we use the clean limit $t^+=0.0$ meV and a delta-function base spectrum $\alpha^2F(\omega)=A\,\delta(\omega-\Omega_E)$ with $\mu^*=0.1$. The results are independent of A, as will be shown later when a scaling theorem is proved. Each curve is labeled by the actual value of Ω_E/T_c used. In all our runs, the critical temperature T_c was set equal to 1.0 meV (11.605 K) and A varied. We note that $h_{c2}(0)$ increases considerably as Ω_E/T_c decreases and that the final few curves acquire an important positive curvature at intermediate values of the reduced temperature t range. This is the distinct signature of the strong-coupling regime.

In Fig. 90, we show results for $h_{c2}(t=0.1)$, which should be close to $h_{c2}(0)$, as a function of T_c/ω_E for both clean (solid curve) and $t^+=100.0$ meV (dotted curve). After a very small initial drop, both curves show an increase through the conventional strong-coupling regime

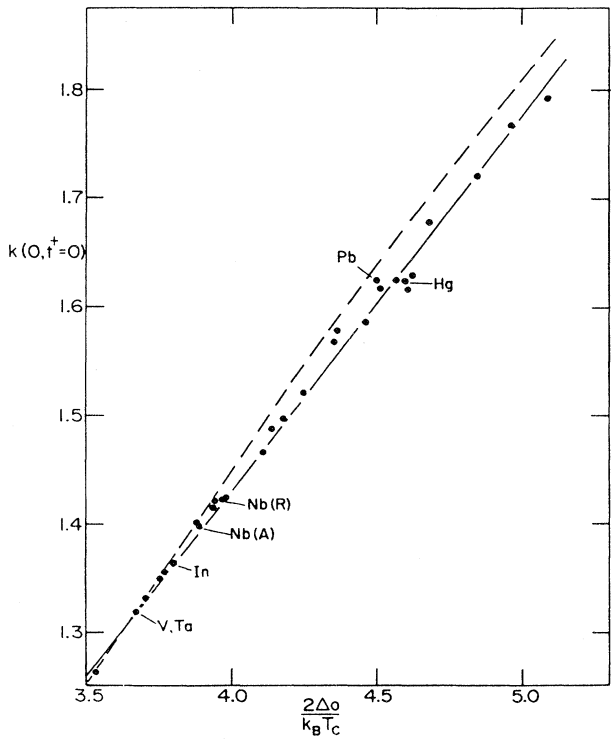

FIG. 87. Ratio $k(0,t^+=0\text{ meV})$ vs $2\Delta_0/k_BT_c$. Equations (7.21) and (7.22) suggest that $2\Delta_0/k_BT_c=2.9k(0,0)-0.13$. This curve is drawn with a solid line and describes the data (solid dots) extremely well. See caption to Fig. 83 and Table XII for full identification of the materials used (solid dots).

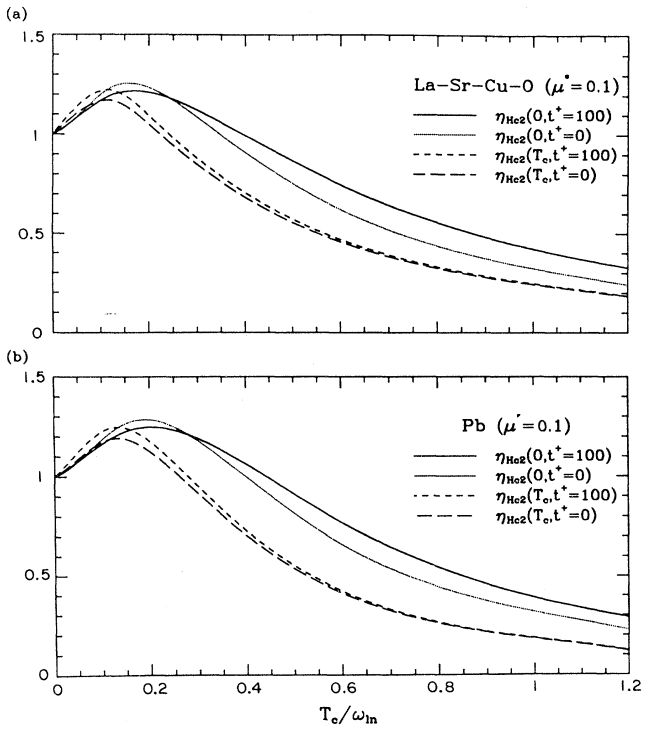

FIG. 88. (a) The strong-coupling correction parameter $\eta_{H_{c2}}(T,t^+)$ is displayed for $T=0$ and $T=T_c$ and for $t^+=0$ and 100 meV. We have used the spectrum calculated by Weber (1987a, 1987b) for $La_{1.85}Sr_{0.15}CuO_4$ with $\mu^*=0.1$. T_c was held fixed at 96 K by scaling the spectrum in height, while the abscissa was scaled in order to sweep through the values of $T_c/\omega_{\ln}$ displayed in the figure. All correction parameters display the same qualitative trend. In the conventional strong-coupling regime ($T_c/\omega_{\ln}\lesssim 0.2$), all the corrections are greater than 1, and modest. However, in the very strong coupling regime ($T_c/\omega_{\ln}\approx 1$), the corrections differ substantially from unity and are less than 1. No significant qualitative difference is noticeable between $t^+=0$ meV and $t^+=100$ meV. (b) The same results are displayed as in (a), but for a Pb spectrum. No qualitative change from (a) is observed, indicating that the results noted in (a) are not very model dependent.

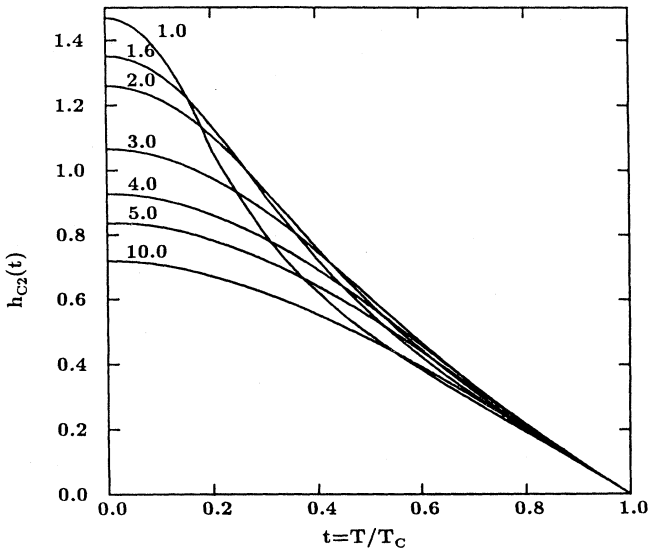

FIG. 89. Reduced temperature (t) variation of $h_{c2}(t)$ for several values of a delta-function base spectra, namely, $\Omega_E/T_c=1.0$, 1.6, 2.0, 3.0, 4.0, 5.0, and 10.0. The curves are for the clean limit, and the BCS value at $t=0$ is 0.73, which falls near our curve for $\Omega_E/T_c=10.0$.

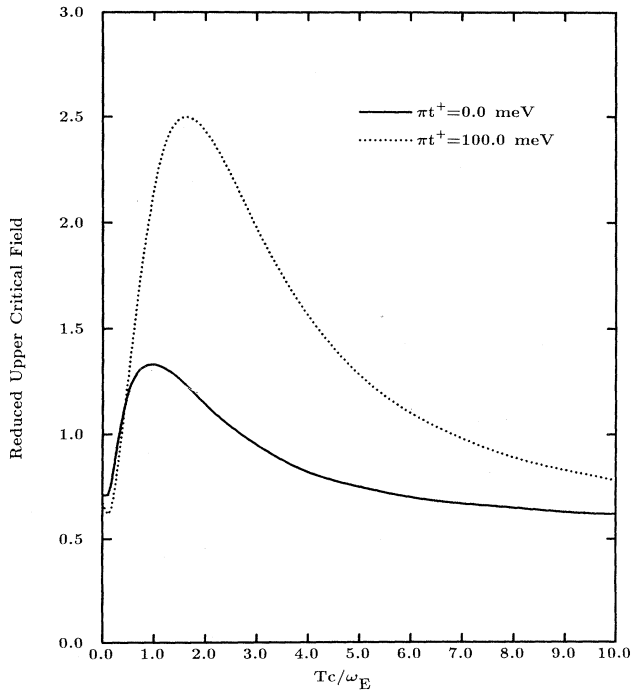

FIG. 90. Reduced upper critical magnetic field at reduced temperature $t=0.1$ as a function of $T_c/\omega_E=0.183\sqrt{\lambda}$ for the clean limit $t^+=0.0$ (solid curve) and $t^+=100.0$ meV (dotted curve).

followed by a maximum, after which the curve drops towards a saturation value, which appears to be about ≈ 0.57 for the clean case. We shall have more to say about this when the asymptotic limit of $h_{c2}(0)$ is studied.

The Ginzburg-Landau parameter $\kappa_1(T,t^+)$ [Marsiglio and Carbotte (1988b)] can also be calculated in the very strong coupling case. We first consider the two limits $T=0$ and $T=T_c$ for $t^+=0$ and $t^+=100$ meV. Results for $\eta_{\kappa_1}(T,t^+)$ are presented in Fig. 91 as a function of $T_c/\omega_{\ln}$. We note first that all curves start at value 1 at $T_c/\omega_{\ln}=0$, which corresponds to BCS theory. As $T_c/\omega_{\ln}$ is increased, both $\eta_{\kappa_1}(0,t^+=0)$, the dotted curve, and $\eta_{\kappa_1}(0,t^+=100$ meV), the solid curve, begin to increase, reaching a maximum before starting to drop towards a value that is slightly above 0.4 and 0.3 at $T_c/\omega_{\ln}=1.2$ for $t^+=100.0$ meV and $t^+=0.0$ meV, respectively. This behavior is the opposite of that found in conventional strong couplers, which all fall in the region before the

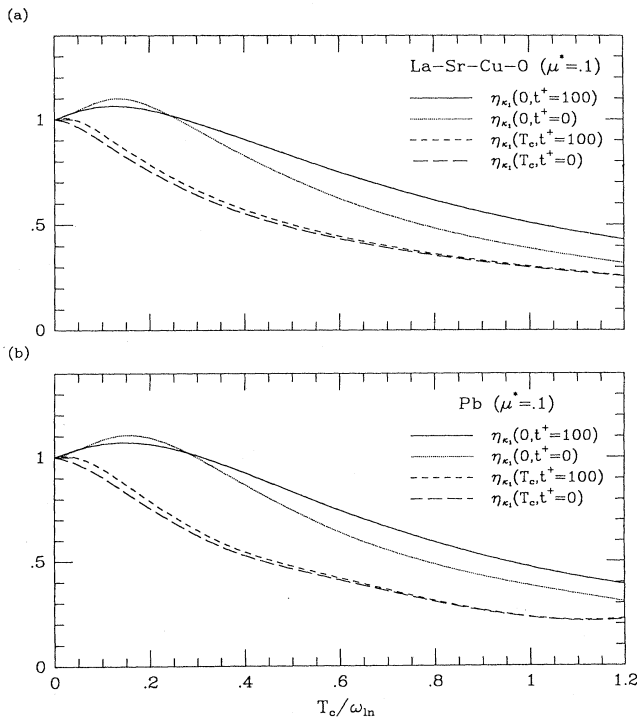

FIG. 91. (a) The strong-coupling parameter $\eta_{\kappa_1}(T,t^+)$ is displayed for $T=0$ and $T=T_c$ for two impurity concentrations $t^+=0$ meV (clean limit) and $t^+=100$ meV (dirty case). The base spectrum used for the electron-phonon spectral density was that for $La_{1.85}Sr_{0.15}CuO_4$ as calculated by Weber. The abscissa in the figure is the parameter $T_c/\omega_{\ln}$ with $\omega_{\ln}$ a characteristic phonon energy first introduced by Allen and Dynes (1975). The conventional strong-coupling regime includes only the first part of the curve for $T_c/\omega_{\ln}\lesssim 0.25$. (b) Same as (a), but here the Pb spectrum is used for the base electron-phonon spectral density of our model.

maximum in the curves of Fig. 91. In contrast to this, the curves for $\eta_{\kappa_1}(T_c,t^+)$ denoted by short and long dashes for $t^+=100.0$ meV and $t^+=0.0$ meV, respectively, are nearly identical, show no maximum, and are both decreased to less than 0.3 at $T_c/\omega_{\ln}=1.2$. The results of Fig. 91 are not very dependent on the shape of the assumed reference spectrum $\alpha^2F(\omega)$, as can be seen when Fig. 91(b) for a Pb base is compared with 91(a), which applies instead for a La-Sr-Cu-O base. The fact that the differences are small gives us confidence in the universality of the qualitative behavior of the curves presented.

Next we consider the parameter $k_1(t,t^+)$ (previously denoted by k), which gives the temperature variation of κ_1 normalized to its value at the critical temperature T_c. Results for the temperature dependence of $k_1(t,t^+=0)$ and $k_1(t,t^+=100)$ are found in Figs. 92(a) and 92(b), respectively. The three systems identified as 1 (solid curve), 2 (dotted curve), and 3 (dashed curve) correspond to $T_c/\omega_{\ln}=1.14$, 0.86, and 0.57, respectively, for a Pb-based spectrum and 1.19, 0.83, and 0.60 for a $La_{1.85}Sr_{0.15}CuO_4$ base. The BCS temperature variation is also shown for comparison and is seen to be completely different from

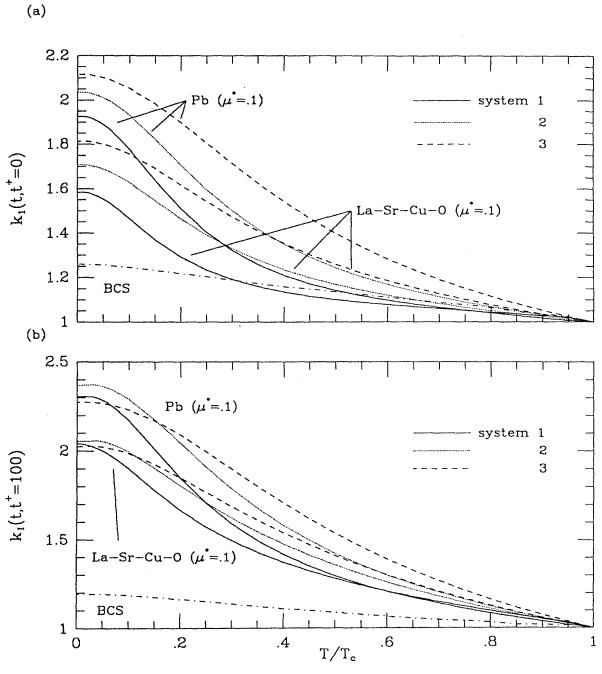

FIG. 92. (a) The reduced quantity $k_1(T,t^+)\equiv\kappa_1(T,t^+)/\kappa_1(T_c,t^+)$ as a function of reduced temperature ($t=T/T_c$) for the clean limit $t^+=0$. We show curves based on the La-Sr-Cu-O and Pb spectra in the very strong coupling limit, which we compare with BCS. For Pb the three systems—1, 2, and 3—correspond, respectively, to $T_c/\omega_{\ln}=1.14$, 0.85, and 0.57. For La-Sr-Cu-O, $T_c/\omega_{\ln}$ equals, instead, 1.19, 0.83, and 0.60, respectively. (b) Same as in Fig. (a), but here $t^+=100$ meV, which corresponds to a reasonably dirty sample.

the very strong coupling case. While the details of the calculated t variation depend somewhat on the base spectrum used, the general trend is roughly the same in the two cases.

H. Asymptotic limits

We next consider asymptotic limits. We start with the dirty-limit case, represented by the superscript "di," for which Eq. (7.6b) applies. It is convenient and conventional to transform Eq. (7.6b) through the change

$$\overline{\Delta}(i\omega_n)\equiv\frac{\tilde{\Delta}(i\omega_n)}{|\tilde{\omega}^0(i\omega_n)|+\rho^{\rm di}} \tag{7.26}$$

which, when substituted into Eq. (7.6b), gives $[\lambda(n-m)\equiv\lambda(i\omega_n-i\omega_m)]$:

$$\overline{\Delta}(i\omega_n)\left[|\omega_n|+\pi T\sum_m\lambda(n-m)\mathrm{sgn}\omega_n\omega_m+\rho^{\rm di}\right]=\pi T\sum_m[\lambda(n-m)-\mu^*]\overline{\Delta}(i\omega_m)\ , \tag{7.27}$$

where use was made of Eq. (7.1b) with the πt^+ term set equal to zero. In Eq. (7.27), the term $n=m$ on the right cancels against the similar term on the left-hand side; hence both sums can be restricted to $m\neq n$ only. This means that the term $\lambda(0)\equiv\lambda$ does not appear in Eq. (7.27). If for the spectral density we take a delta-function model of weight A centered at the Einstein frequency ω_E and define $\overline{B}\equiv B/\sqrt{A\omega_E}$, as before, for any quantity B we arrive at

$$\lambda(m)=\frac{2}{(2\pi\overline{T})^2m^2}\quad[\text{see Eq. (2.27)}] \tag{7.28}$$

for $m\neq0$ and at

$$\frac{\rho^{\rm di}}{\pi T}\overline{\Delta}_n=\sum_{m=1}^{\infty}\left[\lambda(m-n)(1-\delta_{n,m})+\lambda(m+n-1)-\delta_{n,m}\left[2m-1+2\sum_{m'=1}^{m-1}\lambda(m')\right]\right]\overline{\Delta}_m\ , \tag{7.29}$$

where we have set $\mu^*=0$ for convenience. Noting (7.28), we see that Eq. (7.29) makes no reference to material parameters. It will yield a universal material-independent eigenvalue of the form

$$\frac{\rho^{\rm di}}{\pi T}\equiv g(\overline{T})=\frac{eH_{c2}^{\rm di}(T)D}{\pi T}\ , \tag{7.30}$$

where $g(\overline{T})$ is some well-defined universal function of the dimensionless temperature variable $\overline{T}$. In agreement with our previous result of Sec. II, the critical temperature is obtained by setting $g(\overline{T}_c)=0$. This gives $\overline{T}_c=0.2584$ or

$$T_c=0.183\omega_E\sqrt{\lambda} \tag{7.31}$$

[see Eq. 2.29]. From numerical solution of the universal

equation (7.29) for values of $\bar{T}$ below $\bar{T}_c$, we obtain

$$H_{c2}^{di}(T)=\frac{\pi T_c}{eD}k(t)=\frac{0.183\pi}{eD}\omega_E\sqrt{\lambda}\,k(t)\ , \tag{7.32}$$

where $k(t)$ is a universal function of the reduced temperature and is related to $g(\bar{T})$. For t near 1, our numerical work gives

$$H_{c2}^{di}(T)=\frac{2.24\pi T_c}{eD}(1-t)\ , \tag{7.33}$$

which agrees well with the results of Bulaevskii *et al.* [(1988); Bulaevskii and Dolgov (1987a, 1987b)]. Equation (7.32), however, gives results for *any* finite temperature $t>0$, provided the approximation $\omega_E \ll 2\pi T$ is satisfied. Referring to Eq. (7.31), we can transform this condition to read $\sqrt{\lambda}\,t \gg 1$. Instead of plotting the numerical results for $k(t)$, which defines $H_{c2}^{di}(T)$ through (7.32), we have chosen to present instead our results for $h_{c2}^{di}(t)=0.447k(t)$. This is shown as the solid curve in Fig. 93. This curve is really very different from the usual weak-coupling curve for the reduced upper critical field, which has downward curvature. In our case, $h_{c2}^{di}(t)$ is nearly linear over a large range of reduced temperature near $t=1$ and then shows a divergent behavior as $t\to 0$. Strictly speaking, our technique of solution does not permit us to reach the $t=0$ limit, because the condition $\sqrt{\lambda}\,t \gg 1$ must always be met. For $T=0$, Bulaevskii *et al.* (1988) obtain, without proof, the result

$$H_{c2}^{di}(0)=\frac{1.08T_c}{eD}\sqrt{\lambda}=\frac{0.198\omega_E\lambda}{eD} \tag{7.34}$$

and so find that $h_{c2}^{di}(0)=0.45\sqrt{\lambda}$. The λ dependence in (7.34) is certainly consistent with our result that $h_{c2}^{di}(0)\to\infty$ in the limit of infinite λ. Moreover, the result $h_{c2}^{di}(0)=0.45\sqrt{\lambda}$ is confirmed in the numerical work of Schossmann *et al.* (1988), who have calculated $H_{c2}^{di}(0)$ numerically as a function of T_c/ω_E up to a value of about 1.4. Noting that $T_c/\omega_E=0.183\sqrt{\lambda}$, we see that this corresponds to $\sqrt{\lambda}\cong 7.7$, which extends beyond the numerical work of Bulaevskii *et al.* (1988). While it is certainly true that, in this range of λ values, $h_{c2}^{di}(0)$ appears to vary like $\sqrt{\lambda}$ with coefficient ~ 0.43, we may not yet be in the asymptotic limit. Certainly, for any finite impurity concentration, we shall see later that we need to go to much higher values of λ in order to achieve the asymptotic limit.

An approximate analytic form for $H_{c2}(t)$ can be obtained from Eq. (7.29) if we keep a single Matsubara gap, namely, the $m=1$ term. When this is done, we get

$$\rho^{di}\cong\pi T\left[\frac{2}{(2\pi\bar{T})^2}-1\right] \tag{7.35}$$

from which it follows that

$$T_c\cong\frac{1}{2\pi}\omega_E\sqrt{\lambda} \tag{7.36a}$$

and that

$$H_{c2}^{di}(t)\cong\frac{2\pi T_c}{eD}(1-t)\quad\text{for } t\to 1\ ; \tag{7.36b}$$

so,

$$h_{c2}^{di}(t)\cong\frac{1}{2}\left[\frac{1}{t}-t\right]\quad\text{for } t>0\ . \tag{7.36c}$$

This result (dotted curve) is compared with our exact numerical results (solid curve) in Fig. 94. The two curves are surprisingly close. In particular, these both diverge like $1/t$ as $t\to 0$, but with different coefficients.

The arguments used to reduce Eq. (7.1) when πt^+ is finite are similar to those used in the previous section but somewhat different in details. We start by writing

$$|\tilde{\omega}(i\omega_n)|=\pi T\lambda+|\tilde{\omega}_1(i\omega_n)| \tag{7.37}$$

with

$$\tilde{\omega}_1(i\omega_n)=\omega_n+\pi T\sum_{m\neq n}\lambda(n-m)\,\mathrm{sgn}\omega_m+\pi t^+\mathrm{sgn}(\omega_n)\ . \tag{7.38}$$

For $\lambda\to\infty$, we have $\pi T\lambda \gg |\tilde{\omega}_1(i\omega_n)|$ for any finite impurity concentration (πt^+). If it is further assumed that $\pi T\lambda \gg \sqrt{\alpha}$, as will be verified later, the same expansion of the inverse tangent as we used in the previous section can be used with the result that

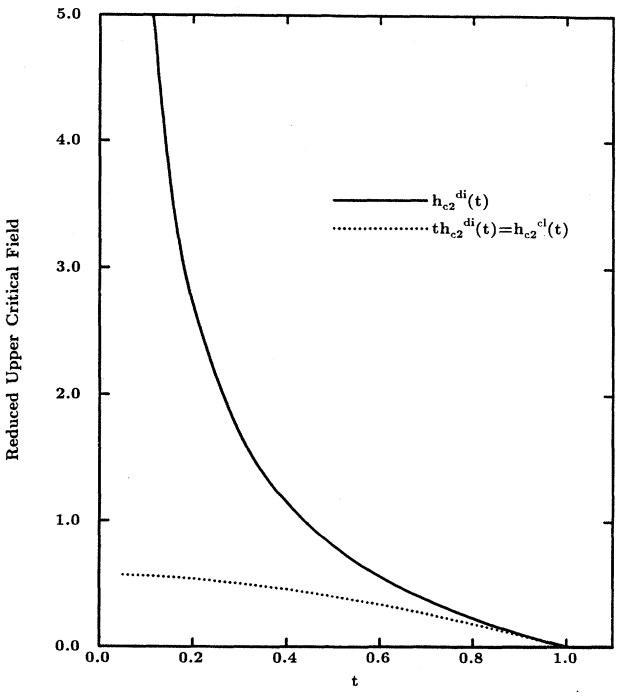

FIG. 93. Asymptotic value ($\lambda\to\infty$) of reduced upper critical field $h_{c2}^{di}(t)$ in the dirty limit (solid line) as a function of reduced temperature for $t>0$. The dotted curve applies to any finite impurity concentration and is related to $h_{c2}^{di}(t)$ by $h_{c2}^{cl}(t)=th_{c2}^{di}(t)$.

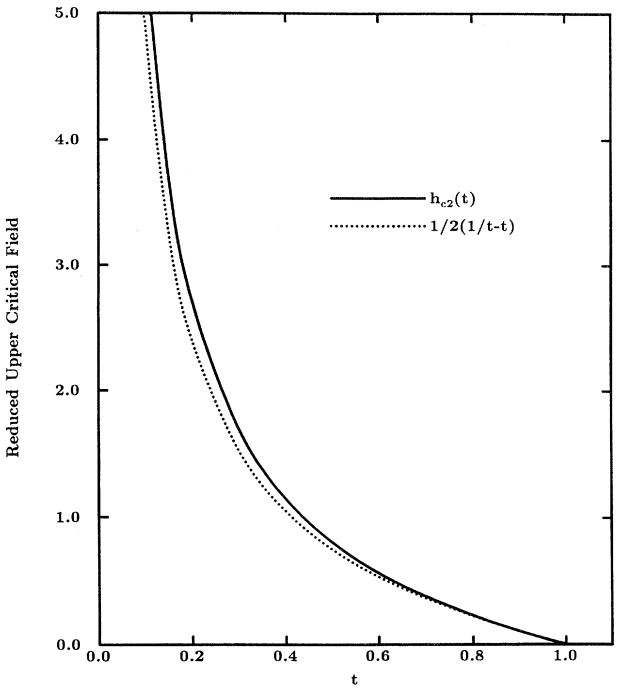

FIG. 94. Reduced upper critical magnetic field $h_{c2}^{di}(t)$ vs reduced temperature t (solid curve) compared with the simple form $\frac{1}{2}(1/t-t)$ (dotted curve).

$$\chi^{-1}(|\tilde{\omega}(i\omega_n)|)-\pi t^+\cong|\tilde{\omega}_0(i\omega_n)|+\frac{1}{3}\frac{\alpha}{\pi T\lambda}\ . \tag{7.39}$$

If we define

$$\rho^{cl}=\frac{1}{3}\frac{\alpha^{cl}}{\pi T\lambda}\ ,$$

where the superscript cl stands for the clean limit, we recover the equation for the dirty limit with the eigenvalue ρ^{di} replaced by ρ^{cl}, from which we immediately conclude that $\rho^{cl}=\rho^{di}$, this means that

$$H_{c2}^{cl}(T)=\frac{6\pi T\lambda}{ev_F^2}eDH_{c2}^{di}(T)\ . \tag{7.40}$$

Substituting (7.32) into (7.40), we find

$$H_{c2}^{cl}(T)=\frac{6\pi^2T_c^2}{ev_F^2}\lambda k(t)t\ , \tag{7.41}$$

so that $H_{c2}^{cl}(T)$ in the $\lambda\to\infty$ limit is determined by the same universal function $k(t)$ previously introduced, except for a numerical coefficient and an extra factor of the reduced temperature t. The impurity content πt^+ has also dropped out. The condition $\pi T\lambda\gg\pi t^+$, which is implied in our derivation, can be rewritten as $\sqrt{\lambda}\,\lambda t\gg t^+/\omega_E$. If we think of taking λ to ∞ by having A fixed and $\omega_E\to 0$, we write $\sqrt{\lambda}\,t\gg t^+/A$, which is always satisfied for any finite t^+ for sufficiently large λ. If, instead, ω_E is fixed and $A\to\infty$, we can again have $\lambda^{3/2}t\gg t^+/\omega_E$ for any fixed value of t^+.

Near $t=1$, i.e., around the critical temperature, we get

$$H_{c2}^{cl}(T)=\frac{13.4\pi^2T_c^2\lambda}{ev_F^2}(1-t)\ , \tag{7.42}$$

which agrees well with the result of Bulaevskii *et al.* (1988), provided we assume they have mistakenly left out a factor of π.

It follows from (7.41) and (7.42) that the clean-limit reduced critical magnetic field is given by

$$h_{c2}^{cl}(t)=th_{c2}^{di}(t)\ . \tag{7.43}$$

Numerical results for $h_{c2}^{cl}(t)$ based on the universal equation (7.29) are shown as the dotted line in Fig. 93. We see that this curve appears to define a well-behaved function of t for small t, so it can safely be extrapolated to $t=0$ to get $h_{c2}^{cl}(0)=0.57$. While we have worked only in the region $\sqrt{\lambda}\,t\gg 1$ and hence $t>0$, we see that the zero-temperature value of $H_{c2}^{cl}(0)$ can be obtained from our extrapolated $h_{c2}^{cl}(0)$ to get

$$H_{c2}^{cl}(0)=\frac{7.64\pi^2T_c^2\lambda}{ev_F^2}\ . \tag{7.44}$$

This result is in serious disagreement with that found by Bulaevskii *et al.* (1988), who get $h_{c2}^{cl}(0)\cong 1.5$ from their numerical work. The problem can easily be traced to the fact that, at $\sqrt{\lambda}\sim 5.5$, which is where these authors stop their calculations, we are, in reality, still far from the asymptotic limit. This is illustrated in Fig. 90 where we showed $h_{c2}(t=0.1)$ as a function of $T_c/\omega_E=0.183\sqrt{\lambda}$. We see that for both the clean limit (solid curve) and for $t^+=100.0$ meV (dotted curve) the curves do not reach their asymptotic limit until beyond $T_c/\omega_E\sim 10$, while Bulaevskii *et al.* stop around 1, which is close to the maximum of the clean-limit curve. This maximum value is almost a factor of 3 larger than the asymptotic value of 0.57. We also note that, while for small λ clean and $t^+=100$ meV curves can differ significantly, the two curves tend towards the same value as λ gets large. This is to be taken as a numerical illustration of the theorem we proved previously, namely, that for $\lambda\to\infty$ the results do not depend on impurity concentration if finite.

We next consider our approximate analytic model solution obtained by using a single-Matsubara-gap approximation. We get from (7.40) and (7.35)

$$H_{c2}^{cl}(T)\cong\frac{6\pi^2\lambda T_c^2}{ev_F^2}(1-t^2)\ , \tag{7.45}$$

from which we find for t near 1

$$H_{c2}^{cl}(t)\cong\frac{12\pi^2\lambda T_c^2}{ev_F^2}(1-t) \tag{7.46}$$

and for $t=0$

$$H_{c2}^{cl}(0)\cong\frac{6\pi^2\lambda T_c^2}{ev_F^2}\ , \tag{7.47}$$

which gives $h_{c2}^{cl}(0)=0.5$ instead of the exact result of 0.57. In addition, our approximate $h_{c2}^{cl}(t)$ is

$$h_{c2}^{cl}(t)\cong\tfrac{1}{2}(1-t^2)\ . \tag{7.48}$$

Comparison of this last result with our exact numerical calculations is given in Fig. 95. We see a remarkable agreement between approximate and exact calculations, except near $t=0$.

Finally, we note that for any t, $H_{c2}^{cl}(t)\propto\lambda^2$ for a fixed ω_E; hence $\sqrt{\alpha}\propto\lambda$. The condition $\pi T\lambda\gg\sqrt{\alpha}$, which we assumed to be satisfied at the beginning of our derivation, can be rewritten (dropping all numerical factors) as $\sqrt{\lambda}\,t\gg1$, a condition which was assumed to hold in our derivation of the dirty-limit critical magnetic field. No further restriction is implied.

I. Functional derivatives

We now work out the functional derivative of $H_{c2}(T)$ with respect to the spectral density $\alpha^2F(\omega)$, since it is useful in many contexts. To proceed, it is convenient to make a transformation from $\tilde{\Delta}(i\omega_n)$ to $\bar{\Delta}_n$ through the equation [Marsiglio, Schossmann, Schachinger, and Carbotte (1987)]

$$\bar{\Delta}_n=\tilde{\Delta}_n(i\omega_n)[\chi^{-1}(\tilde{\omega}(i\omega_n))-\pi t^+]^{-1}\ ; \tag{7.49}$$

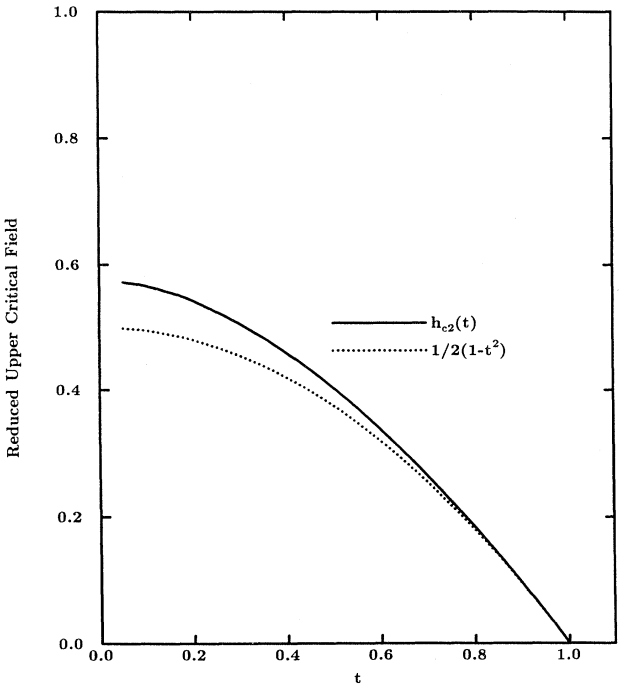

FIG. 95. Asymptotic value ($\lambda\to\infty$) of the reduced upper critical magnetic field $h_{c2}^{cl}(t)$ in the clean limit (solid curve) as a function of reduced temperature (t) compared with the simple form $\frac{1}{2}(1-t^2)$ (dotted curve).

Eq. (7.1) can be rewritten in the form

$$0=\sum_m K_{n,m}\bar{\Delta}_m\ , \tag{7.50}$$

which is a set of linear homogeneous algebraic equations with kernel $K_{n,m}$ given by

$$K_{n,m}=\pi T\left[\lambda(i\omega_n-i\omega_m)-\mu^*-\frac{\delta_{n,m}}{\pi T}[\chi^{-1}(\tilde{\omega}(i\omega_n))-\pi t^+]\right]. \tag{7.51}$$

This kernel depends explicitly on $\alpha^2F(\Omega)$, the temperature T, and the parameter α, which is related to H_{c2} through Eq. (7.1d). Since Eq. (7.51) is symmetric, it follows directly that

$$\frac{\delta\alpha}{\delta\alpha^2F(\Omega)}=-\frac{\sum_{n,m}\bar{\Delta}_n\frac{\delta K_{n,m}}{\delta\alpha^2F(\Omega}\bar{\Delta}_m}{\sum_{n,m}\bar{\Delta}_n\frac{\partial K_{n,m}}{\partial\alpha}\bar{\Delta}_m}\ , \tag{7.52}$$

where $\delta/\delta^2F(\Omega)$ denotes the explicit variation on $\alpha^2F(\Omega)$, keeping α and T constant.

Referring to Eq. (7.51), we can write

$$\frac{\delta K_{n,m}}{\delta\alpha^2F(\Omega)}=\pi T\frac{2\Omega}{\Omega^2+(\omega_n-\omega_m)^2}+\frac{\delta_{n,m}}{\chi^2(\tilde{\omega}(i\omega_n))}\frac{\partial\chi(\tilde{\omega}(i\omega_n))}{\partial\tilde{\omega}(i\omega_n)}\frac{\delta\tilde{\omega}(i\omega_n)}{\delta\alpha^2F(\Omega)} \tag{7.53}$$

with

$$\frac{\partial\chi(\tilde{\omega}(i\omega_n))}{\partial\tilde{\omega}(i\omega_n)}=-\frac{I(\tilde{\omega}(i\omega_n))}{\tilde{\omega}^2(i\omega_n)}\mathrm{sgn}\omega_n\ , \tag{7.54}$$

where we have defined an integral function (related to the exponential integral)

$$I(\tilde{\omega}(i\omega_n))=\int_0^\infty dx\frac{e^{-x}}{1+\alpha x/\tilde{\omega}^2(i\omega_n)} \tag{7.55}$$

in terms of which we can rewrite (7.53) in the form

$$\frac{\delta K_{n,m}}{\delta\alpha^2F(\Omega)}=\pi T\left[\frac{2\Omega}{\Omega^2+(\omega_n-\omega_m)^2}-\frac{\delta_{n,m}I(\tilde{\omega}(i\omega_n))}{\chi^2(\tilde{\omega}(i\omega_n))\tilde{\omega}^2(i\omega_n)}\times\sum_{m'}\frac{2\Omega\,\mathrm{sgn}\omega_m\omega_{m'}}{\Omega^2+(\omega_n-\omega_{m'})^2}\right]. \tag{7.56}$$

We also need to work out the change in $K_{n,m}$ with α,

which is

$$\frac{\partial K_{n,m}}{\partial \alpha}=\frac{\delta_{n,m}}{2\alpha\chi(\tilde{\omega}(i\omega_n))}\left[\frac{I(\tilde{\omega}(i\omega_n))}{\tilde{\omega}(i\omega_n)\chi(\tilde{\omega}(i\omega_n))}-1\right]. \tag{7.57}$$

Everything is now explicit, and formula (7.52) can be evaluated from the solutions to Eqs. (7.1a)–(7.1c).

In Fig. 96, we show our results for $T_c\delta H_{c2}(T)/\delta\alpha^2F(\Omega)$ in the case of pure Nb at various values of the reduced temperature $t=T/T_c$. The horizontal scale is phonon energy in units of T_c, namely, ω/T_c. We note that at very low energies the curve shows a sharp and steep rise toward infinity. This can be interpreted to mean that very low frequency phonons act similarly to ordinary impurities, leading to an increase in the upper critical field $H_{c2}(T)$. This feature is absent in the dirty-limit theory of Rainer and Bergmann. [For work including Pauli limiting see Schossmann, Schachinger, and Carbotte (1987).]

Often one prefers to work with a normalized critical field $h_{c2}(t)$ rather than with $H_{c2}(T)$. By convention, H_{c2} is normalized to T_c times the absolute slope of H_{c2} at T_c and is written in terms of the reduced temperature $t=T/T_c$.

Functional derivatives can be taken at constant absolute temperature T or at constant reduced temperature $t=T/T_c$. These are not the same but are related. Here we wish to keep "t" constant. We note first that [using the notation $\delta Q\equiv(T_c/Q)(\delta Q/\delta\alpha^2F)$, where $\delta/\delta\alpha^2F$ denotes that t is kept constant]

$$\delta h_{c2}(t)=\delta H_{c2}(t)-\delta\left[\left.\frac{dH_{c2}(T)}{dT}\right|_{T_c}\right]-\delta T_c\ . \tag{7.58}$$

To evaluate (7.58) requires a knowledge of the functional derivative of the slope of $H_{c2}(T)$ at T_c which is related to the temperature derivative of the functional derivative of $H_{c2}(T)$ given by Eq. (7.52). Thus we can write

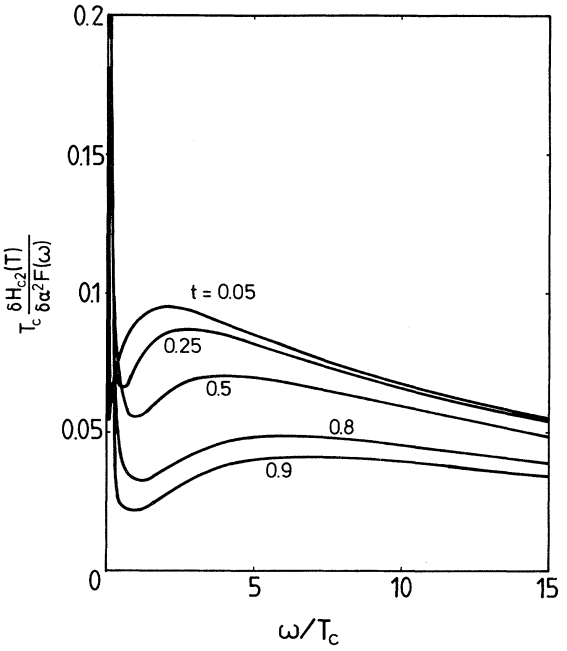

FIG. 96. Functional derivative of the upper critical magnetic field $H_{c2}(T)$ with respect to $\alpha^2F(\Omega)$ (multiplied by T_c) for five different reduced temperatures, $t=0.05$, 0.25, 0.5, 0.8, and 0.9. The plots are for the clean limit ($t^+=0$) and apply to Nb. The phonon frequency (ω) on the horizontal axis is normalized to T_c. Plots for other materials are qualitatively similar. Note the sharp rise at low frequencies preceded by a substantial dip, features that are not found in the dirty limit.

$$\frac{\delta\left[\left.\frac{dH_{c2}(T)}{dT}\right|_{T_c}\right]}{\delta\alpha^2F(\Omega)}=\left.\frac{d^2H_{c2}(T)}{dT^2}\right|_{T_c}\frac{\delta T_c}{\delta\alpha^2F(\Omega)}+\frac{\delta}{\delta\alpha^2F(\Omega)}\left[\left.\frac{dH_{c2}(T)}{dT}\right|_{T_c}\right]. \tag{7.59}$$

We also have

$$\frac{\delta H_{c2}(T)}{\delta\alpha^2F(\Omega)}=\frac{\delta H_{c2}(T)}{\delta\alpha^2F(\Omega)}+\frac{dH_{c2}(T)}{dT}\frac{T}{T_c}\frac{\delta T_c}{\delta\alpha^2F(\Omega)}\ . \tag{7.60}$$

Combining (7.59) and (7.60) with (7.58) leads to the final equation

$$\frac{T_c}{h_{c2}(t)}\frac{\delta h_{c2}(t)}{\delta\alpha^2F(\Omega)}=\frac{T_c}{H_{c2}(t)}\frac{\delta H_{c2}(T)}{\delta\alpha^2F(\Omega)}+\frac{\delta T_c}{\delta\alpha^2F(\Omega)}\left[\frac{T}{H_{c2}(T)}\frac{dH_{c2}(T)}{dT}-\frac{T_c}{\left.\frac{dH_{c2}(T)}{dT}\right|_{T_c}}\left.\frac{d^2H_{c2}(T)}{dT^2}\right|_{T_c}-1\right]$$
$$-\frac{T_c}{\left.\frac{dH_{c2}(T)}{dT}\right|_{T_c}}\left[\frac{d}{dT}\left[\frac{\delta H_{c2}(T)}{\delta\alpha^2F(\Omega)}\right]\right]_{T_c}. \tag{7.61}$$

In their paper, Marsiglio, Schossmann, Schachinger, and Carbotte (1987) also give extensive results for functional derivatives of H_{c2} within the $\lambda^{\theta\theta}$ model and compare with exact results. The equations obtained are rather long. The reader is referred to the original paper for details.

In Fig. 97 we show results for the functional derivative of the reduced critical field $h_{c2}(t)$ at several values of the reduced temperature t in the pure limit for the case of Nb. All curves are small at the highest frequencies considered and exhibit a very broad and large maximum at lower energies before falling through zero and becoming very large and negative, a feature that is missing in the dirty limit. As the temperature is increased, the low-energy node moves towards higher frequencies and the amplitude of the maximum in the functional derivative is suppressed. We conclude from these features that low-frequency phonons always reduce the normalized critical field $h_{ct}(t)$, while phonons between roughly $\omega=2T_c$ and $8T_c$ increase its value.

In Fig. 98, we show results for the functional deriva-

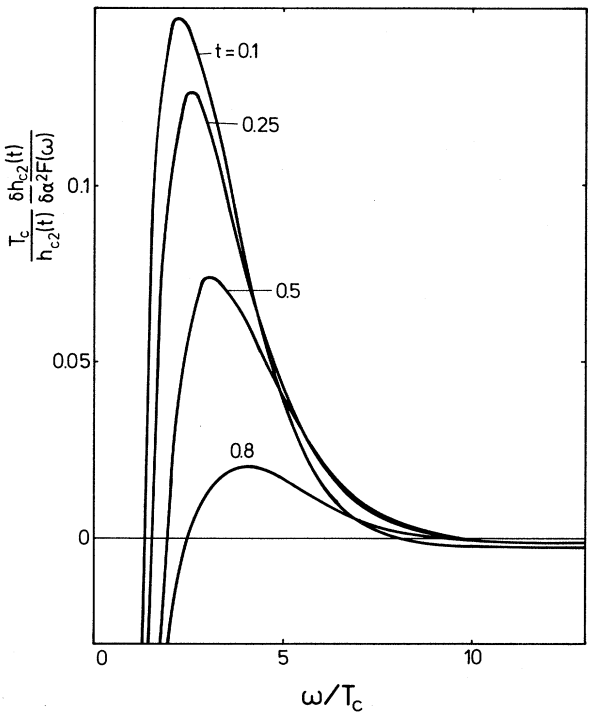

FIG. 97. Normalized functional derivative $[T_c/h_{c2}(t)]$ $\times[\delta h_{c2}(t)/\delta\alpha^2F(\omega)]$ of the reduced critical field $h_{c2}(t)=H_{c2}(t)/|T_c[dH_{c2}(T)/dT]_{T_c}|$ for various reduced-temperature values $t=0.1$, 0.25, 0.5, and 0.8 in the pure limit $t^+=0$ for Nb. The horizontal scale is phonon frequency (ω) normalized to T_c. Note the attenuation of the peak as the temperature is increased. It shifts to slightly higher energy, as does the node at lower ω, after which the functional derivative decreases sharply toward $-\infty$.

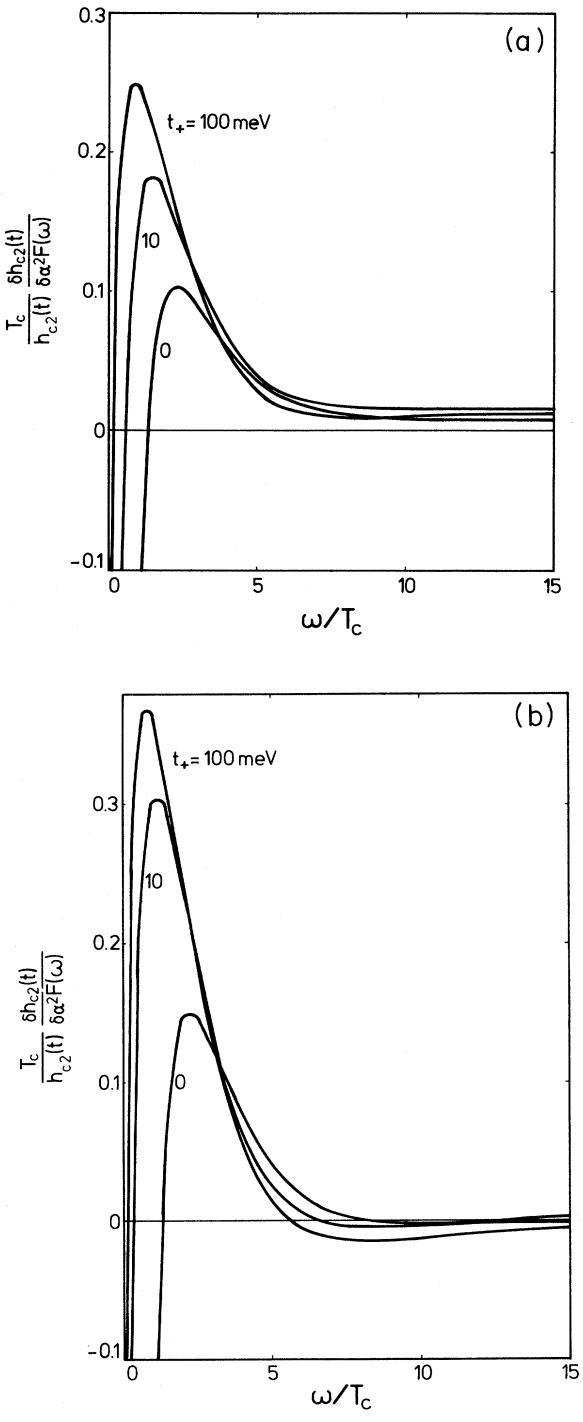

FIG. 98. (a) Normalized functional derivative $[T_c/h_{c2}(t)]$ $\times[\delta h_{c2}(t)/\delta\alpha^2F(\omega)]$ of the reduced critical field $h_{c2}(t)=H_{c2}(T)/|T_c[dH_{c2}(T)/dT]_{T_c}|$ for various impurity concentrations $t^+=0.0$, 10.0, and 100.0 meV at the reduced temperature $t=0.05$ for Nb_3Sn. The horizontal scale is the phonon energy (ω) normalized to T_c. Note the increase in the size of the peak as t^+ increases, as well as the shift of the low-frequency node toward $\omega=0$. In the extreme dirty limit of Rainer and Bergmann the curve goes to zero from above at $\omega=0$. (b) Same as (a), but for Nb.

tive of $h_{c2}(t)$ as a function of impurity concentration for one low value of $t=0.05$. Figures 98(a) and 98(b) apply to Nb_3Sn and Nb, respectively. We note that, particularly at high phonon energies, the functional derivatives are base dependent. For Nb_3Sn they remain positive, while for Nb they can sometimes be negative. Both sets of curves exhibit large maxima at intermediate frequencies before they pass through zero and fall toward $-\infty$ at the lowest frequencies considered. As the impurity concentration is increased, the zero moves toward lower energies so that all low-energy phonons would increase $h_{c2}(t)$ $(t=0.05)$ in the very dirty limit considered by Bergmann and Rainer. Furthermore, the prominent maximum in the curves becomes larger with increasing t^+, indicating that phonon effects are stronger in this region in the dirty limit than they are in the clean limit.

J. Optimum spectrum

We now turn to the problem of optimum spectrum for H_{c2} and related quantities. We will be interested in optimum spectrum for $\eta_{H_{c2}}(T,t^+)$ in the clean and dirty limit for $T=0$ and $T=T_c$. From (7.24), which defines $\eta_{H_{c2}}$, we find for $T=0$

$$\delta\eta_{H_{c2}}(0,t^+)=\delta H_{c2}(0,t^+)-\delta H_{c2}^{\rm BCS}(0,t^+)\ , \tag{7.62}$$

where the first functional derivative is known from our previous work and the second can be obtained by differentiation of (7.17) with $T_c/\omega_{\ln}=0$ in the clean limit and (7.11) in the dirty limit. Such a procedure gives [Akis *et al.* (1988)]

$$\delta H_{c2}^{\rm BCS}(0,t^+=0)=2\delta T_c+2\delta(1+\lambda)\ , \tag{7.63}$$

$$\delta H_{c2}^{\rm BCS}(0,t^+\to\infty)=\delta T_c+\delta(1+\lambda)\ , \tag{7.64}$$

with

$$\delta(1+\lambda)=\frac{T_c}{1+\lambda}\frac{2}{\omega}\ . \tag{7.65}$$

For $T=T_c$, we get

$$\delta\eta_{H_{c2}}(T_c,t^+)=\delta H'_{c2}(T_c,t^+)-\delta H_{c2}^{\prime\rm BCS}(T_c,t^+)\ . \tag{7.66}$$

Again, the first functional derivative is known from our previous work, and the second can be calculated from (7.15) and (7.9) in the clean and dirty limit, respectively, to get

$$\delta H_{c2}^{\prime\rm BCS}(T_c,t^+=0)=\delta T_c+2\delta(1+\lambda) \tag{7.67}$$

and

$$\delta H_{c2}^{\prime\rm BCS}(T_c,t^+\to\infty)=\delta(1+\lambda)\ . \tag{7.68}$$

In Figs. 99 and 100 we plot $\delta\eta_{H_{c2}}(0,0)$ and $\delta\eta_{H_{c2}}(T_c,t^+=500\ \text{meV})$, respectively, as a function of ω/T_c for three different base delta functions as labeled in the caption. An examination of Fig. 88 would lead us to believe that $\eta_{H_{c2}}$ will exhibit a maximum at some energy around $T_c/\omega_{\ln}\cong 0.2$ or $\omega_{\ln}/T_c\sim 5$. This is confirmed by our functional derivative plots. We find, for a base spectrum with $\omega_E/T_c=4.8$ in the case of $H(0,0)$ and 6.7 for $H_{c2}(T_c,t^+=500)$, that the corresponding functional derivative (solid $c2$ curve) is indeed negative everywhere and exactly zero right at the base Einstein frequency, indicating a local maximum has been achieved. The values

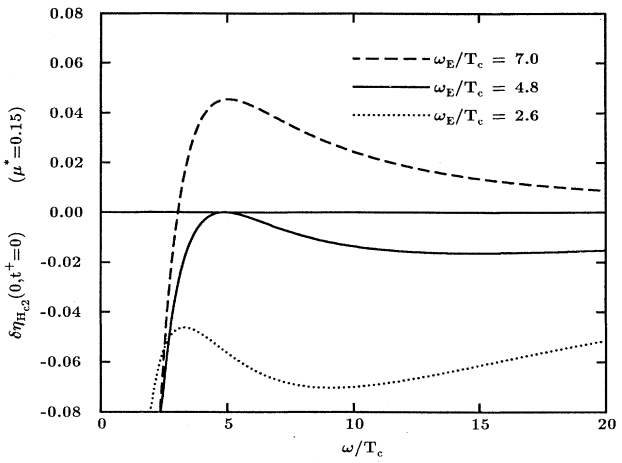

FIG. 99. Functional derivative $\delta\eta_{H_{c2}}$ vs ω/T_c for the case with $T=0$, $t^+=0.0$ meV, and $\mu^*=0.15$ is plotted for three different δ-function spectra, $\alpha^2F(\omega)=A\delta(\omega-\omega_E)$, where ω_E is the Einstein frequency. The solid curve is negative definite and peaks at exactly zero when $\omega=\omega_E$. This indicates a local maximum. The dotted curve has the peak in $\delta\eta_{H_{c2}}$ occurring above ω_E/T_c, and the dashed curve has $\delta\eta_{H_{c2}}$ peaking below ω_E/T_c.

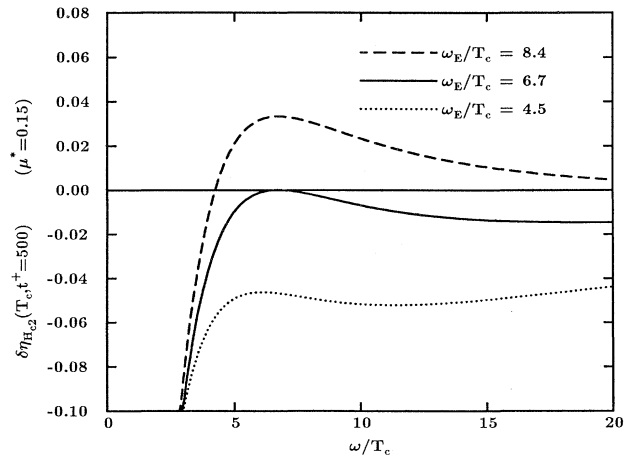

FIG. 100. The same as Fig. 99 except that now $T=T_c$ and $t^+=500.0$ meV.

at maximum obtained are given in Table XIII, and the results are plotted in Figs. 101 and 102 for $\eta_{H_{c2}}(0, t^+=0)$ and $\eta_{H_{c2}}(T_c, t^+=50)$, respectively, as a function of μ^*. On the same plot are also shown results for real materials (solid dots), which all fall below our maximum, as expected.

While we have not stressed it, all these results are independent of the area A taken for the delta function, because a scaling theorem similar to that proved for the thermodynamic properties also holds for H_{c2}. The proof is given here to be complete. For a delta-function spectrum, we can put Eqs. (7.1) and (7.2) into the form

$$\bar{\Delta}(i\omega_n)=\pi\bar{T}\sum_m\left[\frac{2\bar{\omega}_E}{\bar{\omega}_E^2+(\bar{\omega}_m-\bar{\omega}_n)^2}-\mu^*\theta(\omega_c-|\bar{\omega}_m|A)\right]\times\frac{\bar{\Delta}(\omega_m)}{\bar{\chi}^{-1}(\bar{\omega}(i\omega_m))-\pi\bar{t}^+} \tag{7.69}$$

and

$$\bar{\omega}(i\omega_n)=\bar{\omega}_n+\pi\bar{T}\sum_m\frac{2\bar{\omega}_E}{\bar{\omega}_E^2+(\bar{\omega}_m-\bar{\omega}_n)^2}\mathrm{sgn}(\bar{\omega}_m)+\pi\bar{t}^+\mathrm{sgn}(\bar{\omega}_n) \tag{7.70}$$

with $\bar{T}\equiv T/A$, $\bar{\omega}_E\equiv\omega_E/A$, $\bar{\omega}_n\equiv\omega_n/A$, $\bar{\omega}(i\omega_n)\equiv\tilde{\omega}(i\omega_n)/A$, $\bar{t}^+\equiv t^+/A$, $\bar{\Delta}(i\omega_n)\equiv\tilde{\Delta}(i\omega_n)/A$, and finally, $\bar{\chi}(\bar{\omega}_n)\equiv A\chi(\tilde{\omega}_n)$.

From Eq. (7.1c) for $\chi(\tilde{\omega}(i\omega_n))$, one can see that $\bar{\chi}(\tilde{\omega}(i\omega_n))$ has the same form as $\chi(\tilde{\omega}(i\omega_n))$, except that one must replace α with $\bar{\alpha}=\alpha/A^2$ and $\tilde{\omega}(i\omega_n)$ with $\bar{\omega}(i\omega_n)$. In writing the equations in terms of the barred quantities, we have removed the dependence on A except for a very small dependence in the cutoff associated with μ^*. Leavens (1977) followed a similar approach for T_c and, following him, we likewise ignore the small correction required. Given this, $\bar{T}_c$ and $\bar{\alpha}$ become completely independent of A and are only functions of $\bar{\omega}_E$, $\bar{t}^+$, and μ^*. We can therefore write

$$\bar{T}_c=F(\bar{\omega}_E,\mu^*) \tag{7.71}$$

and

$$\bar{\alpha}=H(\bar{\omega}_E,\bar{t}^+,t,\mu^*)\,, \tag{7.72}$$

where $t=T/T_c$. Here, F and H represent universal functions that can be determined from Eqs. (7.69) and (7.70) and from the definition of $\bar{\chi}(\bar{\omega}(i\omega_n))$. In Eq. (7.72), the $\bar{t}^+$ parameter falls out in the clean limit while the dependence is trivial in the dirty limit and does not appear at all in (7.71) as it drops in the T_c equations. Using Eqs. (7.71) and (7.72), we find that T_c is proportional to A and $H_{c2}(T)$ to A^2. From this, one can also conclude that $dH_{c2}(T)/dT$ is proportional to A.

TABLE XIII. Calculated maximum value for the strong-coupling parameter $\eta_{H_{c2}}$ for temperature $T=0$ and $T=T_c$ and for three different impurity concentrations: namely, $t^+=0.0$ (clean limit), $t^+=50.0$ meV, and $t^+=500.0$ meV (dirty sample). Rows 1 to 3 apply to different values of the Coulomb pseudopotential, namely, $\mu^*=0.0514$, 0.15, and 0.225, which should cover the physical range.

	T	0	T_c	0	T_c	0	T_c
μ^*	t^+	0	0	50	50	500	500
0.0514		1.36	1.24	1.30	1.34	1.32	1.39
0.15		1.39	1.27	1.32	1.37	1.34	1.42
0.225		1.41	1.28	1.33	1.39	1.35	1.43

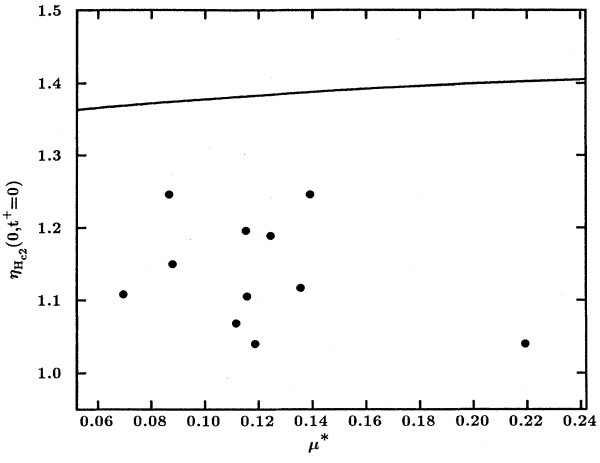

FIG. 101. Maximum possible value of $\eta_{H_{c2}}$ with $T=0$ and $t^+=0.0$ meV plotted as a function of μ^*. The solid dots represent theoretical values for real materials.

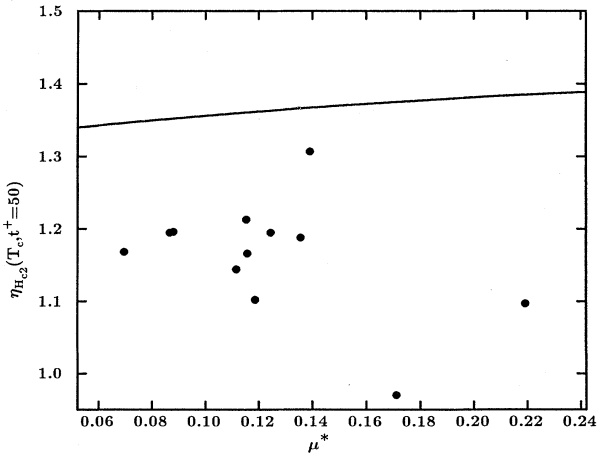

FIG. 102. Maximum possible value of $\eta_{H_{c2}}$ with $T=T_c$ and $t^+=50.0$ meV, plotted as a function of μ^*. The solid dots represent theoretical values for real materials.

VIII. OPTICAL PROPERTIES

A. Formalism

The electromagnetic properties of a BCS superconductor were already discussed in the original paper of Bardeen, Cooper, and Schrieffer (1957). Later, Nam (1967a, 1967b) extended the work to Eliashberg theory. Based on a Kubo formula, he gave complicated but general equations for the current response to an arbitrary external electromagnetic field and also provided some limited numerical results. In particular, for Pb he calculated the zero-temperature, frequency-dependent conductivity. The calculations were later reconsidered and extended by Swihart and Shaw [(1971); Shaw and Swihart (1968)]. Using the same general formalism, based on the imaginary-frequency-axis Matsubara approach, Blaschke and Blocksdorf (1982) computed the surface resistance of several superconductors. The temperature dependence of the dc Josephson current in a superconductor-insulator-superconductor (SIS) tunnel junction was measured and calculated by Lim *et al.* (1970) in Pb and calculated by Vashishta and Carbotte (1973) in $Pb_{0.9}Bi_{0.1}$. The temperature-dependent electromagnetic coherence length was estimated by Kerchner and Ginsberg (1973) using full Eliashberg gap solutions. As well, its zero-temperature reduction over the BCS value was considered. A related quantity, the zero-temperature reduction in the dc Josephson current, was discussed by Ginsberg *et al.* (1976) and by Vashishta and Carbotte (1973). Blezius and Carbotte (1986) have calculated the temperature-dependent London penetration depth for several impurity concentrations in V_3Si. Much more extensive calculations of ferromagnetic properties have been carried out by Blezius *et al.* (1988), who considered the London penetration depth, the electromagnetic coherence length, and the dc Josephson current for an SIS junction, a quantity also related to the local penetration depth. Their aim was to calculate these quantities for many different materials from a knowledge of their spectral density $\alpha^2F(\omega)$ and Coulomb pseudopotential μ^*. In addition, they derived, from microscopic theory, simple semiphenomenological formulas involving the single parameter $T_c/\omega_{\ln}$ and fit the unknown coefficients in the resulting form to the real-material data, so as to provide a simple but useful approximate formula for strong-coupling corrections.

Within linear-response theory, the Fourier transform of the current density [Nam (1967); Scholten *et al.* (1977)] is

$$J_\mu(q;\omega)=-K_{\mu\nu}(q;\omega)A^\nu(q;\omega)\ , \tag{8.1}$$

where $\mu=1,2,3$ corresponds to components x,y,z of the vector **J**, and q and ω are momentum and frequency, respectively. In Eq. (8.1), $A^\nu(q;\omega)$ is the νth component of the vector potential **A** describing the electromagnetic field. $K_{\mu\nu}(q;\omega)$ is a tensor that gives the current-response function and is the Fourier transform of the current-current correlation function.

The electromagnetic properties that interest us here can be expressed in terms of the kernel $K_{\mu\nu}(q;\omega)$ of Eq. (8.1). For example, the zero-frequency penetration depth that describes the penetration of a static magnetic field into the surface of a bulk superconductor is given, for the case of specular reflection, by (Nam (1967a, 1967b)

$$\lambda(T)=\frac{2}{\pi}\int_0^\infty dq\frac{1}{q^2+K(q;0)/4\pi}\ , \tag{8.2}$$

where isotropy was assumed and the temperature dependence of the penetration depth has been made explicit. Note that we have taken the frequency $\omega\to 0$ limit of (8.1), which describes the static situation. Simple explicit equations for $\lambda(T)$ are possible in limiting cases. In the dirty limit, the mean free path (l) of an electron can be reduced greatly because of the increased scattering by impurities. In that case, the electromagnetic response becomes local and only the $q\to 0$ limit of $K(q;0)$ is needed. Carrying out the integration in Eq. (8.2), we get

$$\lambda_l(T)=\left[4\pi\sigma_N T\sum_{n=1}^{\infty}\frac{\Delta^2(i\omega_n)}{\omega_n^2+\Delta^2(i\omega_n)}\right]^{-1/2}\ , \tag{8.3}$$

which depends only on the Matsubara gaps $\Delta(i\omega_n)$. In Eq. (8.3), the subscript "l" stands for local limit, and σ_N is the normal-state conductivity due to impurity scattering only. It is given by

$$\sigma_N=\tfrac{2}{3}N(0)e^2v_F^2\tau_N\ , \tag{8.4}$$

where as before $N(0)$ is the single-spin electronic density of states at the Fermi surface; e, the charge on the electron; v_F, the electron Fermi velocity; and τ_n, the impurity lifetime. The local limit, for which Eq. (8.3) holds, is characterized by the condition $\xi(0)\gg l$, where $\xi(0)$ is the zero-temperature coherence length that will be introduced shortly. Except for an appropriate change of the proportionality constants in Eq. (8.3), $\lambda_l^{-2}(T)$ also gives the critical dc Josephson current $[J_c(T)]$ observed in a superconductor-insulator-superconductor (SIS) tunnel junction (Nam 1967a, 1967b):

$$\frac{J_c(T)}{J_c(0)}=\left[\frac{\lambda_l(0)}{\lambda_l(T)}\right]^2\ . \tag{8.5}$$

When nonlocal effects are important, it is necessary to introduce the Pippard or London limits characterized, respectively, by $\lambda\ll\xi(0)$ and $\lambda\gg\xi(0)$. The Pippard limit is determined through Eq. (8.2), where most of the contribution comes from the $q\to\infty$ region of the integral. The result is

$$\lambda_P(T)=\frac{4}{3\sqrt{3}}\left[\frac{3\pi^2}{v_F}\frac{n}{m}e^2T\sum_{n=1}^{\infty}\frac{\Delta^2(i\omega_n)}{\omega_n^2+\Delta^2(i\omega_n)}\right]^{-1/3} \tag{8.6}$$

where n is the free-electron density and m the electron mass. Equation (8.6) is clearly related to the local limit and therefore need not be discussed further here. The

London limit, which depends mainly on the $q \to 0$ limit of the electromagnetic response function is given by Nam (1967a):

$$\lambda_L(T) = \left[\tfrac{4}{3}\pi N(0) e^2 v_F^2 T \times \sum_{n=1}^{\infty} \frac{\Delta^2(i\omega_n)}{Z(i\omega_n)[\omega_n^2 + \Delta^2(i\omega_n)]^{3/2}} \right]^{-1/2}, \quad (8.7)$$

where we see that the renormalization factor $Z(i\omega_n)$ now enters explicitly, in contrast to the situation that arises for local or Pippard limit.

The final quantity of interest is the electromagnetic coherence length $\xi(T)$, which describes the nonlocality in the electromagnetic response of a superconductor and is given by

$$\lim_{q\to\infty} \frac{qK(q,0)}{K(0,0)} = \frac{3\pi}{4\xi(T)} \quad (8.8)$$

and, more explicitly [Lemberger *et al.* (1978); Blezius and Carbotte (1986)], by

$$\xi(T) = \frac{\frac{v_F}{2} \sum_{n=1}^{\infty} \frac{\Delta^2(i\omega_n)}{Z(i\omega_n)[\omega_n^2 + \Delta^2(i\omega_n)]^{3/2}}}{\sum_{n=1}^{\infty} \frac{\Delta^2(i\omega_n)}{\omega_n^2 + \Delta^2(i\omega_n)}} . \quad (8.9)$$

A comparison of Eqs. (8.3) and (8.7) with (8.9) shows that

$$\left[\frac{\lambda_l(T)}{\lambda_L(T)} \right]^2 = \frac{\xi(T)}{l} , \quad (8.10)$$

where we have introduced the mean free path $l = v_F \tau_N$.

Local and London penetration depths and the coherence length follow directly for a given spectral density $\alpha^2F(\omega)$ and Coulomb pseudopotential μ^*, from numerical solutions of Eqs. (2.1) and (2.2) for the Matsubara gaps $\Delta(i\omega_n)$ and renormalization factors $Z(i\omega_n)$.

B. Comparison with experiment for V_3Si

To illustrate the good agreement that can be achieved with experiment, we consider, in some detail, the case of V_3Si. Christen *et al.* (1984) have measured the temperature variation of the London penetration depth for this material. Their results are presented with error bars in Fig. 103 in the form of $[\lambda(0)/\lambda(T)]^2 - (1-t^4)$ where the two-fluid-model prediction has been subtracted out. We see first that the two-fluid-model temperature variation does not apply for V_3Si. In addition for comparison, we show BCS results (the solid curve with solid dots). These were obtained from our computer programs using the spectrum $\alpha^2F(\omega)$ of aluminum with Eq. (8.7) evaluated exactly from numerical solutions of (2.1) and (2.2). We verified in this way that our programs are capable of reproducing exactly the BCS results. These results clearly do not agree with the measured temperature variation. Three other calculations were carried out, all based on (8.7). The first two were based on the spectrum $\alpha^2F(\omega)$ measured by the tunneling spectroscopy by Kihlstrom (1985). The results are the dot-dashed curve for the clean limit and the dashed curve when a mean free path of 28 nm is included in the calculation. This case agrees very well with experiment and is a little better representation of the data than the pure case. The value $l = 28$ nm is from Christen *et al.* (1984) and corresponds to an impurity scattering time $1/\tau_N = 0.485$ meV. The final curve (dotted) was obtained when the $\alpha^2F(\omega)$ of Bangert *et al.* (1985) was used. This spectrum is not considered to be realistic and does not give agreement with experiment. It is included mainly to illustrate that any arbitrary shape spectrum will not lead to good agreement with data. Our general conclusion is that for V_3Si the temperature variation of the penetration depth is well described by Eliashberg theory and is in significant disagreement with BCS.

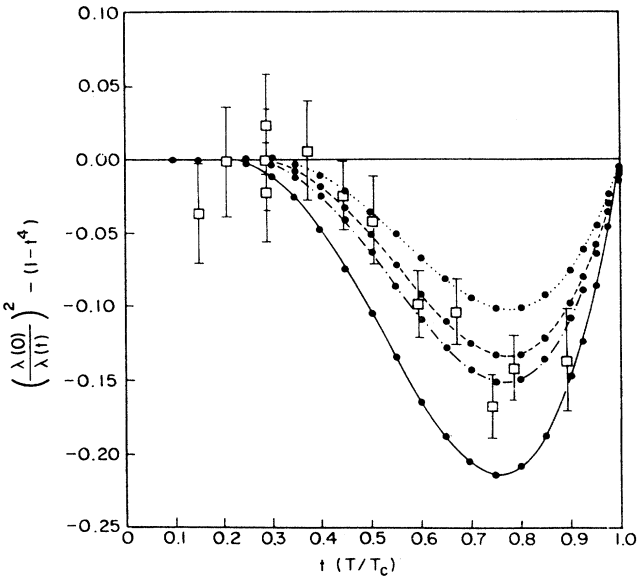

FIG. 103. Strong-coupling difference from the two-fluid prediction of the inverse square of the London-limit penetration depth normalized to its zero-temperature value as a function of temperature normalized with respect to the superconducting critical temperature. The solid curve is both Al and the BCS prediction; the dot-dashed curve is pure Kihlstrom (1985) V_3Si; the short-dashed curve is Kihlstrom (1987) V_3Si with impurities in the amount prescribed by Christen *et al.* (1984); the dotted curve is pure Bangert *et al.* (1985) V_3Si. The data with error bars are those of Christen *et al.* (1984).

We turn now to the absolute magnitude of the coherence distance, $\xi(0)$. For a mean free path of 28 nm, formula (8.9) yields a value of 5.11 nm for a value of Fermi velocity of 1.31×10^7 cm/s taken from the report of Orlando *et al.* (1979), which agrees as well with the value found by Muto *et al.* (1979), accounting for the renormalization factor of $(1+\lambda)$. The value of $\xi(0)$ quoted

above compares well with 5.6 nm, quoted by Orlando *et al.* (1979), and 4.9 nm, by Muto *et al.* (1979), and is about 15 percent larger than would be predicted by a renormalized BCS theory. In this case, $\xi(0)$ is given by the formula $\hbar v_F/[\pi\Delta_0(1+\lambda)]$, which can easily be evaluated. Our conclusion is again that Eliashberg theory works better than does BCS in predicting the measured value of $\xi(0)$ for V_3Si.

C. Reduction to approximate analytic forms

Besides exact numerical solutions of Eqs. (8.6), (8.7), and (8.9), we also want to consider approximate analytic solutions that contain a first correction for strong-coupling corrections to the BCS result for the corresponding quantity. To obtain such approximate equations for the above mentioned electromagnetic properties, we follow our previous work on thermodynamic properties and use the same simple step model for the gap Δ and for the renormalization Z, as described in Appendix B.

Both the local-limit penetration depth and the dc Josephson curent follow from a knowledge of

$$I_l \equiv \pi T \sum_{n=1}^{\infty} \frac{\Delta^2(i\omega_n)}{\omega_n^2+\Delta^2(i\omega_n)} . \tag{8.11}$$

For T near T_c, we can neglect the n dependence of $\Delta(i\omega_n)$, since the sum in (8.11) converges, and get for our model gap $I_l=\pi\Delta_0^2(T)/8T$. To lowest order in $(T-T_c)$, we get from Eq. (B19) of Appendix B

$$y_l(T)\equiv\lambda_l^{-2}(T)=4\sigma_N I_l=\frac{\pi\sigma_N}{2}\frac{F'(T_c)}{G(T_c)}(1-t) \tag{8.12}$$

with $t\equiv T/T_c$, the reduced temperature. Reference to Eqs. (B17a) and (B17b) gives, after some simple algebra,

$$\frac{F'(T_c)}{G(T_c)}=\frac{8\pi^2}{7\xi(3)}T_c\left\{1+\frac{2(\pi T_c)^2}{\lambda}\left[\left[1+\frac{6}{7\xi(3)}\right]a(T_c)-\left[\frac{4}{3}+\frac{2}{7\xi(3)}\right]b\right]\right\} . \tag{8.13}$$

On substituting Eqs. (B25) and (B26) into (8.13), we get

$$T_c\frac{y_l'(T_c)}{4\sigma_N}=\frac{-\pi^3}{7\xi(3)}T_c\left\{1+2\pi^2\left[\frac{T_c}{\omega_{\ln}}\right]^2\alpha_1\left[1.71\ln\left[\frac{1.13\omega_{\ln}}{k_BT_c}\right]-\frac{\alpha_2}{\alpha_1}(1.57)\right]\right\} , \tag{8.14}$$

where α_1 and α_2 are to be treated as arbitrary parameters.

For $T=0$, the sum over Matsubara frequencies in (8.11) can be replaced by an integral, and, ignoring the ω dependence of the gap, we get

$$\frac{y_l(0)}{4\sigma_N}=\frac{\pi}{4}\Delta_0(T=0) , \tag{8.15a}$$

where $\Delta_0(T=0)$ is given in Appendix B [Eq. (B40)]. Combining this with (8.14) and fitting to numerical data yields

$$\frac{y_l(0)}{T_c|y_l'(T_c)|}=0.376\left[1-1.5\left[\frac{T_c}{\omega_{\ln}}\right]-7.6\left[\frac{T_c}{\omega_{\ln}}\right]^2\ln\left[\frac{\omega_{\ln}}{4T_c}\right]\right] . \tag{8.15b}$$

In Fig. 104 (solid dots) we show results for $y_l(0)/[T_c|y_l'(T_c)|]$ in real materials (see Table XIV) based on tunneling-derived kernels, complete numerical solutions of the Eliashberg equations (2.1) and (2.2), and the exact evaluation of formula (8.13). The solid line in Fig. 103 is a visual best fit through the exact numerical data of the form (8.15b). The above derivation did not give a linear term. It was added on, purely on a phenomenological basis, so as to get a really good fit. It appears to be necessary so as to compensate for the approximations made during the derivation of (8.14). The derivation was done for a delta-function spectrum. Exact numerical results in this case are shown as the dashed line in Fig. 103, which is more quadratic near $T_c/\omega_{\ln}=0$. The need for a linear term seems therefore to be due to the frequency spread that occurs in real spectra. As a last point, we note that amorphous Ga falls way off the main-trend curve. This is not surprising, since such a spectrum exhibits considerable weight at low energies; and hence our approximation $\nu/T_c\gg1$ does not apply for all important frequencies (ν).

We next consider the London-limit penetration depth. In analogy with the procedure followed for the local limit, we start by introducing a dimensionless quantity $I_L(T)$ dependent only on the solutions of the Eliashberg equation (2.1) and (2.2). That is, we write

$$I_L(T)\equiv\frac{\lambda_L^{-2}(T)}{\frac{4}{3}N(0)e^2v_F^2}=\pi T\sum_{n=1}^{\infty}\frac{\Delta^2(i\omega_n)}{Z(i\omega_n)[\omega_n^2+\Delta^2(i\omega_n)]^{3/2}} . \tag{8.16}$$

For T near T_c, the sum in (8.16) is sufficiently convergent that we can replace $Z(i\omega_n)$ in each term by its $n=1$ value $(1+\lambda)$. For a constant gap model, we get

$$I_L(T)=+\frac{7\zeta(3)\Delta_0^2(T)}{8(1+\lambda)(\pi T)^2} , \tag{8.17}$$

from which we conclude that

$$\frac{T_c y_L'(T_c)}{\frac{4}{3}N(0)e^2 v_F} = \frac{-1}{1+\lambda}\left\{1+\frac{2(\pi T_c)^2}{\lambda}\left[\left[1+\frac{6}{7\zeta(3)}\right]a(T_c) - \left[\frac{4}{3}+\frac{2}{7\zeta(3)}\right]b\right]\right\}, \quad (8.18)$$

where use was made of formula (8.13) and the definition $y_L(T)\equiv\lambda_L^{-2}(T)$. A similar formula was derived by Masharov (1974a, 1974b) using very different methods.

At zero temperature, we get, converting the sums to integrals in Eq. (8.16) and ignoring the ω dependence in this integral,

$$I_L(0)=\frac{1}{2Z_S(0)} . \quad (8.19)$$

The quantity $Z_S(0)$ is calculated in Appendix B for our model solution, and Eq. (B36) with $\omega=0$ gives

$$Z_S(0)=(1+\lambda)\left[1-\left[\frac{2\Delta_0}{T_c}\right]^2\frac{1}{(2\pi)^2}\frac{(\pi T_c)^2}{1+\lambda}[a(T_c)-b]\right] . \quad (8.20)$$

Using Eqs. (8.18), (8.19), and (8.20), we get, on substituting for $a(T_c)$ and b given by Eqs. (B25) and (B26), respectively, and fitting to real-material data,

$$\frac{y_L(0)}{T_c|y_L'(T_c)|}=0.50\left[1-2.0\left[\frac{T_c}{\omega_{\ln}}\right]-11.0\left[\frac{T_c}{\omega_{\ln}}\right]^2\ln\left[\frac{\omega_{\ln}}{4.5T_c}\right]\right] . \quad (8.21)$$

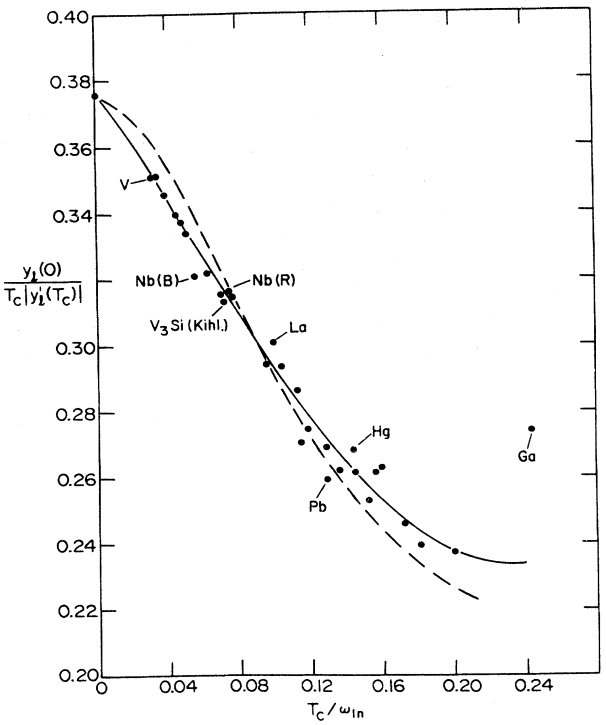

FIG. 104. Ratio $y_l(0)/T_c|y_l'(T_c)|$ vs $T_c/\omega_{\ln}$. The materials, in increasing order of $T_c/\omega_{\ln}$, are Al, V, Ta, Sn, Tl, $Tl_{0.9}Bi_{0.1}$, In, Nb (Butler), Nb (Arnold), $V_3Si(1)$, V_3Si (Kihl.), Nb (Rowell), Mo, $Pb_{0.4}Tl_{0.6}$, La, V_3Ga, Nb_3Al (2), $Nb_3Ge(2)$, $Pb_{0.6}Tl_{0.4}$, Pb, $Nb_3Al(3)$, $Pb_{0.8}Tl_{0.2}$, Hg, Nb_3Sn, $Pb_{0.9}Bi_{0.1}$, $Nb_3Al(1)$, $Nb_3Ge(1)$, $Pb_{0.8}Bi_{0.2}$, $Pb_{0.7}Bi_{0.3}$ and $Pb_{0.65}Bi_{0.35}$. Amorphous Ga has also been included and deviates substantially from the trend. The solid curve corresponds to $y_l(0)/T_c|y_l'(T_c)| = 0.376[1-1.5T_c/\omega_{\ln}-7.6(T_c/\omega_{\ln})^2\ln(\omega_{\ln}/4T_c)]$. Note that a linear term has been required for an accurate fit. The dashed curve corresponds to a series of Einstein spectra with $\mu^*=0$, the model spectra upon which our derivations are based. The trend is quite similar to that of the real materials. However, the initial decrease from BCS is more quadratic, and hence no linear terms would be required. Thus it appears that the effect of the realistic shapes used has been to produce a linear correction below the BCS value.

TABLE XIV. Superconducting properties: optical properties.

Material	$T_c/\omega_{\ln}$	$\frac{\xi(0,t^+=0)}{\xi(T_c,t^+=0)}$	$\frac{y_l(0)}{T_c\lvert y_l'(T_c)\rvert}$	$\frac{y_L(0)}{T_c\lvert y_L'(T_c)\rvert}$
Al	0.004	1.330	0.376	0.500
V	0.031	1.293	0.351	0.454
Ta	0.035	1.292	0.352	0.454
Sn	0.038	1.286	0.346	0.445
Tl	0.046	1.278	0.340	0.434
$Tl_{0.9}Bi_{0.1}$	0.048	1.277	0.338	0.431
In	0.050	1.273	0.334	0.425
Nb (Butler)	0.057	1.261	0.321	0.405
Nb (Arnold)	0.062	1.260	0.322	0.406
V_3Si_1	0.070	1.253	0.315	0.395
V_3Si (Kihl.)	0.071	1.251	0.314	0.393
Nb (Rowell)	0.074	1.255	0.317	0.397
Mo	0.076	1.254	0.315	0.395
$Pb_{0.4}Tl_{0.6}$	0.095	1.233	0.294	0.363
La	0.099	1.244	0.301	0.374
V_3Ga	0.103	1.234	0.294	0.363
Nb_3Al (2)	0.113	1.228	0.286	0.352
Nb_3Ge (2)	0.114	1.211	0.271	0.328
$Pb_{0.6}Tl_{0.4}$	0.119	1.215	0.274	0.333
Pb	0.128	1.195	0.260	0.310
Nb_3Al (3)	0.129	1.219	0.269	0.328
$Pb_{0.8}Tl_{0.2}$	0.136	1.204	0.262	0.316
Hg	0.146	1.215	0.269	0.326
Nb_3Sn	0.146	1.214	0.262	0.318
$Pb_{0.9}Bi_{0.1}$	0.152	1.193	0.253	0.302
Nb_3Al (1)	0.156	1.217	0.262	0.318
Nb_3Ge (1)	0.160	1.218	0.262	0.320
$Pb_{0.8}Bi_{0.2}$	0.172	1.193	0.245	0.293
$Pb_{0.7}Bi_{0.3}$	0.182	1.186	0.239	0.284
$Pb_{0.65}Bi_{0.35}$	0.200	1.194	0.237	0.283
$Pb_{0.5}Bi_{0.5}$	0.320	1.359	0.250	0.340
Ga	0.243	1.342	0.274	0.368
$Pb_{0.75}Bi_{0.25}$	0.288	1.326	0.252	0.333
Bi	0.320	1.380	0.265	0.366

Results of exact numerical solutions for the many real materials (solid dots) identified in previous sections are shown in Fig. 105. A reasonable fit to this data can be obtained only if an additional linear term is introduced phenomenologically as before. The solid line of Fig. 104 corresponds to the form (8.21), which is our final result for strong-coupling corrections.

We note, finally, that the Pippard-limit penetration depth was not explicitly commented on because it does not lead to new results. If we introduce $Z_p(T)\equiv\lambda_p^{-3}(T)$, it follows that

$$\frac{Z_p(0)}{T_c|Z_p'(T_c)|}=\frac{y_l(0)}{T_c|y_l'(T_c)|}\ , \tag{8.22}$$

a quantity already plotted in Fig. 104. In addition as Eq. (8.10) shows, the coherence length is closely related to the local and London limit. Before giving results, it is useful to consider the effect of normal impurity scattering on the gap and renormalization factor, as impurities can enter electromagnetic properties.

No impurities have been included explicitly in the Eliashberg equations (2.1) and (2.2). To include them requires adding to the right-hand side of Eq. (2.1) a term of the form [Daams and Carbotte (1981)]

$$\pi t^+\frac{\Delta(i\omega_n)}{\sqrt{\omega_n^2+\Delta^2(i\omega_n)}}\ , \tag{8.23a}$$

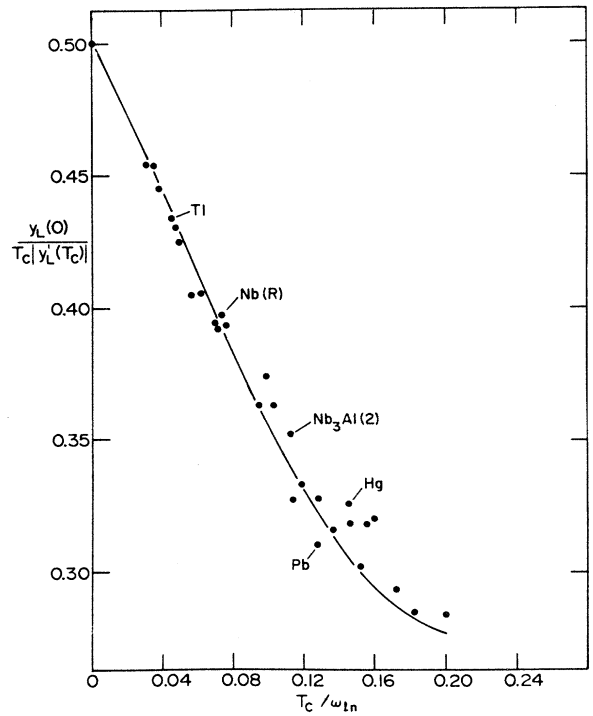

FIG. 105. Ratio $y_L(0)/T_c|y_L'(T_c)|$ vs $T_c/\omega_{\ln}$. See caption of Fig. 104 for identification of materials. The solid curve corresponds to $y_l(0)/T_c|y_l'(T_c)|=0.5[1-2T_c/\omega_{\ln}-11(T_c/\omega_{\ln})^2\ln(\omega_{\ln}/4.5T_c)]$.

and in Eq. (2.2),

$$\pi t^+\frac{1}{\sqrt{\omega_n^2+\Delta^2(i\omega_n)}} \tag{8.23b}$$

with $t^+=1/2\pi\tau_N$ where τ_N is the impurity lifetime. On substituting the modified equation (2.2) into Eq. (2.1), we see that, for an isotropic superconductor, the two impurity terms cancel in the combined equation for the Matsubara gaps. This cancellation agrees with Anderson's theorem [Anderson (1959)], which states that T_c is unaffected by normal impurities in an isotropic superconductor. Of course, when anisotropy is included, the theorem no longer holds, and the effect of normal impurities is to wash out the anisotropy. In the dirty limit, we recover isotropy.

While the impurity contribution drops out of the gaps $\Delta(i\omega_n)$, it remains in the renormalization $Z(i\omega_n)$. For $\lambda_l(T)$, Eq. (8.3) applies and only the $\Delta(i\omega_n)$ are required, so that adding impurities to our equations changes nothing. This is not surprising, since the local limit is derived under the assumption that $l\ll\xi(0)$, i.e., the dirty limit is already built in. It is then only consistent that adding an additional πt^+ term in the Eliashberg equations themselves makes no difference. The situation is different in the London limit, for which Eq. (8.7) applies. $Z(i\omega_n)$ enters explicitly and the πt^+ contribution in a modified equation (2.2) will affect the answer. In fact, in the dirty limit with $\pi t^+\to\infty$, the new term (8.23b) in the Z channel will dominate, and it is appropriate to replace $Z(i\omega_n)$ in Eq. (8.7) by $Z(i\omega_n)\cong\pi t^+/\sqrt{\omega_n^2+\Delta^2(i\omega_n)}$, giving

$$\lambda_L(T)=\left[\frac{4}{3}\pi\frac{N(0)e^2}{\pi t^+}v_F^2T\sum_{n=1}^{\infty}\frac{\Delta^2(i\omega_n)}{\omega_n^2+\Delta^2(i\omega_n)}\right]^{-1/2}\ . \tag{8.24}$$

The constant in the definition of $\lambda_L^{-2}(T)$ is simply $4\pi\sigma_N$, with σ_N given by Eq. (8.4). The London penetration depth in the dirty limit reduces to the local-limit result [Eq. (8.3)].

Equation (8.10) gives a relationship between coherence length and the ratio of local-to-London penetration depth; thus $\xi(T)$ will depend explicitly on impurities. In fact, Eq. (8.9) in the dirty limit gives

$$\xi(T)\cong\frac{v_F}{2\pi t^+}=v_F\tau_N=l\ . \tag{8.25}$$

The coherence length becomes the mean free path.

Results for the ratio $\xi(0)/\xi(T_c)$ for real materials are shown as solid dots in Fig. 106. These results were obtained from exact numerical calculations based on Eqs. (2.1) and (2.2) without an explicit πt^+ term (clean limit) and on the prescription (8.9). The solid curve represents our best visual fit to the data. It is given by

$$\frac{\xi(0)}{\xi(T_c)}=1.33\left[1-0.83\left[\frac{T_c}{\omega_{\ln}}\right]-0.75\left[\frac{T_c}{\omega_{\ln}}\right]^2\ln\left[\frac{\omega_{\ln}}{40T_c}\right]\right]. \tag{8.26}$$

Note that (8.26) was not derived directly from our previous fits to y_l and y_L even though the exact relationship

$$\frac{y_L(0)}{T_c|y_L'(T_c)|}=\frac{\xi(0)}{\xi(T_c)}\frac{y_l(0)}{T_c|y_l'(T_c)|}$$

holds. A new fit to the data on $\xi(0)/\xi(T_c)$ itself was done to increase accuracy.

It is a simple matter to extract from previous work strong-coupling corrections to the various quantities of interest rather than concentrate, as we have done, on dimensionless ratios. If we define as before η_B as the strong-coupling correction to a given quantity B, $B=B^{\rm BCS}\eta_B$, we can find, after a suitable fit to data,

$$\eta_{\lambda_L}(0)=1+1.3\left[\frac{T_c}{\omega_{\ln}}\right]^2\ln\left[\frac{\omega_{\ln}}{13T_c}\right], \tag{8.27}$$

$$\eta_{\lambda_L}(T_c)=1-16\left[\frac{T_c}{\omega_{\ln}}\right]^2\ln\left[\frac{\omega_{\ln}}{3.5T_c}\right], \tag{8.28}$$

$$\eta_{\lambda_l}(0)=1+5\left[\frac{T_c}{\omega_{\ln}}\right]^2\ln\left[\frac{\omega_{\ln}}{3.8T_c}\right]+0.4\left[\frac{T_c}{\omega_{\ln}}\right], \tag{8.29}$$

$$\eta_{\lambda_l}(T_c)=1-2.5\left[\frac{T_c}{\omega_{\ln}}\right]^2\ln\left[\frac{\omega_{\ln}}{1.9T_c}\right], \tag{8.30}$$

$$\eta_{\xi}(0)=1+11\left[\frac{T_c}{\omega_{\ln}}\right]^2\ln\left[\frac{\omega_{\ln}}{4.2T_c}\right]+1.5\left[\frac{T_c}{\omega_{\ln}}\right], \tag{8.31}$$

$$\eta_{\xi}(T_c)=1+17\left[\frac{T_c}{\omega_{\ln}}\right]^2\ln\left[\frac{\omega_{\ln}}{3.4T_c}\right]+1.5\left[\frac{T_c}{\omega_{\ln}}\right]. \tag{8.32}$$

We have chosen not to show fits in these cases, as such graphs are becoming repetitive. The above equations hold approximately only for the conventional strong-coupling regime for which $T/\omega_{\ln}\lesssim 0.25$.

D. Very strong coupling limit

As for other quantities previously considered, it is of interest to go beyond the conventional range and consider much higher values of $T_c/\omega_{\ln}$, which we call the very strong coupling regime. In Figs. 107-109 we show our results for $\eta_{\lambda_l}(T)$ at $T=0$ and $T=T_c$; $\eta_{\lambda_L}(T)$ at $T=0$ and $T=T_c$; and $\eta_{\xi}(T)$ at $T=0$ and $T=T_c$, respectively, up to $T_c/\omega_{\ln}=4.0$. In the case of $\eta_{\lambda_l}(T_c)$, the initial drop as $T_c/\omega_{\ln}$ increases from zero eventually stops when a minimum value is reached, after which this coefficient starts to grow and ends up to be greater than 1. This is in contrast to the behavior found for $\eta_{\lambda_l}(0)$, which simply increases monotonically with some sign of saturation

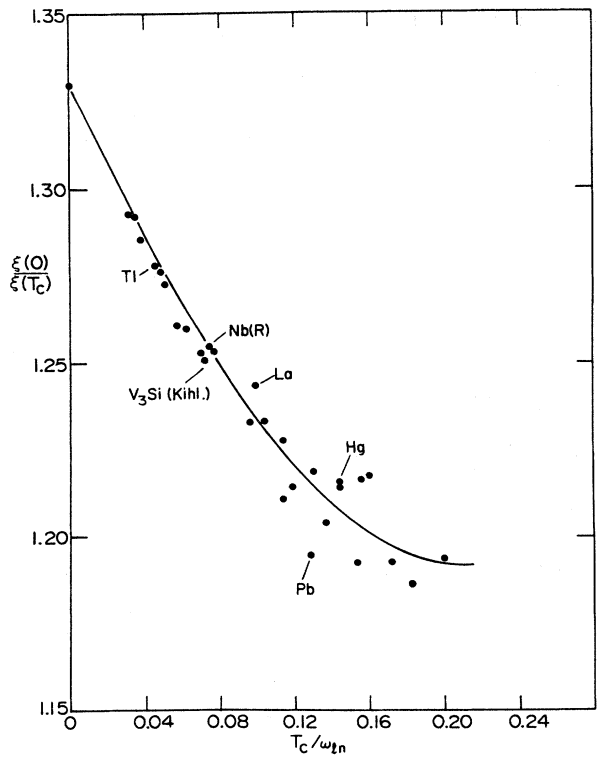

FIG. 106. Ratio $\xi(0)/\xi(T_c)$ vs $T_c/\omega_{\ln}$. See caption to Fig. 104 for identification of materials. The curve corresponds to $\xi(0)/\xi(T_c)=1.33[1-0.83T_c/\omega_{\ln}-0.75(T_c/\omega_{\ln})^2\ln(\omega_{\ln}/40T_c)]$.

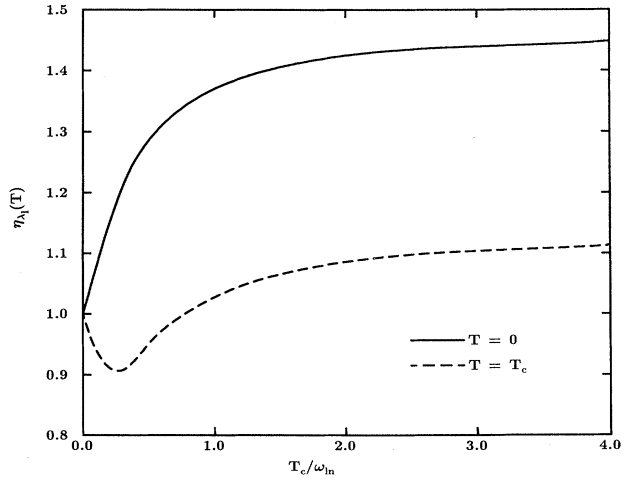

FIG. 107. Strong-coupling correction $\eta_{\lambda_l}(T)$ for the local-limit penetration depth $\lambda_l(T)$ at $T=0$ (solid curve) and $T=T_c$ (dashed curve), as a function of coupling strength $T_c/\omega_{\ln}$.

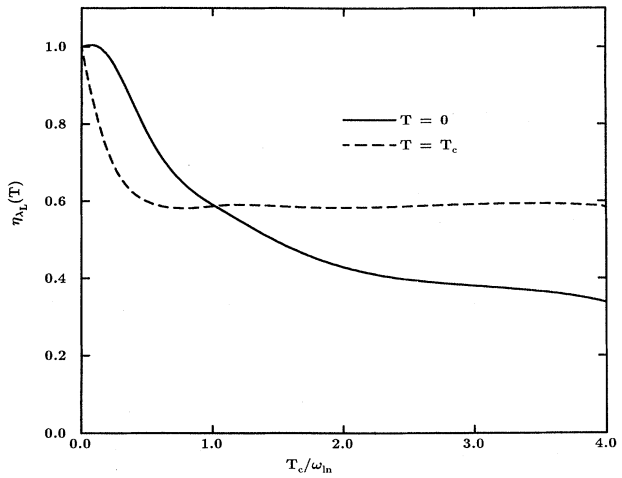

FIG. 108. Strong-coupling correction $\eta_{\lambda_L}(T)$ for the London-limit penetration depth $\lambda_L(T)$ at $T=0$ (solid curve) and $T=T_c$ (dashed curve), as a function of coupling strength $T_c/\omega_{\ln}$.

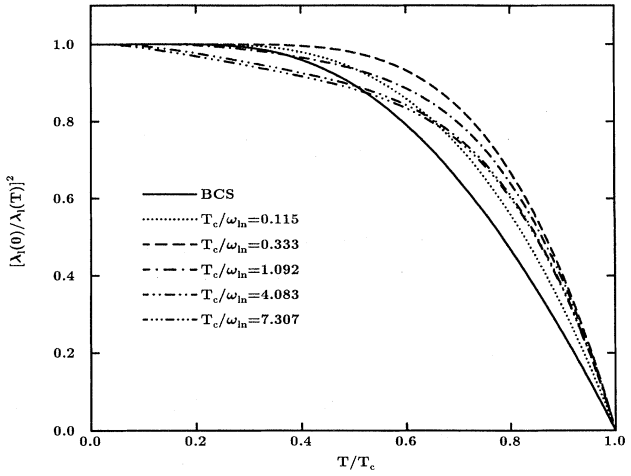

FIG. 110. Temperature variation of the square of the inverse local penetration depth at temperature T normalized to its value at zero temperature for several values of the coupling strength $T_c/\omega_{\ln}$, namely, 0.0 (BCS), 0.115, 0.333, 1.092, 4.083, and 7.307.

occurring when $T_c/\omega_{\ln}$ gets very large. A feature of the curve of $\eta_{\lambda_L}(T_c)$ that is worth noting is that it initially drops very sharply and then levels off to a nearly constant value. By contrast, $\eta_{\lambda_L}(0)$ shows much less variation initially. The curve for $\eta_{\xi}(T_c)$ shows signs of saturation after a fairly rapid increase with increasing value of $T_c/\omega_{\ln}$ at lower values of this parameter. Finally, the curve for $\eta_{\xi}(0)$ is nearly linear and its absolute value becomes remarkably large.

The complete temperature variation of $\lambda_l(T)$ and $\lambda_L(T)$ in the very strong coupling regime is also of interest. These are shown in Figs. 110 and 111, respectively, in the format $[\lambda(0)/\lambda(T)]^2$. For the local limit, the curves first deviate from BCS by showing an upward bulge at all temperatures, but as the coupling is increased a reverse trend is seen in which the tendency is for the curve to fall below BCS at small reduced temperatures and above at the higher values of t. The low-t behavior is fairly flat even for $T_c/\omega_{\ln}=7.3$. For the London limit, the situation is similar at small values of $T_c/\omega_{\ln}$ in the sense that the deviations from BCS are positive; but for large values of $T_c/\omega_{\ln}$, the curves start deviating nega-

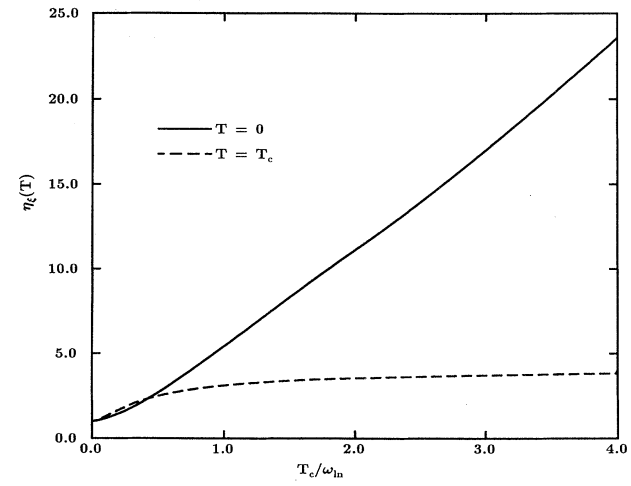

FIG. 109. Strong-coupling correction $\eta_{\xi}(T)$ for the coherence length $\xi(T)$ at $T=0$ (solid curve) and $T=T_c$ (dashed curve), as a function of coupling strength $T_c/\omega_{\ln}$.

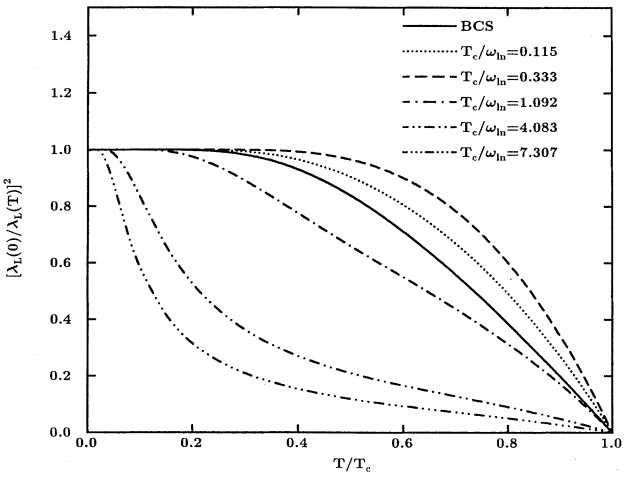

FIG. 111. Temperature variation of the square of the inverse London penetration depth at temperature T normalized to its value at zero temperature for several values of the coupling strength $T_c/\omega_{\ln}$, namely, 0.0 (BCS), 0.115, 0.333, 1.092, 4.083, and 7.307.

tively from BCS for the entire temperature range. In fact, at very large values of $T_c/\omega_{\ln}$, they change curvature and look completely different. The expected flat region at small t, which is taken to be representative of an s-wave superconductor, is missing.

E. Asymptotic limit

Finally, we turn to asymptotic limits. We shall consider both exact numerical results for $\sqrt{\lambda}t \gg 1$ and also the one-Matsubara-gap analytic results. We start with the analytic results first. From Eq. (6.51), we have that the gap $\Delta(T)$ goes like $\sqrt{A\omega_E}(1-t)^{1/2}$ for $t \to 1$, which is the only regime of interest in the one-gap model. Reference to Eq. (8.3) for $\lambda_l(T)$ gives

$$\lambda_l^{-2}(T)=4\sigma_N\omega_E\sqrt{\lambda}(1-t), \quad t\to 1 . \tag{8.33}$$

To get the London limit given by (8.7) is not quite so direct, as we need $Z(1)$ as well as the gap. But from Eq. (6.42), we know that as $\lambda \equiv \lambda(0) \to \infty$

$$Z(1)\cong \frac{\pi T\lambda}{\sqrt{(\pi T)^2+\Delta^2(T)}} , \tag{8.34}$$

so that Eq. (8.7) gives

$$\lambda_L^{-2}(t)=4\left[\frac{ne^2}{m}\right]\frac{1}{\lambda}(1-t), \quad t\to 1 . \tag{8.35}$$

Finally, from (8.10), it follows that

$$\xi(t)=\frac{v_F\hbar}{\lambda^{3/2}\omega_E}, \quad t\to 1 . \tag{8.36}$$

We can also get exact numerical results for these quantities provided $\sqrt{\lambda}t \gg 1$ is assumed. In that case, $\bar{\Delta}(T)$ is independent of any material parameter and can be solved for from Eq. (2.28). If we write $\bar{\Delta}(n)\equiv f_n(t)$, we can rewrite (6.48) for λ_l as

$$\lambda_l^{-2}(t)=\frac{\sqrt{\lambda}\,\omega_E\sigma_N}{\sqrt{2}}g^{-2}(t) \tag{8.37}$$

with the universal function

$$g^{-2}(t)=4\pi\bar{T}_c t\sum_{n=1}^{\infty}\frac{f_n^2(t)}{f_n^2(t)+(\pi\bar{T}_c t)^2(2n-1)^2} . \tag{8.38}$$

The function $g(t)$ is plotted in Fig. 112 where its inverse is also shown and is seen to go to ∞ as $t\to 1$. We find numerically that $g^{-2}(t)=9.64(1-t)$ for t near 1, which is to be compared with the one-gap model which gave $5.66(1-t)$, where we have noted that

$$\left[\sigma_N\frac{\sqrt{\lambda}\,\omega_E}{\sqrt{2}}\right]^{1/2}\lambda_l(t)=\left[\frac{\hbar}{\mu_0}\right]^{1/2}g(t)$$
$$=7.33\times 10^{-4}g(t)\,\frac{\sqrt{\text{meV}}\ \text{m}}{\sqrt{\Omega\,\text{m}}} \tag{8.39}$$

and have reintroduced Planck's constant $\hbar$ and the permeability μ_0. As the temperature is lowered, the one-gap model becomes less valid and our full numerical calculations cannot be compared with any analytic qualitative result. Because Fig. 112 shows that $g(t)$ becomes rather flat as $t\to 0$, it seems reasonable to extrapolate to zero temperature from our lowest temperature, which was $t=0.01$. If we do this, we get $g(0)=0.67$.

The London penetration depth given by the full equation (8.7) can also be related to the universal function $g(t)$ given in (8.38). Referring to (8.35), we obtain, in the asymptotic limit

$$\lambda_L^{-2}(t)=\frac{e^2\mu_0 n}{m\lambda t 2\pi\bar{T}_c}g^{-2}(t) . \tag{8.40}$$

Note the extra factor of t in the denominator of (8.40). Thus

$$\frac{\sqrt{n}\ \lambda_L(t)}{\sqrt{\lambda}}=1.274\bar{\Lambda}\sqrt{t}\ g(t) , \tag{8.41}$$

where

$$\bar{\Lambda}=0.5317\times 10^{-7}\,\text{m}\left[\frac{10^{22}}{\text{cm}^3}\right]^{1/2}$$

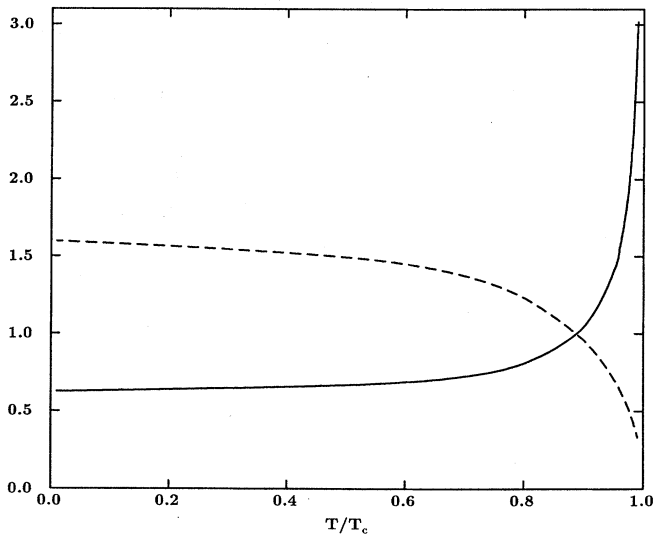

FIG. 112. Universal dimensionless function $g(t)$ (solid line), which determines the temperature dependence of the local penetration depth in the asymptotic limit. The inverse function $g^{-1}(t)$ (dashed curve) is also shown. While our calculations are valid only for $\sqrt{\lambda}t \gg 1$, and so $t>0$ for any large but finite value of λ, the curves for g and g^{-1} are flat over a large temperature range around $t\to 0$; so the value of $g(0)$ can probably be obtained safely by extrapolation of our lowest temperature results ($t=0.01$) on the assumption that at yet lower temperatures the behavior does not change unexpectedly.

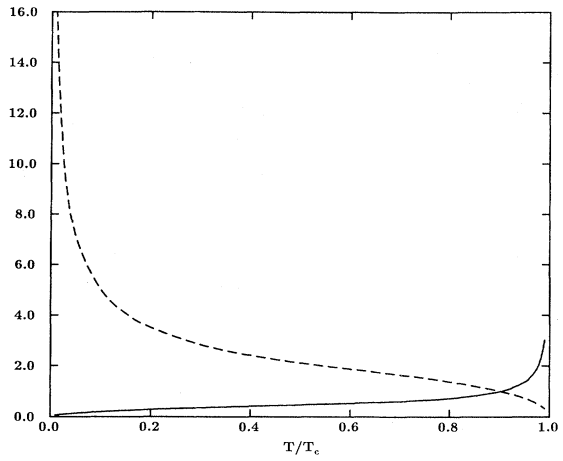

FIG. 113. Universal dimensionless function $\sqrt{t}\,g(t)$ (solid line) and its inverse (dashed line) that determine, respectively, the reduced temperature dependence of the London penetration depth and of its inverse. The calculations are valid only for $\sqrt{\lambda}\,t \gg 1$; so for any large but finite value of λ, we need $t > 0$. Nevertheless, the curve for $\sqrt{t}\,g(t)$ indicates that as $t \to 0$, this function appears to go smoothly to zero as $0.67\sqrt{t}$ at least up to $t = 0.01$.

is the classical penetration depth first introduced by London. The function $\sqrt{t}\,g(t)$ is given in Fig. 113 as is its inverse. The very low temperature dependence of this function is very interesting. While our work is restricted to the asymptotic region with $\sqrt{\lambda}\,t \gg 1$ and so to $t > 0$ for any large, but fixed value of λ, we see again that $\sqrt{t}\,g(t)$ appears to be well behaved as $t \to 0$ and seems to go towards zero. On the other hand, the inverse function, and therefore $\lambda_L^{-1}(t)$, goes to ∞ like $1/\sqrt{t}$ as $t \to 0$. This is a completely different behavior from BCS and is characteristic of the asymptotic limit. It is valid for any finite impurity content and does not map directly into our previous results for the local limit. A word of explanation is perhaps in order. If we assume πt^+ to dominate in the $Z(i\omega_n)$ channel, then, as we have demonstrated, the London limit goes into the local limit. But in the asymptotic limit, we first assume $\lambda \to \infty$; and so any added πt^+ term in the equation for $Z(i\omega_n)$ can be dropped because the second term in

$$Z(i\omega_n) = 1 + \frac{\pi \bar{T}\lambda}{\sqrt{\bar{\omega}_n^2 + \bar{\Delta}_n^2}} + \frac{\pi \bar{T}}{\bar{\omega}_n} \sum_{m \neq n} \lambda(m-n) \frac{\bar{\omega}_m}{\sqrt{\bar{\omega}_m^2 + \bar{\Delta}_m^2}} + \pi \bar{t}^+ \frac{1}{\sqrt{\bar{\omega}_n^2 + \bar{\Delta}_n^2}} \tag{8.42}$$

dominates over the last because $\bar{T}\lambda \gg \bar{t}^+$ for finite t^+. It is a question of which limit is taken first. The "physical" limit is $\bar{T}\lambda \gg \bar{t}^+$ for which the electron-boson scattering dominates over any impurity scattering.

Finally, we look at the asymptotic limit of the coherence length given by Eq. (8.10). Noting that as $\lambda \to \infty$, $Z(i\omega_n)$ can be approximated by Eq. (8.34), we obtain immediately

$$\xi(t) = \frac{v_F \hbar}{2\pi T \lambda} . \tag{8.43}$$

But $T_c = 0.183\sqrt{\lambda}\,\omega_E$ and so

$$\xi(t) = \frac{0.87 v_F \hbar}{\omega_E \lambda^{3/2} t} , \tag{8.44}$$

which is to be contrasted with the approximate result (8.36) valid only for $t = 1$ and, in which case, the numerical factor is 1 rather than 0.87. We note that (8.44) was derived (as for all other formulas in this paper) under the approximation $\sqrt{\lambda}\,t \gg 1$, so that the $1/t$ factor is not a problem.

IX. MAINLY ABOUT THE OXIDES

A. Phonons and high T_c

An argument that is often put forward as evidence that a phonon mechanism cannot be operative [Anderson (1987); Anderson *et al.* (1987)] in the oxide superconductors, in contrast to conventional cases, is based on the simple BCS equation (2.12) for T_c, which we repeat here:

$$k_B T_c = 1.13 \hbar \omega_c \exp\left[-\frac{1+\lambda}{\lambda - \mu^*} \right] . \tag{9.1}$$

The critical temperature $k_B T_c$ has units of energy, and Eq. (9.1) shows that its scale is set by the characteristic exchange boson energy ω_c. Thus if the factor ω_c were to be replaced by an electronic energy that is measured in eV rather than by a phonon energy with magnitude of order 10 meV or so, the critical temperature could be much larger than for a phonon mechanism. This argument, of course, assumes that the range of possible values taken up by the exponent $(1+\lambda)/(\lambda - \mu^*)$ in Eq. (9.1) is roughly comparable for different classes of materials with different mechanisms. That this be so is not at all guaranteed. While the above argument is appealing, it is important to realize that a phonon mechanism cannot be ruled out on the basis of the size of T_c alone. We have already seen in Sec. II, and it is worth repeating here, for emphasis, that for a phonon mechanism with optimum frequency $\omega_E^* = d(\mu^*)A$, $T_c = c(\mu^*)A$, and $\lambda^* = 2A/\omega_E^* = 2/d(\mu^*)$. For $\mu^* = 0.1$, $c(\mu^*) = 0.175$, and $d(\mu^*) = 1.3$, which implies $\lambda^* = 1.54$ and a T_c value of

$$T_c = \frac{c(\mu^*)}{d(\mu^*)} \omega_E^* = 0.135 \omega_E^* . \tag{9.2}$$

In the oxide superconductors, the phonon spectrum extends up to 100 meV, and formula (9.2) gives $T_c \simeq 160$ K

assuming, of course, that the coupling is strong (large A) and exclusively to these high-energy phonons. While an $A \cong 77$ meV is very large compared with our experience in conventional cases, the necessary value of λ is modest and not unusual.

There are other ways to achieve a high value of T_c within a phonon model. For a start, an electron-phonon spectral density $\alpha^2F(\omega)$ has been calculated by Weber (1987a, 1987b) for the case of La-Sr-Cu-O. The calculations are based on the first-principles energy-band results of Mattheiss (1987) and the nonorthogonal tight-binding theory of lattice dynamics developed by Varma and Weber (1979). This framework is highly sophisticated and has proven quite successful in describing the A15 compounds (Weber, 1984a, 1984b). The spectrum obtained in this way is shown as the dashed curve of Fig. 114. It gives a value of T_c equal to 36 K for a standard value of $\mu^*=0.13$ and the value of $\lambda=2.6$. This last quantity is somewhat larger than that found in conventional cases, but not unreasonably so.

Ashauer *et al.* [Ashauer, Lee, and Rammer (1987); Ashauer, Lee, *et al.* (1987); Rammer (1988b, 1989)] have done may additional calculations of T_c applicable to the oxides within an electron-phonon framework [see also Marsiglio and Carbotte (1987c)]. They employ a variety of possible choices for the spectral density, and some of their results are given in Table XV. Besides the result based on Weber's spectrum mentioned above, they consider using for $\alpha^2F(\omega)$ a constant, chosen to give a $T_c=35$ K, times the measured incoherent inelastic neutron-scattering generalized phonon frequency distribution $G(\omega)$ obtained by Renker *et al.* (1987). Additional measurements have been done by Ramirez, Batlogg,

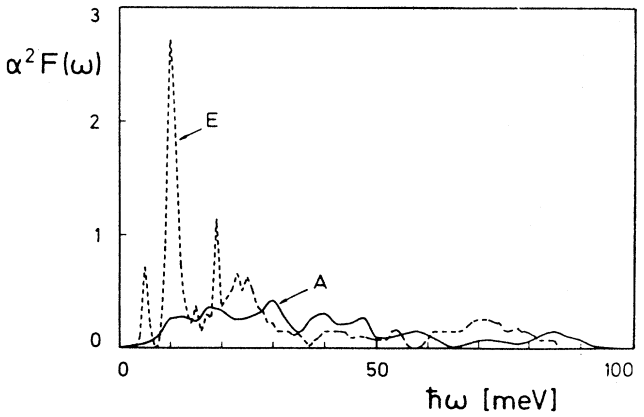

FIG. 114. Spectrum E (dashed curve) is the theoretical Eliashberg function for $La_{1.85}Sr_{0.15}CuO_4$ calculated by Weber (1987a, 1987b). Spectrum A (solid curve), which is given by comparison, is based on the generalized phonon frequency distribution $G(\omega)$ of Renker *et al.* (1988) and gives $T_c=35$ K with $\mu^*=0.0$ [from Ashauer, Lee, and Rammer, (1987)].

TABLE XV. Phonon models for oxides.

	T_c	λ	μ^*
Weber	35	2.6	0.13
$\alpha^2F(\omega)$	91	8.6	0.13
Generalized	35	1.2	0
phonon frequency	35	1.9	0.2
distribution $G(\omega)$	91	3.4	0
	91	5.3	0.2

Aeppli, *et al.* (1987a) and by Brun *et al.* (1987) for the La-Cu-O family; and by Renker *et al.* (1988), Rhyne *et al.* (1987), Bruesch and Buhrer (1988), and Strobel *et al.* (1988) in the Y-Ba-Cu-O family.

The $G(\omega)$ (solid curve) is compared with Weber's $\alpha^2F(\omega)$ (dashed curve) in Fig. 114. The solid curve is considerably harder than the dashed curve which, displays much more weight at lower energies. For the harder spectrum, we see in Table XV that the λ value required to get 35 K is only 1.2 for $\mu^*=0.0$ and 1.9 for $\mu^*=0.2$, to be compared with 2.6 when Weber's calculated spectrum is used. At the present time there is little compelling evidence to prefer one spectrum over the other. Having said this, we point out that the calculations of Weber predict a lattice instability near $La_{1.85}Sr_{0.15}CuO_4$ that is not observed. This is a limitation of his work that we shall return to later. If we consider the case of a 90-K superconductor, Table XV shows that a very large value of λ is needed for a scaled Weber (1987a, 19878b) spectrum (8.6) while a value of $\lambda=3.4$ is sufficient when $G(\omega)$ is used instead. Even smaller values of λ result if the coupling to the higher-energy modes in $G(\omega)$ is preferentially emphasized. To our knowledge there exist no rigorous calculations at present that rule out such values of λ on the basis of lattice stability. It is clear therefore, from the above, that values of T_c of the order of magnitude seen in the oxides with present maximum of 125 K can naturally be accommodated within Eliashberg theory and a pure phonon model, taking note that the theory itself does not address the important question of lattice stability. The need for a new mechanism, if it is required and indeed it is, is to be found elsewhere.

B. Oxygen isotope effect for La-Sr-Cu-O

An argument that is often put forward against an electron-phonon mechanism for the oxides is the partial isotope effect on the oxygen (β_{ox}). This quantity has now been measured by several authors and a useful summary is found in the recent paper by Katayama-Yoshida *et al.* (1988). We consider first the case of La-Sr-Cu-O, and later we shall deal with Y-Ba-Cu-O. The oxygen isotope effect in La-Sr-Cu-O appears to have first been reported almost simultaneously by Batlogg, Cava, *et al.* (1987), who find $\beta_{ox}=0.16\pm0.02$, and by Faltens *et al.* (1987).

In this second paper, the authors find considerable variation with sample, $\beta_{ox}=0.22$ in one case and $\beta_{ox}=0.13$ in another. Their final conclusion is that β_{ox} is not smaller than 0.10 and may possibly be as large as 0.37. A subsequent determination by Bourne *et al.* (1988) reduces the unertainty in the previous work and finds $\beta_{ox}=0.14\pm0.08$. On the other hand, zur Loye *et al.* (1987) quote a value of $\beta_{ox}=0.31$. It is clear from this summary that β_{ox} in La-Sr-Cu-O is significant and probably of the order 0.2.

Weber [Batlogg, Kourauklis, *et al.* (1987)] has calculated the oxygen isotope effect in La-Sr-Cu-O on the basis of his model electron-phonon spectral density. He finds that changing all the isotope masses on the oxygens in the Cu-O planes gives a theoretical value of $\beta_{ox}=0.3$, which is 50 percent larger than our preferred experimental value although, as we have seen, one experiment gives a value that is even larger than the theoretical estimate. It is important to understand clearly that it cannot be concluded from this 50-percent discrepancy that another mechanism besides phonons must be operative in this system. All it means is that, in Weber's spectrum, there is more coupling to the oxygen modes than is indicated in present experiments. In principle, any value of β_{ox} between 0 and 0.5 is compatible with a phonon mechanism, since its actual value depends on the relative coupling to oxygen as opposed to other modes. For $\beta_{ox}=0$ there is no coupling to oxygen, while for $\beta_{ox}=0.5$ there is no coupling to the remaining modes.

C. Analysis of partial isotope effect

A detailed theoretical discussion of β_{ox} has been given by Ashauer, Lee, Rainer, and Rammer (1987). These authors introduce a function $B(\omega)$ that is an integrated differential isotope coefficient $\beta(\omega)$ defined by

$$B(\omega)=\int_{\omega}^{\infty} d\omega'\beta(\omega') , \tag{9.3}$$

where $\beta(\omega)$ is given by (2.63) and represents the contribution to the isotope effect comining from the phonon modes that fall in the energy range between ω and $\omega+d\omega$. Thus $B(\omega)$ gives the contribution coming from all the phonon modes between (ω and ∞).

In Fig. 115, we display the results obtained by Ashauer, Lee, and Rammer (1987) for a 35-K superconductor. The curves shown all occur in pairs, with the solid lines applying to a model with $\mu^*=0$ and the dashed curves for $\mu^*=0.3$. The first set of two curves labeled by A035 and A335, with the first digit referring to the value of μ^* and the last two to the T_c value, makes use of the measured phonon frequency distribution $G(\omega)$ for La-Sr-Cu-O shown in Fig. 114 (solid curve).

From the definition (9.3), $B(0)$ corresponds to the total isotope effect, which is exactly $\frac{1}{2}$ for the model with $\mu^*=0.0$ and somewhat less for $\mu^*=0.3$. As ω is increased, $B(\omega)$ must decrease, and the value at $\omega/\omega_{max}\cong0.5$ is taken by Ashauer *et al.* as representative

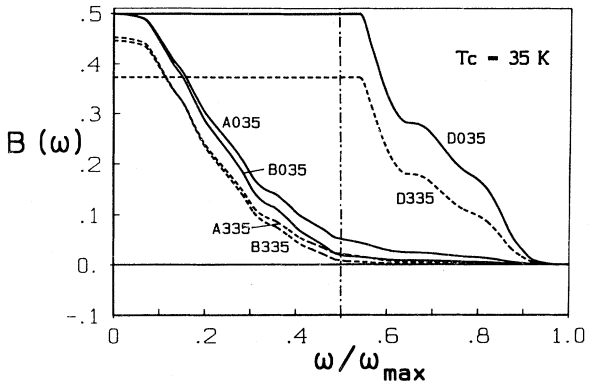

FIG. 115. Calculated isotope effect for a 35-K superconductor. The function $B(\omega)$ yields the total isotope effect at $\omega/\omega_{max}=0.0$ and the oxygen isotope effect at $\omega/\omega_{max}\cong0.5$ (chain-dotted curve). Different curves refer to different model spectra as defined in Ashauer, Lee, and Rammer (1987a) with $\mu^*=0$ (solid curves) and $\mu^*=0.3$ (dashed curves). From Ashauer, Lee, Rainer, and Rammer (1987).

of the oxygen isotope effect on the assumption that all the phonon modes in $G(\omega)$ beyond this frequency represent oxygen motion. This would be the case for a light mass in a one-dimensional lattice. Some evidence for this separation can be found in the Born–von Kármán analyses of Renker *et al.* (1987) based on the generalized phonon frequency distribution in La-Sr-Cu-O shown in Fig. 114 (solid curve). While approximately true, such an idea is not borne out in detail in the shell-model calculations of de Wette *et al.* (1988), who find that some shifting in the lower frequency range always accompanies an oxygen mass change. This is also found in the work of Weber (1987a, 1987b). Keeping this limitation in mind, we, nevertheless, proceed with the model suggested by Ashauer *et al.* because several important points about the partial oxygen isotope effect can be nicely illustrated within this model.

First, for a model based on a constant times $G(\omega)$, which weighs all phonon modes equally, the partial isotope effect β_{ox} is considerably less than the value obtained in Weber's model and is, in fact, lower than the experimental value. Since at this point there is no compelling reason to favor one spectral density over the other, as we have alrady stated, it is clear that to get a model $\alpha^2F(\omega)$ with an oxygen isotope effect equal to the measured value, it is only necessary to assume that the oxygen modes in $G(\omega)$ (assumed to be all phonons above 50 meV) are somewhat more strongly weighted in $\alpha^2F(\omega)$ than are the remaining modes. This could easily be arranged but is premature since the experimental value of β_{ox} remains somewhat uncertain as these are difficult experiments. Furthermore, an infinite number of choices are possible. In model B of Fig. 115, the coupling to the oxygen modes is reduced even further, compared with model A and with Weber's spectrum. This, of course,

gives an even smaller value of β_{ox} and is of little interest as a quantitative model for La-Sr-Cu-O. It does serve to emphasize, however, that the existence of a very small isotope effect β_{ox} on the oxygen mass alone is in no way inconsistent with phonon superconductivity. It simply implies that the coupling to these modes is small. Of course, if the high-energy phonon modes are not importantly involved, we can expect that fairly large values of λ are needed compared with a model in which we are mainly coupled to these modes. This is indeed so for model B compared with A for which $\lambda=1.3$ and 2.0 when $\mu^*=0.0$ and 0.3, respectively. These values are to be compared with 1.2 and 1.9 for model A and the still much smaller values associated with model D, in which we assume coupling only to the oxygen modes beyond 50 meV in $G(\omega)$, and for which $\lambda=0.4$ and 0.9, respectively. For such a model (D), the oxygen isotope effect is large (see Fig. 115), as we might have expected, and is about 0.37 for $\mu^*=0.3$. It is also equal to the total isotope effect. This value for β_{tot} is small compared with a typical value of β for conventional strong coupling. This is not surprising, however, since in model D λ is relatively large. In such a case, we expect from Fig. 115 a value of β_{tot} significantly suppressed below 0.5.

It is clear from the discussion so far that La-Sr-Cu-O has a significant phonon contribution but that a unique model for the electron-phonon spectral density cannot be deduced from a knowledge of β_{ox} alone in the absence of additional constraining information. Knowledge of the total isotope effect would help, although some important ambiguity would still remain, as we shall soon illustrate. In any case, to our knowledge, the La and Cu partial isotope effects have not been measured for La-Sr-Cu-O. In Weber's model, one gets $\beta_{La}=0.02$ and $\beta_{Cu}=0.165$ for a total isotope effect of $\beta_{tot}=0.49$, which is conventional for a strong-coupling superconductor with $\lambda=2.6$ and $\mu^*=0.12$. There is nothing unusual with these values and we have a definite prediction that could be tested. Even if all partial isotope effects were known experimentally, there would still be many ways of modifying the calculated $\alpha^2F(\omega)$ of Weber to accommodate wide variations in these coefficients.

It might be argued that a pure phonon model could be eliminated if β_{tot} were found to be wildly reduced from 0.5, but this could, alternatively, simply indicate a very large value of μ^*, as we saw illustrated in the case of model D.

D. Isotope effect in joint mechanism

An alternative way of obtaining a reduced value for β_{tot} would be to introduce a joint phonon-plus-excitonic mechanism. Here we use the word excitonic in a very general sense and include any boson-exchange mechanisn in which the bosons involved do not depend on the isotopic mass M. If they are assumed to be of high energy compared with T_c, as seems reasonable, we can accommodate them in our theory through an effective μ^* that is negative and represents the sum of the pairing potential for the additional mechanism $N(0)V$ and the Coulomb repulsion μ^*, namely,

$$\mu^*_{eff}=-N(0)V+\mu^* \ . \tag{9.4}$$

For $\mu^*_{eff}=0$, we get a total isotope effect of $\beta_{tot}=0.5$; for μ^*_{eff} dominant over the phonon part, $\beta_{tot}\cong 0.0$. In between, any value of β_{tot} can be reached. At the present time, isotope effect measurements, while helpful and of interest, do not differentiate clearly between a large μ^* and a joint mechanism; we need to examine other evidence, such as the observed thermodynamics and other properties of the superconducting state, to distinguish between various possibilities. Before doing so, it is important to point out that other more exotic effects than the ones considered here can affect the isotope coefficient β, although, at present, our knowledge of these is at best qualitative.

E. Other problems with isotope effect

Energy dependence in the electronic density of states $N(\epsilon)$ on the scale of ω_c can have an important influence on superconductivity [(Lie and Carbotte (1980); Mitrović and Carbotte (1983a, 1983b)] and, in particular, on T_c. This is easily understood within BCS theory. In this model, the pairing potential is taken to be a constant V within $\pm\hbar\omega_c$ of the Fermi energy, and only those electronic states that fall within this energy range participate in the superconducting state. If $N(\epsilon)$ is constant over $\pm\hbar\omega_c$, the information on the states involved is carried by the factor $N(0)$ but, at the very least, some average of $N(\epsilon)$ in the interval ($-\hbar\omega_c$ to $\hbar\omega_c$) is needed when $N(\epsilon)$ varies. As ω_c changes because of changes in ionic mass M, this average will change, since different values of $N(\epsilon)$ will be involved. The isotope effect will therefore be changed by $N(\epsilon)$ and depend on the detail of its energy variation [Combescot and Labbé (1988)].

Another effect not included in Eliashberg theory that can change the isotope coefficient are anharmonic corrections. These have been discussed most recently by Dreschsler and Plakida (1987, 1988). A related effect, but more specific to the oxides, has been described by Phillips (1987). On the other hand, Fisher *et al.* (1988) have considered how zero-point motion can change β. All these are interesting possibilities, but the theory of these effects is not yet well developed and much work remains to be done before a definitive assessment of their relative importance is available.

We turn next to other properties of the superconducting state. For this task we shall start with Weber's spectrum even though, as we have pointed out, it predicts an oxygen isotope effect about 50 percent larger than the measured value. Other deficiencies of the model have been summarized by Pickett (1989). Here we mention only one. It predicts a structural transition just beyond

the composition 15 percent Sr to be due to a soft breathing mode, while Birgeneau *et al.* (1987) find that it is due to a soft tilt mode. Nevertheles, Weber's $\alpha^2F(\omega)$ can still serve as a useful basis for a first attempt at a comparison of predicted superconducting properties with experimental results with an aim at obtaining information on mechanism. Schossmann, Marsiglio and Carbotte (1987) present results of extensive calculations of this kind, which we now review.

F. Thermodynamics for La-Sr-Cu-O, experimental uncertainties

In Table XVI, we enter the values obtained for certain conventional parameters useful in characterizing the spectrum and also give results of Eliashberg calculations for the dimensionless quantities $2\Delta_0/k_BT_c$, $\Delta C(T_c)/\gamma T_c$, $\gamma T_c^2/H_c^2(0)$, and $h_c(0)$. These are the gap-to-critical-temperature ratio, the specific-heat jump normalized to its "normal-state value," the Sommerfeld constant γ times the square of the critical temperature divided by the square of the zero-temperature thermodynamic critical magnetic field, and the reduced thermodynamic critical field, respectively. Also entered in brackets for comparison are the BCS values. On comparison of these two sets of values, we conclude that if La-Sr-Cu-O is a phonon superconductor, it will behave in a significantly different way from a BCS superconductor, and if the apppropriate quantities are measured, we should be able to get important information on mechanism. Unfortunately, the experimental situation is far from satisfactory at this time. First, all properties involving normal-state Sommerfeld constant γ have not been measured with any reliability because γ is difficult to obtain. The critical temperature is sufficiently high that the normal-state specific heat at this temperature is dominated by the phonon contribution, which is not well known since a Debye model is not adequate. Furthermore, the critical magnetic fields are so large at low temperature that it is impossible to force the material to become normal and hence to measure γ directly. Another possibility is to use the Pauli susceptibility. Unfortunately, a Stoner enhancement factor also enters this quantity [Salamon and Bardeen (1988)], which is not well known but may be large. In a recent estimate, Jaffe (1989) suggests that it could be as large as a factor of 2. The derived electronic density-of-states factor is therefore quite uncertain. Yet another method is to derive γ from the slope of the upper critical magnetic field, but this also requires an analysis, which can lead to significant errors, as we shall discuss in some detail later. Furthermore, there is no consensus, at the moment, as to the exact experimental value of the slope, as can be seen in Table XVII (see also Table XVIII) for Y-Ba-Cu-O).

The general conclusion of all this is that γ is not well known at the moment because of experimental uncertainties and because of the need to extract it indirectly from data through a model-dependent analysis. A similar situation holds for the ratio $2\Delta_0/k_BT_c$. Considerable controversy remains about the value of the gap, as can be seen in Table XVII where we have compiled data as of the spring of 1988 [Marsiglio (1988)]. Inclusion of more recent data does not change the general picture. Far-infrared measurements tend to give values of the gap ratio near BCS although Timusk and Tanner (1989) have presented arguments that appear to invalidate much of the analysis on which these values depend. In general, tunneling measurements give values that are rather higher, although there are a few exceptions. Another problem is that La-Sr-Cu-O is very anisotropic in its normal-state properties, so the gap is expected to be highly anisotropic, making it difficult to compare experimental results with the theoretical prediction of Table XVI. Another difficulty with tunneling is that the coherence length perpendicular to the CuO planes is very short, and tunneling typically probes only within one coherence length of the surface. On this scale, the surface could well not be representative of the bulk. In view of these limitations, it may not be surprising that tunneling results tend to be quite erratic, even from measure-

TABLE XVI. Characteristics and predictions based on Weber's spectrum for $\alpha^2F(\omega)$ in La-Sr-Cu-O.

T_c	λ	μ^*	A	$\omega_{\ln}$	$T_c/\omega_{\ln}$	γ
35 K	2.6	0.14	22.0 meV	14.0 meV	0.23	6.1 mJ/(mol K^2)

$\frac{\Delta C(T_c)}{\gamma T_c}$	$\frac{2\Delta_0}{k_BT_c}$	$\frac{\gamma T_c^2}{H_c^2(0)}$	$h_c(0)$	$\Delta C(T_c)/T_c$
2.8(1.43)	5.3(3.54)	0.124(0.168)	0.48(0.58)	17 mJ/(mol K^2)

$-\frac{dH_c(T)}{dT}\Big\|_{T_c}$ $\left[\frac{\text{mT}}{\text{K}}\right]$
17

ments at different spots on the same sample. Anomalous structure is also seen in some I-V curves, and the gap edge is never completely well defined with some leakage current into the gap region, of origin as yet uncertain. In some interpretations, the far-infrared measurements also give significant absorption below twice the gap value where there should be none. This possibly indicates the existence of states within the gap, which would make any interpretation of the data less clear. For all these reaons, no definitive conclusions can be reached at this time based on the theoretical predictions of Table XVI. All that can be said, after careful consideration of the available data, is that $2\Delta_0/k_BT_c$ in La-Sr-Cu-O is possibly lower than the 5.3 value predicted on the basis of Weber's spectrum [Carbotte and Marsiglio (1989)]. This would favor a joint phonon-plus-exciton mechanism as does β_{ox}, in one interpretation at least. It could also mean that a harder spectrum is favored over that calculated by Weber, as is indicated from inelastic incoherent neutron measurements of the generalized frequency distribution $G(\omega)$.

The specific-heat jump at T_c [$\Delta C(T_c)$] has been measured by several groups. There is, unfortunately, considerable disagreement for this measurement as well (see Table XVII). It is clear that there is significant sample dependence. This is exemplified by the fact that while the normal-state resistivity remains linear up to T_c in some samples, in others there is an upturn before the material becomes superconducting. Furthermore, many of the experimental results were obtained on polycrystalline

TABLE XVII. Experimental results for LaSrCuO.

(a) Gap to critical temperature ratio

$\frac{2\Delta_0}{k_BT_c}$	Reference
2.4	Walter *et al.*, 1987
1.6–2.7	Sulewski, Sievers, *et al.*, 1987
2.5	Schlesinger, Collins, Kaiser, and Holtzberg, 1987
2.9–4.5	Bonn *et al.*, 1987
5.2–9.1	Hawley *et al.*, 1987
<4.5	Kirtley, Tsuei, Park, Chi, Rozen, and Shafer, 1987
5–8.7	Pan, Ng *et al.*, 1987
4.07–4.78	Ekino *et al.*, 1987
4.5–5.8	Moreland, Clark *et al.*, 1987
3–6	Leiderer *et al.*, 1987
3.5–4.0	van Bentum, van de Leemput *et al.*, 1987
0.7–2.7	Degiorgi *et al.*, 1987
8–18	Naito *et al.*, 1987
2.6	Sulewski, Noh *et al.*, 1987
1.3±0.2	Lee *et al.*, 1987
5	Zavaritzky *et al.*, 1987
4.7	Sato *et al.*, 1987
7±2	Pan, Ng, and de Lozanne, 1987
2 (c axis)	Schlesinger, 1987

(b) Slope of the upper critical field

$\lvert H'_{c2}(T_c)\rvert$ (T/K)	Reference
2.2–5.0	Orlando *et al.*, 1987a
1.51	Kwok *et al.*, 1987
1.7	Okuda *et al.*, 1987a
2.7–6.0	Kobayashi *et al.*, 1987
0.3∥, 4⊥	Hidaka, Enomoto, Suzuki, Oda, and Murakami, 1987
1.8	Nakao *et al.*, 1987a
2.13	Capone *et al.*, 1987
1.3–4.0	Osofsky *et al.*, 1987
2	Zavaritsky *et al.*, 1987

(b) Slope of the upper critical field

$\lvert H'_{c2}(T_c)\rvert$ (T/K)	Reference
2.1±0.1	Braginski *et al.*, 1987
2.2	van Bentum, van Kempen *et al.*, 1987
2.0–3.7	Renker *et al.*, 1987

(c) Specific-heat jump at T_c

$\frac{\Delta C(T_c)}{T_c}\left[\frac{\text{mJ}}{\text{mol K}^2}\right]$	Reference
7.6±1.8	Batlogg, Raminz *et al.*, 1987
20±5	Dunlap *et al.*, 1987
16.8	Decroux *et al.*, 1987
8.8	Finnemore *et al.*, 1987
22–26	Kitazawa, Atake, Ishii *et al.*, 1987
11	Uchida, Takagi, Kitazawa, and Tanaka, 1987; Uchida, Takagi, Hasegawa *et al.*, 1987
9.9	Phillips *et al.*, 1987
10±2	Ramirez, Batlogg, Aeppli *et al.*, 1987
6.5	Bourne, Zettl *et al.*, 1987

(d) Band-structure density of states

$N_B(E_F)\left[\frac{\text{states}}{\text{eV Cu-atom spin}}\right]$	Reference
0.66	Mattheiss, 1987
0.6 (0.95)[a]	Freeman *et al.*, 1987
0.82	Temmerman *et al.*, 1987
0.82	Takegahara *et al.*, 1987
0.62 (1.08)[a]	Papaconstantopoulos *et al.*, 1987
0.83	Fujiwara and Hatsugai, 1987
1.03	Oguchi, 1987

[a]With doping $x=0.15$.

samples. There is evidence that while the superconductivity is bulk, it is not, by any means, always 100 percent bulk. There can be both metallic and insulating components present. Moreover, the granularity of the samples can vary, and this feature can affect superconducting properties. Keeping these limitations in mind, on careful analysis of the available data given in Table XVII, which covers the period up until the spring of 1988 only but is sufficient for our present purpose, Carbotte and Marsiglio (1989) come up with a preferred experimental value of 17 mJ/(mol K^2) for $\Delta C(T_c)/T_c$ in La-Sr-Cu-O. This value, however uncertain, can be used in conjunction with our theoretical prediction of $\Delta C(T_c)/\gamma T_c = 2.8$ to extract a value of the normal-state Sommerfeld constant and use it

TABLE XVIII. Experimental results for YBaCuO.

(a) Gap-to-critical-temperature ratio

$\frac{2\Delta_0}{k_B T_c}$	Reference
3.5±0.3	Genzel *et al.*, 1987
3.5	Thomas, Bhatt *et al.*, 1987
3.7–5.6	Kirtley, Collins *et al.*, 1987
1.6–3.4	Kirtley, Collins *et al.*, 1987
2.3–3.5	Thomas, Ng *et al.*, 1987
2.5–4.2	Wrobel *et al.*, 1987
1.3±0.2	Lee *et al.*, 1987
3.3	Vuong *et al.*, 1987
3.2	Bonn, Greedan *et al.*, 1987
11	Ng *et al.*, 1987
4.5–6.0⊥	Kirtley, Collins *et al.*, 1987
3.9–4.8∥	Kirtley, Collins *et al.*, 1987
4.8	Moreland, Ekin *et al.*, 1987
3.8–4.5	Ekino and Akimitsu, 1987
10	Iguchi *et al.*, 1987
13	Kirk *et al.*, 1987
3.9	Crommie *et al.*, 1987
3.2±0.4	van Bentum, van Kempen *et al.*, 1987
7–13	Escdero *et al.*, 1987
3.5	Thomas, Ng *et al.*, 1987
5±0.2	Polturak *et al.*, 1987
3.4±1.5	Lyons *et al.*, 1987
4.8±0.5	Barone *et al.*, 1987
~8	Schlesinger, Collins, Kaiser, and Holtzberg, 1987
75	Zavaritsky *et al.*, 1987
3.9	Tulina *et al.*, 1987
3.8	Bazhenov *et al.*, 1987

(b) Slope of the upper critical field

$\lvert H'_{c2}(T_c)\rvert$ (T/K)	Reference
1.3 (50%)	Wu, Ashburn *et al.*, 1987
3 (10%)	Wu, Ashburn *et al.*, 1987
2.5 (50%)	Ramirez, Batlogg, Cava *et al.*, 1987
1.2	Muto *et al.*, 1987
2.4	Muto *et al.*, 1987
2.3∥, 0.46–0.71⊥	Worthington *et al.*, 1987
4.6 (10%)	Junod *et al.*, 1987
0.6 (0%)	Junod *et al.*, 1987
1.25	Song *et al.*, 1987
3.8 (50%)	Takita *et al.*, 1987
1.0 (1%)	Takita *et al.*, 1987

(b) Slope of the upper critical field

$\lvert H'_{c2}(T_c)\rvert$ (T/K)	Reference
2.35 (50%)	Okuda *et al.*, 1987b
0.37⊥ (50%)	Hidaka, Enomoto, Suzuki, Oda, Katsui, and Murakami, 1987
1.95∥ (50%)	Hidaka, Enomoto, Suzuki, Oda, Katsui, and Murakami, 1987
2.2 (50%)	Apfelstedt *et al.*, 1987
1.8 (50%)	Nakao *et al.*, 1987b
2.2–3.6 (50%)	Fuller *et al.*, 1987
1.75 (50%)	Schinder *et al.*, 1987
5.3 (10%)	Schinder *et al.*, 1987
3∥, 0.9⊥ (100%)	Iye *et al.*, 1987
1.27 (50%)	Takabatake *et al.*, 1987
4.7 (90%)	Ousset *et al.*, 1987
1.9±0.2	Braginski, 1987
1.3 (50%), 5 (onset)	Orlando *et al.*, 1987b
1.9 (50%)	Panson *et al.*, 1987
2.9 (50%)	Orlando *et al.*, 1987c
5.3 (90%)	Orlando *et al.*, 1987c
3±0.3	Laborde *et al.*, 1987

(c) Specific-heat jump at T_c

$\frac{\Delta C(T_c)}{T_c}\left[\frac{\text{mJ}}{\text{mol K}^2}\right]$	Reference
18	Nevitt *et al.*, 1987
15.5	Inderhees *et al.*, 1987
1.32	Zhaojia *et al.*, 1987
16	van Miltenburg *et al.*, 1987
7	Kitazawa, Atake, Kisho *et al.*, 1987
11±2	Li *et al.*, 1987
23±5	Ayache *et al.*, 1987
13	Junod, Bezinge *et al.*, 197
20	Beckman *et al.*, 1987

(d) Band-structure density of states

$N_B(E_F)\left[\frac{\text{states}}{\text{eV Cu-atom spin}}\right]$	Reference
1.5	Mattheis and Hamann, 1987
0.56 (0.4)[a] (0.26)[b]	Massida *et al.*, 1987
1.1 (0.92–0.97)[c]	Herman *et al.*, 1987

[a] $y=0.1$.
[b] $y=0.2$
[c] $y=0.5$.

to investigate the consistency of the data with strong-coupling theory. The value of γ extracted in this way is 6.1 mJ/(mol K^2), which is consistent with some of the other estimates found in the literature. We can calculate from γ a value for the single-spin electronic density of states $N(0)$ at the Fermi energy. A useful formula to accomplish this aim is

$$N(0)\left[\frac{\text{states}}{\text{eV f.u. spin}}\right]=\frac{0.212}{1+\lambda}\gamma\left[\frac{\text{mJ}}{\text{mol K}^2}\right]. \quad (9.5)$$

The value for $N(0)$ obtained from (9.5) for our favored value of γ is $N(0)=0.36$ states/(eV f.u. spin). If we assume that all the important electron-electron correlation effects are included in the band-structure calculations for La-Sr-Cu-O, we can compare the above value with band-structure results. The band-structure density of states, in the parent undoped compound La_2-Cu-O_4, has been obtained by several groups, and some results are summarized in Table XVII. A first objection to this table is that band structure predicts a metal with half-filled band, while, experimentally, La_2CuO_4 is an antiferromagnetic insulator. However, as doping is introduced, the metallic stage is reached before superconductivity sets in, and it can be argued that band-structure theory then becomes valid. From Table XVII, it is clear that there is general agreement that $N(0)\cong 0.65$ states/(eV f.u. spin) when the doping is not accounted for. Two values entered in brackets in Table XVII(d) include doping in a rigid-band model. Freeman *et al.* (1987) and Papaconstantopoulos *et al.* (1987) find for $La_{1.85}Sr_{0.15}CuO_4$ 0.95 and 1.1 states/(eV f.u. spin), respectively. These values are 3 times larger than our value estimated on the basis of specific-heat data and Weber's $\alpha^2F(\omega)$ spectrum. This argues for a smaller λ value in $La_{1.85}Sr_{0.15}CuO_4$, which could be achieved through a hardening of the electron-phonon spectrum with more coupling to the higher frequency modes than is indicated in Weber's work, or it could mean that we have a joint phonon-excitonic mechanism. The first possibility is rather mundane in the present context, and the theory developed in previous sections would apply without modification. It is, however, probably not consistent with the measured partial isotope effect on the oxygen. If we assign no errors to the numbers used in the analysis, which we certainly cannot, this first possibility would also require rather small values of λ for a T_c of 36 K, but it remains a possibility, considering the uncertainties that persist in the data. The second possibility of a joint phonon-plus-excitonic mechanism is more interesting and will be studied in some detail. Before doing this, we describe the extraction of γ from critical magnetic-field data to stress the difficulties with such analysis.

The upper critical magnetic field has been measured near T_c by many groups. Again, as Table XVII indicates, there is significant variation in the slope at T_c $[H'_{c2}(T_c)]$ not only from sample to sample, but also depending on whether the onset or midpoint of the resistivity drop is used. Strictly speaking, the onset point should be used, but the polycrystalline samples and the possible fluctuations above T_c complicate this simple prescription. Moreover, anisotropy [Teichler (1977)] now plays a more significant role, as measurements on single crystals indicate. We proceed, nonetheless, with the isotropic theory, noting that simple modifications are required to treat an anisotropic electron gas.

The measured slope can also be used to give an independent estimate of the Sommerfeld constant γ through the relation [Carbotte and Marsiglio (1989)]

$$H'_{c2}(T_c)=-4.48\times 10^4\gamma\rho(\Omega\,\text{cm})\eta_{H_{c2}}(T_c)\ (\text{Oe K}^{-1})\ ; \quad (9.6)$$

$\rho(\Omega\,\text{cm})$ is the residual resistivity in $\Omega\,cm$. The factor $\eta_{H_{c2}}(T_c)$, first introduced by Bergmann and Rainer (1973), takes into account strong-coupling effects. It remains within 30 percent of unity for a moderate strong-coupling material and so is not an important factor in this regime. The problematic factor is $\rho(\Omega\,\text{cm})$. Normally, the residual resistivity is found by measuring the zero-temperature normal-state resistance; in this manner, the phonon-assisted resistance is removed. This is impossible, however, in the oxides; moreover, extrapolation is difficult—the linear resistivity behavior is not well understood, and sometimes there is a sharp rise just before T_c. In some resistivity measurements, the extrapolation would cause $\rho(T=0)$ to be very near to zero, which is not understood. Kwok *et al.* (1987) used $\rho(T_c)$ in their analysis and obtained $\gamma\approx 4.9$ mJ/(mol K^2). A linear extrapolation to zero temperature gives a resistivity of just more than half that at T_c, so that we get $\gamma\approx 8$ mJ/(mol K^2), assuming ($\eta_{H_{c2}}\approx 1$ for LSCO). This is in reasonable agreement with our previous estimate for γ. It is clear, however, that considerable uncertainty remains in such analyses.

G. Joint mechanism

Excitonic superconductivity was first suggested as a theoretical possibility in 1964 by Little (1964) and Ginzburg (1964a, 1964b). The idea is very similar to that involving phonons, except that the polarization leading to an attractive interaction is not due to a movement of the ions themselves but rather to movements of electrons (say, on the ion cores perhaps not within the superconducting CuO planes). This polarization will result in a net positively charged region of space to which a conduction electron will be attracted. Little (1964) envisioned a one-dimensional geometry with conduction chains along side "exciton" chains. The two types of electrons (conduction and those that produce the excitons) are then physically separated from one another. Ginzburg (1964a, 1964b, 1965) considered a two-dimensional geometry with a metallic layer sandwiched between two dielectric layers. This geometry was later investigated in detail by

Allender *et al.* (1973), within the Eliashberg formalism. There are many objections to the idea of excitonic superconductivity, which have been neatly summarized by Little (1987). We shall not reiterate them here, but simply note that many can be overcome under the proper conditions. Perhaps the most serious problem is that vertex corrections may become important [Migdal (1958a, 1958b); Grabowski and Sham (1984)], since the ratio of the electron mass to exciton mass is no longer small. We shall nonetheless proceed, following Allender *et al.* (1973), and ignore this complication.

The most compelling reason for considering excitonic superconductivity is associated with this last problem, in that the mediating boson (exciton) now has an electronic energy scale. Hence, in the simple BCS picture, T_c will be significantly enhanced because the prefactor is now $\omega_{ex} \gg \omega_D$. Theoretical work [see the many articles in *Novel Superconductivity* edited by Wolf and Kresin (1987)] has also suggested the possiblity of excitonic superconductivity in the high-T_c oxides [Gallo *et al.* (1987); Yu *et al.* (1987)]. Several experiments have indicated that excitons may be playing a role in these materials. Far-infrared optical meaurements [Etemad *et al.* (1987); Herr *et al.* (1987); Kamaras *et al.* (1987); Orenstein *et al.* (1987)] reveal an increased absorption at high frequencies (0.44 eV in YBCO and 0.37 eV in LSCO), which may be due to an exciton mode being present. Moreover, the presence of the increased absorption has been shown to be strongly correlated with the presence of superconductivity in the material [Varma *et al.* (1987); Timusk and Tanner (1989)].

In what follows, we scale down the electron-phonon spectrum calculated by Weber while, at the same time, we increase the excitonic contribution, which we model by an Einstein spectrum located at $\omega_{ex}=500$ meV. The relative weighting of the phonon (λ) and exciton (λ_{ex}) contributions are then adjusted, keeping $T_c=36$ K. We have used $\mu^*(\omega_c=1.53 \text{ eV})=0.15$. The results for the isotope effect coefficient β_{ox} are illustrated in Fig. 116 as a function of $\lambda_{ex}/\lambda_{tot}$. We note that when only phonons are present ($\lambda_{ex}/\lambda_{tot}=0$), β_{ox} is near 0.275, whereas, when only excitons are present, the isotope coefficient approaches zero, as is expected. In these calculations, we have used Weber's calculated spectrum with ^{16}O replaced by ^{18}O in the planes. We also note that, had the isotope coefficient been measured to be near zero, the phonons could not have played a significant role, since the increase in β_{ox} from zero is relatively steep. The value for the pure phonon case would be slightly higher, except that there is a μ^* present. The small maximum near $\lambda_{ex}/\lambda_{tot}=0$ is indicative of the fact that as λ_{ex} increases from zero it initially has the effect of representing a negative μ^* and hence tends to cancel some of the effect of the existing μ^*. The manner in which the isotope effect was calculated followed the method used by Rainer and Culetto (1979). They kept the cutoff in the Δ channel fixed and simply shifted the frequencies in the $\alpha^2F(\nu)$ spectrum downwards in inverse proportion to the square root

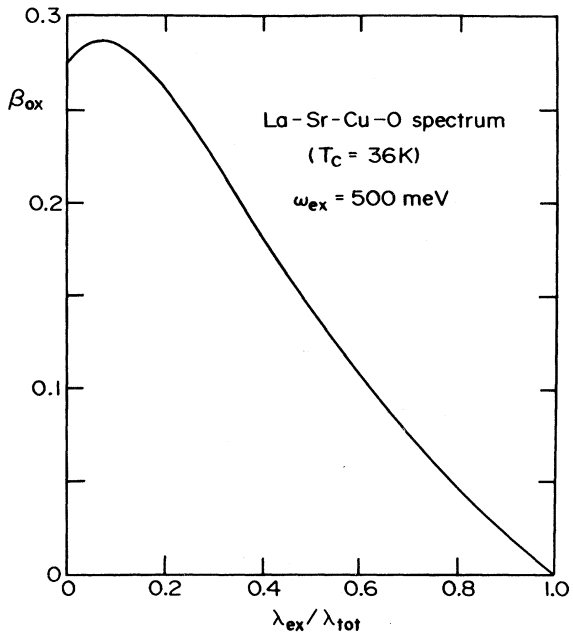

FIG. 116. Isotope-effect coefficient β_{ox} vs $\lambda_{ex}/\lambda_{tot}$, with $\mu^*=0.15$ for a combined phonon and exciton spectrum. This calculation uses Weber' spectral functions with and without oxygen replacement in the Cu-O planes. The experimentally measured, preferred value $\beta_{ox}=0.16\pm0.02$ gives rather stringent constraints on the possible value of $\lambda_{ex}/\lambda_{tot}$ within this model.

of the mass change. This method contrasts with the more complicated procedure [Leavens (1974)] of referring the cutoff to the phonon spectrum so that μ^* acquires an artificial mass dependence through its cutoff. We have the added advantage of having Weber's more accurate calculation of the phonon frequency shifts at our disposal as well.

Figure 116 allows us to decide on the ratio of λ_{ph} to λ_{ex} in LSCO on the basis of the isotope-effect measurement alone. Taking into account the axial-site oxygen isotope effect, we require $\beta_{ox}\approx0.14$ in Fig. 116, which determines $\lambda_{ex}/\lambda_{tot}\approx0.5$. This choice will depend somewhat on our choice for μ^* and ω_{ex}, as well as the manner in which we simply scaled Weber's $\alpha^2F(\nu)$ spectrum. However, for definiteness and for purposes of illustration, we fix $\lambda_{ex}/\lambda_{tot}=0.5$ and investigate other properties. Results are summarized in Table XIX for this value of $\lambda_{ex}/\lambda_{tot}$

TABLE XIX. Results for joint mechanism.

Property	BCS	$\delta=0.5$	$\delta=0.25$	$\delta=0.0$
$2\Delta_0/k_BT_c$	3.53	4.0	4.4	5.3
$\Delta C(T_c)/\gamma T_c$	1.43	1.7	2.1	2.8
$\gamma T_c^2/H_c^2(0)$	0.168	0.153	0.140	0.124
$h_c(0)$	0.576	0.55	0.52	0.48
	$\delta=\lambda_{ex}/\lambda_{tot}$			

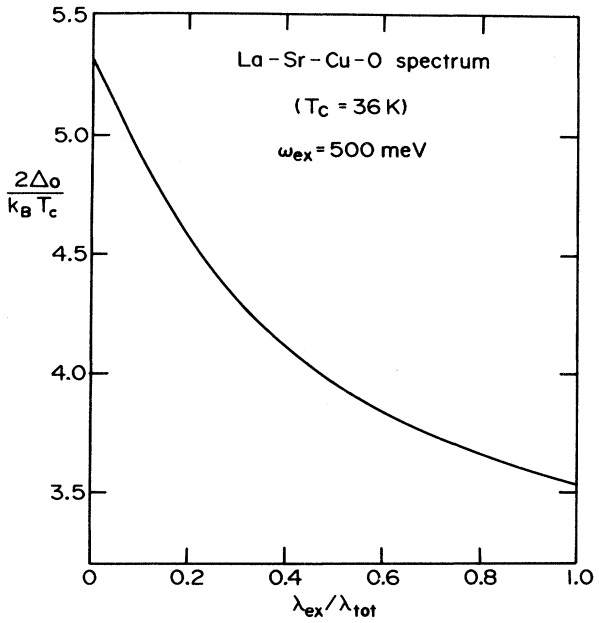

FIG. 117. $2\Delta_0/k_BT$ vs $\lambda_{ex}/\lambda_{tot}$ for the combined phonon-exciton model considered in the text. A choice of $\lambda_{ex}/\lambda_{tot}\approx 0.5$ implies $2\Delta_0/k_BT_c\approx 4$, which is in better agreement with far-infrared measurements of the gap edge than a pure phonon model with Weber's calculated $\alpha^2F(\omega)$.

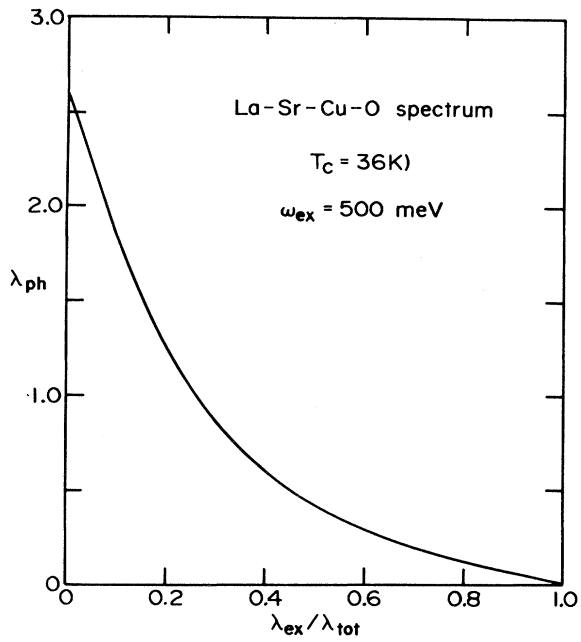

FIG. 119. Phonon contribution (λ_{ph}) to the total mass renormalization as a function of $\lambda_{ex}/\lambda_{tot}$ for a combined phonon-exciton model.

and compared with neighboring cases.

Figure 117 displays the gap ratio $2\Delta_0/k_BT_c$ as a function of $\lambda_{ex}/\lambda_{tot}$. Again, in the pure phonon case, we have simply Weber's spectrum, so that the results of the previous section apply, and $2\Delta_0/k_BT_c=5.3$. In the other extreme, a purely excitonic mechanism implies that $T_c/\omega_{ln}\approx 0.006$, so that a BCS result will be achieved. Our choice of $\lambda_{ex}/\lambda_{tot}$ implies that $2\Delta_0/k_BT_c\approx 4$ (see also Table XIX), which is certainly in the thick of things, as far as experiments go (see Table XVII). This and ensuing results will differ slightly from those of Marsiglio *et al.* (1987b), where the choice of $\lambda_{ex}/\lambda_{tot}\approx 0.4$ was made based on the calculated full isotope effect. The normalized specific-heat jump $\Delta C(T_c)/\gamma T_c$ is illustrated in Fig. 118; $\lambda_{ex}/\lambda_{tot}=0.5$ implies $\Delta C(T_c)/\gamma T_c=1.7$ (see also Table XIX). Here, again, we cannot check this against experiment, but instead rely on it to determine γ. We use, once again, the experimental value $\Delta C(T_c)/T_c=17$ mJ/(mol K^2) (see Table XVII), so that $\gamma\approx 10$ mJ/(mol K^2). To determine the density of states, we need to know λ_{tot}. Figure 119 illustrates λ_{ph} versus $\lambda_{ex}/\lambda_{tot}$, from which λ_{tot} can be determined for $\lambda_{ex}/\lambda_{tot}=0.5$. We find $\lambda_{tot}\approx 0.9$. Using Eq. (9.5), we find $N(0)=1.12$ states/(eV f.u. spin). This value is far more consistent with the values 0.95 and 1.08 determined through band-structure calculations than the value determined directly from Weber's spectrum (0.36 in the same units), and hence lends support to the combined phonon-exciton model for LSCO. The degree of agreement can be varied, however, by adjustment of choice of $\lambda_{ex}/\lambda_{tot}$ and by variation of μ^*, not to mention the choice of the experimental value of $\Delta C(T_c)/T_c$. What is clear, however, is that significant improvement has been achieved over the pure phonon model.

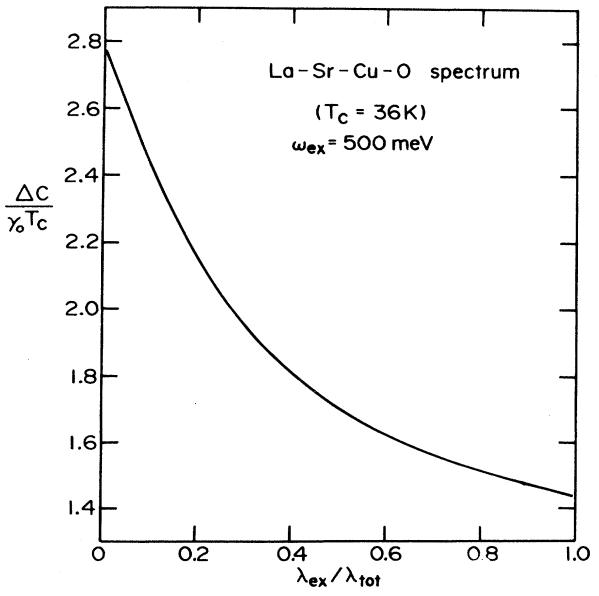

FIG. 118. Normalized specific-heat jump at T_c, $\Delta C(T_c)/\gamma T_c$, as a function of $\lambda_{ec}/\lambda_{tot}$ for a combined phonon-exciton model.

While the possibility of a combined phonon-exciton

model looks very promising, the existing experimental information is not sufficient to rule out entirely a pure phonon model, which remains a distinct possibility for La-Sr-Cu-O.

H. Specific to Y-Ba-Cu-O

We now turn to the case of Y-Ba-Cu-O with a critical temperature of 96 K. Weber and Mattheis (1988) have calculated the electron-phonon mass renormalization for this case. Varma and Weber's (1979) technique of nonorthogonal tight-binding theory of lattice dynamics [see also Weber (1984a, 1984b)] based on the band-structure calculations of Mattheiss and Hamann (1987) was applied with the result that λ is found to be quite small, perhaps of order 0.5, and leads to, at most, 19–30 K for T_c. For a critical discussion of the limitations of the work of Weber and Mattheiss (1988) and for reference to other relevant articles, the reader is referred to the review of Pickett (1989). The failure of present state-of-the-art numerical calculations of the electron-phonon interaction can be taken as the first indication that some other mechanism is operative, although the phonons can be expected to play some role since the value of λ is not likely to be insignificant. An independent determination of λ from consideration of resistivity data gives smaller values of order $\lesssim 0.21$ for Y-Ba-Cu-O and $\lesssim 0.1$ for La-Sr-Cu-O [Gurvitch and Fiory (1987a, 1987b); Gurvitch *et al.* (1988)].

In the absence of a successful calculation of the electron-phonon spectral density in Y-Ba-Cu-O, which gives a T_c of 96 K, we can begin our discussion of thermodynamic properties on the basis of Weber's spectrum for La-Sr-Cu-O scaled upward by a constant amount to get the measured T_c. No new calculations are needed, and we can rely on the results obtained in the previous sections in the limit of very strong coupling. Noting that $T_c/\omega_{\ln} \approx 0.22$ for La-Sr-Cu-O, we expect it to be ≈ 0.6 for Y-Ba-Cu-O on the assumption that the electron-phonon spectral density is not too different in shape from the dashed curve of Fig. 114. In Fig. 38, we showed $2\Delta_0/k_B T_c$ as a function of $T_c/\omega_{\ln}$ and conclude that this dimensionless ratio should be about 7 in this material. In Table XVIII we show a compilation of early experimental results for this quantity by Marsiglio (1988). As for La-Sr-Cu-O, there is a great deal of variability from one experiment to the next and no firm conclusion can be made. Some experiments show large values, while others favor a BCS-like $2\Delta_0/k_B T_c$, which is expected if some high-energy electronic boson-exchange mechanism is operative.

The data on the specific-heat jump also does not help in sorting out which possibility $T_c/\omega_{\ln} \sim 0.6$ or 0.0 is the correct one. In fact, from one curve for $\Delta C(T_c)/\gamma T_c$ versus $T_c/\omega_{\ln}$ in the very strong coupling limit shown in Fig. 59, we expect this dimensionless ratio to be close to the BCS value in both limits. Of course, we cannot easily compare with experiment, as the Sommerfeld constant γ is not well known experimentally at this time for the same reasons as we have discussed for La-Sr-Cu-O. Under such circumstances, we can use the theoretical value for $\Delta C(T_c)/T_c$ to estimate the electronic density of states at the Fermi energy and compare with results of band-structure calculations.

In Table XVIII we have compiled some early results for the jump divided by T_c [Marsiglio (1988)]. Again there is a great deal of scatter, but a preferred value might be 15 mJ/(mol Cu-atom K^2). If we use this value of $\Delta C(T_c)/T_c$ with $\Delta C(T_c)/\gamma T_c \equiv f = 1.43$, we obtain $N(0)(1+\lambda) = 2.2$ states/(eV Cu-atom spin). Table XVIII also lists some values of $N(0)$ calculated from band structure. With $\lambda \approx 0.5$, we would obtain $N(0) \sim 1.5$ states/(eV Cu-atom spin) in agreement with the upper limit of the calculated values (see Table XVIII). Higher values of λ would violate the BCS assumption. With $f = 2.8$, $N(0)(1+\lambda) = 1.1$ states/(eV Cu-atom spin). Choosing $\lambda \approx 1.5$–3.0 gives $N(0) \sim 0.28$–0.45 states/(eV Cu-atom, spin), which agrees with Massidda *et al.* (1987) values including doping. Finally, to represent the very strong coupling limit, we use the $\lambda = 30$ spectrum. Then, $f \approx 0.6$, so that $N(0)(1+\lambda) = 5.3$ states/(eV Cu-atom spin) and hence $N(0) \approx 0.2$ states/(eV Cu-atom spin). This is just below the range indicated by Massidda *et al.* (1987) calculations with doping.

On the basis of the existing data, then, it is not possible to favor one or the other of these possibilities. Many uncertainties exist in the analysis itself. The bulk specific-heat capacity should be used, whereas most of the measurements were performed on polycrystalline samples with Meissner effects as low as 25 percent at low temperatures. Moreover, Deutscher *et al.* (1980) have noted that granularity in a sample tends to reduce the specifc-heat jump [Ebner and Stroud (1985)]. Finally, anisotropy is known to reduce the jump as well. All of these effects point toward larger γ values than is obtained in this analysis, and hence, larger mass renormalization, which would favor the very strong coupling limit. However, Fermi-liquid effects have been ignored, and these may also play a large role in contributing to a mass renormalization. Finally, the disagreement in values for $N(0)$ produced by band-structure theorists is also disturbing and, at this stage prevents this sort of analysis from being quantitative.

I. Isotope effect for Y-Ba-Cu-O

The oxygen isotope effect in Y-Ba-Cu-O seems to have been measured first by Batlogg, Kourouklis, *et al.* (1987c) and by Bourne, Crommie, *et al.* (1987b). In the first paper, a change in T_c of less than 0.2 percent is observed on replacement of 75 percent of ^{16}O by ^{18}O ($\beta_{ox} = 0.0 \pm 0.02$), while the second, by the Berkeley group, finds $\beta_{ox} = 0.0 \pm 0.027$. Later, a new determination

of β_{ox} by some of the Berkeley group [Leary *et al.* (1987)] gave a finite $\beta_{ox}=0.05$. Another measurement by Morris *et al.* (1988) gave a change of critical temperature 0.2 ± 0.05 K for an 88 percent substituted sample, and Benitez *et al.* (1988) found 0.16 ± 0.06 K for 90 percent ^{18}O. A most recent publication by Yvon *et al.* (1989) finds 0.4 ± 0.1 K confirming the value of $\beta_{ox}=0.05$. An informative review and criticism of previous measurements is also given. On the other hand, another very recent paper by Hoen *et al.* (1989) gives $\beta_{ox}\cong0.019\pm0.004$. It is clear from all this that the isotope effect in Y-Ba-Cu-O is small but measurable. Very recent data by Franck *et al.* (1989) gave a different story. In a careful study using different preparation methods and measurements, they concluded that β_{ox} is perhaps as large as 0.1 and possibly even larger. While still small, these new measurements would indicate that the phonons are certainly involved. There are also some measurements of the isotope effect on the Cu and Ba site. In this case, all measurements agree that they are both very small and often below resolution. Bourne, Zettl, *et al.* (1987) consider both Cu and Ba substitutions and quote $\beta_{Cu}=0.0\pm0.07$ and $\beta_{Ba}=0.0\pm0.1$. Lin *et al.* (1988) find no shift on the Cu within a resolution of 0.2 K, while Vasiliev and co-workers [Vasiliev and Luschikov (1988); Vasiliev *et al.* (1988)] find $\beta_{Cu}=0.01\pm0.03$. Finally, Hidaka *et al.* (1988) obtain zero for β_{Ba} within a resolution of 0.15 K. It would appear that, if the present data on the various partial isotope effects in Y-Ba-Cu-O stand up to future scrutiny, the total effect is probably small but could be significant and perhaps larger than 0.1. Even if this value remains uncertain, it indicates that a joint phonon-plus-electronic mechanism is involved in Y-Ba-Cu-O. This is an appealing possibility, because it gives a fairly consistent picture for all superconductors. The conventional ones would fall in the pure phonon limit while La-Sr-Cu-O could be a mixture of phonon plus exciton with, finally, Y-Ba-Cu-O dominantly but not exclusively an electronic superconductor. This possibility has led us to consider an excitonic superconductor perturbed somewhat by a small but not insignificant phonon contribution (Akis and Carbotte, 1989b). Under such circumstances, it is of interest to understand how significantly superconducting properties might deviate from BCS laws and so, possibly, give information on mechanism.

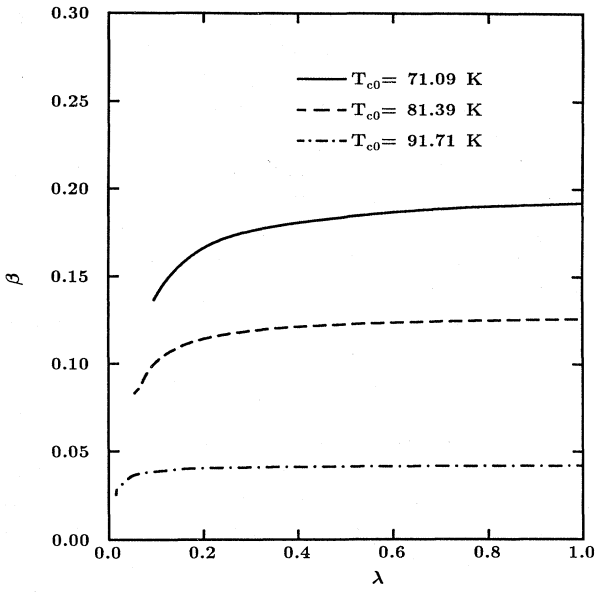

FIG. 120. Total isotope effect β as a function of phonon frequency ω_E in a combined phonon-exciton model for a 96-K superconductor. The excitonic part is modeled by a negative effective μ^*_{eff}, which defines a T_{c0}—the critical temperature when the phonons are neglected. $T_{c0}=71.1$ K for the solid curve, 81.4 K for the dashed curve, and 91.7 K for the dot-dashed curve.

J. Excitonic superconductivity

To illustrate the main results obtained, we consider the specific case of Y-Ba-Cu-O with T_c set equal to 96 K in all our calculations [Marsiglio and Carbotte (1987b, 1988a)]. In addition, the phonon spectral density is taken to be a delta function of the form $\alpha^2F(\omega)=\frac{1}{2}\lambda_{ph}\omega_E\delta(\omega-\omega_E)$ with the Einstein frequency set at a phonon energy. Furthermore, assuming that the second mechanism involves a high-energy boson, we treat it in

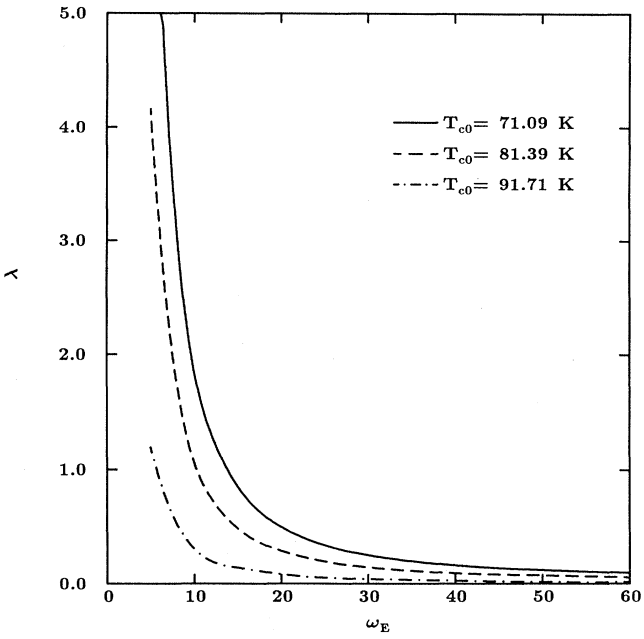

FIG. 121. Electron-phonon mass renormalization λ as a function of phonon energy ω_E for 96-K superconductor with combined exciton-phonon mechanism. For labels on the curves, see Fig. 120.

an effective negative $\mu^*_{\rm eff}$ approximation and, instead of quoting $\mu^*_{\rm eff}$ and the associate cutoff, we simply use T_{c0} as the parameter. Here, T_{c0} is the critical temperature that would result if we have only an excitonic mechanism and so $\lambda_{\rm ph}=0$. In Fig. 120, we show results for the total isotope effect of a 96-K superconductor as a function of phonon energy ω_E and three different values of excitonic contribution, namely, $T_{c0}=71.1$ K (solid curve), 81.4 K (dashed curve), and 91.7 K (dot-dashed curve). As T_{c0} is decreased, the phonons play a more significant role in T_c and must account for an ever increasing difference $(96-T_{c0})$ K. As we would expect, the isotope effect is also increased. What is, perhaps, somewhat surprising is that the total β is not a rapidly increasing function of decreasing ω_E for a given value of T_c. In fact, the curves are rather flat and completely different from the corresponding variation in $\lambda_{\rm ph}\equiv\lambda$, which we show in Fig. 121. In this case, λ is seen to remain small if ω_E is large even for $T_{c0}=71.1$ K; but as ω_E decreases below 20 meV, the rise of λ is very rapid and its value can be larger than 1. It is important to note also that even for $\lambda=1$, which implies quite a significant coupling to the phonons, β can still remain small and below 0.05, which is smaller than our preferred experimental estimate of 0.1 or even a little larger. This is contrary to the expectation of Pattnaik and Newns (1989). For this to occur, however, it is necessary that the electron-phonon coupling be dominantly with low-energy phonons around 5 meV in the specific example considered in the figure.

In Fig. 122, we show the normalized specific-heat jump at T_c, $\Delta C(T_c)/\gamma T_c$ as a function of phonon energy for a 96-K superconductor in a combined phonon-exciton model. Again, solid, dashed, and dot-dashed curves apply to $T_{c0}=71.1$, 81.4, and 91.7 K, respectively, with the last cases certainly not inconsistent with the presently available isotope-effect data. It is seen that if the phonon contribution is mainly from coupling to phonons above 20 meV, we do not get significant differences from pure BCS. If, however, the coupling is predominantly to modes around 10 meV, the calculations predict that $\Delta C(T_c)/\gamma T_c$ can fall significantly below BCS, a prediction that is consistent with our previous, very strong coupling results for a single-mechanism case. In both calculations, T_c is of the order of ω_E. This can occur because T_c is large due to a very large electron-phonon interaction or because it is mainly due to some excitonic contribution. The behavior of most other dimensionless ratios is found to be similar and opposite to usual strong-coupling behavior. An exception is the gap-to-critical-temperature ratio $2\Delta_0/k_BT_c$, which we show in Fig. 123. In this case, we always obtain values above the BCS value of 3.54. For large values of ω_E, the deviations are small for each of the cases considered and, in fact, remain fairly small until ω_E is around 20 meV, in which case $2\Delta_0/k_BT_c$ can start rising quite significantly, particularly if T_{c0} is not too near T_c and there is significant room for

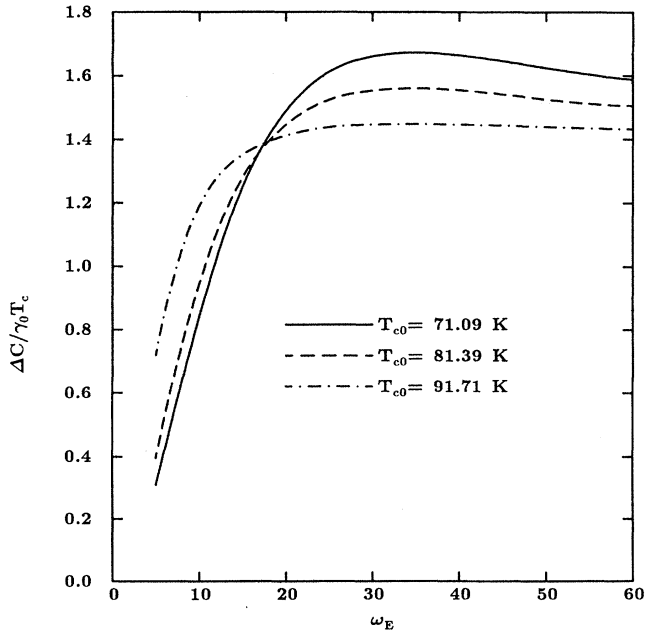

FIG. 122. Normalized specific-heat jump at T_c, $\Delta C(T_c)/\gamma T_c$, as a function of phonon energy ω_E for a 96-K superconductor with combined exciton-phonon mechanism. For labels on the curves, see Fig. 120.

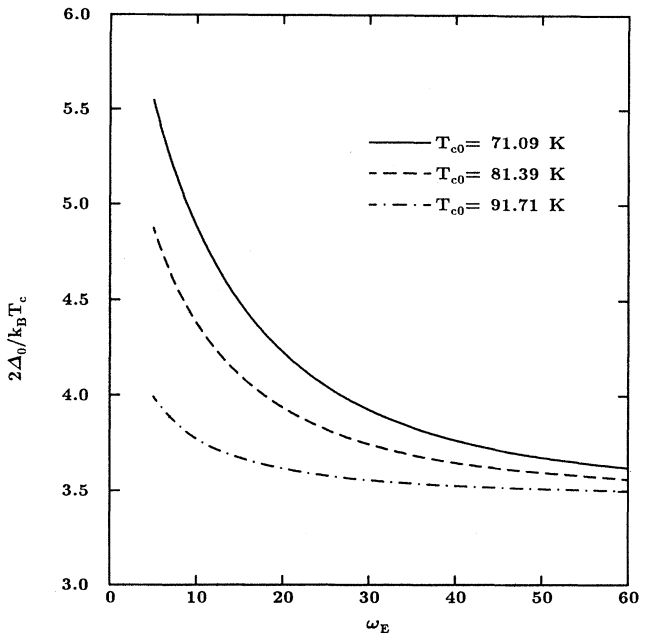

FIG. 123. Dimensionless ratio of gap to critical temperature $2\Delta_0/k_BT_c$ as a function of phonon energy ω_E for a 96-K superconductor with combined exciton-phonon mechanism. For labels on the curves, see Fig. 120.

a phonon contribution.

A general conclusion from all this is that a superconductor with high T_c and small but finite total isotope effect which is described through a joint phonon-plus-exciton mechanism can show interesting deviations from pure BCS behavior that could be looked for. Unfortunately, the data in Y-Ba-Cu-O are not sufficiently well defined to allow any definitive conclusion at this time. The variability of the data and the lack of any consensus represent a serious problem in comparisons between theory and experiment.

K. Slope of specific heat at T_c

A quantity of particular interest that needs to be mentioned is the specific-heat jump and its slope near T_c. Another is the temperature dependence of the London-limit penetration depth. The slope of the specific-heat jump near T_c has been measured in recent experiments [Junod *et al.* (1988); Loram and Mirza (1988)] and has been found to be particularly sharp. The dimensionless ratio of slope to jump, which is independent of value of the Sommerfeld constant γ can be as high as 14. We have seen in Sec. VI, Fig. 73, that such a large value is inconsistent with the theoretical maximum of about 5, which comes from Eliashberg theory, whatever the size, shape, or origin of the kernels entering the isotropic version of these equations. It is certainly also consistent with the pure BCS behavior expected for a pure excitonic superconductor and must be taken as a puzzle at this point.

L. Temperature dependence of penetration depth

The story on the temperature variation of the London penetration depth is different. Strong-coupling calculations for this quantity have been presented by Blezius *et al.* (1988) and by Rammer (1988a). Measurements using muon spin relaxation are numerous. Some are by Gygax *et al.* (1987), Aeppli *et al.* (1987), Kossler *et al.* (1987), Harshman *et al.* (1987, 1989), Cooke *et al.* (1988, 1989), Kiefl *et al.* (1988), Naughton *et al.* (1988), Schenck (1988), and Lichti *et al.* (1989). Alternative techniques can also be used. See, for example, Fiory *et al.* (1988) and Mitra *et al.* (1989).

In Fig. 124, we reproduce the strong-coupling results obtained by Blezius *et al.* (1988) and the comparison with the data of Kiefl *et al.* (1988) for Y-Ba-Cu-O. What is plotted is the deviation of the penetration depth in the

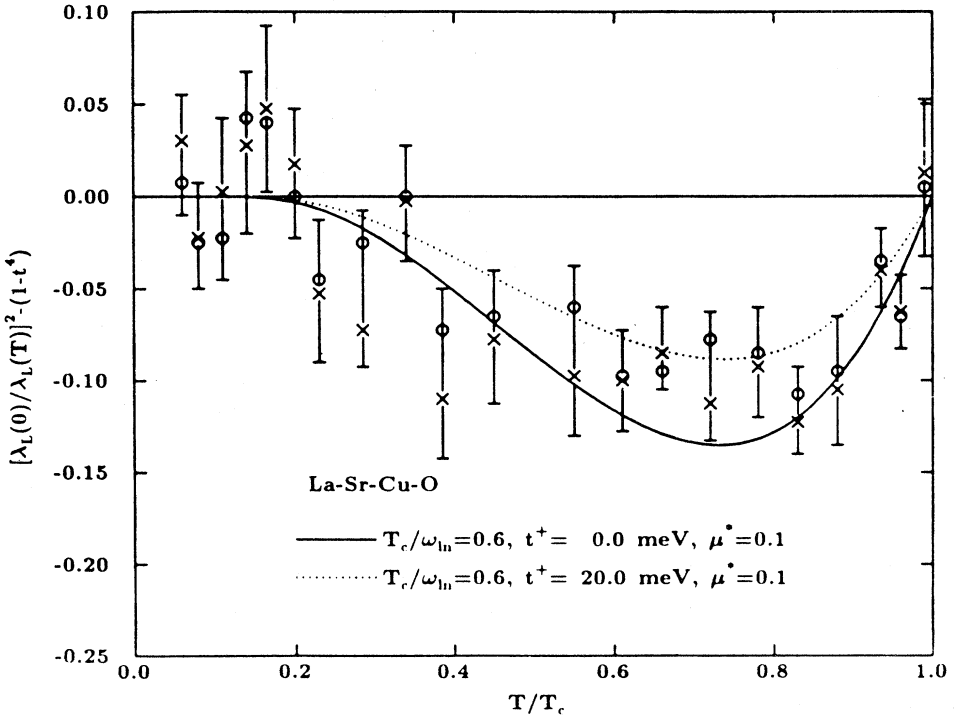

FIG. 124. Temperature dependence of the London penetration depth deviation function $[\lambda_L(0)/\lambda_L(T)]^2-(1-t^4)$ as a function of reduced temperature $t \equiv T/T_c$ for a model of Y-Ba-Cu-O based on a rescaling of Weber's $\alpha^2F(\omega)$ for La-Sr-Cu-O with $T_c/\omega_{\ln}=0.6$. The solid curve is in the clean limit and the dotted curve is for $t^+=20.0$ meV. The data are by Kiefl *et al.* (1988).

London limit from the two-fluid-model prediction, namely,

$$\left[\frac{\lambda_L(0)}{\lambda_L(T)}\right]^2 - (1-t^4) , \tag{9.7}$$

where $t \equiv T/T_c$ is the reduced temperature. The calculations are for a strong-coupling model with $T_c/\omega_{\ln}=0.6$, a value suggested previously. We see good agreement with experiment for an impurity content represented by $t^+=20.0$ meV. We note that the observed and calculated deviations fall below the two-fluid model except, perhaps, near zero temperature.

In Fig. 125, we show a similar comparison between an independent strong-coupling calculation by Rammer (1988a) and the data of Harshman *et al.* (1987). What is plotted is

$$\left[\frac{\lambda(0)}{\lambda(T)}\right]^2 \text{ vs } T/T_c . \tag{9.8}$$

Also shown in the figure are the BCS dirty- and clean-limit curves. The data (+) certainly fall outside the region defined by the two weak-coupling (dashed line) curves, but do fall between the strong-coupling curves (solid line) for clean (lower curve) and dirty (upper curve) limit, respectively. More recent data from muon spin-relaxation measurements at the Clinton P. Anderson Meson Physics Facility (LAMPF) at Los Alamos [Lichti *et al.* (1989)] fall nearly on the dirty-limit strong-coupling curve of Rammer (1988a) and are above the two-fluid prediction. On the other hand, the data of Fiory *et al.* (1988) and of Mitra *et al.* (1989) show a BCS weak-coupling behavior. These data are more consistent with the idea of a joint phonon-plus-electronic boson-exchange mechanism. The data that agree with pure strong-coupling calculations have the problem that the measured value for the total isotope effect is violated. As a general conclusion, we see once more that present data show too much variation to be useful in differentiating with certainty between various models.

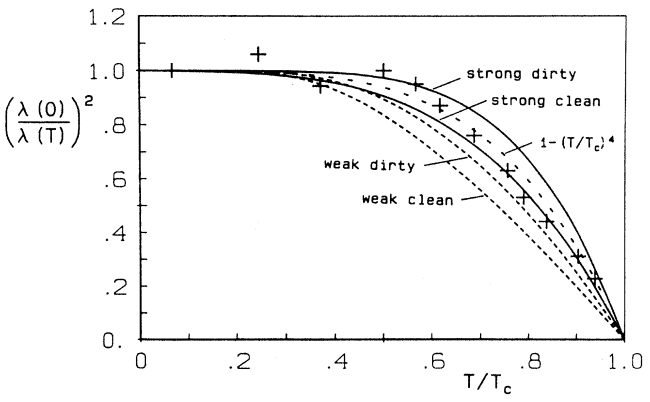

FIG. 125. Temperature dependence of the magnetic penetration depth in weak- and strong-coupling theory. The dashed curves labeled by "weak dirty" and "weak clean" correspond to BCS. The two-fluid-model result $(1-t^4)$ is also shown and compared with the strong-coupling results (solid curve) labeled by "strong dirty" and "strong clean." The data with which $[\lambda(0)/\lambda(T)]^2$ is compared are from Harshman *et al.* (1987).

X. CONCLUSIONS

For conventional superconductors, Eliashberg theory with tunneling-derived kernels yields a remarkably accurate description of the observed thermodynamics and other properties which, in general, are found not to obey BCS universal laws. The theory also allows for the introduction of concepts such as functional derivatives with respect to the spectral density $\alpha^2F(\omega)$, which fall outside a BCS description. Interesting questions, such as the effectiveness of a particular frequency ω on T_c or some other property, can be addressed and answered.

Application of the concepts of Eliashberg theory (with single or joint mechanism) to the high-T_c oxides is inconclusive at the present time, mainly because of the large variation that exists in the data. With better data, it should be possible to say something about mechanism and discover the energy scale associated with the pairing interaction.

ACKNOWLEDGMENTS

Over the years, I have had many stimulating discussions with my students and postdoctoral fellows on the subject of this review. I wish to thank, in particular, R. Akis, J. Blezius, J. M. Coombes, J. M. Daams, C. R. Leavens, F. Marsiglio, B. Mitrović, E. Schachinger, M. Schossmann, and W. Stephan. E. J. Nicol and E. Schachinger read most of the manuscript and made many constructive comments. E. Schachinger also helped with some of the final organization of the paper. I have been supported financially by the Natural Sciences and Engineering Council of Canada (NSERC), by the Ontario Center for Materials Research (OCMR), and by the Canadian Institute for Advanced Research (CIAR).

APPENDIX A: FUNCTIONAL DERIVATIVE OF T_c WITH $\alpha^2F(\omega)$ IN TWO-SQUARE-WELL MODEL

We begin with the linearized form of the Eliashberg equations (2.1) and (2.2) using $\tilde{\Delta}_n \equiv \Delta(i\omega_n)Z(i\omega_n)$ and $\tilde{\omega}_n \equiv \omega_n Z(i\omega_n)$. They are

$$\tilde{\Delta}_n = \pi T_c \sum_m [\lambda(m-n)-\mu^*(\omega_n)] \frac{\tilde{\Delta}_m}{|\tilde{\omega}_m|} \tag{A1}$$

and

$$\tilde{\omega}_n = \omega_n + \pi T_c \sum_m \lambda(m-n)\mathrm{sgn}(\omega_m) \tag{A2}$$

with $\lambda(m-n)\equiv\lambda(i\omega_m-i\omega_n)$. Consider a system for which the base $\alpha_0^2F(\omega)$ is augmented by a term of $\epsilon\delta(\omega-\omega_0)$ with $\epsilon\to 0$. In this case

$$\lambda(m-n)\to\lambda(m-n)+\epsilon\frac{2\omega_0}{\omega_0^2+(\omega_n-\omega_m)^2}\ , \tag{A3}$$

where we will treat the first term in the two-square-well model (or $\lambda^{\theta\theta}$ model), while the second is infinitesimal and can be accounted for exactly. In the $\lambda^{\theta\theta}$ model

$$\sum_m \lambda(m-n)\,\mathrm{sgn}(\omega_m)$$

has $(2n-1)$ terms that do not cancel in pairs, and so we get for (A2)

$$|\tilde{\omega}_n|=(1+\lambda)|\omega_n|+\epsilon f_n \tag{A4}$$

with

$$f_n=\pi T_c\sum_m\frac{2\omega_0\,\mathrm{sgn}(\omega_n\omega_m)}{\omega_0^2+(\omega_n-\omega_m)^2}\ . \tag{A5}$$

Substituting (A4) into (A1), retaining only the lowest-order terms in ϵ, and applying the $\lambda^{\theta\theta}$ model to the finite term, gives

$$\tilde{\Delta}_n=\pi T_c\left[\frac{\lambda-\mu^*}{1+\lambda}\right]\sum_m\frac{\tilde{\Delta}_m}{|\omega_m|}+\frac{\pi T_c\epsilon}{1+\lambda}\sum_m\left[\frac{2\omega_0}{\omega_0^2+(\omega_n-\omega_m)^2}-\frac{\lambda-\mu^*}{1+\lambda}\frac{f_m}{|\omega_m|}\right]\frac{\tilde{\Delta}_m}{|\omega_m|}\ . \tag{A6}$$

The first term in (A6) is independent of n and denoted by $\tilde{\Delta}$, while the second is proportional to ϵ and denoted by $\epsilon\delta\tilde{\Delta}_n$. We get

$$\delta\tilde{\Delta}_n=\frac{\pi T_c}{1+\lambda}\sum_m\left[\frac{2\omega_0}{\omega_0^2+(\omega_n-\omega_m)^2}-\frac{\lambda-\mu^*}{1+\lambda}\frac{f_m}{|\omega_m|}\right]\frac{\tilde{\Delta}}{|\omega_m|} \tag{A7}$$

and

$$\tilde{\Delta}=\pi T_c\left[\frac{\lambda-\mu^*}{1+\lambda}\right]\sum_m\frac{(\tilde{\Delta}+\epsilon\delta\tilde{\Delta}_m)}{|\omega_m|}\ . \tag{A8}$$

Substitution of (A7) into (A8) gives the eigenvalue equation

$$1=\pi T_c\left[\frac{\lambda-\mu^*}{1+\lambda}\right]\sum_m\frac{1}{|\omega_m|}+\epsilon(\pi T_c)^2\left[\frac{\lambda-\mu^*}{1+\lambda}\right]\sum_{mm'}\left[\frac{2\omega_0}{\omega_0^2+(\omega_m-\omega_{m'})^2}-\frac{\lambda-\mu^*}{1+\lambda}\frac{f_{m'}}{|\omega_{m'}|}\right]\frac{1}{|\omega_m||\omega_{m'}|}\frac{1}{1+\lambda}\ . \tag{A9}$$

When $\epsilon=0$ (A9) reduces to the usual BCS equation for T_c^0, namely,

$$1=\pi T_c^0\left[\frac{\lambda-\mu^*}{1+\lambda}\right]\sum_m\frac{1}{|\omega_m^0|}\ , \tag{A10}$$

where superscript "0" denotes the case of no perturbation. In the second term, on the right-hand side of (A9), we can use unperturbed quantities everywhere, since the entire equation is already proportional to ϵ. In addition, if the sum over m is performed first, the second term in the curly bracket can be reduced using (A10). On changing the left-hand side of (A9) to T_c^0 through Eq. (A10), we arrive at the result

$$\ln\left[\frac{T_c^0+\delta T_c}{T_c^0}\right]\cong\frac{\delta T_c}{T_c^0}=\frac{\epsilon(\pi T_c^0)}{1+\lambda}\left[\pi T_c^0\sum_{mm'}\frac{2\omega_0}{\omega_0^2+(\omega_m^0-\omega_{m'}^0)^2}\frac{1}{|\omega_m^0|}\frac{1}{|\omega_{m'}^0|}-\sum_{m'}\frac{f_{m'}^0}{|\omega_{m'}^0|^2}\right]\ . \tag{A11}$$

Finally, reference to (A5) gives

$$\frac{\delta T_c}{\delta\alpha^2F(\omega_0)}\equiv\lim_{\epsilon\to 0}\frac{\delta T_c}{\epsilon}=\frac{T_c}{1+\lambda}(\pi T_c)^2\sum_{mm'}\left[\frac{2\omega_0}{\omega_0^2+(\omega_m-\omega_{m'})^2}\right]\left[\frac{1}{|\omega_m||\omega_{m'}|}-\frac{\mathrm{sgn}(\omega_m\omega_{m'})}{|\omega_{m'}|^2}\right]\ , \tag{A12}$$

where we have dropped the superscripts "0", as they are no longer needed. Finally, introducing the dimensionless parameter $\bar{\Omega}\equiv\omega_0/T_c$, we arrive at

$$\frac{\delta T_c}{\delta\alpha^2F(\omega_0)}=\frac{1}{1+\lambda}G(\bar{\Omega}) \tag{A13}$$

with the universal function

$$G(\bar{\Omega})=\sum_{mm'}\frac{2\bar{\Omega}}{\bar{\Omega}^2+4\pi^2(m-m')^2}\times\left[\frac{1}{|2m-1||2m'-1|}-\frac{\mathrm{sgn}(2m-1)(2m'-1)}{|2m'-1|^2}\right]\ . \tag{A14}$$

The term $m'=m$ drops out of the double sum in (A14) because in that case the term in the curly bracket is exactly zero. It is convenient to rewrite (A14) in the form

$$G(\bar{\Omega})=\sum_{n=1}^{\infty}\frac{4\bar{\Omega}}{\bar{\Omega}^2+4\pi^2n^2}B_n \tag{A15}$$

where

$$B_n=\sum_{m=1}^{n}\left[\frac{2}{n}\frac{1}{2m-1}+\frac{2}{(2m-1)^2}\right]-\frac{\pi^2}{4}\ , \tag{A16}$$

which is our final formula. The B_n's are just numbers, and the first few terms in (A15) give $G(\bar{\Omega})$ qualitatively.

APPENDIX B: DERIVATION OF STRONG-COUPLING CORRECTIONS

In this appendix we outline in detail the derivation of strong-coupling corrections. It is divided into two sections. The first describes the derivation of thermodynamic properties. In the second section, critical magnetic-field properties are derived.

1. Thermodynamics

a. $T\sim T_c$

Equations (2.1) and (2.2) are expanded near T_c (small Δ_m):

$$Z_S(\omega_n)\Delta(\omega_n)=\pi T\sum_{m=-N_0+1}^{N_0}\lambda(i\omega_n-i\omega_m)\frac{\Delta_0}{|\omega_m|}\left[1-\frac{1}{2}\frac{\Delta_0^2}{\omega_m^2}+\frac{3}{8}\frac{\Delta_0^4}{\omega_m^4}\right], \tag{B1}$$

$$Z_S(\omega_n)=Z_N(\omega_n)+\frac{\pi T}{\omega_n}\int_0^{\infty}2\nu\,d\nu\,\alpha^2F(\nu)\sum_{m=-N_0+1}^{N_0}\frac{\mathrm{sgn}\omega_m}{\nu^2+(\omega_m-\omega_n)^2}\left[-\frac{1}{2}\frac{\Delta_0^2}{\omega_m^2}+\frac{3}{8}\frac{\Delta_0^4}{\omega_m^4}\right]. \tag{B2}$$

Here the subscript S (N) means superconducting (normal), and $N_0=\omega_0/2\pi T+\frac{1}{2}$ enumerates the Matsubara frequencies in the sums. However, the convergence is sufficiently rapid that N_0 can be replaced by infinity. The summations are folded to the domain $[0,\infty]$. In the Z channel [Eq. (B2)], this procedure results in sums like

$$\sum_{m=1}^{\infty}\frac{1}{\omega_m^{2i-1}}\frac{1}{(\nu^2+\omega_m^2+\omega_n^2)^2}\times\left[1+\frac{4\omega_m^2\omega_n^2}{(\nu^2+\omega_m^2+\omega_n^2)^2}+\cdots\right]. \tag{B3}$$

Noting that $\omega_n=\pi T(2n-1)$, and only small n is required, one sees that terms of $O(T_c/\nu)^6$ have been neglected, consistent with our assumption, $T_c\ll\nu$. These terms would contribute, however, in the free-energy formula [Eq. (5.1)], to $O(T_c/\nu)^2$ and hence should be retained. Howver, for the sake of simplicity, and since coefficients will be fitted to numerical data in the end anyway, we have dropped them. The required sums are

$$U_i\equiv 4\pi T\sum_{m=1}^{\infty}\frac{1}{\omega_m^{2i-1}}\frac{1}{(\omega_m^2+a_n^2)^2} \tag{B4}$$

and

$$V_i\equiv 4\pi T\sum_{m=1}^{\infty}\frac{1}{\omega_m^{2i-1}}\frac{4\omega_m^2\omega_n^2}{(\omega_m^2+a_n^2)^4}\ . \tag{B5}$$

Here, $a_n^2\equiv\nu^2+\omega_n^2$, and $i=1,2,3,\ldots$. In accordance with the remarks made above, only $i=1,2$ are required in Eq. (B4) and all i can be neglected in Eq. (B5). These are readily evaluated in terms of digamma functions, which can then be expanded as follows:

$$U_1\equiv\frac{2}{a_n^4}\left[\ln\frac{1.13a_n}{k_BT}-\frac{1}{2}\right]$$
$$U_2\equiv\frac{7}{2}\frac{\zeta(3)}{(\pi T)^2}\frac{1}{a_n^4}\ ; \tag{B6}$$

$\zeta(3)$ is the Riemann zeta function [$\zeta(3)\approx 1.202\cdots$]. It is easy to show $V_1=O(T/\nu)^4$. Equation (B2) becomes

$$Z_S(\omega_n)-Z_N(\omega_n)=-\Delta_0^2(T)\int_0^{\infty}2\nu\,d\nu\,\alpha^2F(\nu)\frac{1}{(\nu^2+\omega_n^2)^2}\left[\ln\frac{1.13\sqrt{\nu^2+\omega_n^2}}{k_BT}-\frac{1}{2}\right]+\frac{21}{16}\Delta_0^4(T)\frac{\zeta(3)}{(\pi T)^2}\int_0^{\infty}2\nu\,d\nu\,\alpha^2F(\nu)\frac{1}{(\nu^2+\omega_n^2)^2}\ . \tag{B7}$$

At this point we also write the expansion for the Bardeen-Stephen free-energy formula:

$$\frac{\Delta F}{N(0)}\equiv\frac{F_S-F_N}{N(0)}=-2\pi T\sum_{m=1}^{\infty}Z_N(\omega_m)\left[\frac{1}{4}\frac{\Delta_0^4}{\omega_m^3}-\frac{1}{4}\frac{\Delta_0^6}{\omega_m^5}\right]-2\pi T\sum_{m=1}^{\infty}[Z_S(m)-Z_N(m)]\left[\frac{1}{2}\frac{\Delta_0^2}{\omega_m}-\frac{1}{8}\frac{\Delta_0^4}{\omega_m^3}\right]. \tag{B8}$$

As will be seen below, the variation of $Z_N(\omega_m)$ with m is not large. In the first sum we can safely replace $Z_N(m)$ by its constant value at, say, $m=1$. However, in the second sum, the first term is nonconvergent with a constant value for $Z_S(m)-Z_N(m)$; hence the n dependence must be retained in Eq. (B7). It will be dropped, however, in the argument of the logarithm, to facilitate the calculation. An identical expansion can be performed for $Z_N(n)$, with the result

$$Z_N(\omega_n)=1+\lambda-\tfrac{1}{3}(\pi T)^2[(2n-1)^2-1]\times\int_0^{\infty}2\nu\,d\nu\,\alpha^2F(\nu)\frac{1}{\nu^4}. \tag{B9}$$

The constant value to be used in the first term of Eq. (B8) now depends on our choice of n. For $n=1$, there is a no strong-coupling correction; $Z_N=1+\lambda$, which is the $\lambda^{\theta\theta}$ result. For higher value of n a strong-coupling correction results. We prefer to use the former value, since it is exact for $n=1$. This is seen most readily from the exact equation for $Z_N(\omega_n)$:

$$Z_N(\omega_n)=1+\frac{\pi T}{\omega_n}\left[\lambda(0)+2\sum_{m=1}^{n-1}\lambda(m)\right]. \tag{B10}$$

In fact, our choice for Z_N will be consistent with our use of the zero-temperature Sommerfeld constant γ in the ratio $\Delta C(T_c)/\gamma T_c$. This choice also omits strong-coupling corrections arising from electron-phonon coupling at nonzero temperatures, as described by Grimvall (1968, 1969, 1981) and Kresin and Zaitsev (1978b).

Similar remarks apply to the Δ channel. Equation (B1) can be reduced to

$$Z_S(n)\Delta_0=\Delta_0\int_0^{\infty}2\nu\,d\nu\,\alpha^2F(\nu)[P_1+Q_1-\tfrac{1}{2}\Delta_0^2(P_2+Q_2)+\tfrac{3}{8}\Delta_0^4(P_3+Q_3)], \tag{B11}$$

where

$$P_i\equiv\sum_{m=1}^{\infty}\frac{2\pi T}{\omega_m^{2i-1}}\frac{1}{\omega_m^2+a_n^2} \tag{B12}$$

and

$$Q_i\equiv\sum_{m=1}^{\infty}\frac{2\pi T}{\omega_m^{2i-3}}\frac{4\omega_n^2}{(\omega_m^2+a_n^2)^3}. \tag{B13}$$

These sums are

$$P_1=\frac{1}{a_n^2}\ln\frac{1.13a_n}{k_BT}-\frac{(\pi T)^2}{6a_n^4}, \tag{B14a}$$

$$P_2=\frac{7}{4}\frac{\zeta(3)}{(\pi T)^2}\frac{1}{a_n^2}-\frac{1}{a_n^4}\ln\frac{1.13a_n}{k_BT}, \tag{B14b}$$

$$P_3=\frac{31}{16}\frac{\zeta(5)}{(\pi T)^4}\frac{1}{a_n^2}-\frac{7}{4}\frac{\zeta(3)}{(\pi T)^2}\frac{1}{a_n^4}, \tag{B14c}$$

$$Q_1=\frac{\omega_n^2}{a_n^4}, \tag{B14d}$$

$$Q_2=Q_3=O(1/a_n^6). \tag{B14e}$$

We evaluate Eq. (B11) for small n (specifically, $n=1$) and define

$$a(T)\equiv\int_0^{\infty}2\nu\,d\nu\,\alpha^2F(\nu)\frac{1}{\nu^4}\ln\frac{1.13\nu}{k_BT} \tag{B15a}$$

and

$$b(T)\equiv\int_0^{\infty}2\nu\,d\nu\,\alpha^2F(\nu)\frac{1}{\nu^4}. \tag{B15b}$$

The gap equation (B11) becomes [using $Z_S(n=1)$]

$$1=F(T)+\Delta_0^2G(T)+\Delta_0^4J(T), \tag{B16}$$

where

$$F(T)=\frac{\lambda}{1+\lambda}\ln\frac{1.13\omega_{\ln}}{k_BT}-\frac{(\pi T)^2}{1+\lambda}[a(T)-\tfrac{4}{3}b], \tag{B17a}$$

$$G(T)=\frac{-\lambda}{1+\lambda}\frac{7}{8}\frac{\zeta(3)}{(\pi T)^2}+\frac{3}{2}\frac{a(T)}{1+\lambda}+[\tfrac{7}{8}\zeta(3)-\tfrac{1}{2}]\frac{b}{1+\lambda}, \tag{B17b}$$

$$J(T)=\frac{\lambda}{1+\lambda}\frac{93}{128}\frac{\zeta(5)}{(\pi T)^4}-\frac{93}{128}\frac{\zeta(5)}{(\pi T)^2}\frac{b}{1+\lambda}-\frac{63}{32}\frac{\zeta(3)}{(\pi T)^2}\frac{b}{1+\lambda}. \tag{B17c}$$

The T_c equation is given by $1=F(T_c)$, with the result

$$T_c=1.13\omega_{\ln}\exp\left[-\left[\frac{1+\lambda}{\lambda}\right]\right]\left[1-\frac{(\pi T_c)^2}{\lambda}[a(T_c)-\tfrac{4}{3}b]\right]. \tag{B18}$$

This is not an accurate T_c equation, but it will prove useful later. The gap parameter (near T_c) is obtained from Eq. (B16):

$$\Delta_0^2(T)=-\frac{F'}{G}(T-T_c)\left[1+\left[\frac{1}{2}\frac{F''}{F'}-\frac{G'}{G}+\frac{F'J}{G^2}\right](T-T_c)\right], \tag{B19}$$

where it is understood that the derivatives are with respect to temperature, and the functions are evaluated at T_c. Equation (B19), along with Eq. (B7), is to be substituted into Eq. (B8). Summations in the second term are required, but of the form encountered previously, (U_1). The result is

$$\frac{\Delta F}{N(0)}=\frac{1}{2}\frac{(1+\lambda)^2}{\lambda}[\Delta_0^4K(T)+\tfrac{4}{3}\Delta_0^6L(T)], \tag{B20}$$

where

$$K(T)=G_0(T)-\frac{TF_0'(T)}{1+\lambda}\left[c(T)-a(T)+\frac{b}{4}\right] \tag{B21a}$$

and

$$L(T)=J_0(T)+\frac{3}{2}\frac{G_0(T)}{1+\lambda}\left[a(T)-\frac{b}{2}\right]. \tag{B21b}$$

A new strong-coupling correction, defined by

$$c(T)=\int_0^\infty 2\nu\,d\nu\,\alpha^2F(\nu)\frac{1}{\nu^4}\ln^2\frac{1.13\nu}{k_BT}, \tag{B22}$$

is required. The "0" subscripts in Eqs. (B21) signify that the strong-coupling corrections in Eqs. (B17) are not present. The specific-heat difference near T_c is given by the thermodynamic formula

$$\Delta C(T)=-T\frac{d^2\Delta F}{dT^2}, \tag{B23}$$

so that after some tedious algebra, one obtains

$$\frac{\Delta C(T)}{\gamma T_c}=f+(1-t)g, \tag{B24}$$

where f and g are defined below.

To simplify the formulas for f and g, we write

$$a(T_c)=\frac{\alpha_1}{\omega_{\ln}^2}\int_0^\infty 2\nu\,d\nu\,\alpha^2F(\nu)\frac{1}{\nu^2}\ln\frac{1.13\nu}{k_BT_c}=\frac{\alpha_1}{\omega_{\ln}^2}\lambda\ln\frac{1.13\omega_{\ln}}{k_BT_c}. \tag{B25}$$

The first equality follows for a given spectrum from the mean value theorem of calculus; α_1 can be chosen to compensate for the averaging. The second equality follows from the definition of $\omega_{\ln}$ [Eq. (2.16)]. Similarly,

$$b=\frac{\alpha_2}{\omega^2}\lambda \tag{B26}$$

and

$$c(T_c)=\frac{\alpha_3}{\omega_{\ln}^2}\lambda\ln\frac{1.13\omega_{\ln}}{k_BT_c}\ln\frac{1.13\omega_{\ln}}{\beta_3k_BT_c}. \tag{B27}$$

In Eq. (B27), the weak-coupling T_c equation can be used:

$$\ln\frac{1.13\omega_{\ln}}{k_BT_c}=\frac{1+\lambda}{\lambda}. \tag{B28}$$

The result is an equation of the form

$$f=1.43\left[1+\left[\frac{\pi T_c}{\omega_{\ln}}\right]^2\left[z_1\ln\frac{1.13\omega_{\ln}}{k_BT_c}-z_2-\frac{z_3}{\ln\frac{1.13\omega_{\ln}}{k_BT_c}}\right]\right]. \tag{B29}$$

We note that for a δ-function spectrum, the $\alpha_i,\beta_e\equiv1$, and in fact we expect that even for realistic spectra, $\alpha_i\approx\beta_3\approx1$. With this approximation, $z_1\approx5.9$, $z_2\approx5.3$, and $z_3\approx0.2$. Hence we drop the last term in Eq. (B29). Equation (B29) becomes

$$f\equiv\frac{\Delta C(T_c)}{\gamma T_c}=1.43\left[1+a_1\left[\frac{T_c}{\omega_{\ln}}\right]^2\ln\left[\frac{\omega_{\ln}}{b_1T_c}\right]\right], \tag{B30}$$

where

$$a_1=\pi^2\left[\left[4+\frac{24}{7\zeta(3)}\right]\alpha_1-\frac{8}{7\zeta(3)}\alpha_3\right], \tag{B31a}$$

$$b_1=\frac{1}{1.13}\exp\left[\frac{\frac{16}{3}\alpha_2+\frac{8}{7\zeta(3)}\alpha_2-\frac{8}{7\zeta(3)}\alpha_3\ln\beta_3-\frac{8}{7\zeta(3)}\alpha_1}{\left[4+\frac{24}{7\zeta(3)}\right]\alpha_1-\frac{8}{7\zeta(3)}\alpha_3}\right]. \tag{B31b}$$

Equations (B31) are not used to determine a_1 and b_1. Rather, they are fit to numerical data (Table X). The result is $a_1=53$ and $b_1=3$. We note that for $\alpha_i=\beta_3=1$, Eqs. (B31) yield $a_1=58$ and $b_1=2$, remarkably close to the accurate fit. Similarly, for g we obtain

$$g=-3.77\left[1+a_2\left[\frac{T_c}{\omega_{\ln}}\right]^2\ln\left[\frac{\omega_{\ln}}{b_2T_c}\right]\right], \tag{B32}$$

where a_2 and b_2 are functions of α_i and β_3. The fitted values are $a_2=117$ and $b_2=2.9$, whereas our estimates would be (fortuitously) $a_2=117$ and $b_2=3.1$.

b. $T=0$

At zero temperature the Eliashberg equations are modified according to the prescription $2\pi T\sum_\omega \to \int d\omega$. The equation for $Z_S(\omega)$ is folded to the domain $[0,\infty]$, with the result that it can be written

$$Z_S(\omega)=1+4\int_0^\infty \nu\, d\nu\, \alpha^2F(\nu)(A_1+A_2)\,, \tag{B33}$$

where

$$A_1=\int_0^\infty d\omega' \frac{\omega'^2}{\sqrt{\omega'^2+\Delta_0^2}}\frac{1}{(\omega'^2+a_0^2)^2} \tag{B34a}$$

and

$$A_2=\int_0^\infty d\omega' \frac{4\omega^2\omega'^2}{\sqrt{\omega'^2+\Delta_0^2}}\frac{1}{(\omega'^2+a_0^2)^4}\,. \tag{B34b}$$

Here again $a_0^2\equiv\omega^2+\nu^2$. The results are

$$A_1=\frac{1}{2a_0^2}-\frac{\Delta_0^4}{2a_0^4}\left[\ln\frac{2a_0}{\Delta_0}-1\right] \tag{B35a}$$

and

$$A_2=\frac{1}{3}\frac{\omega^2}{a_0^4}\,. \tag{B35b}$$

Other contributions are of higher order. The net result is

$$Z_S(\omega)=Z_N(\omega)+\Delta_0^2\int_0^\infty \frac{2\nu\, d\nu\, \alpha^2F(\nu)}{(\nu^2+\omega^2)^2}\times\left[1-\ln\frac{2\sqrt{\nu^2+\omega^2}}{\Delta_0}\right]; \tag{B36}$$

$Z_N(\omega)$ can be evaluated exactly:

$$Z_N(\omega)=1+\frac{1}{\omega}\int_0^\infty 2\, d\nu\, \alpha^2F(\nu)\tan^{-1}\left[\frac{\omega}{\nu}\right]. \tag{B37}$$

Recall that we have used a constant model for $\Delta(\omega)$ and $Z_S(\omega)$. Hence it should not matter at what frequency we evaluate Eq. (B37), as long as it is small. However, there is a dependence, and once again we will choose $\omega=0$. Then $Z_N(0)=1+\lambda$, and there is no strong-coupling correction. This is again consistent with use of the Sommerfeld constant γ in the ratio $\gamma T_c^2/H_c^2(0)$, for example. Note, moreover, that for evaluation of the free-energy difference, the ω dependence for $Z_S(\omega)-Z_N(\omega)$ must be retained in Eq. (B36), except in the logarithm, once again. One can argue that a more appropriate frequency at which to evaluate $Z_N(\omega)$, and subsequently $\Delta(\omega)$, is Δ_0, the gap edge, since this defines the gap edge. However, it must be kept in mind that this calculation is on the imaginary axis, so that corrections proportional to ω^2 actually have the opposite sign from the correction on the real axis [since $\omega^2=-(i\omega)^2$]. Hence it is more accurate to evaluate at $\omega=0$.

The gap channel is treated similarly, with the result

$$Z_S(0)\Delta_0=\Delta_0\int_0^\infty 2\nu\, d\nu\, \alpha^2F(\nu)(A_3+A_4)\,, \tag{B38}$$

where

$$A_3=\int_0^\infty \frac{d\omega'}{\sqrt{\omega'^2+\Delta_0^2}}\frac{1}{\omega'^2+a_0^2} \tag{B39a}$$

and

$$A_4=\int_0^\infty \frac{d\omega'}{\sqrt{\omega'^2+\Delta_0^2}}\frac{4\omega^2\omega'^2}{(\omega'^2+a_0^2)^3}\,. \tag{B39b}$$

Evaluation of these integrals is straightforward. Combining with Eq. (B36) evaluated at $\omega=0$, we obtain

$$\Delta_0=2\omega_{\ln}\exp\left[-\left[\frac{1+\lambda}{\lambda}\right]\right]\left[1+\frac{3}{2}\frac{\Delta_0^2}{\lambda}(a-\tfrac{5}{6}b)\right]. \tag{B40}$$

Here, a and b are the same functions (within BCS) as in the previous section (evaluated at $T=T_c$). Combining Eq. (B18) with (B40), we obtain

$$\frac{2\Delta_0}{k_BT_c}=3.53\left[1+a_3\left[\frac{T_c}{\omega_{\ln}}\right]^2\ln\left[\frac{\omega_{\ln}}{b_3T_c}\right]\right], \tag{B41}$$

where

$$a_3=[\tfrac{3}{8}(3.53)^2+\pi^2]\alpha_1 \tag{B42a}$$

and

$$b_3=\frac{1}{1.13}\exp\left[\frac{\frac{5}{16}(3.53)^2+\frac{4}{3}\pi^2}{\frac{3}{8}(3.53)^2+\pi^2}\frac{\alpha_2}{\alpha_1}\right]. \tag{B42b}$$

The values first fit by Mitrović, Zarate, and Carbotte (1984) are $a_3=12.5$ and $b_3=2$ (see Table IV). The values we would obtain by setting $\alpha_i\approx 1$ are $a_3=14.5$ and $b_3=2.9$, which again are not much different from the best fit.

The free-energy difference at $T=0$ within our model is written

$$\frac{\Delta F}{N(0)}=-\int_0^\infty d\omega\left[Z_N(\omega)\left[\sqrt{\omega^2+\Delta_0^2}+\frac{\omega^2}{\sqrt{\omega^2+\Delta_0^2}}-2\omega\right]+[Z_S(\omega)-Z_N(\omega)](\sqrt{\omega^2+\Delta_0^2}-\omega)\right]. \tag{B43}$$

In the first term, $Z_N(\omega)=1+\lambda$ is used. In the second, Eq. (B36) must be used to retain convergence. The integrals are easily performed with the result

$$\frac{\Delta F}{N(0)}=-\tfrac{1}{2}(1+\lambda)\Delta_0^2\left[1-\frac{\Delta_0^2}{1+\lambda}(c-a)\right]. \tag{B44}$$

Then, using $\gamma=\frac{2}{3}\pi^2N(0)(1+\lambda)$ along with Eq. (B41), we obtain

$$\frac{\gamma T_c^2}{H_c^2(0)}=0.168\left[1-a_4\left[\frac{T_c}{\omega_{\ln}}\right]^2\ln\left[\frac{\omega_{\ln}}{b_4T_c}\right]\right], \tag{B45}$$

where

$$a_4=29\alpha_1-3.1\alpha_3\,, \tag{B46a}$$

$$b_4=\frac{1}{1.13}\exp\left[\frac{34.1\alpha_2-3.1\alpha_1-3.1\alpha_3\ln\beta_3}{2.9\alpha_1-3.1\alpha_3}\right]. \tag{B46b}$$

The fits to numerical data give $a_4=12.2$, $b_4=3$; the estimates are $a_4=26$, $b_4=2.9$, in error by a (more realistic) factor of 2. The ingredients are also present to calculate the reduced thermodynamic critical field, $h_c(0)\equiv H_c(0)/T_c|H_c'(T_c)|$. We obtain an equation,

$$h_c(0)=0.576\left[1-a_5\left[\frac{T_c}{\omega_{\ln}}\right]^2\ln\left[\frac{\omega_{\ln}}{b_5T_c}\right]\right], \tag{B47}$$

with a fit $a_5=13.4$ and $b_5=3.5$. We note that the properties $\Delta C/\gamma T_c$, $\gamma T_c^2/H_c^2(0)$, and $h_c(0)$ are not independent. Rutger's relation provides the thermodynamic identity

$$h_c(0)=\left[4\pi\frac{\gamma T_c^2}{H_c^2(0)}\frac{\Delta C}{\gamma T_c}\right]^{-1/2}. \tag{B48}$$

Our choices for the various coefficients do not satisfy Eq. (B48) exactly to $O(T_c/\omega_{\ln})^2$. Hence, when manipulating the final equations [Eqs. (B30), (B41), (B45), (B47)], all terms should be retained.

2. Upper critical magnetic field (dirty limit)

a. $T\sim T_c$

We use the same model as that used in Part 1. Moreover, near T_c,$\rho(T)$ is very small. A folding of the summation in Eq. (7.6b) to positive m gives the equation

$$(1+\lambda)\Delta_0=\Delta_0\int_0^\infty 2\nu\,d\nu\,\alpha^2F(\nu)\times\left[P_1+Q_1-\frac{\rho(T)}{1+\lambda}(P_2+Q_2)\right], \tag{B49}$$

where

$$P_i\equiv\sum_{m=1}^{\infty}\frac{2\pi T}{\omega_m^i}\frac{1}{\omega_m^2+a_n^2} \tag{B50a}$$

and

$$Q_i\equiv\sum_{m=1}^{\infty}\frac{2\pi T}{\omega_m^{i-2}}\frac{4\omega_n^2}{(\omega_m^2+a_n^2)^3}\,. \tag{B50b}$$

These are evaluated in terms of digamma functions and expanded in powers of $(T/\nu)^2$. The result is

$$P_1=\frac{1}{\nu^2}\ln\frac{1.13\nu}{k_BT}-\frac{(\pi T)^2}{\nu^4}\left[\ln\frac{1.13\nu}{k_BT}-\frac{1}{3}\right], \tag{B51a}$$

$$P_2=\frac{\pi}{4T}\left[\frac{1}{\nu^2}-\frac{2T}{\nu^3}-\frac{(\pi T)^2}{\nu^4}\right], \tag{B51b}$$

$$Q_1=\frac{(\pi T)^2}{\nu^4}\,. \tag{B51c}$$

Using similar definitions as in Part 1 of this appendix, we obtain

$$1=F(T)+\frac{\rho(T)}{2\pi T(1+\lambda)}G(T)\,, \tag{B52}$$

where $F(T)$ is given by Eq. (B17a), and $G(T)$ is defined

$$G(T)\equiv-\frac{\pi^2}{2}\left[\frac{\lambda}{1+\lambda}-2T\frac{d}{1+\lambda}-(\pi T)^2\frac{b}{1+\lambda}\right]. \tag{B53}$$

A new moment is required,

$$d\equiv\int_0^\infty 2\frac{d\nu}{\nu^2}\alpha^2F(\nu)\,,$$

and will lead to a strong-coupling term that is linear in $T_c/\omega_{\ln}$. The derivative $\rho'(T_c)$ is easily obtained from Eq. (B52). The result is

$$T_c|\rho'(T_c)|=\frac{4T_c}{\pi}(1+\lambda)\left[1+2\frac{T_c}{\lambda}d+4\frac{T_c^2}{\lambda^2}d^2+\frac{(\pi T_c)^2}{\lambda}[2a(T_c)-\tfrac{8}{3}b]\right]. \tag{B54}$$

b. $T=0$

The same prescription is used as before; the limit $\omega\to0$ is used, with the result

$$(1+\lambda)\Delta_0=\Delta_0\int_0^\infty 2\nu\,d\nu\,\alpha^2F(\nu)I(\nu,\bar\rho)\,, \tag{B55}$$

where

$$I(\nu,\bar\rho)\equiv\int_0^\infty d\omega'\frac{1}{\omega'^2+\nu^2}\frac{1}{\omega'+\bar\rho(0)}=\frac{1}{\nu^2}\ln\frac{\nu}{\bar\rho(0)}+\frac{\pi}{2}\frac{\bar\rho(0)}{\nu^3}-\frac{\bar\rho^2(0)}{\nu^4}\ln\frac{\nu}{\bar\rho(0)} \tag{B56}$$

and $\bar{\rho}(0)\equiv\rho(0)/(1+\lambda)$. Using the T_c equation (B18), we easily obtain

$$\rho(0)=\frac{\pi T_c}{2e^{\gamma}}(1+\lambda)\left[1+\frac{\pi}{4e^{\gamma}}\frac{\pi T_c}{\lambda}d+\frac{3}{2}\left[\frac{\pi}{4e^{\gamma}}\right]^2\left[\frac{\pi T_c}{\lambda}\right]^2 d^2+\frac{(\pi T_c)^2}{\lambda}\left[\frac{4e^{2\gamma}-1}{4e^{2\gamma}}a(T_c)-\frac{4}{3}b\right]\right], \tag{B57}$$

where $\gamma\approx 0.577\ldots$ is Euler's constant. Equations (B54) and (B57) are readily combined; using (B25) and (B26) along with $d\equiv\alpha_4\lambda/\omega_{\ln}$, we obtain an equation of the form

$$h_{c2}(0,\infty)=0.693\left[1-a_1\frac{T_c}{\omega_{\ln}}-a_2\left[\frac{T_c}{\omega_{\ln}}\right]^2\ln\frac{\omega_{\ln}}{b_1 T_c}\right]. \tag{B58}$$

An Einstein model gives $a_1=0.61$, $a_2=11.3$, and $b_1=3.7$. The fitted parameters are considerably different, as indicated in Sec. VII.

3. Upper critical magnetic field (clean limit)

a. $T\sim T_c$

Near T_c, expansions similar to those in the dirty limit apply, since $\alpha(T)$ is small. We obtain the equation

$$1+\lambda=\int_0^{\infty}2\nu\,d\nu\,\alpha^2F(\nu)[P_1+Q_1-\tfrac{1}{3}\tilde{\alpha}(T)(P_2+Q_2)], \tag{B59}$$

where the P_i and Q_i are the same as those defined in Eqs. (B12) and (B13). Using Eqs. (B14) we obtain

$$1=F(T)+\tilde{\alpha}(T)G(T), \tag{B60}$$

where now

$$G(T)\equiv-\frac{7}{12}\frac{\zeta(3)}{(\pi T)^2}\frac{\lambda}{1+\lambda}+\frac{7}{12}\zeta(3)\frac{b}{1+\lambda}+\frac{1}{3}\frac{a(T)}{1+\lambda} \tag{B61}$$

and $\tilde{\alpha}(T)\equiv\alpha(T)/(1+\lambda)^2$. We find

$$T_c|\tilde{\alpha}'(T_c)|=\frac{12}{7\zeta(3)}(\pi T_c)^2\times\left\{1+\frac{(\pi T_c)^2}{\lambda}\left[\left[2+\frac{4}{7\zeta(3)}\right]a(T_c)-\frac{8}{3}b\right]\right\}. \tag{B62}$$

b. $T=0$

In the limit $\omega\to 0$ we find

$$1+\lambda=\frac{2}{\sqrt{\tilde{\alpha}(0)}}\int_0^{\infty}2\nu\,d\nu\,\alpha^2F(\nu)I(\nu,\tilde{\alpha}(0)), \tag{B63}$$

where

$$I(\nu,\tilde{\alpha}(0))=\int_0^{\infty}\frac{d\omega}{\omega^2+\nu^2}\int_0^{\infty}dq\,e^{-q^2}\tan^{-1}\left[\frac{\sqrt{\tilde{\alpha}(0)}q}{\omega}\right]. \tag{B64}$$

This double integral cannot be done analytically. However, as was done by Marsiglio, Schossmann, Schachinger, and Carbotte (1987), we use the approximation

$$\chi(\omega)=\frac{1}{1+\lambda}\frac{1}{\omega+c},$$

which was found to be quite accurate. Here, the constant c will contain strong-coupling corrections and is given by $c=\sqrt{\tilde{\alpha}(0)}\,e^{-\gamma/2-1}$. Within BCS, $c^{\rm BCS}=(\pi/2)e^{-\gamma}T_c$. The integral is now elementary. We obtain

$$\tilde{\alpha}(0)=\left[\frac{\pi}{2}\right]^2 e^{-\gamma+2}T_c^2\left\{1+\frac{\pi^2}{2}e^{-\gamma}T_c\frac{d}{\lambda}+\frac{\pi^2}{4}e^{-2\gamma}\left[\pi T_c\frac{d}{\lambda}\right]^2+\frac{2(\pi T_c)^2}{\lambda}\left[\left[1-\frac{e^{-2\gamma}}{4}\right]a(T_c)-\frac{4}{3}b\right]\right\}. \tag{B65}$$

Hence $h_{c2}(0,0)$ is of the form

$$h_{c2}(0,0)=0.727\left[1+a_1\frac{T_c}{\omega_{\ln}}-a_2\left[\frac{T_c}{\omega_{\ln}}\right]^2\ln\frac{\omega_{\ln}}{b_2 T_c}\right]. \tag{B66}$$

An Einstein model gives $a_1=2.8$, $a_2=6.25$, and $b_2=3$. The parameters determined through a fit to numerical data are very different: $a_1=0$, $a_2=2.7$, and $b_2=20$. We have found that the linear term is not required.

REFERENCES

Abrikosov, A. A., 1957, Sov. Phys. JETP **5**, 1174 [Zh. Eksp. Teor. Fiz. **32**, 1442 (1957)].

Abrikosov, A. A., and L. P. Gor'kov, 1960, Zh. Eksp. Teor. Fiz. **39**, 1781.

Abrikosov, A. A., and L. P. Gor'kov, 1961, Sov. Phys. JETP. **12**, 1243.

Abrikosov, A. A., L. P. Gor'kov, and I. E. Dzyaloshinksii, 1963 *Methods of Quantum Field Theory in Statistical Physics* (Prentice-Hall, Englewood, Cliffs, NJ).

Aeppli, G., R. J. Cava, E. J. Ansaldo, J. H. Brewer, S. R.

Kreitzman, G. M. Luke, D. R. Noakes, and R. F. Kiefl, 1987, Phys. Rev. B **35**, 7129.
Akis, R., and J. P. Carbotte, 1989a, J. Low. Temp. Phys. **76**, 65.
Akis, R., and J. P. Carbotte, 1989b, Physica C **159**, 395.
Akis, R., and J. P. Carbotte, 1989c, Physica C **162-163**, 1491.
Akis, R., F. Marsiglio, and J. P. Carbotte, 1989, Phys. Rev. B **39**, 2722.
Akis, R., F. Marsiglio, E. Schachinger, and J. P. Carbotte, 1988, Phys. Rev. B **37**, 9318.
Allen, P. B., 1972, Phys. Rev. B **6**, 2577.
Allen, P. B., 1974, Solid State Commun. **14**, 937.
Allen, P. B., 1975, in *Dynamical Properties of Solids,* edited by G. K. Horton and A. A. Maradudin (North-Holland, Amsterdam), Vol. 3, p. 95.
Allen, P. B., 1980, in *Modern Trends in the Theory of Condensed Matter,* edited by A. Pekalski and J. Przystawa (Springer, New York), p. 388.
Allen, P. B., and M. L. Cohen, 1969, Phys. Rev. **187**, 525.
Allen, P. B., and R. C. Dynes, 1975, Phys. Rev. B **12**, 905.
Allen, P. B., and B. Mitrović, 1982, in *Solid State Physics,* edited by H. Ehrenreich, F. Seitz, and D. Turnbull (Academic, New York), Vol. 37, p. 1.
Allender, D., J. Bray, and J. Bardeen, 1973, Phys. Rev. B 7, 1020.
Alterovitz, S., and D. E. Mapother, 1975, Phys. Rev. B **11**, 139.
Ambegaokar, V., and A. A. Griffin, 1965, Phys. Rev. **137**, A1151.
Anderson, J. R., and A. V. Gold, 1963, Phys. Rev. **139**, A1459.
Anderson, P. W., 1959, J. Phys. Chem. Solids **11**, 26.
Anderson, P. W., 1987, Science **235**, 1196.
Anderson, P. W., G. Baskaran, Z. Zou, and T. Hsu, 1987, Phys. Rev. Lett. **58**, 2790.
Apfelstedt, I., R. Flükiger, R. Meir-Hirmer, B. Obst, C. Politis, W. Schauer, F. Weiss, and H. Wühi, 1987, in *Proceedings of the 18th International Conference on Low Temperature Physics—LT 18,* edited by Y. Nagaoka (Jpn. J. Appl. Phys. **26**, Suppl. **26-3**, 1181).
Appapillai, M., and A. R. Williams, 1973, J. Phys. F **3**, 759.
Arbman, G., and T. Jarlborg, 1978, Solid State Commun. **26**, 857.
Arnold, G. B., 1978, Phys. Rev. B **18**, 1076.
Arnold, G. B., J. Zasadzinski, J. W. Osmun, and E. L. Wolf, 1980, J. Low Temp. Phys. **40**, 225.
Arnold, G. B., J. Zasadzinski, and E. L. Wolf, 1978, Phys. Lett. A **69**, 136.
Ashauer, B., W. Lee, D. Rainer and J. Rammer, 1987, Physica **148B**, 243.
Ashauer, B., W. Lee, and J. Rammer, 1987, Z. Phys. B **67**, 147.
Axe, J. D., and G. Shirane, 1973, Phys. Rev. B **8**, 1965.
Ayache, C., B. Barbara, E. Bonjour, R. Calemczuk, M. Couach, and J. H. Henry, 1987, Solid State Commun. **64**, 247.
Bangert, W., J. Geerk, and P. Schweiss, 1985, Phys. Rev. B **31**, 6066.
Baquero, R., and J. P. Carbotte, 1983, J. Low Temp. Phys. **51**, 135.
Baquero, R., J. M. Daams, and J. P. Carbotte, 1981, J. Low Temp. Phys. **42**, 585.
Bardeen, J., L. N. Cooper, and J. R. Schrieffer, 1957, Phys. Rev. **108**, 1175.
Bardeen, J., and M. Stephen, 1964, Phys. Rev. **136**, A1485.
Barone, A., A. Di Chiara, G. Peluso, U. Scotti di Uccio, A. M. Cucolo, R. Vaglio, F. C. Matacotta, and E. Oliz, 1987, Phys. Rev. B **36**, 7121.
Batlogg, B., R. J. Cava, A. Jayaraman, R. B. van Dover, G. A. Kourouklis, S. Sunshine, D. W. Murphy, L. W. Rupp, H. S. Chen, A. White, K. T. Short, A. M. Mujsce, and E. A. Rietman, 1987, Phy. Rev. Lett. **58**, 2333.
Batlogg, B., G. Kourouklis, W. Weber, R. J. Cava, A. Jayaraman, A. E. White, K. T. Short, L. W. Rupp, and E. A. Rietman, 1987, Phys. Rev. Lett. **59**, 912.
Batlogg, B., A. D. Raminz, R. J. Cava, R. B. van Dover, and E. A. Rietman, 1987, Phys. Rev. B **35**, 5340.
Batlogg, B., J. P. Remeika, R. C. Dynes, H. Barz, A. S. Cooper, and J. P. Garno, 1982, in *Superconductivity in d- and f-Band Metals,* edited by W. Buckel and W. Weber (Kernforschungszentrum, Karlsruhe), p. 401.
Bazhenov, A. V., A. V. Gorbunov, N. V. Klassen, S. F. Kondakov, I. V. Kukushkin, V. D. Kulakovskii, O. V. Misochko, V. B. Tiimofeev, L. I. Chernyshova, and B. N. Shepel, 1987, in *Novel Superconductivity,* edited by S. A. Wolf and V. Z. Kresin (Plenum, New York), p. 893.
Beckman, O., L. Lundgren, P. Nordblad, I. Sandlund, P. Svedlindh, T. Lundström, and S. Rundqvist, 1987, Phys. Lett. A **125**, 425.
Bednorz, J. G., and K. A. Müller, 1986, Z. Phys. B **64**, 189.
Benitez, E. L., J. J. Lin, S. J. Poon, W. E. Farneth, M. K. Crawford, and E. M. McCarron, 1988, Phys. Rev. B **38**, 5025.
Bergmann, G., and D. Rainer, 1973, Z. Phys. **263**, 59.
Birgeneau, R. J., C. Y. Chen, D. R. Gabbé, H. P. Jenssen, M. D. Kastner, C. J. Petters, P. J. Picone, T. Thio, T. R. Thurston, H. L. Tuller, J. D. Axes, B. Bone, and G. Shirane, 1987, Phys. Rev. Lett. **59**, 1329.
Blaschke, R., and R. Brocksdorf, 1982, Z. Phys. B **49**, 99.
Blezius, J., R. Akis, F. Marsiglio, and J. P. Carbotte, 1988, Phys. Rev. B **38**, 179.
Blezius, J. W., and J. P. Carbotte, 1986, Phys. Rev. B **33**, 3509.
Blezius, J. W., and J. P. Carbotte, 1987, Phys. Rev. B **36**, 3622.
Blezius, J. W., and J. P. Carbotte, 1988, J. Low Temp. Phys. **73**, 255.
Bonn, D. A., J. E. Greedan, C. V. Stager, T. Timusk, M. G. Doss, S. L. Herr, K. Kamarás, and D. B. Tanner, 1987, Phys. Rev. Lett. **58**, 2249.
Bonn, D. A., *et al.*, 1987, Phys. Rev. B **35**, 8843.
Bourne, L. C., M. F. Crommie, A. Zettl, H. zur Loye, S. W. Keller, K. L. Leary, A. M. Stacy, K. J. Chang, M. L. Cohen, and D. E. Morris, 1987, Phys. Rev. Lett. **58**, 2337.
Bourne, L. C., S. Hoen, M. F. Crommie, W. N. Creger, A. Zettl, Marvin L. Cohen, L. Bernardez, J. Kinney, and D. E. Moris, 1988, Solid State Commun. **67**, 707.
Bourne, L. C., A. Zettl, T. W. Barbee, III, and M. L. Cohen, 1987, Phys. Rev. B **36**, 3190.
Braginski, A. I., 1987, in *Novel Superconductivity,* edited by S. A. Wolf and V. Z. Kresin (Plenum, New York), p. 935.
Brock, J. C. F., 1969, Solid State Commun. **7**, 1798.
Brockhouse, B. N., T. Arase, G. Coglioti, K. R. Rao, and A. D. B. Woods, 1962, Phys. Rev. **128**, 1099.
Brockhouse, B. N., E. D. Hallman, and S. C. Ng, 1968, in *Magnetic and Inelastic Scattering of Neutrons in Metals,* edited by T. J. Rowland and P. A. Beck (Gordon and Breach, London).
Brown, A., M. W. Zemansky, and H. A. Boorse, 1953, Phys. Rev. **92**, 52.
Bruesch, P., and W. Buhrer, 1988, Z. Phys. B **70**, 1.
Brun, Torben, M. Grimsditch, K. E. Gray, R. Bhadra, V. Maroni, and C.-K. Loong, 1987, Phys. Rev. B **35**, 8837.
Bulaevskii, L. N., and O. V. Dolgov, 1987a, JETP Lett. **45**, 526.
Bulaevskii, L. N., and O. V. Dolgov, 1987b, Pis'ma Zh. Eksp. Teor. Fiz. **45**, 413.
Bulaevskii, L. N., O. V. Dolgov, and M. O. Ptitsyn, 1988, Phys.

Rev. B **38**, 11 290.
Butler, W. H., F. J. Pinski, and P. B. Allen, 1979, Phys. Rev. B **19**, 3708.
Butler, W. H., H. G. Smith, and N. Wakabayaski, 1977, Phys. Rev. Lett. **39**, 1004.
Cai, J., G. Ji, H. Wu, J. Cai, and C. Gong, 1979, Sci. Sin. **22**, 417.
Capone, D. W., II, D. G. Hinks, J. D. Jorgensen, and K. Zhang, 1987, Appl. Phys. Lett. **9**, 543.
Carbotte, J. P., 1969, in *Superconductivity,* edited by P. R. Wallace (Gordon and Breach, London), Vol. 1, p. 491.
Carbotte, J. P., 1982, in *Superconductivity in d- and f-Band Metals,* edited by W. Buckel and W. Weber (Kernforschungszentrum, Karlsruhe), p. 487.
Carbotte, J. P., 1987a, Sci. Prog. (London) **71**, 329.
Carbotte, J. P., 1987b, in *Novel Superconductivity,* edited by S. A. Wolf and V. Z. Kresin, (Plenum, New York), p. 73.
Carbotte, J. P., and R. C. Dynes, 1968, Phys. Rev. **172**, 476.
Carbotte, J. P., and F. Marsiglio, 1989, in *Studies of High Temperature Superconductors,* edited by A. Narlikar (Nova Science, New York), p. 64.
Carbotte, J. P., F. Marsiglio, and B. Mitrović, 1986, Phys. Rev. B **33**, 6135.
Carbotte, J. P., and P. Vashishta, 1971, Can. J. Phys. **49**, 1493.
Cava, R. J., R. B. van Dover, B. Batlogg, and E. A. Rietman, 1987, Phys. Rev. Lett. **58**, 408.
Chanin, G., and J. P. Torre, 1972, Phys. Rev. B **5**, 4357.
Chen, J. T., L. E. Wenger, C. J. McEwan, and E. M. Logothetis, 1987, Phys. Rev. Lett. **58**, 1972.
Chen, T. T., J. T. Chen, J. D. Leslie, and H. J. T. Smith, 1969, Phys. Rev. Lett. **22**, 526.
Chou, C., D. White, and H. L. Johnston, 1958, Phys. Rev. **109**, 788.
Christen, D. K., H. R. Kerchner, S. T. Sekula, and Y. K. Chang, 1984, in *Proceedings of the Seventeenth International Conference on Low Temperature Physics, Part II,* edited by U. Eckern, A. Schmid, W. Weber, and H. Wühl (North-Holland, Amsterdam), p. 1035.
Chu, C. W., P. H. Hor, R. L. Meng, L. Gao, Z. J. Huang, and Y. Q. Wang, 1987, Phys. Rev. Lett. **58**, 405.
Clement, J. R., and E. H. Quinnell, 1952, Phys. Rev. **85**, 502.
Cohen, M., and P. W. Anderson, 1972, in *Superconductivity in d- and f-Band Metals,* AIP Conference Proceedings No. 4, edited by D. H. Douglass (AIP, New York), p. 17.
Combescot, R., 1984, Europhys. Lett. **10**, 177.
Combescot, R., 1989, Physica C **162-164**, 1507.
Combescot, R., and J. Labbé, 1988, Physica C **153-155**, 204.
Cooke, D. W., R. L. Hutson, R. S. Kwok, M. Maez, H. Rempp, M. E. Schillaci, J. L. Smith, J. O. Willis, R. L. Lichti, K. C. B. Chan, C. Boekema, S. P. Weathersby, J. A. Flint, and J. Oostens, 1988, Phys. Rev. B **37**, 9401.
Cooke, D. W., R. L. Hutson, R. S. Kwok, M. Maez, H. Rempp, M. E. Schillaci, J. L. Smith, J. O. Willis, R. L. Lichti, K. C. B. Chan, C. Boekema, S. P. Weathersby, and J. Oostens, 1989, Phys. Rev. B **39**, 2748.
Coombes, J. M., and J. P. Carbotte, 1986a, J. Low Temp. Phys. **63**, 431.
Coombes, J. M., and J. P. Carbotte, 1986b, Phys. Rev. B **34**, 4622.
Coombes, J. M., and J. P. Carbotte, 1987, Phys. Rev. B **35**, 6643.
Coombes, J. M., and J. P. Carbotte, 1988, Phys. Rev. B **38**, 8697.
Corsan, J. M., and A. J. Cook, 1969, Phys. Lett. A **28**, 500.
Cowan, W., and J. P. Carbotte, 1978, Phys. Lett. A **64**, 470.
Cowley, E. R., 1974, Solid State Commun. **14**, 587.
Crommie, M. F., L. C. Bourne, A. Zettl, Marvin L. Cohen, and A. Stacy, 1987, Phys. Rev. B **35**, 8853.
Daams, J. M., 1979, Ph.D. thesis (McMaster University).
Daams, J. M., and J. P. Carbotte, 1978, Can. J. Phys. **56**, 1248.
Daams, J. M., and J. P. Carbotte, 1980a, J. Low Temp. Phys. **40**, 135.
Daams, J. M., and J. P. Carbotte, 1980b, Solid State Commun. **33**, 585.
Daams, J. M., and J. P. Carbotte, 1981, J. Low Temp. Phys. **43**, 263.
Daams, J. M., J. P. Carbotte, M. Ashraf, and R. Baquero, 1984, J. Low Temp. Phys. **55**, 1.
Daams, J. M., J. P. Carbotte, and R. Baquero, 1979, J. Low Temp. Phys. **35**, 547.
Daams, J. M., B. Mitrović, and J. P. Carbotte, 1981, Phys. Rev. Lett. **46**, 65.
Decker, D. L., D. E. Mapother, and R. W. Shaw, 1958, Phys. Rev. **112**, 1888.
Decroux, M., and Ø. Fischer, 1982, in *Superconductivity in Ternary Compounds,* edited by M. B. Maple and Ø. Fischer (Springer, New York), Vol. 2, p 57.
Decroux, M., A. Junod, A. Bezinge, D. Cattani, J. Cors, J.L. Jorda, A. Stettler, M. François, K. Yvon, Ø. Fischer, and J. Muller, 1987, Europhys. Lett. **3**, 1035.
Degiorgi, L., E. Kaldis, and P. Wachter, 1987, Solid State Commun. **64**, 873.
Deutscher, G., O. Entin-Wohlman, S. Fishman, and Y. Shapira, 1980, Phys. Rev. B **21**, 5041.
de Wette, F. W., J. Prade, A. D. Kulkarni, U. Schröder, and W. Kress, 1988, Phys. Rev. B **38**, 6583.
Dolgov, O. V., and A. A. Lolubov, 1988, Int. J. Mod. Phys. B **1**, 1089.
Dolgov, O. V., and E. G. Maksimov, 1982a, Sov. Phys. Usp. **25**, 688.
Dolgov, O. V., and E. G. Maksimov, 1982b, Usp. Fiz. Nauk **138**, 95.
Dreschsler, S. L., and N. M. Plakida, 1987, Phys. Status Solidi B **144**, K113.
Dreschsler, S. L., and N. M. Plakida, 1988, Physica C **153-155**, 206.
Dunlap, B. D., M. V. Nevitt, M. Slaski, T. E. Klippert, Z. Sungaila, A. G. McKale, D. W. Capone, R. B. Poeppel, and B. K. Fladermeyen, 1987, Phys. Rev. B **35**, 7210.
Dynes, R. C., 1972, Solid State Commun. **10**, 615.
Dynes, R. C., J. P. Carbotte, D. W. Taylor, and C. K. Campbell, 1969, Phys. Rev. **178**, 713.
Dynes, R. C., J. P. Carbotte, and E. J. Woll, 1968, Solid State Commun. **6**, 101.
Ebner, C., and D. Stroud, 1985, Phys. Rev. B **31**, 165.
Ekino, T., and J. Akimitsu, 1987, Jpn. J. Appl. Phys. **26**, L452.
Ekino, T., J. Akimitsu, M. Sato,and S. Hosoya, 1987, Solid State Commun. **62**, 535.
Eliashberg, G. M., 1960a, Sov. Phys. JETP **11**, 696.
Eliashberg, G. M., 1960b, Zh. Eksp. Teor. Fiz. **38**, 966.
Escudero, R., L. Renón, T. Akachi, R. A. Barrio, and J. Tagüeña-Martínez, 1987, Phys. Rev. B **36**, 3910.
Etemad, S., D. E. Aspnes, M. K. Kelly, R. Thompson, J. M. Tarascon, and G. W. Hull, 1987, Phys. Rev. B **37**, 3396.
Faltens, T. A., W. K. Ham, S. W. Keller, K. J. Leary, J. N. Michaels, A. M. Stacy, H. zur Loye, D. E. Morris, T. W. Barbee, III, L. C. Bourne, M. L. Cohen, S. Hoen, and A. Zettl, 1987, Phys. Rev. Lett. **59**, 915.

Ferreira da Silva J., E. A. Burgemeister, and Z. Dokoupil, 1969, Physica **41**, 409.
Finnemore, D. K., R. N. Shelton, J. R. Clem, R. W. McCallun, H. C. Ku, R. E. McCarley, S. C. Chen, P. Klavins, and V. Kogan, 1987, Phys. Rev. B **35**, 5319.
Finnemore, D. K., T. F. Stromberg, and C. A. Swenson, 1966, Phys. Rev. **149**, 231.
Fiory, A. T., A. F. Hebard, P. M. Mankiewich, and R. E. Howard, 1988, Phys. Rev. Lett. **61**, 1419.
Fisher, D. S., A. J. Millis, B. Shraiman, and R. N. Bhatt, 1988, Phys. Rev. Lett. **61**, 482.
Franck, J. P., J. Jung, G. J. Salomons, W. A. Miner, and M. A.-K. Mohamed, J. Chrzanowski, S. Gygax, J. C. Irwin, D. F. Mitchell, and I. Sproule, 1989, Physica C **164**, 753.
Freeman, A. J., J. Yu, and C. L. Fu, 1987, Phys. Rev. B **36**, 7111.
Fujiwara, T., and Y. Hatsugai, 1987, Jpn. J. Appl. Phys. **26**, L716.
Fuller, W. W., M. S. Osofsky, L. E. Toth, S. B. Qadri, S. H. Lawrence, R. A. Hein, D. U. Gubser, T. L. Francavilla, and S. A. Wolf, 1987, in *Proceedings of the 18th International Conference on Low Temperature Physics—LT 18,* edited by Y. Nagaoka (Jpn. J. Appl. Phys. **26**, Suppl. 26-3, 1189).
Galkin, A. A., A. I. D'yachenko, and V. M. Svistunov, 1974, Sov. Phys. JETP **39**, 1115 [Zh. Eksp. Teor. Fiz. **66**, 2262 (1974)].
Gallo, C. F., L. R. Whitney, and P. J. Walsh, 1987, in *Novel Superconductivity,* edited by S. A. Wolf and V. Z. Kresin (Plenum, New York), p. 385.
Geerk, J., J. M. Rowell, P. H. Schmidt, F. Wuchner, and W. Schaver, 1982, in *Superconductivity in d- and f-Band Metals,* edited by W. Buckel and W. Weber (Kernforschungszentrum, Karlsruhe), p. 23.
Geilikman, B. T., and V. Z. Kresin, 1965, Fiz. Tverd. Tela (Leningrad) **1**, 3294.
Geilikman, B. T., and V. Z. Kresin, 1966, Sov. Phys. Solid State **7**, 2659.
Geilikman, B. T., V. Z. Kresin, and N. F. Masharov, 1975, J. Low Temp. Phys. **18**, 241.
Genzel, L., A. Wittlin, J. Kulm, H. Mattausch, W. Bauhofer, and A. Simon, 1987, Solid State Commun. **63**, 843.
Gilat, G., 1965, Solid State Commun. **3**, 101.
Ginsberg, D. M., R. E. Harris, and R. C. Dynes, 1976, Phys. Rev. B **14**, 990.
Ginzburg, V. L., 1964a, Zh. Eksp. Teor. Fiz. **47**, 2318.
Ginzburg, V. L., 1964b, Phys. Lett. **13**, 101.
Ginzburg, V. L., 1965, Sov. Phys. JETP **20**, 1549.
Ginzburg, V. L., and D. A. Kirzhnits, 1982, *High Temperature Superconductivity* (Consultants Bureau, New York).
Gladstone, G., M. A. Jensen, and J. R. Schrieffer, 1969, in *Superconductivity,* edited by R. D. Parks (Marcel Dekker, New York), Vol. 2, p. 665.
Glötzel, D., D. Rainer, and H. R. Schober, 1979, Z. Phys. B **35**, 317.
Gor'kov, L. P., 1959a, Zh. Eksp. Teor. Fiz. **36**, 1918.
Gor'kov, L. P., 1959b, Sov. Phys. JETP **9**, 1364.
Grabowski, M., and L. J. Sham, 1984, Phys. Rev. B **29**, 6132.
Grimvall, G., 1968, J. Phys. Chem. Solids **29**, 1221.
Grimvall, G., 1969, Phys. Kondens. Mater. **9**, 283.
Grimvall, G., 1981, *The Electron-Phonon Interaction in Metals* (North-Holland, New York).
Gurvitch, M., and A. T. Fiory, 1987a, Phys. Rev. Lett. **59**, 1337.
Gurvitch, M., and A. T. Fiory, 1987b, in *Novel Superconductivity,* edited by S. A. Wolf and V. Z. Kresin (Plenum, New York), p. 663.
Gurvitch, M., A. T. Fiory, L. S. Schemeyer, R. T. Cava, G. P. Espinosa, and J. V. Waszczak, 1988, Physica C **153-155**, 1369.
Gygax, F. N., B. Hitti, E. Lippelt, A. Schenck, D. Cattani, J. Cors, M. Decroux, O. Fischer, and S. Barth, 1987, Europhys. Lett. **4**, 473.
Hansen, H. H., R. L. Pompi, and T. M. Wu, 1973, Phys. Rev. B **8**, 1042.
Harmon, B. N., and S. K. Sinha, 1976, in *Superconductivity in d- and f-Band Metals,* edited by D. H. Douglass (Plenum, New York), p. 391.
Harmon, B. N., and S. K. Sinha, 1977, Phys. Rev. B **16**, 3919.
Harris, R. E., R. C. Dynes, and D. M. Ginsberg, 1976, Phys. Rev. B **14**, 993.
Harshman, D. R., G. Aeppli, E. J. Ansaldo, B. Batlogg, J. H. Brewer, J. F. Carolan, R. J. Cava, M. Celio, A. C. D. Chaklader, W. N. Hardy, S. R. Kreitzman, G. M. Luke, D. R. Noakes, and M. Senba, 1987, Phys. Rev. B **36**, 2386.
Harshman, D. R., L. F. Schneemeyer, J. V. Waszezak, G. Aeppli, R. J. Cava, B. Batlogg, L. W. Rupp, E. J. Ansaldo, and D. L. Williams, 1989, Phys. Rev. B **39**, 851.
Hauser, J. J., D. D. Bacon, and W. H. Haemmerle, 1966, Phys. Rev. **151**, 296.
Hawley, M. E., K. E. Gray, D. W. Capone, II, and D. G. Hinks, 1987, Phys. Rev. B **35**, 7224.
Heine, V., P. Nozieres, and J. W. Wilkins, 1966, Philos. Mag. **13**, 741.
Helfand, E., and N. R. Werthamer, 1964, Phys. Rev. Lett. **13**, 686.
Helfand, E., and N. R. Werthamer, 1966, Phys. Rev. **147**, 288.
Herman, F., R. V. Kasowick, and W. Y. Hsu, 1987, Phys. Rev. B **36**, 6912.
Herr, S. L., K. Kamarás, C. D. Porter, M. G. Doss, D. B. Tanner, D. A. Bonn, J. E. Greedan, C. V. Stager, and T. Timusk, 1987, Phys. Rev. B **36**, 733.
Hershfeld, A. T., H. A. Leupold, and H. A. Boorse, 1962, Phys. Rev. **127**, 1501.
Hidaka, T., T. Matsui, and Y. Nakagawa, 1988, Jpn. J. Appl. Phys. **27**, Part 2, L553.
Hidaka, Y., Y. Enomoto, M. Suzuki, M. Oda, A. Katsui, and T. Murakami, 1987, in *Proceedings of the 18th International Conference on Low Temperature Physics—LT 18,* edited by Y. Nagaoka (Jpn. J. Appl. Phys. **26**, Suppl. 26-3, 1133).
Hidaka, Y., Y. Enomoto, M. Suzuki, M. Oda,and T. Murakami, 1987, Jpn. J. Appl. Phys. **26**, Part 2, L377.
Hirsch, J. E., and F. Marsiglio, 1989a, Physica **162-164**, 591.
Hirsch, J. E., 1989b, Physica C **158**, 326.
Hirsch, J. E., 1989c, Phys. Lett. A **138**, 83.
Hirsch, J. E., and F. Marsiglio, 1989, Phys. Rev. B **39**, 11 515.
Hoen, S., W. N. Creager, L. C. Bourne, M. F. Crommie, T. W. Barbee, III, L. Cohen, and A. Zettl, 1989, Phys. Rev. B **39**, 2269.
Iguchi, I., H. Watanabe,Y. Kasai, T. Mochiku, A. Sugishita, and E. Yamaka, 1987, Jpn. J. Appl. Phys. **26**, L645.
Inderhees, S. E., M. B. Salamon, T. A. Friedmann, and D. M. Ginsberg, 1987, Phys. Rev. B **36**, 2401.
Ishikawa, M., and L. E. Toth, 1971, Phys. Rev. **13**, 1856.
Iye, Y., T. Tamegai, H. Takeya, and H. Takei, 1987, Jpn. J. Appl. Phys. **26**, L1057.
Jaffe, J. E., 1989, Phys. Rev. B **40**, 2558.
Junod, A., A. Bezinge, D. Cattani, J. Cors, M. Decroux, Ø. Fischer, P. Genoud, L. Hoffmann, J.-L. Jorda, J. Muller, and E. Walker, 1987, in *Proceedings of the 18th International Conference on Low Temperature Physics—LT 18,* edited by Y.

Nagaoka (Jpn. J. Appl. Phys. **26**, Suppl. 26-3, 1021).
Junod, A., A. Bezinge, D. Eckert, T. Graf, and J. Muller, 1988, Physica C **152**, 495.
Junod, A., J. L. Jorda, and J. Muller, 1986, J. Low Temp. Phys. **62**, 301.
Junod, A., *et al.*, 1987, Europhys. Lett. **4**, 247.
Kamarás, K., C. D. Porter, M. G. Doss, S. L. Herr, D. B. Tanner, D. A. Bonn, J. E. Greedon, A. H. O'Reilly, C. V. Stager, and T. Timusk, 1987, Phys. Rev. Lett. **59**, 919.
Karakosov, A. E., E. G. Maksimov, and S. A. Mashkov, 1975, Zh. Eksp. Teor. Fiz. **68**, 1937.
Karakosov, A. E., E. G. Maksimov, and S. A. Mashkov, 1976, Sov. Phys. JETP **41**, 971.
Katayama-Yoshida, H., T. Hirooka, *et al.*, 1988, Physica C **156**, 481.
Kerchner, H. R., and D. M. Ginsberg, 1973, Phys. Rev. B **8**, 3190.
Khan, F. S., and P. B. Allen, 1980, Solid State Commun. **36**, 481.
Kiefl, R. F., T. M. Riseman, G. Aeppli, E. J. Ansaldo, J. F. Carolan, R. J. Cava, W. N. Hardy, D. R. Harshman, N. Kaplan, J. R. Kempton, S. R. Kreitzman, G. M. Luke, B. X. Yang, and D. L. Williams, 1988, Physica C **153-155**, 757.
Kieselmann, G., and H. Rietschel, 1982, J. Low Temp. Phys. **46**, 27.
Kihlstrom, K. E., 1985, Phys. Rev. B **32**, 2891.
Kihlstrom, K. E., and T. H. Geballe, 1981, Phys. Rev. B **24**, 4101.
Kimhi, D. B., and T. H. Geballe, 1980, Phys. Rev. Lett. **45**, 1039.
Kirk, M. D., *et al.*, 1987, Phys. Rev. B **35**, 8850.
Kirtley, J. R., R. T. Collins, Z. Schlesinger, W. J. Gallagher, R. L. Sandstrom, T. R. Dinger, and D. A. Chance, 1987, Phys. Rev. B **35**, 8846.
Kirtley, J. R., C. C. Tsuei, S. I. Park, C. C. Chi, J. Rozen, and M. W. Shafer, 1987, Phys. Rev. B **35**, 7216.
Kirtley, J. R., C. C. Tsuei, S. I. Park, C. C. Chi, J. Rozen, M. W. Shafer, W. J. Gallagher, R. L. Sandstrom, T. R. Dinger, and D. A. Chance, 1987, in *Proceedings of the 18th International Conference on Low Temperature Physics—LT 18,* edited by Y. Nagaoka (Jpn. J. Appl. Phys. **26**, Suppl. 26-3, 997).
Kirzhnits, D. A., E. G. Maksimov, and D. I. Khomskii, 1973, J. Low Temp. Phys. **10**, 79.
Kitazawa, K., T. Atake, H. Ishii, H. Sato, H. Takagi, S. Uchida, Y. Saito, K. Fueki, and S. Tanaka, 1987, Jpn. J. Appl. Phys. **26**, L748.
Kitazawa, K., T. Atake, K. Kisho, T. Hasegawa, H. Takagi, S. Uchida, Y. Saito, K. Fueki, S. Tanaka, and M. Sakai, 1987, Jpn. J. Appl. Phys. **26**, L751.
Klein, B. M., L. L. Boyer, D. A. Papconstantopoulos, and L. F. Mattheiss, 1978, Phys. Rev. B **18**, 6411.
Klein, B. M., D. A. Papaconstantopoulos, and L. F. Mattheiss, 1980, in *Superconductivity in d- and f-Band Metals,* edited by H. Suhl and M. B. Maple (Academic, New York), p. 455.
Knapp, G. S., S. D. Bader, H. V. Culvert, F. Y. Fradin, and T. E. Klipper, 1975, Phys. Rev. B **11**, 4331.
Kobayashi, N., T. Sasaoka, K. Oh-ishi, M. Kikuchi, M. Furuyama, T. Sasaki, K. Nato, Y. Syono, and Y. Muto, 1987, Jpn. J. Appl. Phys. **26**, L757.
Kossler, W. J., J. R. Kempton, X. H. Yu, H. E. Schone, Y. J. Uemura, A. R. Moodenbaugh, and M. Suenaga, 1987, Phys. Rev. B **35**, 7133.
Kotov, B. A., N. M. Okuneva, and E. L. Plachenova, 1968a, Fiz. Tverd. Tela (Leningrad) **10**, 513.
Kotov, B. A., N. M. Okuneva, and E. L. Plachenova, 1968b, Sov. Phys. Solid State **10**, 402.
Kresin, V. Z., 1987, Solid State Commun. **63**, 725.
Kresin, V. Z., and V. P. Parkhomenko, 1974, Fiz. Tverda. Tela (Leningrad) **16**, 3363.
Kresin, V. Z., and V. P. Parkhomenko, 1975, Sov. Phys. Solid State **16**, 2180.
Kresin, V. Z., and G. O. Zaitsev, 1978a, Zh. Eksp. Teor. Fiz. **74**, 1886.
Kresin, V. Z., and G. O. Zaitsev, 1978b, Sov. Phys. JETP **47**, 983.
Kung, C., H. Wu, C. Tsai, and K. Chi, 1978, Sci. Sin. **21**, 62.
Kus, F. W., and J. P. Carbotte, 1979, Solid State Commun. **29**, 715.
Kwo, J., and T. H. Geballe, 1981, Phys. Rev. B **23**, 3230.
Kwok, W. K., G. W. Crabtree, D. G. Hinks, D. W. Capone, J. D. Jorgensen, and K. Zhang, 1987, Phys. Rev. B **35**, 5343.
Laborde, O., J. L. Tholence, P. Lejay, A. Sulpice, R. Tournier, J. J. Capponi, C. Michel, and J. Provost, 1987, Solid State Commun. **63**, 877.
Leary, K. J., H. zur Loye, S. W. Keller, T. A. Faltens, W. K. Ham, J. N. Michaels, and A. M. Stacy, 1987, Phys. Rev. Lett. **59**, 1236.
Leavens, C. R., 1974, Solid State Commun. **15**, 1329.
Leavens, C. R., 1975, Solid State Commun. **17**, 1499.
Leavens, C. R. 1977, J. Phys. F **7**, 1911.
Leavens, C. R., and J. P. Carbotte, 1971, Can. J. Phys. **49**, 724.
Leavens, C. R., and J. P. Carbotte, 1972, Ann. Phys. (N.Y.) **70**, 338.
Leavens, C. R., and J. P. Carbotte, 1974, J. Low Temp. Phys. **14**, 195.
Leavens, C. R., and J. P. Carbotte, 1977, Ferroelectricity **16**, 295.
Leavens, C. R., and E. W. Fenton, 1980, Solid State Commun. **33**, 597.
Leavens, C. R., and D. Ritchie, 1984, in *Proceedings of the 17th International Conference on Low Temperature Physics–LT 17,* edited by U. Eckern, A. Schmidt, W. Weber, and H. Wühl (Physica B **126**, 1045).
Leavens, C. R., and D. S. Ritchie, 1985, Solid State Commun. **53**, 137.
Lee, M., M. Yudkowsky, W. P. Halperin, J. Thiel, S.-J. Hwu, and K. R. Poeppelmeir, 1987, Phys. Rev. B **36**, 2378.
Leiderer, P., R. Feile, B. Renker, and D. Ewert, 1987, Z. Phys. B **67**, 25.
Lemberger, T. R., D. M. Ginsberg, and G. Rickayzen, 1978, Phys. Rev. B **18**, 6057.
Leung, H. K., J. P. Carbotte, D. W. Taylor, and C. R. Leavens, 1976a, Can. J. Phys. **54**, 1585.
Leung, H. K., J. P. Carbotte, D. W. Taylor, and C R. Leavens, 1976b, J. Low Temp. Phys. **24**, 2534.
Leupold, H. A., and H. A. Boorse, 1964, Phys. Rev. **134**, A1322.
Li, Q., G. Lu, K. Wu, Y. Zhou, C. Li, and D. Yin, 1987, Solid State Commun. **64**, 209.
Lichti, R. L., K. C. B. Chan, D. W. Cooke, and C. Boekema, 1989, Appl. Phys. Lett. **54**, 2361.
Lie, S. G., and J. P. Carbotte, 1980, Solid State Commun. **35**, 129.
Lim, C. S., J. D. Leslie, H. J. T. Smith, P. Vashishta, and J. P. Carbotte, 1970, Phys. Rev. B **2**, 1651.
Lin, Quan, *et al.*, 1988, Solid State Commun. **65**, 869.
Little, W. A., 1964, Phys. Rev. **134**, A1416.
Little, W. A., 1987, in *Novel Superconductivity,* edited by S. A. Wolf and V. Z. Kresin (Plenum, New York), p. 341.

Loram, J. W., and K. A. Mirza, 1988, Physica C **153-155**, 1020.
Lou, L. F., and W. J. Tomasch, 1972, in *Low Temperature Physics—LT 13,* edited by K. D. Timmerhaus, W. J. O'Sullivan, and E. F. Hammel (Plenum, New York), p. 599.
Lyons, K. B., S. H. Liou, M. Hong, H. S. Chen, J. Kwo, and T. J. Negran, 1987, Phys. Rev. B **36**, 5592.
Maeda, H., Y. Tanaka, M. Fukutomi, and T. Asano, 1988, Jpn. J. Appl. Phys. **27**, L209.
Maki, K., 1969, in *Superconductivity,* edited by R. D. Parks (Marcel Dekker, New York), Vol. 2, p. 1035.
Marsiglio, F., 1988, Ph.D. thesis (McMaster University).
Marsiglio, F., R. Akis, and J. P. Carbotte, 1987a, Phys. Rev. B **36**, 5245.
Marsiglio, F., R. Akis, and J. P. Carbotte, 1987b, Solid State Commun. **64**, 905.
Marsiglio, F., R. Akis, and J. P. Carbotte, 1988, Physica C **153-155**, 227.
Marsiglio, F., and J. P. Carbotte, 1985, Phys. Rev. B **31**, 4192.
Marsiglio, F., and J. P. Carbotte, 1986, Phys. Rev. B **33**, 6141.
Marsiglio, F., and J. P. Carbotte, 1987a, Phys. Rev. B **36**, 3633.
Marsiglio, F., and J. P. Carbotte, 1987b, Phys. Rev. B **36**, 3937.
Marsiglio, F., and J. P. Carbotte, 1987c, Solid State Commun. **63**, 419.
Marsiglio, F., and J. P. Carbotte, 1988a, Rev. Solid State Sci. **1**, 423.
Marsiglio, F., and J. P. Carbotte, 1988b, Solid State Commun. **65**, 1175.
Marsiglio, F., J. P. Carbotte, and E. Schachinger, 1986, J. Low Temp. Phys. **65**, 305.
Marsiglio, F., J. M. Coombes, and J. P. Carbotte, 1987, Phys. Rev. B **35**, 3219.
Marsiglio, F., M. Schossmann, and J. P. Carbotte, 1988, Phys. Rev. B **37**, 4965.
Marsiglio, F., M. Schossmann, E. Schachinger, and J. P. Carbotte, 1987, Phys. Rev. B **35**, 3226.
Marsiglio, F., P. J. Williams, and J. P. Carbotte, 1989, Phys. Rev. B **39**, 9595.
Masharov, N. F., 1974a, Fiz. Tverd. Tela (Leningrad) **16**, 2342.
Masharov, N. F., 1974b, Sov. Phys. Solid State **16**, 1524.
Massidda, J. Yu, A. J. Freeman, and D. D. Koelling, 1987, Phys. Lett. A **122**, 198.
Mattheiss, L. F., 1970, Phys. Rev. B **1**, 373.
Mattheiss, L. F., 1987, Phys. Rev. Lett. **58**, 1028.
Mattheiss, L. F., and D. R. Hamann, 1987, Solid State Commun. **63**, 395.
Mattheiss, L. F., L. R. Testardi, and W. W. Yao, 1978, Phys. Rev. B **17**, 4640.
McKnight, S. W., B. L. Bean, and S. Perkowitz, 1979, Phys. Rev. B **19**, 1437.
McKnight, S. W., S. Perkowitz, D. B. Tanner, and L. R. Testardi, 1979, Phys. Rev. B **19**, 5689.
McMillan, W. L., 1968, Phys. Rev. **167**, 331.
McMillan, W. L., and J. M. Rowell, 1965, Phys. Rev. Lett. **14**, 108.
McMillan, W. L., and J. M. Rowell, 1969, in *Superconductivity,* edited by R. D. Parks (Marcel Dekker, New York), Vol. 1, p. 561.
Meservey, R., and B. B. Schwartz, 1969, in *Superconductivity,* edited by R. D. Parks (Marcel Dekker, New York), Vol. 1, p. 117.
Migdal, A. B., 1958a, Sov. Phys. JETP **34**, 996.
Migdal, A. B., 1958b, Zh. Eksp. Teor. Fiz. **34**, 1438.
Mitra, Sreeparna, J. H. Cho, W. C. Lee, D. C. Johnston, and V. C. Kogan, 1989, Phys. Rev. B **40**, 2674.
Mitrović, B., and J. P. Carbotte, 1981a, J. Low Temp. Phys. **43**, 131.
Mitrović, B., and J. P. Carbotte, 1981b, Solid State Commun. **40**, 249.
Mitrović, B., and J. P. Carbotte, 1981c, Solid State Commun. **37**, 1009.
Mitrović, B., and J. P. Carbotte, 1982, Solid State Commun. **41**, 695.
Mitrović, B., and J. P. Carbotte, 1983a, Can. J. Phys. **61**, 784.
Mitrović, B., and J. P. Carbotte, 1983b, Phys. Rev. B **28**, 2477.
Mitrović, B., and J. P. Carbotte, 1986, Phys. Rev. B **33**, 591.
Mitrović, B., C. R. Leavens, and J. P. Carbotte, 1980, Phys. Rev. B **21**, 5048.
Mitrović, B., E. Schachinger, and J. P. Carbotte, 1984, Phys. Rev. B **29**, 6187.
Mitrović, B., H. G. Zarate, and J. P. Carbotte, 1984, Phys. Rev. B **29**, 184.
Moore, D. F., R. B. Zubeck, and M. R. Beasley, 1977, Bull. Am. Phys. Soc. **22**, 289.
Moore, D. F., R. B. Zubeck, J. M. Rowell, and M. R. Beasley, 1979, Phys. Rev. B **20**, 2721.
Morel, P., and P. W. Anderson, 1962, Phys. Rev. **125**, 1263,
Moreland, J., A. F. Clark, H. C. Ku, and R. H. Shelton, 1987, Cryogenics **27**, 227.
Moreland, J., J. W. Ekin, L. F. Goodrich, T. E. Capobianco, A. F. Clark, J. Kwo, M. Hong, and S. H. Liou, 1987, Phys. Rev. B **35**, 8856.
Morris, D. E., R. M. Kuroda, A. G. Markelz, J. H. Nickel, and J. T. T. Wei, 1988, Phys. Rev. B **37**, 5936.
Müller, P., N. Nücker, W. Reichardt, and A. Müller, 1982, in *Superconductivity in d- and f-Band Metals,* edited by W. Buckel and W. Weber (Kernforschungszenturm, Karlsruhe), p. 19.
Muto, Y., N. Kobayashi, and Y. Syono, 1987, in *Novel Superconductivity,* edited by S. A. Wolf and V. Z. Kresin (Plenum, New York), p. 787.
Muto, Y., N. Toyota, K. Noto, K. Akutsu, M. Isino,and T. Fukase, 1979, J. Low Temp. Phys. **34**, 617.
Naito, M., *et al.*, 1987, Phys. Rev. B **35**, 7228.
Nakao, K., N. Miura, S. Uchida, H. Takagi, S. Tanaka, K. Kishio, J. Shimoyama, K. Kitazawa, and Kazuo Fueki, 1987a, Jpn. J. Appl. Phys. **26**, Part 2, L413.
Nakao, K., N. Miura, S. Uchida, H. Takagi, S. Tanaka, K. Kishio, J. Shimoyama, K. Kitazawa, and K. Fueki, 1987b, in *Proceedings of the 18th International Conference on Low Temperature Physics—LT 18,* edited by Y. Nagaoka (Jpn. J. Appl. Phys. **26**, Suppl. 26-3, 1187).
Nam, S. B., 1967a, Phys. Rev. B **156**, 470.
Nam, S. B., 1967b, Phys. Rev. B **156**, 487.
Nambu, Y., 1960, Phys. Rev. **117**, 648.
Neighbor, J. E., J. F. Cochran, and C. A. Shiffman, 1967, Phys. Rev. **155**, 384.
Nevitt, M. V., G. W. Crabtree, and T. E. Klippert, 1987, Phys. Rev. B **36**, 2398.
Ng, K. W., S. Pan, A. L. de Lozanne, A. J. Panson, and J. Talvacchio, 1987, in *Proceedings of the 18th International Conference on Low Temperature Physics—LT 18,* edited by Y. Nagaoka (Jpn. J. Appl. Phys. **26**, Suppl. 26-3, 993).
Niel, L., N. Giesinger, H. W. Weber, and E. Schachinger, 1985, Phys. Rev. B **32**, 2976.
Novotny, V., and P. P. M. Meincke, 1975, J. Low Temp. Phys. **18**, 147.
Oguchi, T., 1987, Jpn. J. Appl. Phys. **26**, L417.
Ohtsuka, T., and Y. Kimura, 1971, Physica **55**, 562.
Okuda, K., S. Noguchi, A. Yamagishi, K. Sugiyama, and M.

Date, 1987a, Jpn. J. Appl. Phys. **26**, L822.
Okuda, K., S. Noguchi, A. Yamagishi, K. Sugiyama, and M. Date, 1987b, in *Proceedings of the 18th International Conference on Low Temperature Physics—LT 18,* edited by Y. Nagaoka (Jpn. J. Appl. Phys. **26**, Suppl. 26-3, 1172).
Orenstein, J., G. A. Thomas, D. H. Rapkine, C. G. Betha, B. F. Levine, R. J. Cava, E. A. Rietman, and D. W. Johnson, Jr., 1987, Phys. Rev. B **36**, 729.
Orlando, T. P., and M. R. Beasley, 1981, Phys. Rev. Lett. **46**, 1598.
Orlando, T. P., A. Delive, S. Fomer, E. J. McNiff, Jr., J. M. Tarascon, J. H. Greene, W. R. McKinnon, and G. W. Hull, 1987a, Phys. Rev. B **35**, 5347.
Orlando, T. P., A. Delive, S. Fomer, E. J. McNiff, Jr., J. M. Jarascon, J. H. Greene, W. R. McKinnon, and G. W. Hull, 1987b, Phys. Rev. B **35**, 7249.
Orlando, T. P., A. Delive, S. Fomer, E. J. McNiff, Jr., J. M. Jarascon, J. H. Greene, W. R. McKinnon, and G. W. Hull, 1987c, Phys. Rev. B **36**, 2394.
Orlando, T. P., E. J. McNiff, Jr., S. Foner, and M. R. Beasley, 1979, Phys. Rev. B **19**, 4545.
Osofsky, M. S., *et al.*, 1987, in *Novel Superconductivity,* edited by S. A. Wolf and V. Z. Kresin (Plenum, New York), p. 807.
Ousset, J. C., M. F. Ravet, M. Maurer, J. Durand, J. P. Ulnet, H. Rakoto, and S. Askenazy, 1987, Europhys. Lett. **4**, 743.
Owen, C. S., and D. J. Scalapino, 1971, Physica **55**, 691.
Padamsee, H., J. E. Neighbor, and C. A. Shiffman, 1973, J. Low Temp. Phys. **12**, 387.
Pan, S., K. W. Ng, A. L. de Lozanne, J. M. Tarascon, and L. H. Greene, 1987a, Phys. Rev. B **35**, 7220.
Pan, S., K. W., Ng, and A. L. de Lozanne, 1987, in *Novel Superconductivity,* edited by S. A. Wolf and V. Z. Kresin (Plenum, New York), p. 1029.
Panson, A. J., A. I. Braginski, J. R. Gavaler, J. K. Hulm, M. A. Jamocko, H. C. Pohl, A. M. Stewert, J. Talvacchio, and G. R. Wagner, 1987, Phys. Rev. B **35**, 8774.
Papaconstantopoulos, D. A., W. E. Picket, H. Krakauer, and L. L. Boyer, 1987, in *Proceedings of the 18th International Conference on Low Temperature Physics—LT 18,* edited by Y. Nagaoka (Jpn. J. Appl. Phys. **26**, Suppl. 26-3, 1091).
Park, J. C., J. E. Neighbor, and C. A. Shiffman, 1974, Phys. Lett. A **50**, 9.
Pattnaik, P. C., and D. M. Newns, 1989, Physica C **157**, 13.
Peter, M., J. Ashkenazi, and M. Dacorogna,, 1977, Helv. Phys. Acta **50**, 267.
Phillips, J. C., 1987, Phys. Rev. B **35**, 861.
Phillips, N. E., R. A. Fischer, S. E. Lacy, C. Marcenat, J. A. Olsen, W. K. Ham, and A. M. Stacy, 1987, in *Novel Superconductivity,* edited by S. A. Wolf and V. Z. Kresin (Plenum, New York), p. 739.
Pickett, W. E., 1980, Phys. Rev. B **21**, 3897.
Pickett, W. E., 1982, Phys. Rev. B **26**, 1186.
Pickett, W. E., 1989, Rev. Mod. Phys. **61**, 433.
Pinski, F. J., P. B. Allen, and W. H. Butler, 1978, J. Phys. (Paris) Colloq. **C6**, 472.
Polturak, E., and B. Fischer, 1987, Phys. Rev. B **36**, 5586.
Prohammer, M., and E. Schachinger, 1987, Phys. Rev. B **36**, 8353.
Rainer, D., 1986, in *Progress in Low Temperature Physics,* edited by D. F. Brewer (North-Holland, Amsterdam), Vol. 10, p. 371.
Rainer, D., and G. Bergmann, 1974, J. Low Temp. Phys. **14**, 501.
Rainer, D., and F. J. Culetto, 1979, Phys. Rev. B **19**, 2540.
Ramirez, A. P., B. Batlogg, G. Aeppli, R. J. Cava, and E. A. Rietman, 1987, Phys. Rev. B **35**, 8833.
Ramirez, A. P., B. Batlogg, R. J. Cava, L. Schneemeyer, R. B. van Dover, E. A. Rietman, and J. V. Waszczak, 1987, in *Novel Superconductivity,* edited by S. A. Wolf and V. Z. Kresin (Plenum, New York), p. 689.
Rammer, J., 1988a, Europhys. Lett. **5**, 77.
Rammer, J., 1988b, Physica C **153-155**, 1625.
Rammer, J., 1989, in *Studies of High Temperature Superconductors,* edited by A. Narlikar (Nova Science, New York), p. 116.
Renker, B., F. Gompf, E. Gering, N. Nüker, B. Ewert, W. Reichhardt, and H. Rietschel, 1987, Z. Phys. B **67**, 15.
Renker, B., F. Gompf, E. Gering, G. Roth, W. Reichhardt, D. Ewert, H. Rietschel, and H. Mutka, 1988, Z. Phys. B **71**, 437.
Reuter, G. E., and E. H. Sondheimer, 1948, Proc. R. Soc. London, Ser. A **195**, 336.
Rhyne, J. J., D. A. Neumann, J. A. Gotaas, F. Beech, L. Toth, S. Lawrence, S. Wolf, M. Osofsky, and D. U. Gubser, 1987, Phys. Rev. B **36**, 2294.
Rickayzen, G., 1965, *Theory of Superconductivity* (Wiley, New York),
Rickayzen, G., 1980, *Green's Functions and Condensed Matter* (Academic, Toronto).
Rietschel, H., and H. Winter, 1979, Phys. Rev. Lett. **43**, 1256.
Rietschel, H., H. Winter, and W. Reichart, 1980, Phys. Rev. B **22**, 4284.
Roberts, B. W., 1976, J. Phys. Chem. Ref. Data **5**, 581.
Robinson, R., and J. Rowell, 1972, private communication.
Rohrer, H., 1960, Helv. Phys. Acta **33**, 675.
Rowell, J. M., 1976, Solid State Commun. **19**, 1131.
Rowell, J. M., and R. C. Dynes, 1970, in *Proceedings of the International Conference on Phonons,* edited by M. A. Nusimovici (Flammarion, Paris), p. 150.
Rowell, J. M., W. L. McMillan, and R. C. Dynes, 1970, private communication.
Roy, A. P., and B. N. Brockhouse, 1970, Can. J. Phys. **48**, 1781.
Rusinov, A. I., 1969a, Zh. Eksp. Teor. Fiz. **56**, 2043.
Rusinov, A. I., 1969b, Sov. Phys. JETP **29**, 1101.
Salamon, M. B., and J. Bardeen, 1988, Phys. Rev. Lett. **59**, 2615.
Sato, M., S. Shamoto, M. Onoda, M. Sera, K. Fukuda, S. Hosoya, J. Akimitsu, T. Ekino, and K. Imaeda, 1987, in *Novel Superconductivity,* edited by S. A. Wolf and V. Z. Kresin (Plenum, New York), p. 927.
Sauerzopf, F. M., E. Moser, H. W. Weber, and F. A. Schmidt, 1987, J. Low Temp. Phys. **66**, 191.
Scalapino, D. J., 1969, in *Superconductivity,* edited by R. D. Parks (Marcel Dekker, New York), Vol. 1, p. 449.
Scalapino, D. J., J. R. Schrieffer, and J. W. Wilkins, 1966, Phys. Rev. **148**, 263.
Scalapino, D. J., Y. Wada, and J. C. Swihart, 1965, Phys. Rev. Lett. **14**, 102.
Schachinger, E., J. M. Daams, and J. P. Carbotte, 1980, Phys. Rev. B **22**, 3194.
Schachinger, E., M. Prohammer, E. Seidl, and H. W. Weber, 1988, Physica C **153–155**, 247.
Schachinger, E., W. Stephan, and J. P. Carbotte, 1988, Phys. Rev. B **36**, 5003.
Schachinger, E., H. G. Zarate, M. Schossmann, and J. P. Carbotte, 1986, J. Low Temp. Phys. **63**, 1.
Schell, G., H. Winter, and H. Rietschel, 1980, in *Superconductivity in d- and f-Band Metals,* edited by H. Suhl and M. B. Maple (Academic, New York), p. 465.
Schenck, A., 1988, Physica C **153-155**, 1127.

Schinder, W., A. Grassmann, P. Schmitt, J. Ströbel, H. Niederhofer, G. Adrian, G. Saemann-Ischenko, and H. Adrian, 1987, in *Proceedings of the 18th International Conference on Low Temperature Physics—LT 18,* edited by Y. Nagaoka (Jpn. J. Appl. Phys. **26**, Suppl. 26-3, 1199).
Schlesinger, Z., R. T. Collins, D. L. Kaiser, and F. Holtzberg, 1987, Phys. Rev. Lett. **59**, 1958.
Schlesinger, Z., R. T. Collins, M. W. Shafer, and E. M. Engler, 1987, Phys. Rev. B **36**, 5275.
Schlesinger, Z., R. U. Greene, J. G. Bednorz, and K. A. Müller, 1987, Phys. Rev. B **35**, 5334.
Scholten, P. D., J. D. Lejeune, W. M. Saslow, and D. G. Naugle, 1977, Phys. Rev. B **16**, 1068.
Schossmann, M., and J. P. Carbotte, 1986, Phys. Rev. B **34**, 1550,
Schossmann, M., and J. P. Carbotte, 1989, Phys. Rev. B **39**, 4210.
Schossmann, M., J. P. Carbotte, and E. Schachinger, 1988, J. Low Temp. Phys. **70**, 537.
Schossmann, M., F. Marsiglio, and J. P. Carbotte, 1987, Phys. Rev. B **36**, 3627.
Schossmann, M., and E. Schachinger, 1986, Phys. Rev. B **33**, 6123.
Schossmann, M., E. Schachinger, and J. P. Carbotte, 1987, Phys. Rev. B **36**, 8360.
Schrieffer, J. R., 1964, *Theory of Superconductivity* (Benjamin, New York).
Schrieffer, J. R., D. J. Scalapino, and J. W. Wilkins, 1963, Phys. Rev. Lett. **10**, 336.
Schweiss, B. P., B. Renker, E. Schneider, and W. Reichardt, 1976, in *Superconductivity in d- and f-Band Metals,* edited by D. H. Douglass (Plenum, New York), p. 189.
Shaw, W., and J. C. Swihart, 1968, Phys. Rev. Lett. **20**, 1000.
Shen, L. Y., 1972, Phys. Rev. Lett. **29**, 1082.
Sheng, Z. Z., and A. M. Hermann, 1988, Nature **332**, 138.
Shiba, H., 1968, Prog. Theor. Phys. **40**, 435.
Shiffman, C. A., J. F. Cochran, and M. Garber, 1963, J. Phys. Chem. Solids **24**, 1369.
Shirane, G., and J. D. Axe, 1971, Phys. Rev. B **4**, 1957.
Skalski, S. S., O. Betbeder-Matibet, and P. R. Weiss, 1964, Phys. Rev. **136**, A1500.
Sleight, A. W., J. L. Gillson, and P. E. Bierstedt, 1975, Solid State Commun. **17**, 27.
Song, S. N., S. J. Hwu, K. Poppelmeier, T. O. Mason, and J. B. Ketterson, 1987, in *Proceedings of the 18th International Conference on Low Temperature Physics—LT 18,* edited by Y. Nagaoka (Jpn. J. Appl. Phys. **26**, Suppl. 26-3, 1039).
Stedman, R., L. Almqvist, and G. Nilsson, 1967, Phys. Rev. **162**, 549.
Stewart, G. R., 1979, Solid State Commun. **30**, 415.
Stroble, P., P. Monceau, J. L. Tholence, R. Currat, A. J. Dianoux, J. J. Caponi, and J. G. Bednorz, 1988, Physica C **153-155**, 282.
Stromberg, T. F., and C. A. Swenson, 1962, Phys. Rev. Lett. **9**, 370.
Subramanian, M. A., J. C. Calabrese, C. C. Torardi, J. Gopalakrishnan, T. R. Askew, R. B. Flippen, K. J. Morrissey, U. Chowdhury, and A. W. Sleight, 1988, Nature **332**, 420.
Sulewski, P. E., T. W. Noh, J. T. McWhirter, and A. J. Sievers, 1987, Phys. Rev. B **36**, 5735.
Sulewski, P. E., A. J. Sievers, S. E. Russek, H. D. Hallen, D. K. Lathrop, and R. A. Buhrman, 1987, Phys. Rev. B **35**, 5330.
Swihart, J. C., 1962, IBM J. Res. Dev. **6**, 14.
Swihart, J. C., 1963, Phys. Rev. **131**, 73.
Swihart, J. C., D. J. Scalapino, and Y. Wada, 1965, Phys. Rev. Lett. **14**, 106.
Swihart, J. C., and W. Shaw, 1971, in *Superconductivity,* edited by F. Chilton (North-Holland, Amsterdam), p. 678.
Takabatake, T., M. Ishikawa, Y. Nakazawa, I. Oguro, T. Sakakibara, and T. Goto, 1987, Jpn. J. Appl. Phys. **26**, L978.
Takegahara, K., H. Harima, and A. Yanase, 1987, Jpn. J. Appl. Phys. **26**, L352.
Takita, K., T. Ippōshi, T. Uchino, H. Akinaga, H. Katoh, and K. Masuda, 1987, in *Proceedings of the 18th International Conference on Low Temperature Physics—LT 18,* edited by Y. Nagaoka (Jpn. J. Appl. Phys. **26**, Suppl. 26-3, 1043).
Tedrow, P. M., and R. Meservey, 1982, Phys. Rev. B **25**, 171.
Teichler, H., 1977, in *Anisotropy Effects in Superconductors,* edited by H. W. Weber (Plenum, New York), p. 7.
Temmerman, W. M., G. M. Stocks, P. J. Durham, and P. A. Sterne, 1987, J. Phys. F **17**, L135.
Testardi, L. R., and L. F. Mattheiss, 1978, Phys. Rev. Lett. **41**, 1612.
Thomas, G. A., R. N. Bhatt, A. Millis, R. Cava, and E. Rietman, 1987, in *Proceedings of the 18th International Conference on Low Temperature Physics—LT 18,* edited by Y. Nagaoka (Jpn. J. Appl. Phys. **26**, Suppl. 26-3, 1001).
Thomas, G. A., H. K. Ng, A. J. Millis, R. N. Bhatt, R. Cava, E. A. Rietman, D. W. Johnson, Jr., G. G. Espinosa, and J. M. Vandenberg, 1987, Phys. Rev. B **36**, 846.
Timusk, T., and D. B. Tanner, 1989, in *Physical Properties of High Temperature Superconductors,* edited by D. M. Ginsberg (World Scientific, Singapore), Vol. 1, p. 339.
Tomlinson, P. G., and J. P. Carbotte, 1976, Phys. Rev. B **13**, 4738.
Tomlinson, P. G., and J. P. Carbotte, 1977, Can. J. Phys. **55**, 751.
Tomlinson, P. G., and J. C. Swihart, Phys. Rev. B **19**, 1867.
Toxen, A. M., 1965, Phys. Rev. Lett. **15**, 462.
Truant, P. T., and J. P. Carbotte, 1973, Can. J. Phys. **51**, 922.
Tulina, N. A., V. A. Borodin, V. F. Kondakov, and L. I. Chernyshova, 1987, in *Novel Superconductivity,* edited by S. A. Wolf and V. Z. Kresin (Plenum, New York), p. 889.
Uchida, S., H. Takagi, T. Hasegawa, K. Kishio, S. Tajima, K. Kitazawa, K. Fueki, and S. Tanaka, 1987, in *Novel Superconductivity,* edited by S. A. Wolf and V. Z. Kresin (Plenum, New York), p. 855.
Uchida, S., H. Takagi, K. Kitazawa, and S. Tanaka, 1987, Jpn. J. Appl. Phys. **26**, L1.
Uemura, Y. J., V. J. Emery, A. R. Moodenbaugh, M. Suenaga, D. C. Johnston, A. J. Jacobson, J. T. Lewandowski, J. H. Brewer, R. F. Kiefl, S. R. Kreitzman, G. M. Luke, T. Riseman, C. E. Stronach, W. J. Kossler, J. R. Kempton, X. H. Yu, D. Opie, and H. E. Schone, 1988, Phys. Rev. B **38**, 9280.
van Bentum, P. J. M., L. E. C. van de Leemput, L. W. M. Schreurs, P. A. A. Teunissen, and H. van Kempen, 1987, Phys. Rev. B **36**, 843.
van Bentum, P. J. M., H. van Kempen, L. E. C. van de Leemput, J. A. A. J. Perenboom, L. W. M. Schreurs, and P. A. Teunissen, 1987, Phys. Rev. B **36**, 5279.
van Miltenberg, J. C., A. Schuijff, K. Kadowaki, M. van Sprang, J. Q. A. Koster, Y. K. Huang, A. A. Menovsky, and H. Barten, 1987, Physica B&C **146**, 319.
Varma, C. M., 1982, in *Superconductivity in d- and f-Band Metals,* edited by W. Buckel and W. Weber (Kernforschungszentrum, Karlsruhe), p. 603.
Varma, C. M., S. Schmitt-Rink, and E. Abrahams, 1987, Solid State Commun. **3**, 3.

Varma, C. M., and W. Weber, 1979, Phys. Rev. B **19**, 6142.
Vashishta, P., and J. P. Carbotte, 1973, Phys. Rev. B **7**, 1874.
Vasiliev, B. V., and V. I. Luschikov, 1988, Physica C **153-155**, 261.
Vasiliev, B. V., V. I. Lushchikov, and V. V. Sikolenko, 1988, JETP Lett. **47**, 334 [Pis'ma Zh. Eksp. Teor. Fiz. **47**, 276 (1988)].
Vidberg, H. J., and J. W. Serene, 1977, J. Low Temp. Phys. **29**, 179.
Vuong, T. H. H., D. C. Tsui, V. J. Goldman, P. H. Hon, R. L. Ming, and C. W. Chu, 1987, Solid State Commun. **63**, 525.
Wada, Y., 1964, Phys. Rev. **135**, A1481.
Walter, U., M. S. Sherwin, A. Stacy, P. L. Richards, and A. Zettl, 1987, Phys. Rev. B **35**, 5327.
Wang, Z., Z. Zhou, D. Mao, X. Zhang, and H. Wu, 1980, Acta Phys. Sci. **29**, 863.
Weber, H. W., and E. Schachinger, 1988, Helv. Phys. Acta **61**, 478.
Weber, W., 1984a, in *Electronic Structure of Complex Systems,* Vol. 113 of *Nato Advanced Study Institute Series B: Physics,* edited by P. Phariseau and W. Temmerman (Plenum, New York), p. 345.
Weber, W., 1984b, Physica B **126**, 217.
Weber, W., 1987a, Phys. Rev. Lett. **58**, 1371.
Weber, W., 1987b, Phys. Rev. Lett. **58**, 2154(E).
Weber, W., and L. F. Mattheiss, 1988, Phys. Rev. B **37**, 599.
Werthamer, N. R., E. Helfand, and P. C. Hohenberg, 1966, Phys. Rev. **147**, 295.
Werthamer, N. R., and W. L. McMillan, 1967, Phys. Rev. **158**, 415.
Whitmore, M., 1984, J. Low Temp. Phys. **56**, 129.
Wolf, E. L., and G. B. Arnold, 1982, Phys. Rep. **91**, 32.
Wolf, E. L., and R. J. Noer, 1979, Solid State Commun. **30**, 391.
Wolf, E. L., and J. Zasadzinski, 1974, Phys. Lett. A **62**, 165.
Wolf, E. L., J. Zasadzinski, J. W. Osmun, and G. R. Arnold, 1979, Solid State Commun. **31**, 321.
Wolf, S. A., and V. Z. Kresin, 1987, Eds., *Novel Superconductivity* (Plenum, New York).
Worthington, T. K., W. J. Gallagher, and T. R. Dinger, 1987, Phys. Rev. Lett. **59**, 1160.
Wrobel, J. M., S. Wang, S. Gygax, B. P. Clayman, and L. K. Peterson, 1987, Phys. Rev. B **36**, 2368.
Wu, H., and G. Ji, 1979, Sci. Sin. **22**, 514.
Wu, H., C.-H. Tsai, C. Kung, K. Chi, and C.-T. Tsai, 1977 Sci. Sin. **20**, 583.
Wu, H., Z. Weng, G. Ji, and Z. Zhou, 1987, J. Phys. Chem. Solids **48**, 395.
Wu, H., Z. Zhou, Z. Wang, and X. Zhang, 1980, Acta Phys. Sin. **29**, 409.
Wu, M. K., J. R. Ashburn, C. J. Torng, P. H. Hor, R. L. Meng, L. Gao, Z. J. Huang, Y. Q. Wang, and C. W. Chu, 1987, Phys. Rev. Lett. **58**, 908.
Yu, J., S., Massidda, A. J. Freeman, and D. D. Koeling, 1987, Phys. Lett. A **122**, 203.
Yvon, P. J., R. B. Schwartz, C. B. Pierce, L. Bernardez, A. Cenners, and R. Meisenheimer, 1989, Phys. Rev. B **39**, 6690.
Zarate, H. G., and J. P. Carbotte, 1983a, Phys. Rev. B **27**, 194.
Zarate, H. G., and J. P. Carbotte, 1983b, Solid State Commun. **48**, 273.
Zarate, H. G., and J. P. Carbotte, 1984, J. Low Temp. Phys. **57**, 291.
Zarate, H. G., and J. P. Carbotte, 1985, J. Low Temp. Phys. **59**, 19.
Zarate, J. G., and J. P. Carbotte, 1987, Phys. Rev. B **35**, 3256.
Zasadzinski, J., D. M. Burnell, E. L. Wolf, and G. B. Arnold, 1982, Phys. Rev. B **25**, 1662.
Zasadzinski, J., W. K. Schubert, E. L. Wolf, and G. B. Arnold, 1980, in *Superconductivity in d- and f-Band Metals,* edited by H. Suhl and M. B. Maple (Academic, New York), p. 159.
Zavaritsky, N. V., V. N. Zavaritsky, and S. V. Petrov, 1987, in *Novel Superconductivity.* edited by S. A. Wolf and V. Z. Kresin (Plenum, New York), p. 871.
Zhaojia, C., Z. Yong, Y. Hongshun, C. Zuyan, Z. Dongnin, Q. Yitai, W. Baimei, and Z. Qirui, 1987, Solid State Commun. **64**, 685.
Zhou, Z., H. Wu, D. Mao, and Y. Gu, 1980, Sci. Sin. **23**, 1379.
zur Loye, H.-C., K. J. Leary, S. W. Keller, W. K. Ham, T. A. Faltens, J. N. Michaels, and A. M. Stacy, 1987, Science **238**, 1558.